# IDENTIFYING DISCREPANCIES BETWEEN INWARD AND OUTWARD ELECTRON TRANSFER IN *SHEWANELLA ONEIDENSIS*

By

Shaylynn Delaney Miller

A DISSERTATION

Submitted to
Michigan State University
in partial fulfillment of the requirements
for the degree of

Biochemistry and Molecular Biology – Doctor of Philosophy

2025

## ABSTRACT

Addressing the climate crisis requires not a single breakthrough, but a suite of well-understood, adaptable solutions spanning technology, policy, and practice. To limit warming to no more than 1.5°C above pre-industrial levels, we must approach net zero carbon dioxide ($CO_2$) emissions around the mid-twenty first century. However, achieving this will require a coordinated effort across multiple disciplines, with combinations of biology and technology playing a crucial role in supporting these initiatives. One promising biotechnology, microbial electrosynthesis (MES), has the potential to significantly reduce net $CO_2$ emissions if implemented on an industrial scale. In future MES systems, microbial species capable of extracellular electron transfer (ET) and carbon fixing reactions could recycle $CO_2$ from industrial emissions directly into useful organic molecules.

While MES and its key components (the bacteria-electrode interface and ET), could become valuable tools in the broader effort to lower net $CO_2$ emissions, fundamental questions remain for even the most well-understood extracellular ET pathway, the Mtr pathway. The Mtr pathway is the metal reducing pathway from *Shewanella oneidensis*, a bacterium that can use extracellular electron acceptors when the available oxygen is insufficient for respiration (outward ET). The Mtr pathway is also bidirectional, an important feature for a model organism used to study MES. Because MES requires a robust bacteria-electrode interface for electron transfer into the bacterium (inward ET), the bidirectionality of the Mtr pathway provides an excellent vehicle for studying the mechanisms and bottlenecks that constrain inward ET in *S. oneidensis* or comparable systems. Despite the established bidirectionality of the Mtr pathway, there is a persistent asymmetry between outward and inward ET, with outward electron transfer being

consistently higher in magnitude. Tefft and TerAvest (2019) developed an *S. oneidensis* strain expressing butanediol dehydrogenase (Bdh), a non-native NADH-dependent enzyme. The enzymatic reaction Bdh catalyzes, acetoin reduction to 2,3-butanediol, can act as an indicator of electron transfer to cytoplasmic carriers via NADH dehydrogenases. However, this direction is the opposite of the respiratory direction and is thermodynamically limited for inward ET.

In Chapter 2, I use a thermodynamic model to compare inward ET through *S. oneidensis* NADH dehydrogenases under three energetic coupling scenarios, along with a qualitative changes in membrane potential at the single cell level for electrode-attached *S. oneidensis*. In Chapter 3, I compare the extracellular component of inward and outward ET by using two thermodynamically favorable ET paths. Under conditions with and without a redox mediator for *S. oneidensis*, I use chronoamperometry and cyclic voltammetry to conclude that inward and outward ET occur through different mechanisms for anaerobic *S. oneidensis*. In Chapter 4, I investigate the impact of pre-culture medium on inward ET ability. Pre-cultured in minimal rather than rich medium increased inward ET. Using differential protein analysis I found that pre-culture in minimal medium appears to prime *S. oneidensis* for inward ET more effectively than pre-culture in rich medium. Growth in minimal medium made proteins in energy conserving pathways more abundant, and proteins from translational processes less abundant.Together, Chapters 2, 3, and 4 describe bottlenecks along the inward ET pathway that, if alleviated, could lessen or eliminate the discrepancy between inward and outward ET rates in *S. oneidensis*.

To my nieces and nephews: Elijah, Valentina, Valeria, Micah, and any yet to arrive. I hope that in some small way I can help give you a better world to grow up in.

## ACKNOWLEDGEMENTS

Science isn't done in a vacuum, unless of course you're referring to a literal vacuum.

Hahaha, anyway, thank you guys for always filling the void.

It means more than my words will ever convey.

First, thank you to Anne Casper for inviting a kid from your freshman biology class to join your lab. You started this, and I certainly would not be about to defend this dissertation if you hadn't given me that chance.

Thank you to all the friends from in and out of the lab along the way, and a particular thank you to all the labmates I've grown up with, both as a scientist and as a person, since starting research 15 years ago.

To Michaela, thank you for always striving to be an excellent science mentor, and just as importantly, an excellent human being.

To my parents, sister, and all my family: Thank you for always encouraging my curiosity, I love you so much and I hope to always do the same for you.

To Dad specifically, because you might actually read my dissertation: Yes, I already know about the typo on page whatever…Entirely unrelated question, have you cracked the double cipher yet?

There are too many names to list to acknowledge all the people I want to thank. Know that if you've been an important part of my life, you're in this. However, the name that this page isn't complete without is Stefania, my best friend and my wife. I love you and the little family we have, and I'm so thrilled to start the next part of our lives together with Oliver, our sweet little cat boy, who is finally safe and healthy at home.

## TABLE OF CONTENTS

# Chapter 1. Extracellular electron transfer in *Shewanella oneidensis*

## 1. 1. Microbial Bioelectrochemical Systems: Connecting the Biological with the Electrochemical

Systems that interconvert biological and electrochemical information have enabled a range of biotechnologies to emerge over the last several decades. Microbial fuel cells (MFCs) for energy generation, biosensors for environmental monitoring, and microbial electrosynthesis (MES) for recycling carbon dioxide into new compounds are just a few examples of the uses of bioelectrochemical systems (BESs).[1,2] At the core of BESs is the biological-electrochemical interface, where information and/or energy is exchanged between biological and electrical systems. The biological side of this interface can involve anything from live bacterial cells capable of extracellular electron transfer (ET) to individual inorganic molecules secreted by microbes. Configurations of BESs can also exist without direct participation of living organisms. A bioelectrochemical interface could involve ET via isolated redox active proteins, or electron carrying molecules. However, what all BESs have in common is controlled ET between biological and electrochemical components. Whether mediated by whole cells, isolated proteins, or diffusible electron carriers, the efficiency, specificity, and directionality of this transfer dictates the performance of BESs.[3,4] Understanding the mechanisms governing these interactions is critical for improving BES efficiency, scalability, and applicability across different fields.

Among the many emerging biotechnologies, MES has garnered attention due to the worsening climate crisis and the need to reach net zero carbon dioxide emissions by the mid-21$^{st}$ century to avoid the worst consequences of climate change.[5–7] MES sounds like an ideal biotechnology to decrease net carbon emissions because it converts inorganic carbon sources (e.g., $CO_2$) into organic carbon compounds (sugars, biofuel precursors,

etc.) and stores electrical energy. However, we have yet to reach a profitable combination of ET rate and energy conversion efficiency.[6] Improvements to current density (electrons/time/electrode surface area), changes in BES design, and decreased electrode material cost are among the factors that could contribute to a financially feasible industrial scale MES system.[7,8] Improving current density requires a deeper understanding of extracellular ET mechanisms and how they can be controlled in BESs. In this dissertation I will delve further into the topic of extracellular ET using the model organism, *Shewanella oneidensis* and its metal reducing (Mtr) pathway, the most thoroughly understood extracellular ET pathway to date.[9–15]

### 1. 2. *Shewanella oneidensis*: At the bio-electrochemical interface

#### 1. 2. 1 An overview of *Shewanella oneidensis* and the Mtr pathway

*S. oneidensis* MR-1, first isolated from Oneida Lake (NY, USA) in the 1980s, as evolved a flexible respiratory strategy, and respires aerobically but also uses alternate terminal electron acceptors for respiration when oxygen is scarce.[16–21] Before reaching an extracellular electron acceptor, electrons from oxidized substrates (e.g., lactate) are transported via cytoplasmic electron carrying molecules (e.g., NADH) to membrane bound dehydrogenases (e.g., NADH dehydrogenase). From there, the cytoplasmic electron carrier is oxidized, the quinone pool is reduced, and electrons can pass to CymA, a multiheme cytochrome in the *S. oneidensis* inner membrane.[22,23] From CymA, small periplasmic cytochromes, such as CctA, carry electrons across the periplasmic space, to the Mtr pathway embedded in *S. oneidensis'* outer membrane.[23] The Mtr pathway is composed of multiheme cytochromes, which allow *S. oneidensis* to reduce extracellular electron acceptors like insoluble metals and electrodes (Figure 1-1A).[10,15,24] The Mtr pathway consists of several proteins (MtrA, MtrB, MtrC, and OmcA), of which MtrA, MtrC,

and OmcA are multi-heme cytochromes, while MtrB is a β-barrel protein embedded in the outer membrane.[15] MtrA and MtrC span the inside of the MtrB β-barrel from the periplasmic side to the cell surface.[15] The structure that results is akin to an insulated 'biological wire' that allows electron flow across the outer membrane.[14,15] On the cell surface, MtrC and OmcA are both available for electron exchange with extracellular surfaces and molecules.[25]

In addition to outward ET (Figure 1-1A), where electrons from cellular metabolism flow

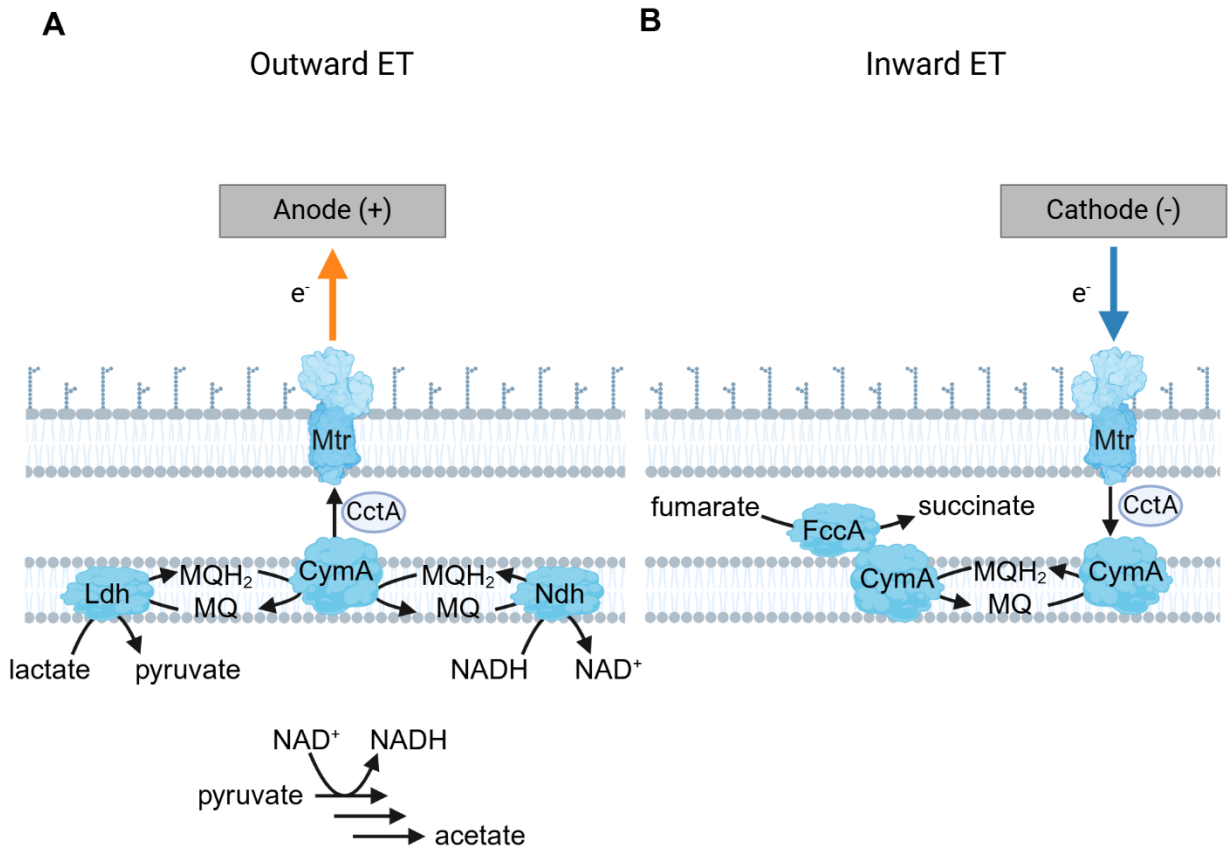


*Figure 1-1. Examples of extracellular electron transfer in Shewanella oneidensis. (A) Outward electron transfer (Outward ET) also known as extracellular electron donation (EED). This is the extracellular electron transfer direction that wild type* S. oneidensis *would perform during cellular respiration. (B) Example of inward electron transfer (Inward ET) also known as extracellular electron uptake (EEU). The electron donor here is a negatively poised electrode and the electron acceptor is fumarate, as was the case when Ross et al. (2011) established that the Mtr pathway is bidirectional. The above figure was adapted from Miller et al. (2025, preprint).[29]*

out along the multiheme cytochromes of the Mtr pathway and reduce a natural electron acceptor or positively-poised electrode (anode), work by Ross et al. (2011) established that the Mtr pathway can also support inward ET (Figure 1-1B).[9] Ross et al. (2011) demonstrated inward ET in *S. oneidensis* by showing that it could use electrons from a negatively-poised electrode (cathode) to reduce fumarate to succinate in the periplasm.[9] Work by Rowe et al. (2018) further demonstrated a physiologically important role for inward ET in *S. oneidensis*, as inward ET to oxygen represented a source of cellular energy acquisition without a carbon source.[26] Rowe et al. (2021) continued this work, describing evidence for alternate ET pathways for inward ET that were independent of outward ET.[12]

*S. oneidensis* can also support inward ET to the cytoplasm when the proton-translocating NADH dehydrogenase, Nuo, has sufficient proton motive force (PMF) to drive the thermodynamically unfavorable step in reverse (Figure 1-2).[27,28] In the first use of this system, Tefft and TerAvest (2019) supplied additional PMF by expressing proteorhodopsin, a light driven proton pump.[27] However, Ford and TerAvest (2023) later established that trace oxygen (~1% dissolved oxygen) could also provide PMF by activating native proton pumping oxidases, as shown in Figure 1-2.[28]

As discussed in the previous section, biotechnologies like MES rely on microbial systems capable of electrode-driven intracellular reduction reactions. The ability of *S. oneidensis* to use electrons from a cathode to drive cytoplasmic reduction reactions makes it a valuable model organism for identifying and resolving bottlenecks that limit inward ET.[27] The directional asymmetry in magnitude that persists for outward and inward ET has yet to be resolved.[29] Even when comparing thermodynamically favorable ET pathways,

inward ET only matches approximately one tenth the magnitude of outward ET. Throughout this work, a particular focus will be on studying the bottlenecks responsible for this directional ET asymmetry.[29]

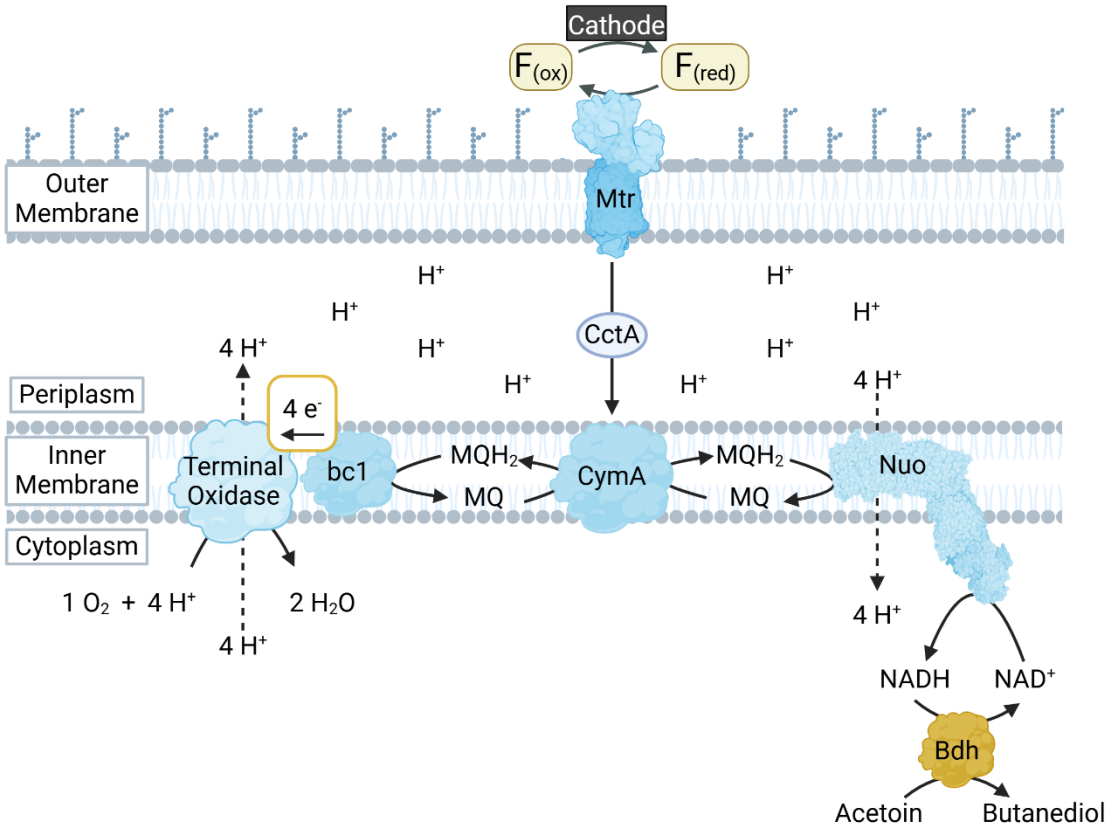


*Figure 1-2. Inward ET from a cathode to the cytoplasm in* S. oneidensis *as described by Tefft and TerAvest (2019) and Ford and TerAvest (2023).[27,28] Proteins native to* S. oneidensis *are in blue and the heterologously expressed protein, butanediol dehydrogenase (Bdh) is yellow. Bdh converts acetoin into butanediol in an NADH-dependent manner and acts as an indicator of successful electron transfer across the inner membrane. Nuo is a proton-pumping NADH dehydrogenase, CymA is a multi-heme cytochrome in the inner membrane, $MQH_2$ is menaquinol, MQ is menaquinone, CctA is a periplasmic multi-heme cytochrome, and F(red) and F(ox) are the reduced and oxidized forms of flavin, respectively. Dashed arrows represent proton translocation across the inner membrane, while solid arrows show the direction of ET.*

### 1. 2. 2 Flavin-mediated extracellular ET

While we have known that *S. oneidensis* can reduce extracellular electron acceptors for several decades, some fundamental aspects of the extracellular ET process have only

recently been uncovered. Numerous models of the mechanism by which electrons travel from the OMCs (MtrC and OmcA) to insoluble electron acceptors have been proposed over the years.[18] In 2008, Marsili et al. and von Canstein et al., both demonstrated that the soluble redox shuttles mediating extracellular ET in *S. oneidensis* were flavins, common enzymatic cofactors. [11,18,30] Specifically, *S. oneidensis* can produce flavin mononucleotide (FMN), riboflavin (RF), and flavin adenine dinucleotide (FAD) and secrete RF and FMN extracellularly at up to μM concentrations. [11,13,30] Additional work by Kotloski and Gralnick (2013) further demonstrated the importance of secreted flavins for extracellular ET with a knockout mutant of the bacterial flavin adenine dinucleotide exporter (*bfe*); the mutant strain, *S. oneidensis Δbfe*, could make flavins but not secrete them extracellularly suggesting that soluble flavins are responsible for ~75% of extracellular ET, a result consistent with the 70% previously estimated by Marsili et al. (2008).[11,13] While the importance of flavins to *S. oneidensis* ET has been clearly established, the mechanism by which they enhance the ET rate remains less clear. Given that the majority of ET relies on flavin-mediated pathways and that discrepancies persist between inward and outward ET, further characterization of the underlying mechanisms is essential.

Work by Paquete et al. (2014) supported the originally proposed diffusion-based model, as their results were consistent with a transient interaction between OMCs and soluble flavins.[31] However, other OMC-flavin behavior reported by Okamoto et al. (2013) was not compatible with a purely diffusion-based model.[32] Indeed, Okamoto et al. (2013) reported that their results supported ET through a one-electron transfer, an OMC-flavin interaction that is consistent with a semiquinone flavocytochrome, not the two-electron transfer

expected for ET through flavin diffusion.[32] There is mounting evidence for a hybrid mechanism, where flavins can act either through diffusion or as a flavocytochrome complex depending on the environmental context.[33–35] In the hybrid model of flavin-mediated ET, the transition between diffusion and a flavocytochrome complex is dependent on a highly conserved disulfide bond in the OMCs.[35] The ability to toggle the semiquinone form on and off protects *S. oneidensis* from forming reactive oxygen species via the reactive flavocytochrome, while maintaining the ability to use the kinetically more rapid semiquinone form under anaerobic conditions.[33–35] As shown in Figure 1-3, in the presence of oxygen the disulfide bond is intact and the OMC-flavin interaction becomes transient, favoring the diffusive mode of ET, and under anaerobic conditions, the disulfide bond is reduced, allowing ET through the flavocytochrome when the multiheme cytochromes are continuously reduced by catabolic processes. [33–35]

The ability of *S. oneidensis* to toggle between diffusive and flavocytochrome-bound ET modes highlights that bidirectionality in an extracellular ET pathway does not imply that the directions operate in a mechanistically equivalent manner. Identifying the source of these asymmetries can reveal bottlenecks that limit inward ET relative to outward ET in *S. oneidensis*. By identifying disparities between inward and outward ETs in *S. oneidensis*, we can pinpoint key locations in the extracellular ET pathway where optimization could enhance the inward ET required for biotechnologies like microbial electrosynthesis.

### 1. 3. Research overview

As discussed above, Tefft and TerAvest (2019) established that an engineered strain of *S. oneidensis* could drive cytoplasmic reduction reactions on a cathode.[27] While this system provided proof-of-concept for inward ET to cytoplasmic $NAD^+$, it remained unclear which of *S. oneidensis'* four NADH dehydrogenases were essential for inward ET to the cytoplasm.[27,36] Tefft et al. (2022) confirmed that Nuo and Nqr1, a proton-pumping and

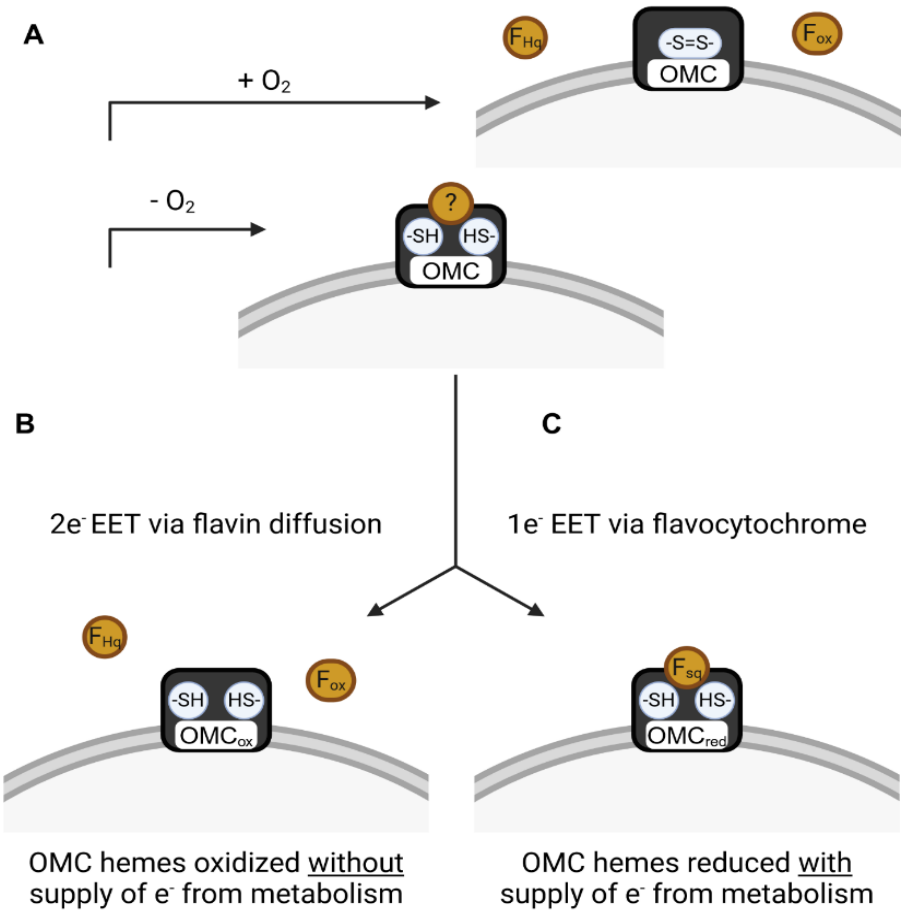


*Figure 1-3. An updated flavin mediated electron transfer model: A highly conserved disulfide bond toggles between a bound flavocytochrome mode under anaerobic conditions and an unbound diffusive flavin mode under aerobic conditions.[33–35] $F_{ox}$, $F_{sq}$, and $F_{Hq}$, represent the fully oxidized, partially reduced semiquinone, and fully reduced flavin states. (A) the disulfide bond and associate flavin interaction with (+$O_2$) or without (-$O_2$) oxyegen. Pannels B and C show two conditions without oxygen, where the OMCs are either reduced (Panel A) or oxidized (Panel B) depending on the availabilioty of electrons from metabolism.*

sodium-pumping NADH dehydrogenases, respectively, were required to support inward ET to cytoplasmic $NAD^+$.[37] Ford and TerAvest (2023) demonstrated that *S. oneidensis* can support inward ET with PMF generated by its native proton-pumping oxidases, instead of using the light-driven proton pump.[28] These studies further established the utility of *S. oneidensis* as a model organism for studying microbial extracellular ET, a fundamental requirement for MES and many biotechnologies. Still, among the lingering questions pertaining to extracellular ET in *S. oneidensis* is the difference in ET rate for outward and inward ET processes.[29]

From the experimental evidence reported by Tefft et al. (2019), Tefft et al. (2022), and Ford et al. (2023), I hypothesized that an ion-motive force (IMF), such as proton or sodium motive force (SMF), would be required to drive inward ET to the cytoplasm. However, it remained plausible that the equilibrium of the thermodynamically limiting step at the respiratory NADH dehydrogenases could be shifted to favor inward ET, even in the absence of a steady supply of IMF. In Chapter 2, I address this question with a thermodynamic model to calculate the available Gibbs free energy under three energetic coupling scenarios. For each scenario (PMF coupled, SMF coupled, and energetically uncoupled) I modeled the Gibbs free energy available under biologically relevant conditions for *S. oneidensis* in terms of membrane potential and pH difference across the inner membrane, while assuming either a highly reduced or highly oxidized quinone pool. I complemented my computational approach by adapting an experimental technique developed by Pirbadian et al. (2020) that allows fluorescence microscopy of *S. oneidensis* cells in a BES.[38] By adapting their set-up, I performed the first qualitative measurement of membrane potential changes in *S. oneidensis* actively performing inward ET to the

cytoplasm. Together, the results of my thermodynamic model and experimental approach in Chapter 2 are consistent with inward ET from a cathode to cytoplasmic $NAD^+$ being both IMF-dependent and IMF-limited.

In Chapter 3, I adapted the BES protocol from Tefft et al. (2019) to directly compare the flavin-mediated component of inward and outward ET in *S. oneidensis*, for the first time. To isolate the extracellular component of extracellular ET, I compared two thermodynamically favorable pathways with varying concentrations of supplemental flavin. By analyzing the two extracellular ET directions using chronoamperometric and cyclic voltametric potentiometry, I conclude that under anaerobic conditions, inward and outward ET 1) have different dependencies on supplemental flavin and 2) follow distinct ET mechanisms.

In Chapter 4, I observed that growth medium choice, prior to inoculation in a BES, can alter performance during inward ET. Differential proteomic analysis of electrode-attached cells revealed that growth in minimal medium primes the *S. oneidensis* proteome for inward ET. Pre-culture in minimal medium led to a proteome shift towards energy conserving pathways that overlap with components of the inward ET pathway, including *nuo*, a now established bottleneck for inward ET.

## REFERENCES


1. Kneuer L, Wurst R, Gescher J. *Shewanella oneidensis*: Biotechnological Application of Metal-Reducing Bacteria. In: ; 2024. doi:10.1007/10_2024_272

2. Dessì P, Rovira-Alsina L, Sánchez C, et al. Microbial electrosynthesis: Towards sustainable biorefineries for production of green chemicals from CO2 emissions. *Biotechnol Adv*. 2021;46. doi:10.1016/j.biotechadv.2020.107675

3. Karthikeyan R, Singh R, Bose A. Microbial electron uptake in microbial electrosynthesis: a mini-review. *J Ind Microbiol Biotechnol*. 2019;46(9-10):1419-1426. doi:10.1007/s10295-019-02166-6

4. Zhang S, Jiang J, Wang H, Li F, Hua T, Wang W. A review of microbial electrosynthesis applied to carbon dioxide capture and conversion: The basic principles, electrode materials, and bioproducts. *Journal of $CO_2$ Utilization*. 2021;51:101640. doi:10.1016/j.jcou.2021.101640

5. Masson-Delmotte V, Zhai P, Pörtner HO, et al. IPCC, 2018: Global Warming of 1.5°C. An IPCC Special Report on the impacts of global warming of 1.5°C above pre-industrial levels and related global greenhouse gas emission pathways, in the context of strengthening the global response to the threat of climate change, sustainable development, and efforts to eradicate poverty. *Intergovernmental Panel on Climate Change*. Published online 2019:616. doi:10.1017/9781009157940

6. Prévoteau A, Carvajal-Arroyo JM, Ganigué R, Rabaey K. Microbial electrosynthesis from CO2: forever a promise? *Curr Opin Biotechnol*. 2020;62:48-57. doi:10.1016/j.copbio.2019.08.014

7. Jourdin L, Sousa J, Stralen N van, Strik DPBTB. Techno-economic assessment of microbial electrosynthesis from CO2 and/or organics: An interdisciplinary roadmap towards future research and application. *Appl Energy*. 2020;279:115775. doi:10.1016/j.apenergy.2020.115775

8. Zhang L, Zhang Y, Liu Y, et al. High power density redox-mediated Shewanella microbial flow fuel cells. *Nat Commun*. 2024;15(1):8302. doi:10.1038/s41467-024-52498-w

9. Ross DE, Flynn JM, Baron DB, Gralnick JA, Bond DR. Towards Electrosynthesis in Shewanella: Energetics of Reversing the Mtr Pathway for Reductive Metabolism. Xu S yong, ed. *PLoS One*. 2011;6(2):e16649. doi:10.1371/journal.pone.0016649

10. Coursolle D, Baron DB, Bond DR, Gralnick JA. The Mtr respiratory pathway is essential for reducing flavins and electrodes in *Shewanella oneidensis*. *J Bacteriol*. 2010;192(2):467-474. doi:10.1128/JB.00925-09

11. Marsili E, Baron DB, Shikhare ID, Coursolle D, Gralnick JA, Bond DR. Shewanella secretes flavins that mediate extracellular electron transfer. *Proc Natl Acad Sci U S A*. 2008;105(10):3968-3973. doi:10.1073/pnas.0710525105

12. Rowe AR, Salimijazi F, Trutschel L, et al. Identification of a pathway for electron uptake in *Shewanella oneidensis*. *Commun Biol*. 2021;4(1). doi:10.1038/s42003-021-02454-x

13. Kotloski NJ, Gralnick JA. Flavin electron shuttles dominate extracellular electron transfer by *Shewanella oneidensis*. *mBio*. 2013;4(1). doi:10.1128/mBio.00553-12

14. Firer-Sherwood M, Pulcu GS, Elliott SJ. Electrochemical interrogations of the Mtr cytochromes from Shewanella: Opening a potential window. *Journal of Biological Inorganic Chemistry*. 2008;13(6):849-854. doi:10.1007/s00775-008-0398-z

15. Edwards MJ, White GF, Butt JN, Richardson DJ, Clarke TA. The Crystal Structure of a Biological Insulated Transmembrane Molecular Wire. *Cell*. Published online 2020. doi:10.1016/j.cell.2020.03.032

16. Kaila VRI, Wikström M. Architecture of bacterial respiratory chains. *Nat Rev Microbiol*. 2021;19(5):319-330. doi:10.1038/s41579-020-00486-4

17. Gralnick JA, Newman DK. Extracellular respiration. *Mol Microbiol*. 2007;65(1):1-11. doi:10.1111/j.1365-2958.2007.05778.x

18. Gralnick JA, Bond DR. Electron Transfer Beyond the Outer Membrane: Putting Electrons to Rest. Published online 2023. doi:10.1146/annurev-micro-032221

19. Shi L, Rosso KM, Clarke TA, Richardson DJ, Zachara JM, Fredrickson JK. Molecular Underpinnings of Fe(III) Oxide Reduction by *Shewanella oneidensis* MR-1. *Front Microbiol*. 2012;3(FEB):50. doi:10.3389/fmicb.2012.00050

20. Fredrickson JK, Romine MF, Beliaev AS, et al. Towards environmental systems biology of Shewanella. *Nat Rev Microbiol*. 2008;6(8):592-603. doi:10.1038/NRMICRO1947

21. Kouzuma A. Molecular mechanisms regulating the catabolic and electrochemical activities of *Shewanella oneidensis* MR-1. *Biosci Biotechnol Biochem*. 2021;85(7):1572-1581. doi:10.1093/bbb/zbab088

22. G McMillan DG, Marritt SJ, Butt JN, C Jeuken LJ. Menaquinone-7 Is Specific Cofactor in Tetraheme Quinol Dehydrogenase CymA. Published online 2012. doi:10.1074/jbc.M112.348813

23. Sun W, Lin Z, Yu Q, Cheng S, Gao H. Promoting Extracellular Electron Transfer of *Shewanella oneidensis* MR-1 by Optimizing the Periplasmic Cytochrome c Network. *Front Microbiol*. 2021;12. doi:10.3389/fmicb.2021.727709

24. Fonseca BM, Paquete CM, Neto SE, Pacheco I, Soares CM, Louro RO. Mind the gap: Cytochrome interactions reveal electron pathways across the periplasm of *Shewanella oneidensis* MR-1. *Biochemical Journal*. 2013;449(1):101-108. doi:10.1042/BJ20121467

25. Babanova S, Cornejo J, Nealson K, et al. Outer membrane cytochromes/flavin interactions in Shewanella spp.—A molecular perspective . *Biointerphases*. 2017;12(2):021004. doi:10.1116/1.4984007

26. Rowe AR, Rajeev P, Jain A, et al. Tracking electron uptake from a cathode into Shewanella cells: Implications for energy acquisition from solid-substrate electron donors. *mBio*. 2018;9(1). doi:10.1128/mBio.02203-17

27. Tefft NM, Teravest MA. Reversing an Extracellular Electron Transfer Pathway for Electrode-Driven Acetoin Reduction. *ACS Synth Biol*. 2019;8(7):1590-1600. doi:10.1021/acssynbio.8b00498

28. Ford KC, Teravest MA. The Electron Transport Chain of *Shewanella oneidensis* MR-1 can Operate Bidirectionally to Enable Microbial Electrosynthesis. *Appl Environ Microbiol*. Published online December 20, 2023. doi:10.1101/2023.08.11.553014

29. Miller SD, Ford KC, TerAvest MA. Outward and inward electron transfer occur through distinct mechanisms for anaerobic S. oneidensis. *Unsubmitted Intended journal: Bioelectrochemistry*. Published online 2025.

30. Von Canstein H, Ogawa J, Shimizu S, Lloyd JR. Secretion of flavins by Shewanella species and their role in extracellular electron transfer. *Appl Environ Microbiol*. 2008;74(3):615-623. doi:10.1128/AEM.01387-07

31. Paquete CM, Fonseca BM, Cruz DR, et al. Exploring the molecular mechanisms of electron shuttling across the microbe/metal space. *Front Microbiol*. 2014;5(JUN). doi:10.3389/fmicb.2014.00318

32. Okamoto A, Hashimoto K, Nealson KH, Nakamura R. Rate enhancement of bacterial extracellular electron transport involves bound flavin semiquinones. *Proc Natl Acad Sci U S A*. 2013;110(19):7856-7861. doi:10.1073/pnas.1220823110

33. Hong G, Pachter R. Bound Flavin-Cytochrome Model of Extracellular Electron Transfer in *Shewanella oneidensis*: Analysis by Free Energy Molecular Dynamics Simulations. *Journal of Physical Chemistry B*. 2016;120(25):5617-5624. doi:10.1021/acs.jpcb.6b03851

34. Norman MP, Edwards MJ, White GF, et al. A Cysteine Pair Controls Flavin Reduction by Extracellular Cytochromes during Anoxic/Oxic Environmental Transitions. Brennan RG, ed. *mBio*. Published online January 16, 2023. doi:10.1128/mbio.02589-22

35. Edwards MJ, White GF, Norman M, et al. Redox Linked Flavin Sites in Extracellular Decaheme Proteins Involved in Microbe-Mineral Electron Transfer. *Sci Rep*. 2015;5(December 2014):1-11. doi:10.1038/srep11677

36. Duhl KL, Tefft NM, TerAvest MA. *Shewanella oneidensis* MR-1 utilizes both sodium- and proton-pumping NADH dehydrogenases during aerobic growth. *Appl Environ Microbiol*. 2018;84(12). doi:10.1128/AEM.00415-18

37. Tefft NM, Ford K, TerAvest MA. NADH dehydrogenases drive inward electron transfer in *Shewanella oneidensis* MR-1. *Microb Biotechnol*. Published online 2022. doi:10.1111/1751-7915.14175

38. Pirbadian S, Chavez MS, El-Naggar MY. Spatiotemporal mapping of bacterial membrane potential responses to extracellular electron transfer. *Proc Natl Acad Sci U S A*. Published online August 3, 2020. doi:10.1073/pnas.2000802117

# Chapter 2. Energetic constraints of metal-reducing bacteria as biocatalysts for microbial electrosynthesis

Shaylynn D. Miller[1], Kathryne C. Ford[2,3], Megan C. Gruenberg Cross[1], Michaela A. TerAvest[1]*

[1]Department of Biochemistry and Molecular Biology, Michigan State University, East Lansing, MI, USA

[2]Department of Microbiology and Molecular Genetics, Michigan State University, East Lansing, MI, USA

[3]Department of Chemical and Biomolecular Engineering, North Carolina State University, Raleigh, NC, USA

## 2. 1. Author contributions

All authors contributed to preliminary discussions conceptualizing the thermodynamic model. SM and KF performed preliminary calculations for the model. MGC did extensive literature review of topical papers. SM further developed the preliminary thermodynamic calculations into the multicompartment free energy model. SM and MT worked together to interpret the results of the thermodynamic model. SM and MT conceptualized the microscopy compatible bioelectrochemical system experiments. SM performed all microscopy experiments, troubleshooting and processed the resulting data. SM and MT interpreted the microscopy experiment results. SM wrote the initial drafts of the manuscript. All authors contributed to editing and revising the manuscript and have approved the submitted manuscript.

## 2. 2. Abstract

As outlined by the 2018 Intergovernmental Panel on Climate Change, we need to approach global net zero $CO_2$ emissions by approximately 2050 to prevent warming

beyond 1.5°C and the associated environmental tipping points. Future microbial electrosynthesis (MES) systems could decrease net $CO_2$ emissions by capturing it from industrial sources. MES is a process where electroactive microorganisms convert the carbon from $CO_2$ and reduction power from a cathode into reduced organic compounds. However, no MES system has attained an efficiency compatible with a financially feasible scale-up. To improve MES efficiency, we need to consider the energetic constraints of extracellular electron uptake (EEU) from an electrode to cytoplasmic electron carriers like $NAD^+$. In many microbes, EEU to the cytoplasm must transit through the respiratory quinone pool (Q-pool). However, electron transfer from the Q-pool to cytoplasmic $NAD^+$ is thermodynamically unfavorable. Here, we model the thermodynamic barrier for Q-pool-dependent EEU using the well-characterized bidirectional electron transfer pathway of *Shewanella oneidensis*, which has NADH dehydrogenases that are energetically coupled to the proton-motive force (PMF), the sodium-motive force (SMF), or are uncoupled. We also tested our hypothesis that Q-pool-dependent EEU to $NAD^+$ is ion-motive force (IMF)-limited in *S. oneidensis* expressing butanediol dehydrogenase (Bdh), a heterologous NADH-dependent enzyme. We assessed membrane potential changes in *S. oneidensis* expressing Bdh on a cathode at the single-cell level pre to post injection with acetoin, the Bdh substrate.

We modeled the Gibbs free energy change for electron transfer from respiratory quinones to NADH under conditions reflecting changes in membrane potential, pH, reactant to product ratio, and energetically coupled IMF. Of the 40 conditions modeled for each method of energetic coupling (PMF, SMF, and uncoupled), none were thermodynamically favorable without PMF or SMF. We also found that the *S. oneidensis* membrane potential

decreased upon initiation of EEU to $NAD^+$ on a cathode.

Our results suggest that Q-pool-dependent EEU is both IMF-dependent and is IMF-limited in a proof-of-concept system. Because microbes that rely on Q-pool-dependent EEU are among the most genetically tractable and metabolically flexible options for MES systems, it is important that we account for this thermodynamic bottleneck in future MES platform designs.

**2. 3. Introduction**

The Intergovernmental Panel on Climate Change's *Special Report: Global Warming of 1.5°C* estimates that global temperatures will reach 1.5°C above their pre-industrial level between the years 2030 and 2052 with present warming rates.[1] To avoid reaching 1.5°C warming and future environmental tipping points, we need to decrease net greenhouse gas emissions, particularly $CO_2$.[1] One option for decreasing net $CO_2$ emission involves harnessing biological carbon-fixing reactions to convert inorganic carbon (e.g., $CO_2$) into organic carbon molecules. Some microorganisms can perform electrode-driven carbon fixation in a process called microbial electrosynthesis (MES). During MES, carbon from $CO_2$ is covalently bonded into organic carbon molecules with reducing power from an extracellular electrode.[2–5] On an industrial scale, MES systems could decrease net greenhouse gas emissions by recycling $CO_2$ waste into organic carbon products at major emission sources.[6,7]

Organisms suitable for industrial-scale MES span many genera; however, a pervasive issue, even at small scales, is low current density (electrons/time/electrode area), which remains far below what will be required for industrial scale-up.[2,7,8] Certain autotrophic species, such as the chemoautotrophs *Acetobacterium woodii* and *Sporomusa ovata*, and the photoautotroph *Rhodopseudomonas palustris*, can perform MES, where electron flow

from a cathode provides the reducing power required for carbon fixing reactions in a bioelectrochemical system (BES).[9–13] To date, the highest current density magnitude reported for a pure culture MES system was -17.5 mA·cm$^{-2}$, using *A. woodii*.[14] However, MES current density magnitudes produced by wildtype autotrophic species remain incompatible with industrial scale-up.[15] MES systems can involve either mixed (multiple species) or pure cultures (a single species), both of which offer benefits and drawbacks. While mixed cultures can offer greater current density magnitudes, here we will focus on pure cultures to better pinpoint EEU bottlenecks.[16]

MES requires electron flow from a negatively-poised electrode (cathode) to bacteria. However, the natural electron flow direction for most species, from bacteria to positively-poised electrode (anode), has been more extensively studied. Bacteria able to reduce an anode, such as metal-reducing bacteria, have the metabolic flexibility and sufficiently robust electron transport pathways to respire via an extracellular terminal electron acceptor.[17] The metal-reducing bacterium *Geobacter sulfurreducens* is an apt example of the magnitude of the anodic current density that can be achieved in a BES with a thick, electrically connected biofilm (~ 0.9 mA·cm$^{-2}$).[18] However, to reach economic viability given present material and electricity costs Jourdin et al. (2020) estimated, in their techno-economic assessment of $CO_2$-fed MES, that MES systems will require a current density magnitude of -50 to -100 mA·cm$^{-2}$.[7,8,15] Recent work with *Shewanella oneidensis*, another metal-reducing bacterium, suggests that substantial improvements to current density may be possible without a thick electroactive biofilm; Zhang et al. (2024) showed that in a microbial flow fuel cell with artificial redox mediators, *S. oneidensis* could produce current densities exceeding 40 mA·cm$^{-2}$.[19] While still an emerging approach, it is likely that a

combination of improvements to BESs, either through structural or biological engineering could make MES systems financially feasible methods of decreasing net carbon emissions. However, even if microbial current densities reliably reached tens of $mA \cdot cm^{-2}$, the issue of EEU for MES remains.[15]

Metal-reducing bacteria have yet to mirror their anodic current density magnitudes on a cathode. To resolve this discrepancy, we must first understand which steps limit EEU. *S. oneidensis* has the most thoroughly characterized electron transport pathway of all metal-reducers, the Mtr pathway.[20–25] Because *S. oneidensis*' Mtr pathway is well understood and bidirectional, it is an excellent system to study and improve EEU in metal-reducing bacteria. During EEU, an organism directs electron flow through pathways tied to its energy conservation strategy.[26] For example, ion-motive force (IMF) drives ion-gradient phosphorylation, allowing organisms to conserve energy by coupling exergonic redox reactions to endergonic ion-translocations.[10,27–33] These exergonic redox reactions from catabolism to final electron acceptor(s) also define the routes available for EEU.

EEU occurs either through a series of conductive proteins in the cell membrane or via small molecules that can diffuse across lipid membranes, such as $H_2$ (Figure 2-1A).[2,6,10,11,13,20,21,26,34,35] $H_2$-mediated EEU in acetogens and methanogens relies on $H_2$ diffusion to soluble cytoplasmic hydrogenases, allowing electrons to bypass the quinone pool by diffusing into the cell as molecular hydrogen (Figure 2-1B).[10,11,36,37] However, in non-diffusive EEU, electrons must cross lipid membranes using membrane-integrated proteins and quinones, lipid-soluble redox-active molecules.[38,39] Microbial respiratory chains can flexibly combine different quinone reductases and quinol oxidases, but each combination shares the intermediate component, the quinone pool (Q-pool).[13,38–43] While

either EEU mechanism, Q-pool dependent or independent, could enable MES systems to reach economically viable current densities, their advantages and energetic constraints are distinct. We will focus on Q-pool-dependent EEU, as this mechanism encompasses a wide range of genetically tractable microorganisms (Figure 2-1).

As discussed above, an organism's electron transport chain is closely tied to its means of energy conservation. While some steps of the respiratory electron transport chain are freely reversible ($\Delta G \sim 0$), the redox reactions that are coupled to IMF generation must be thermodynamically favorable ($\Delta G << 0$), and far from equilibrium. Note that 'freely reversible' commonly refers to Gibbs free energy changes within ± 6 to 10 kJ · $mol^{-1}$.[44,45] The thermodynamically favorable direction for electrons to flow is from a lower to higher reduction potential.[27,46,47] Ion-translocating NADH dehydrogenases are among the enzymes that couple ion translocation with electron transfer from low potential electron donors like NADH to the Q-pool. Q-pool-dependent EEU uses this step in reverse, resulting in a thermodynamically unfavorable ($\Delta G >> 0$) electron transfer.[48]

In this work, we address an example of the thermodynamically unfavorable electron transfer in *S. oneidensis* expressing butanediol dehydrogenase (Bdh), as previously described by members of our group.[48] Bdh is an NADH-dependent enzyme, non-native to *S. oneidensis*, that converts acetoin to 2,3-butanediol.[48] Figure 2-2B shows the free energy landscape for EEU in *S. oneidensis* expressing Bdh (referred to as MR-1+Bdh in the remainder of this chapter). For Steps 1-6 of EEU (Figure 2-2), the free energy landscape favors EEU (net negative $\Delta G$). The $\Delta G$ available for Step 7 depends on the energy-coupling ability of the catalyzing NADH dehydrogenase. *S. oneidensis* has four NADH dehydrogenases, Nuo ($H^+$-pumping), Nqr1 and Nqr2 ($Na^+$-pumping), and Ndh

(uncoupled).[49,50] When Step 7 occurs without energetic coupling, EEU is thermodynamically unfavorable in Step 7 (Figure 2-2), however, when coupled with proton motive force (PMF) or sodium motive force (SMF), Step 7 shifts in the forward direction (as written) leaving the entire pathway thermodynamically favoring EEU (net negative ΔG). To overcome the potential bottleneck in Step 7 that may limit Q-pool-dependent MES, it is crucial that we identify the conditions under which this reaction becomes thermodynamically favorable for EEU. Q-pools contain multiple quinone species; however, we will assume menaquinone-7 (MQ)/menaquinol-7 ($MQH_2$) because this couple is responsible for 85% of EEU in *S. oneidensis*.[20,22] Menaquinone also has a lower redox potential than the other predominant quinone species, ubiquinone, and is therefore a better electron donor for NADH generation.[51]

Given the free energy landscape for EEU in *S. oneidensis* MR-1+Bdh (Figure 2-2), we expect NADH dehydrogenase activity to be thermodynamically favorable for EEU only when energetically coupled to IMF. To determine if IMF is thermodynamically required for EEU in MR-1+Bdh, we calculated the multicompartment free energy for Step 7 under a range of biologically relevant conditions (i.e., variations in pH, reactant to product ratio, and membrane potential voltage). These ΔG calculations assume that Step 7 was catalyzed by either Nuo (translocation of 4 $H^+$ per NADH), Nqr (translocation of 2 Na+ per NADH), or Ndh (uncoupled, 0 ions per NADH). In this way, we determined whether Step 7 can be driven forward (negative ΔG) by manipulating contextual variables (e.g., by increasing electrode potential to over-reduce the quinone pool) or if a source of energetically coupled IMF is thermodynamically required.

We expect that EEU in *S. oneidensis* is not only IMF-dependent but also IMF-limited

under biologically relevant conditions. By comparing the current densities supported by different sections of the Mtr pathway, we can hypothesize the location of the rate-limiting step for EEU. Our previous work, Tefft and TerAvest (2019) and Tefft et al. (2022), used a comparable BES set up; we observed current density for EEU to fumarate (|-8.7 $\mu A \cdot cm^{-2}$|) that was approximately 14 times greater in magnitude than to cytoplasmic $NAD^+$ (|-0.62 $\mu A \cdot cm^{-2}$|), where IMF was supplied by proteorhodopsin (PR), a light-dependent proton pump.[48,52] Prior to exiting the Q-pool, both electron transfer pathways include the freely reversible free energy landscape depicted in Figure 2-2, Steps 1-6. Note that the term 'free energy landscape' refers to the sequential free energy changes along each step of the pathway, illustrating the relative thermodynamic barriers of the process.[53] The difference in thermodynamic favorability lies in the path through which electrons leave the Q-pool. Electron transfer from menaquinol to fumarate is catalyzed by fumarate reductase, a thermodynamically favorable reaction ($\Delta G'° = -11.9 \pm 7.0$ $kJ \cdot mol^{-1}$) that does not depend on energetic coupling to IMF.[54] To determine if Q-pool-dependent EEU is IMF limited, we used a fluorescence microscopy technique described by Pirbadian et al. (2020). [55] Pirbadian et al. (2020) showed that thioflavin T (ThT), a fluorescent cationic dye, can be used as a proxy for membrane potential in *S. oneidensis* imaged on a transparent electrode. As Figure 2-2 illustrates, when acetoin (the Bdh substrate) is present, MR-1+Bdh has an NADH-dependent electron acceptor in the cytoplasm. From our previous work, Ford and TerAvest (2023), we know that even an ostensibly anaerobic BES with active nitrogen bubbling has ~1% dissolved oxygen; this oxygen concentration is sufficient for the proton-pumping terminal oxidase to supply the PMF needed to drive EEU to cytoplasmic $NAD^+$ in *S. oneidensis* (Figure 2-2A).[56] We imaged MR-1+Bdh on a

cathode while monitoring membrane potential change (i.e., the voltage across the inner membrane), pre- to post-injection with either acetoin or the solvent control, water.

In this work, we used computational and experimental methods to further define the thermodynamic bottleneck that limits Q-pool-dependent EEU, and by extension, Q-pool-dependent MES systems.

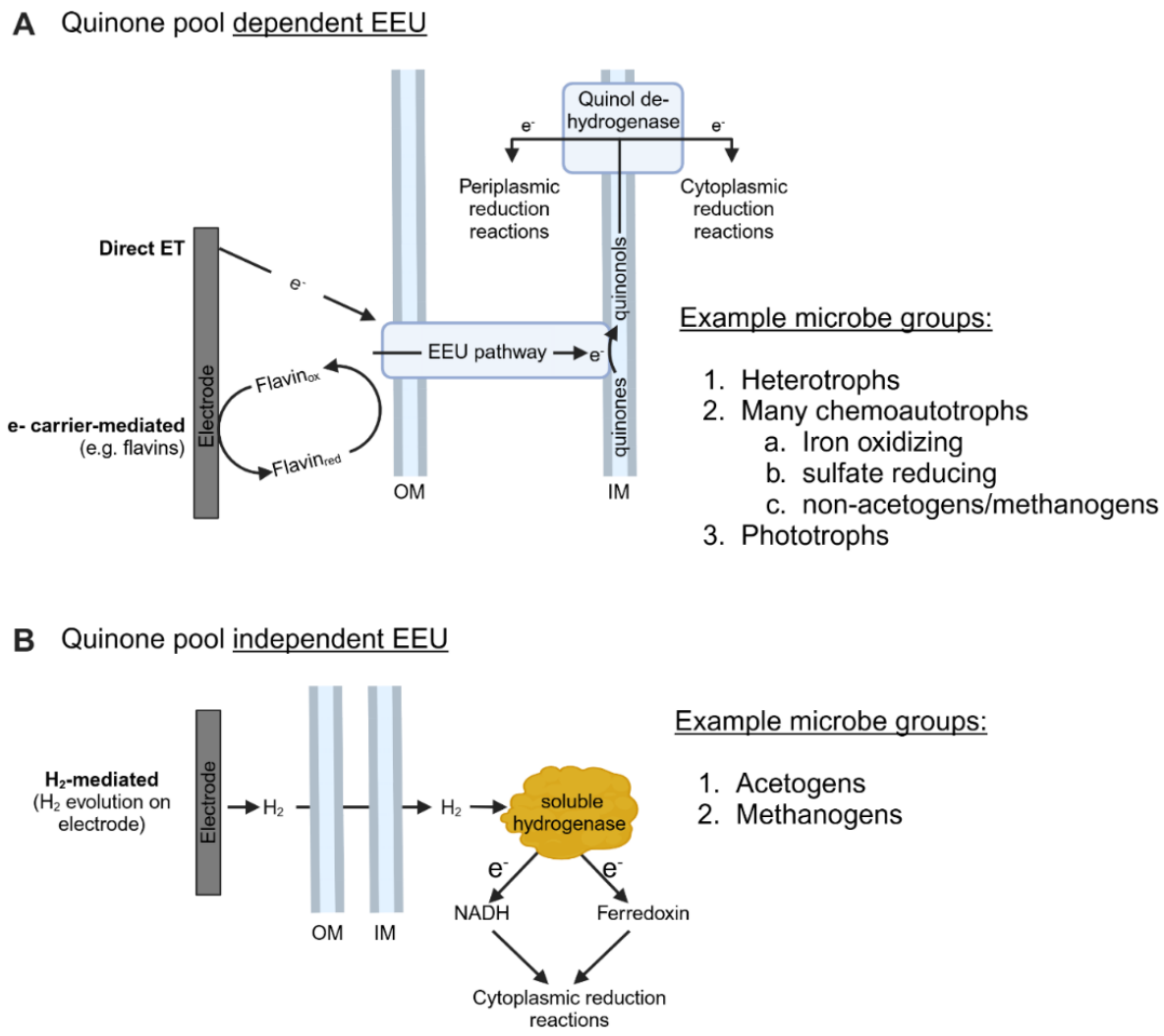


*Figure 2-1. (A) Extracellular electron uptake (EEU) through the respiratory quinone pool (Q-pool). (B) EEU that bypasses the Q-pool via H2 diffusion to soluble cytoplasmic hydrogenases. Note that these examples assume either a wildtype or engineered organism capable of EEU to the cytoplasm. Many species in these categories cannot perform EEU in their wildtype form. Electrons (e-), outer membrane (OM) and inner membrane (IM).*

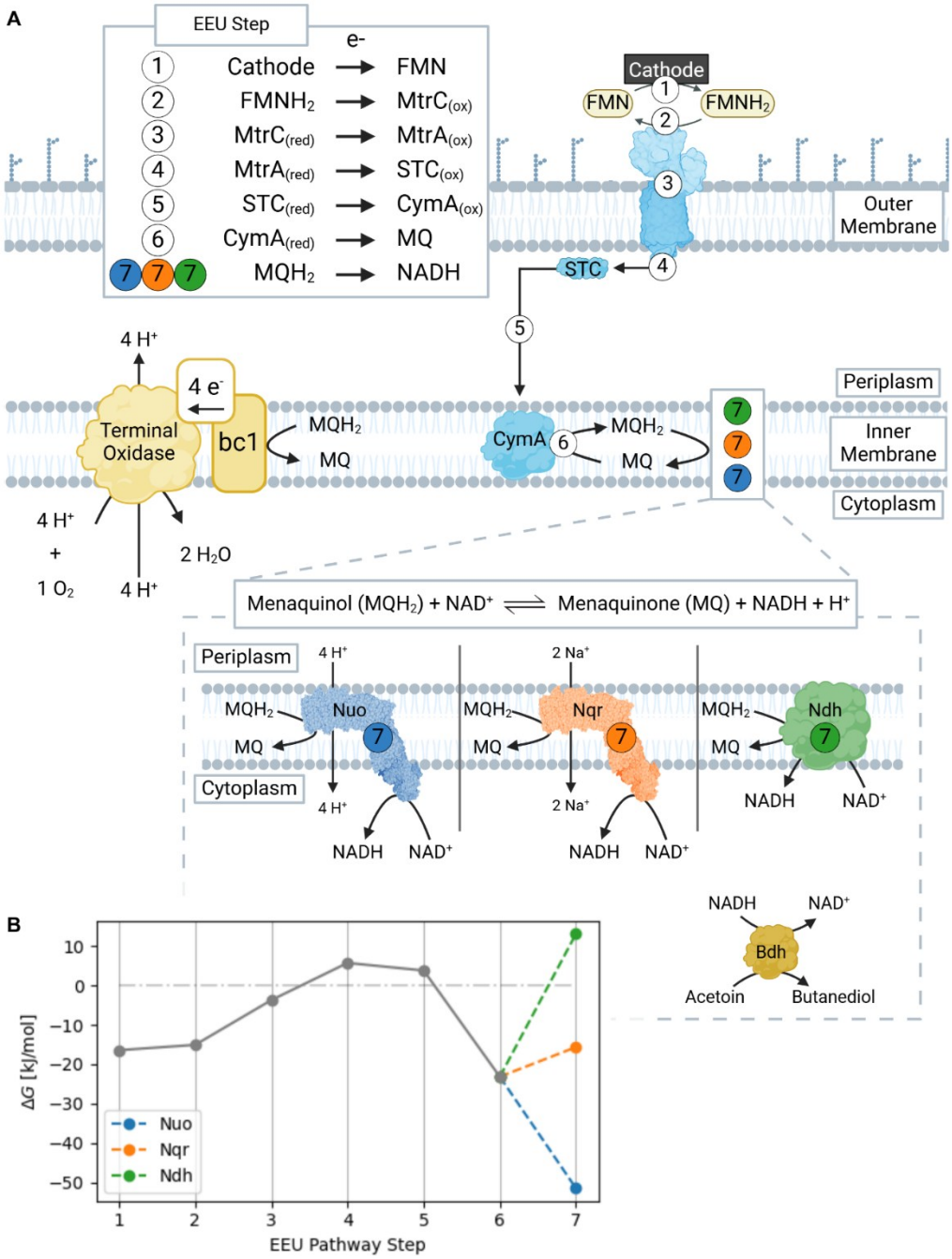


*Figure 2-2. (A) EEU in* S. oneidensis *from an electrode to NAD⁺, where the PMF is supplied by a proton-pumping terminal oxidase. The thermodynamically distinct paths of electron transfer to three differently coupled NADH dehydrogenases (Nuo, Nqr, and Ndh). (B) The free energy (ΔG) associated with each step of the pathway in panel A. For Step 7, a negative free energy means that EEU across the quinone pool is thermodynamically favorable and a positive free energy means that EEU across the quinone pool to cytoplasmic NAD⁺ is thermodynamically unfavorable. MQ, menaquinone-7; $MQH_2$, menaquinol-7; FMN, flavin mononucleotide; $FMNH_2$, reduced flavin mononucleotide; STC, small tetraheme cytochrome; MtrABC, proteins of the Mtr pathway; Bdh, butanediol dehydrogenase; bc1, bc1 complex; e⁻, electron.*[57]

## 2. 4. Methods

### 2. 4. 1 Reactions and Equations.

#### 2.4.1.1 Step 7: The reaction for Figure 2-2, Step 7.

$$Menaquinol\ (MQH_2) + NAD^+ \overset{NADH\ dehydrogenase}{\Longleftrightarrow} Menaquinone\ (MQ) + NADH + H^+$$

#### 2.4.1.2 Equation 1: Standard biochemical free energy with multicompartment adjustment.

$$\Delta G'^{\circ}_{(multicompartment)} = \Delta G'^{\circ} + \boldsymbol{N_{ion} RT\ ln}\left(\frac{[\boldsymbol{ion}]_{final}}{[\boldsymbol{ion}]_{initial}}\right) + \boldsymbol{Q_{charge} F \Delta \phi}$$

#### 2.4.1.3 Equation 2: Overall free energy change for Step 7 taking place in the periplasm and cytoplasm.

$$\Delta G = \Delta G'^{\circ}_{(multicompartment)} + RT\ln\left(\frac{[MQ][NADH]}{[MQH_2][NAD^+]}\right)$$

### 2. 4. 2 Multicompartment Gibbs free energy calculations.

We calculated the multicompartment free energy for Step 7, assuming either Nuo (4 $H^+$ per NADH), Nqr1 (2 $Na^+$ per NADH), or Ndh (uncoupled, 0 ions per NADH) catalyzed the reaction. Standard biochemical free energy (ΔG'°) calculations in a single cellular compartment use the assumption that reactants and products are in a uniform aqueous solution. However, when a reaction involves ion translocation across a membrane, the aqueous solutions on either side of the membrane cannot be assumed internally consistent.[54] In this work, we calculated $\Delta G'^{\circ}_{(multicompartment)}$ using the eQuilibrator 3.0 Python-based Application Programming Interface (API).[54,58] eQuilibrator 3.0 API accounts for the differences in pH, charge, and ion concentrations between cellular compartments by adding compartment-specific adjustments to the standard biochemical free energy of a reaction ($\Delta_r G'^{\circ}$) to calculate the multicompartment standard free energy ($\Delta G'^{\circ}_{(multicompartment)}$) shown in Equation 1. These adjustments are critical for reactions that

involve ion transport from an initial compartment (e.g., periplasm) to a final compartment (e.g., cytoplasm). In Equation 1, the multicompartment adjustment includes terms for the ion concentration ([ion]) for both the initial and final compartments, the membrane voltage ($\Delta\phi$) and the stoichiometry of ions transported; $N_{ion}$ represents the number of ions transported, while $Q_{charge}$ is the total charge transported across the inner membrane. Additionally, F is Faraday's constant (-96.5 $kC \cdot mol^{-1}$), R is the gas constant (8.31447 x $10^{-3}$ $kJ \cdot K^{-1} \cdot mol^{-1}$), and T is temperature in Kelvin (289.15 K).[54,59,60] Once the $\Delta G'^{\circ}_{(multicompartment)}$ is calculated with Equation 1, it can be plugged into Equation 2 to calculate the overall free energy change ΔG for Step 7. [54,60]

We also calculated the Gibbs free energy changes in Figure 2-2B using Equations 1 and 2, to demonstrate a snapshot of the free energy landscape for EEU through the Mtr pathway to *S. oneidensis'* three types of NADH dehydrogenases (PMF-linked, SMF-linked, uncoupled). Cytoplasmic pH was set to 7.6, periplasmic pH to 7.3, the quinone pool at 80% reduced, an $NAD^+$ to NADH ratio favoring EEU (15:1), and a membrane potential of -0.15V. Note that Figure 2-2B is an explanatory aid to complement our hypothesis, not part of our results for this work. For this reason, the input values need only be within a physiologically relevant range for the sake of the example not varried incrementally as done for the data in Figure 2-4.

**2. 4. 3 Biologically relevant parameter definitions.**

In the context of this work, 'biologically relevant' indicates that a value, or range of values, was chosen because it is physiologically relevant to bacteria that are neutrophilic and mesophilic. The percentage of reduced quinones in the Q-pool was assumed to be on the edge of the experimentally determined minimum and maximum, 0.1% reduced and 90% reduced, respectively.[61,62] The Mtr pathway in *S. oneidensis* primarily interacts with the

quinone pair menaquinone/menaquinol via CymA in the inner membrane.[63] The reaction quotient for Step 7 is $\frac{[MQ][NADH]}{[MQH_2][NAD^+]}$, meaning that the ratios of [$NAD^+$] to [NADH] and [$MQH_2$] to [MQ] contribute symmetrically to the overall Gibbs free energy change of Step 7 (Equation 2). Because both ratios impact the thermodynamic favorability of Step 7 in a mathematically equivalent manner, through the natural logarithm term $ln\left(\frac{[MQ][NADH]}{[MQH_2][NAD^+]}\right)$, we held the [$NAD^+$] to [NADH] ratio constant. The ratio of [$NAD^+$] to [NADH] used in all free energy calculations was 15:1, representing an NAD(H) pool that is 93.7% oxidized. Additionally, because ratios remain difficult to measure accurately, we chose a 15:1 ratio because it is physiologically plausible and favors EEU.[64,65] By assuming a consistent and highly oxidized NAD(H) pool, paired with either a highly oxidized or highly reduced Q-pool, we decreased the complexity of the modeled scenarios, while ensuring that we included the situations most likely to favor EEU for comparing the relative abilities of energetic coupling via Nuo, Nqr, and Ndh.

**2. 4. 4 Bioelectrochemical system (BES) preparation.**

Pirbadian et al. (2020) demonstrated that the fluorescent cationic dye Thioflavin T (ThT) can be used to visualize membrane potential changes in *S. oneidensis* in response to extracellular electron transfer at an anode.[55] In this work, we used an experimental set-up similar to Pirbadian et al. (2020) to visualize membrane potential changes during EEU for *S. oneidensis* on a cathode following a period of anodic electrode potential (+0.2 V vs a saturated Ag/AgCl reference electrode).[55] Each single-chamber BES consisted of a borosilicate glass culture tube that was cut to approximately 7 cm in length from the flanged end. The working electrode was an indium-tin-oxide (ITO) coated glass cover slip measuring 22 x 40 mm with a thickness of 0.16 to 0.19 mm and a sheet resistance of 70-

100 Ω/□ (SPI Supplies, Thickness #1.5, Cat. # 06498-AB). A titanium wire was connected to the ITO slip with CCC carbon adhesive (Electron Microscopy Sciences, Cat. # 12664). The cut end of the culture tube was adhered to the center of the conductive side of the ITO slip with a two-part epoxy following manufacturer instructions (Polytec PT, Cat. # EP 653-T). To provide electrical insulation and structural support, the epoxy was also spread over the remaining exposed portions of the ITO surface and the attachment point of the titanium wire. The counter electrode was a coiled titanium wire, and the reference electrode was Ag/AgCl in saturated KCl in a glass tube with a magnesia stick frit (Sigma Aldrich, Cat. # 31408-1EA). The counter and reference electrodes were held in place and the BES sealed with a butyl rubber septum stopper. Figure 2-3A shows a diagram of the microscopy experimental setup.

**2. 4. 5 Bacterial culture preparation and BES inoculation.**

We used the strain *S. oneidensis* MR-1 carrying plasmid pBBR1-Bdh (i.e., strain MR-1+Bdh), created by Tefft and TerAvest (2019), for all microscopy experiments.31 The enzyme butanediol dehydrogenase (Bdh) was constitutively expressed from a plasmid conferring kanamycin resistance, pBBR1. For each biological replicate, we inoculated 5 ml of Miller's Lysogeny Broth (LB) supplemented with kanamycin (kan, 50 $\mu g \cdot ml^{-1}$) with a single colony of MR-1+Bdh. Each culture grew to an $OD_{600}$ of 3.47 to 4.66. After growth in LB+kan, cultures were centrifuged (8,500 x g for 3 minutes) and resuspended in 50 ml of M5 minimal medium (1.29 mM $K_2HPO_4$, 1.65 mM $KH_2PO_4$, 7.87 mM NaCl, 1.70 mM $NH_4SO_4$, 475 µM $MgSO_4 \cdot 7H_2O$, 100 mM HEPES, 50 $\mu g \cdot ml^{-1}$ kanamycin, 1X Wolfe's mineral solution (excluding both casamino acids and $AlK(SO_4)_2 \cdot 12\ H_2O$), and 1X Wolfe's vitamin solution (excluding riboflavin) to wash cells.31,43,53 Following the wash in minimal medium, the culture was again centrifuged (8,500 x g for 3 minutes), then

standardized to an $OD_{600}$ of 0.2 in M5 minimal medium.

**2. 4. 6 Electrochemical experiments with fluorescence monitoring.**

The BES was inoculated with 7 ml of the standardized culture of MR-1+Bdh. The three-electrode, single-chamber BES was connected to a potentiostat (VMP, BioLogic USA) with the working electrode potential set to +0.2 V vs a saturated Ag/AgCl reference electrode for 15 to 17 hours; during this time, 99.9% $N_2$ gas (Airgas) was bubbled into the BES (Figure S 2-1). All medium was then removed from the BES, barring 0.5 ml that remained to avoid drying cells on the ITO electrode.[55] The BES was filled to a total of 8.5 ml with M5 minimal medium +10 μM ThT and remained electrically connected to the potentiostat for 30 minutes prior to beginning fluorescence microscopy, with the working electrode potential set to +0.2 V vs the saturated Ag/AgCl reference electrode.

During microscopy, an anaerobic serum bottle was connected to the BES via neoprene tubing to prevent changes in pressure or oxygenation during injections. To prepare the anaerobic serum bottle, the container was autoclave sterilized, filled with 50 ml of M5 minimal medium, 10 μM ThT, and 1 mM acetoin, then sealed with a butyl rubber stopper and connected to two lines of sterile neoprene tubing. Nitrogen was bubbled into the bottle and tubing for a minimum of 16 hours. Due to the light sensitivity of ThT, the serum bottle was wrapped in aluminum foil during this time to prevent photodegradation. The three biological replicates that received a water injection rather than acetoin used anaerobic bottles that contained M5 minimal medium +10 μM ThT.

To determine if EEU to the cytoplasm is IMF-limited in *S. oneidensis* +Bdh, we imaged live cells on a transparent ITO electrode to measure membrane potential before and after injecting 0.17 ml of 50 mM acetoin (1 mM working concentration). Fluorescence images were acquired with an inverted Zeiss Axio Observer D1 microscope with a Plan-

Apochromat 63x/1.40 Oil DIC objective. Each BES was connected to an anerobic bottle, prepared as described above. All fluorescence images for ThT were collected with the Zeiss Axio Observer D1 GFP filter cube. Once *S. oneidensi*s cells were visualized on the ITO electrode, a portable potentiostat (Rodeostat, IO Rodeo) was connected to maintain the following working electrode potentials (vs saturated Ag/AgCl reference electrode) and timeframes: +0.2 V (40 minutes), -0.5V (120 minutes). We collected electric current once per second with a single-channel three-electrode Rodeostat. We plotted all current vs time curves with a 60-second simple moving average. The first injection of either acetoin (1 mM) or water control occurred at 70 minutes out of the total 160-minute time series. The second injection of either carbonyl cyanide m-chlorophenyl hydrazone (CCCP, 125 μM) or ethanol control occurred at 130 minutes out of the total 160-minute timeseries. CCCP is a protonophore, which collapses the membrane voltage and pH gradient across the membrane.[67] Each image time series had an interval of 2 minutes. All injections were prepared in an anaerobic chamber and transported in a BD GasPak System container.

**2. 4. 7 Fluorescence Microscopy Image Analysis.**

Carl Zeiss image (CZI) files were processed with ImageJ version 1.53t. The background fluorescence was subtracted from each image using the default rolling ball radius setting (50.0 pixels) with smoothing disabled. ImageJ's analysis tool 'Analyze Particles' was used to gather ThT fluorescence data for individual cells from each background subtracted image. The mean fluorescence intensity was calculated for every bacterial cell. Individual bacterial cell fluorescence was used to calculate the mean fluorescence at each timepoint. The collective average of the three biological replicates could then be calculated. The corresponding standard error of the mean (sem) for both the experimental (acetoin) and control (water) groups is also shown. We report standard error of the mean

rather than standard deviation because each group mean reflects variation between biological replicates, not within a single replicate.

We note that the fluorescence data throughout this work were collected using a fluorescence microscope that required manual re-focusing adjustments approximately 30–45 seconds prior to each image. As this process introduced slight point-to-point variability in the measurements, unrelated to the true fluorescence dynamics, we limit our interpretation to longer trends rather than individual point-to-point variations. Despite this technical limitation, the broad trends over longer periods remained consistent and comparable across biological replicates.

**2. 4. 8 Statistical Analysis.**

We measured the intraexperiment response in ThT fluorescence (ΔThT) and electric current (ΔI) following injection with either acetoin or water. The pre-injection timeframe was 40 to 70 minutes, and the post-injection timeframe was 71 to 128 minutes. We evaluated statistical significance with a Welch's t-test. The null hypothesis assumption was that there would be no difference in either ΔThT or ΔI when comparing the experimental group (acetoin injection) to the control group (water injection). The cutoff for statistical significance was $p<0.05$. Both the experimental and control groups had three independent biological replicates of *S. oneidensis* +Bdh. All additional data processing was done in Python with numpy 1.23.4, scipy 1.9.3, pandas 1.2.5, and matplotlib 3.6.0.

**2. 4. 9 Data availability.**

Gibbs free energy changes were calculated using eQuilibrator 3.0 API in Python 3.9.7 with the following package dependencies: seaborn 0.11.2, scipy 1.8.1, pandas 1.3.4, numpy 1.22.4, matplotlib 3.4.3, cvxpy 1.2.1. The source code and raw data for the free energy calculations and the microscopy experiments are available on request.

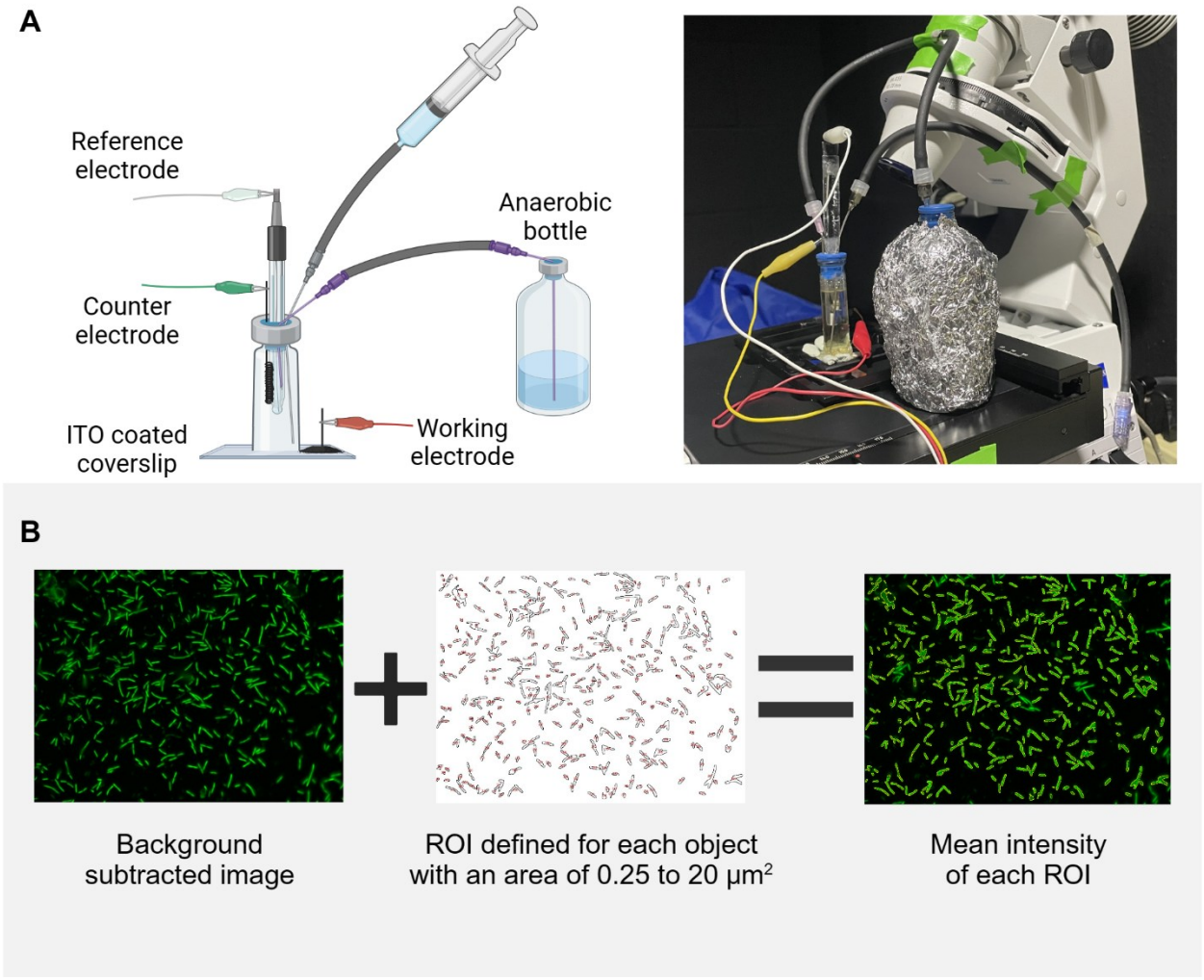


*Figure 2-3. Experimental setup and analysis workflow for our microscopy-compatible bioelectrochemical system (BES). (A) Diagram of our BES, the design of which was based on Pirbadian et al. (2020). To minimize $O_2$ changes in the BES during injection, the BES was connected to an anaerobic bottle containing a media reservoir and head space. On the right-hand side is a picture of our BES setup. The aluminum foil on the bottle was present to protect ThT in the media from photodegradation while $N_2$ bubbled into the media bottle overnight. (B) For each timepoint, the background fluorescence was subtracted in ImageJ. Regions of interest (ROI) were defined for individual cells, or small groups of cells, that fit into the defined area of 0.25 to 20 μm². For each timepoint of a biological replicate, the mean ThT intensity was the background-subtracted mean fluorescence intensity of the ROIs. Some cell drift out of the field of view (FOV) was uncontrollable, however, we strove to maintain the FOV for each biological replicate to keep the laser exposure time, and any resulting changes in membrane permiability to ThT, consistent for each timepoint.*

## 2. 5. Results

### 2. 5. 1 Q-pool-dependent EEU to cytoplasmic $NAD^+$ is IMF-dependent.

We calculated the ΔG for Step 7 in *S. oneidensis* when catalyzed by three energetically distinct NADH dehydrogenases. Nuo and Nqr are energetically coupled to IMF, translocating 4 $H^+$ and 2 $Na^+$ per NADH, respectively, while Ndh is not coupled to IMF. For each NADH dehydrogenase, we modeled the ΔG of Step 7 in response to biologically relevant changes in the reaction quotient ($\frac{[MQ][NADH]}{[MQH_2][NAD^+]}$), membrane potential ($\Delta\phi$), ion-transport stoichiometry, and pH difference across the inner membrane (Equations 1 and 2, Methods).

For the 40 conditions modeled for each type of energetic coupling in Figure 2-4, Step 7 was thermodynamically favorable (ΔG < 0) in 0/40 (0%) of scenarios when energetically uncoupled, 12/40 (30%) when SMF-coupled, and 31/40 (77.5%) when PMF-coupled. A high reactant-to-product ratio (90% reduced) of menaquinol ($MQH_2$) to menaquinone (MQ), increased the available free energy for Step 7 under all energetic coupling conditions compared to a low ratio of $MQH_2$:MQ (0.1% reduced); however, a shift in the reactant-to-product ratio alone was not sufficient to make Step 7 favorable in the absence of IMF (ΔG > 0). We only show reactant-to-product ratios for $MQH_2$ to MQ, because the NAD(H) pool is held constant in our models at 93.7% oxidized to favor EEU, as described in the Methods section.

For each value of periplasmic pH (i.e., 5, 6, 7, and 8) modeled, the cytoplasmic pH was held constant (pH=7.5). Change in the periplasmic pH only reversed the thermodynamically favored direction of Step 7 when energetically coupled to SMF or PMF. When Ndh was used, ΔG was not dependent on membrane potential. When Step

7 was catalyzed by Nqr or Nuo in our model, a greater membrane potential magnitude (-0.2 V) yielded the most thermodynamically favorable ΔG for a given column. The ion involved in energetic coupling determined whether an acidic or basic periplasmic pH was the most favorable for EEU (ΔG<0). When we modeled the ΔG for Step 7 catalyzed by Nuo (PMF-coupled) an acidic periplasmic pH was the most thermodynamically favorable for EEU (Figure 2-4C). However, when we modeled the ΔG assuming Nqr (SMF-coupled), a basic periplasmic pH was more thermodynamically favorable for EEU for a given row in Figure 2-4B. These results support the hypothesis that energetic coupling to IMF is required for Step 7 to proceed in the EEU direction.

**2. 5. 2 Q-pool-dependent EEU to cytoplasmic $NAD^+$ is IMF-limited.**

To determine whether EEU was IMF-limited, we used a small (<10 ml) single-chamber bioelectrochemical system (BES) designed for simultaneous fluorescence imaging and electrochemical measurements, as shown in Figure 2-3. Using this microscopy compatible-BES, we measured the membrane potential and electric current produced by MR-1+Bdh on a cathode. We observed that when acetoin was added, ThT fluorescence decreased significantly compared to the water control, indicating that electron transfer to acetoin was an IMF sink that significantly altered the membrane potential (Figure 2-5). When water was injected instead of acetoin, no change in ThT fluorescence or current occurred. There was no significant difference in cathodic current before and after acetoin injection, however, this is not unexpected given the low cell density in the experimental setup. The PMF uncoupler, CCCP, was injected 60 minutes after acetoin injection. Following CCCP injection, ThT fluorescence did not decrease further, suggesting that cells may have been completely depolarized after acetoin injection. We confirmed that CCCP injection in this system caused membrane depolarization by injecting CCCP into

systems with *S. oneidensis* MR-1+Bdh using lactate as an electron donor and oxygen as an electron acceptor in the electrochemical cell without an applied voltage (Figure S 2-2) Aerobic lactate metabolism provides NADH to the ion translocating NADH dehydrogenases and subsequent build-up of membrane potential.[68] Under these conditions, ThT fluorescence decreased by 50% upon CCCP injection (Figure S 2-2). When lactate was the electron donor and oxygen the electron acceptor, pre-CCCP ThT fluorescence (~7,000 procedure defined unit, p.d.u.) was ~3.5X higher than for *S. oneidensis* with the cathode as the electron donor and acetoin as the electron acceptor (~2,000p.d.u.).

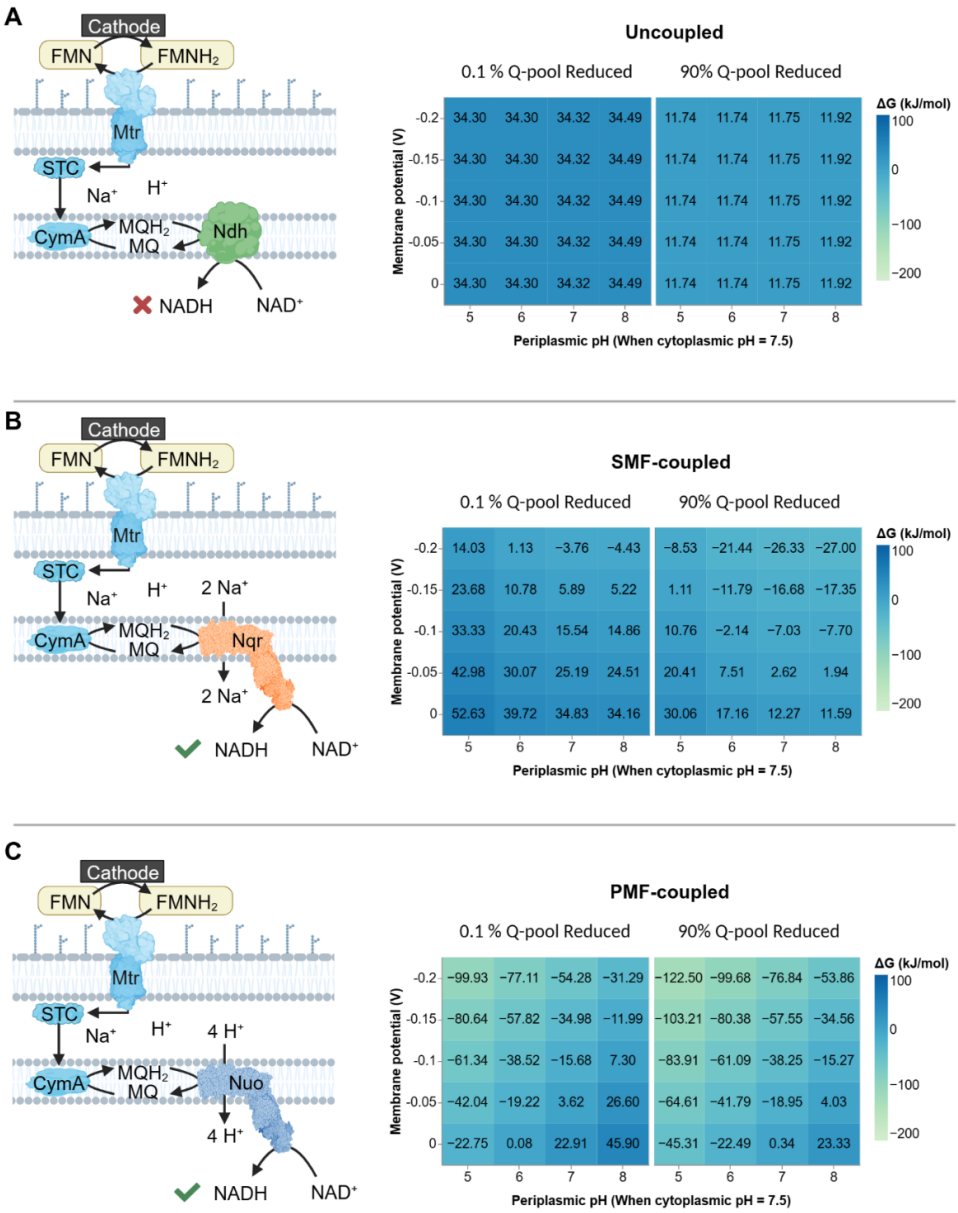


*Figure 2-4. Gibbs free energy predicted for Reaction 1 under various biologically relevant conditions (non-extremophile). In A-C) a diagram of the associated EEU pathway is on the left and the results of our thermodynamic model are on the right. Each heatmap shows the ΔG calculated for Reaction 1 where the Q-pool is either primarily oxidized or reduced, 0.1% reduced and 90% reduced respectively. For both an oxidized and reduced Q-pool, we modeled various combinations of membrane potential and periplasmic pH. As Reaction 1 occurs across a membrane, we calculated ΔG using Equations 1 and 2. Mtr represents the MtrA, MtrB, and MtrC proteins from the Mtr pathway. Small tetraheme cytochromes (STC) are electron carriers in the periplasmic space. FMN and $FMNH_2$ are the oxidized and reduced forms of flavin mononucleotide, respectively. Arrows indicate the direction of electron flow (excluding the ion-translocating arrows). The quinone pool (Q-pool) contains menaquinone (MQ) and menaquinol ($MQH_2$).*

## 2. 6. Discussion

To reduce net carbon emissions at industrial sources via MES systems, we must first address the current density bottlenecks that limit EEU. Here, we described the thermodynamic bottleneck that limits Q-pool-dependent EEU in *S. oneidensis*, a constraint applicable to several genera of MES candidate organisms. EEU through the Mtr pathway, a well-characterized and bidirectional ET route in *S. oneidensis*, is thermodynamically reversible prior to exiting the Q-pool in Step 7. We calculated the multicompartment free energy change available to Step 7 under biologically relevant conditions (non-extremophile). Thermodynamic calculations showed that Q-pool-dependent EEU requires energetic coupling to IMF for Step 7 to be thermodynamically favorable under all conditions modeled (Figure 2-4). We also hypothesized that Q-pool-dependent EEU is IMF-limited.

As discussed by Mancini et al. (2019), for a membrane potential indicator to display Nernstian behavior, extensive optimization must occur under all experimental contexts.[69] While this level of optimization was impractical for this study, we were able to assess membrane potential changes with ThT qualitatively by restricting fluorescence intensity comparison to individual biological replicates, then comparing the pre- to post-injection ΔThT for the acetoin and water-control groups. When acetoin is added, the periplasm loses positively charged ions either as protons or sodium ions via NADH dehydrogenase, which decreases the magnitude of the membrane potential voltage. As cations leave the periplasm, the corresponding drop in capacitive negative charge (-OH) on the cytoplasmic side of the inner membrane decreases the attraction for positively charged ThT, leading to a decrease in its abundance inside individual cells.[55,69]

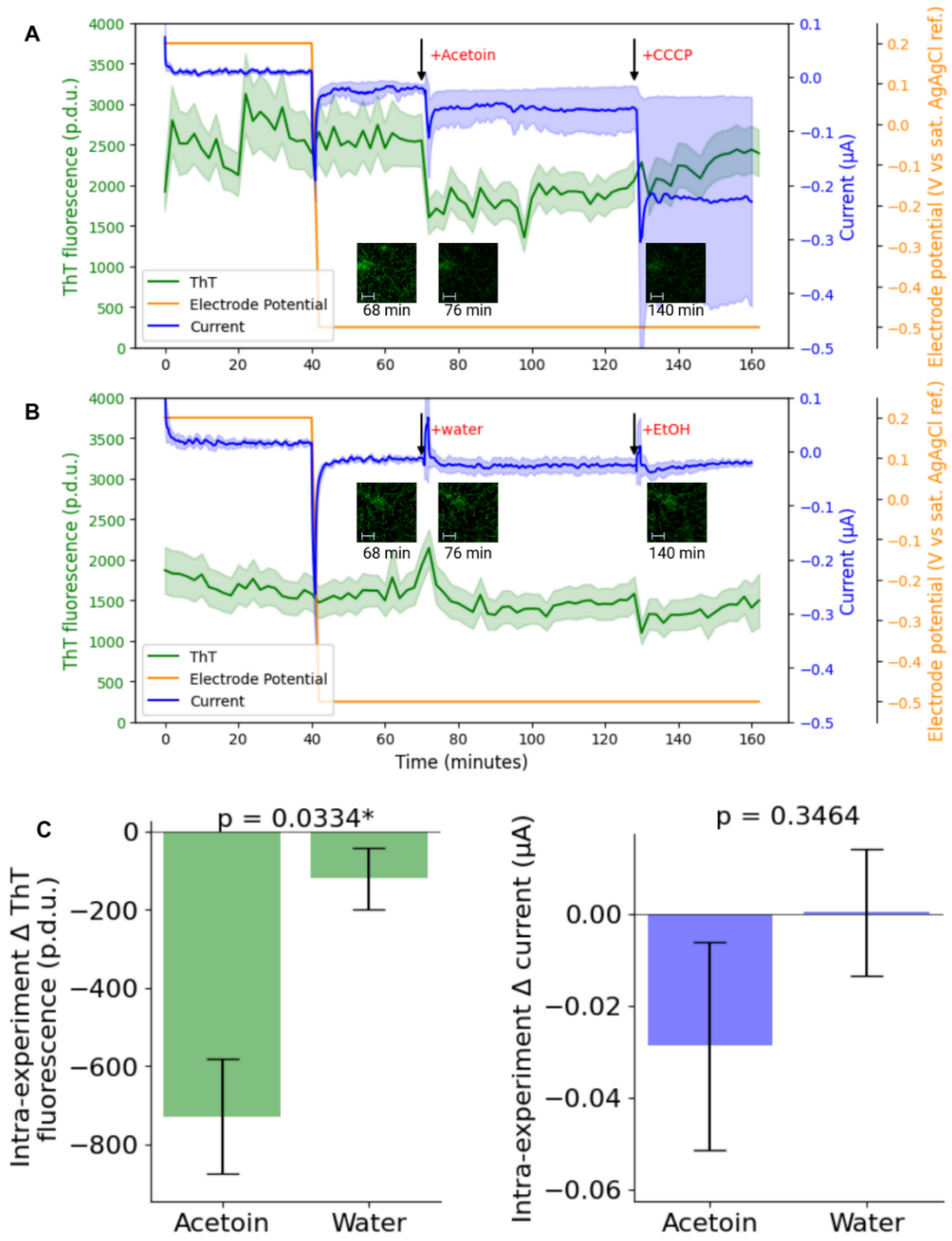


*Figure 2-5. ThT fluorescence and electrical current simultaneously measured in microscopy-compatible BESs. (A) and (B) show the applied electrode potential (orange), ThT fluorescence (green), and current (purple) plotted as fuctions of time. In (A) the two injections were acetoin and CCCP. (B) Shows the same experimental procedure performed with the solvent controls injected, water and ethanol (EtOH) respectively. (C) Shows the mean ± SEM (standard error of the mean) for the pre- to post-injection difference in ThT fluorescence (left, green) and electric current (purple, right). In (C) Intra-experiment refers to the pre- to post-injection change, for either acetoin or water within a single biological replicate; ΔThT or Δcurrent are the mean ± SEM of three biological replicates for either the acetoin injection (Acetoin, n=3) or the solvent control (Water, n=3). The * symbol indicates statistical significance.*

We found that acetoin but not the solvent control (water), triggered a sustained decrease in membrane potential ($p=0.0334$), suggesting that EEU was IMF-limited. ThT fluorescence following acetoin injection dropped by 727.7 ± 145.6 p.d.u, whereas the ThT fluorescence following the solvent control (water) injection dropped by 119.2 ± 78.5 p.d.u. Additionally, CCCP did not further lower ThT fluorescence after the acetoin-dependent decrease, indicating that the membrane was already depolarized. Complete depolarization suggests that inward electron transfer depletes IMF faster than it can be replaced and therefore IMF generation is the rate limiting step for EEU under these conditions.

Our finding that Q-pool-dependent EEU in *S. oneidensis* MR-1+Bdh, an engineered heterotrophic bacterium, is both IMF-dependent and IMF-limited aligns with the mechanisms observed in wildtype autotrophic organisms where EEU drives energy-conserving pathways through the Q-pool. As reviewed in Gupta et al. (2020), autotrophs relying on Q-pool-dependent EEU require a source of IMF for carbon fixation.[13] Similarly, Guzman et al. (2019) demonstrated that *R. palustris* requires PMF for electrode-driven carbon fixation.[9] Past work with *S. oneidensis* is also consistent with IMF-dependent EEU to the cytoplasm.[48,52,56,70,71] Tefft and TerAvest (2019) reported EEU in *S. oneidensis* +Bdh +PR (proteorhodopsin), where PR, a light-driven proton pump, provided PMF.[48] On a cathode, *S. oneidensis* +Bdh +PR, rapidly responded to changes in light, indicating that EEU might be PMF-limited.[48] Rowe et al. (2018 and 2021) showed that *S. oneidensis* can perform EEU to the Q-pool with PMF supplied natively by proton-pumping terminal oxidases.[70,71] Ford and TerAvest (2023) demonstrated that PMF from terminal oxidases was also sufficient to drive EEU to the cytoplasm in place of PR in *S. oneidensis* +Bdh.[56]

Tefft et al. (2022) found that CCCP interfered with EEU to the cytoplasm, but not to fumarate reductase (FccA) in the periplasm.[52] As illustrated by Ross et al. (2011), 85% of EEU to FccA must go through the quinone pool.[20] Considered together, Tefft et al. (2022) and Ross et al. (2011) highlight that EEU to the Q-pool is not PMF-dependent, however, electron transfer from the reduced quinone pool to cytoplasmic $NAD^+$ is PMF-dependent.[20,52]

As shown by our model, Step 7 could be thermodynamically favorable for EEU with a consistent supply of IMF. Future work could optimize expression of both $H^+$-pumping oxidases and dissolved oxygen concentration to provide sufficient PMF for EEU, without reaching harmful concentrations of $H_2O_2$ from oxygen reduced on the cathode.[56] Under optimized conditions, it is possible that IMF would no longer be limiting for EEU. If this occurs, and discrepancies between anodic and cathodic current density magnitudes persist, future research directions could include enzymatic engineering.

We can improve the feasibility of MES as a scalable biotechnology by identifying and optimizing the IMF sources able to drive EEU in metal-reducers. The utility of the efficient electron transport pathways in metal-reducing bacteria are not limited to MES systems from a given species or genus. Indeed, the two requirements of MES have been independently demonstrated through heterologous expression: TerAvest et al. (2014) showed that *E. coli* expressing the Mtr pathway could directly link metabolic oxidation to electrode reduction; and Antonovsky et al. (2016) engineered a strain of *E. coli* capable of fixing $CO_2$ into organic carbon molecules.[72–74] In the future, engineered heterotrophic species, and/or their heterologously expressed EEU pathways, could increase current density magnitudes well into the range required for MES to be a scalable and sustainable

biotechnology.

## Declarations

### Ethics Approval and Consent to Participate

Not applicable.

### Availability of Data and Materials

Free energy changes were calculated using eQuilibrator 3.0 API in Python 3.9.7; see Methods section for package dependencies. The source code and raw data for either the free energy calculations or the microscopy experiments are available on request.

### Competing Interests

The authors declare that they have no competing interests.


### Funding

Our work was funded by the NSF CAREER award 1750785 to MT.

### Acknowledgements

We thank Dr. Sahand Pirbadian and Dr. Moh El-Naggar, of the El-Naggar Lab (University of Southern California) for helpful discussions, emails, and components for our BES prototype. We also thank members of the TerAvest lab, particularly Nicholas Tefft, for contributing to topical conversations for this project. Thank you to the Ducat Lab (Michigan State University) for use of their fluorescence microscope. Our work was funded by the NSF CAREER award 1750785 to M. TerAvest.


### Authors' Information


#### Corresponding Author

Michaela A. TerAvest – ORCID: 0000-0002-5435-3587; Email: teraves2@msu.edu

#### Authors

Shaylynn D. Miller – ORCID: 0009-0007-6351-0517

Kathryne C. Ford – ORCID: 0000-0002-6357-9318

Megan C. Gruenberg Cross – ORCID: 0000-0002-9158-9900

## 2. 7. Supplementary Information

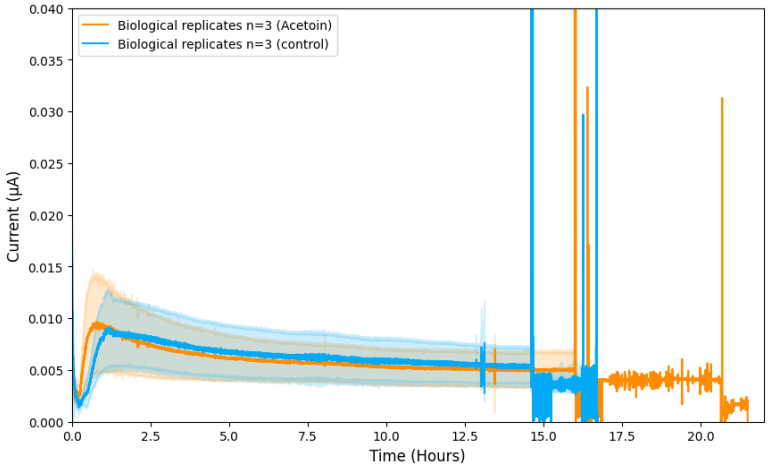


*Figure S 2-1. BES preparation for microscopy. Electrical current (µA) vs time (hours) prior to microscopy for each biological replicate in Figure 2-5. The working electrode potential was set to +0.2 V vs a saturated Ag/AgCl reference electrode for 15 to 17 hours prior to removing the minimal medium and replacing it with minimal medium plus ThT; during this time, 99.9% $N_2$ gas (Airgas) was bubbled into the BES. One replicate (the single orange line extending out past 20 hours) had a longer period between medium replacement and microscopy due to a brief tornado evacuation to the basement.*

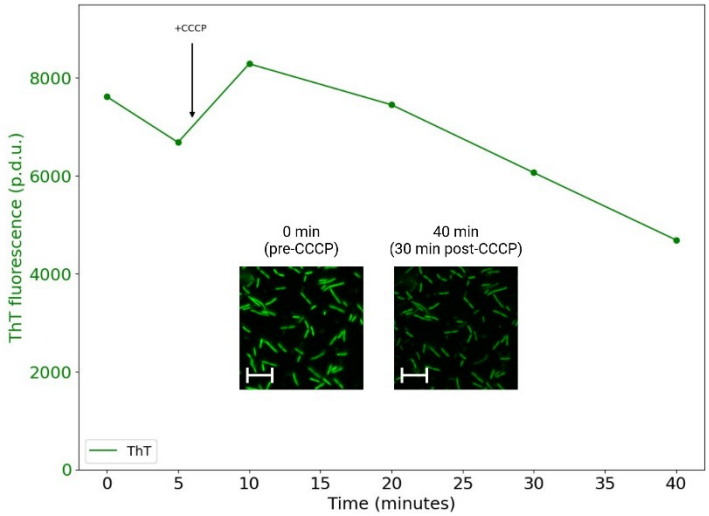


*Figure S 2-2. Thioflavin T fluorescence (ThT) over time. To demonstrate that the lack of membrane potential drop following CCCP injection in Figure 2-5 was not due to faulty technique or damaged CCCP, we imaged S. oneidensis MR-1 +Bdh in aerobic M5 minimal media with 20mM lactate in the same manner as all other injections in this work. As expected, CCCP decreased ThT fluorescence.*

## REFERENCES


1. Masson-Delmotte V, Zhai P, Pörtner HO, et al. IPCC, 2018: Global Warming of 1.5°C. An IPCC Special Report on the impacts of global warming of 1.5°C above pre-industrial levels and related global greenhouse gas emission pathways, in the context of strengthening the global response to the threat of climate change, sustainable development, and efforts to eradicate poverty. *Intergovernmental Panel on Climate Change*. Published online 2019:616. doi:10.1017/9781009157940

2. Karthikeyan R, Singh R, Bose A. Microbial electron uptake in microbial electrosynthesis: a mini-review. *J Ind Microbiol Biotechnol*. 2019;46(9-10):1419-1426. doi:10.1007/s10295-019-02166-6

3. Zhang S, Jiang J, Wang H, Li F, Hua T, Wang W. A review of microbial electrosynthesis applied to carbon dioxide capture and conversion: The basic principles, electrode materials, and bioproducts. *Journal of $CO_2$ Utilization*. 2021;51:101640. doi:10.1016/j.jcou.2021.101640

4. Rabaey K, Rozendal RA. Microbial electrosynthesis - Revisiting the electrical route for microbial production. *Nat Rev Microbiol*. 2010;8(10):706-716. doi:10.1038/nrmicro2422

5. Nevin KP, Woodard TL, Franks AE, Summers ZM, Lovley DR. Microbial electrosynthesis: Feeding microbes electricity to convert carbon dioxide and water to multicarbon extracellular organic compounds. *mBio*. 2010;1(2). doi:10.1128/mBio.00103-10

6. Dessì P, Rovira-Alsina L, Sánchez C, et al. Microbial electrosynthesis: Towards sustainable biorefineries for production of green chemicals from CO2 emissions. *Biotechnol Adv*. 2021;46. doi:10.1016/j.biotechadv.2020.107675

7. Jourdin L, Burdyny T. Microbial Electrosynthesis: Where Do We Go from Here? *Trends Biotechnol*. 2021;39(4):359-369. doi:10.1016/j.tibtech.2020.10.014

8. Prévoteau A, Carvajal-Arroyo JM, Ganigué R, Rabaey K. Microbial electrosynthesis from CO2: forever a promise? *Curr Opin Biotechnol*. 2020;62:48-57. doi:10.1016/j.copbio.2019.08.014

9. Guzman MS, Rengasamy K, Binkley MM, et al. Phototrophic extracellular electron uptake is linked to carbon dioxide fixation in the bacterium Rhodopseudomonas palustris. *Nat Commun*. 2019;10(1):1-13. doi:10.1038/s41467-019-09377-6

10. Kremp F, Roth J, Müller V. A Third Way of Energy Conservation in Acetogenic Bacteria. *Microbiol Spectr*. 2022;10(4). doi:10.1128/spectrum.01385-22

11. Schuchmann K, Müller V. Autotrophy at the thermodynamic limit of life: A model

for energy conservation in acetogenic bacteria. *Nat Rev Microbiol*. 2014;12(12):809-821. doi:10.1038/nrmicro3365

12. Gupta D, Guzman MS, Bose A. Extracellular electron uptake by autotrophic microbes: physiological, ecological, and evolutionary implications. *J Ind Microbiol Biotechnol*. 2020;47(9-10):863-876. doi:10.1007/s10295-020-02309-0

13. Gupta D, Guzman MS, Bose A. Extracellular electron uptake by autotrophic microbes: physiological, ecological, and evolutionary implications. *J Ind Microbiol Biotechnol*. 2020;47(9-10):863-876. doi:10.1007/s10295-020-02309-0

14. Jourdin L, Raes SMT, Buisman CJN, Strik DPBTB. Critical biofilm growth throughout unmodified carbon felts allows continuous bioelectrochemical chain elongation from CO2 up to caproate at high current density. *Front Energy Res*. 2018;6(MAR):7. doi:10.3389/fenrg.2018.00007

15. Jourdin L, Sousa J, Stralen N van, Strik DPBTB. Techno-economic assessment of microbial electrosynthesis from CO2 and/or organics: An interdisciplinary roadmap towards future research and application. *Appl Energy*. 2020;279:115775. doi:10.1016/j.apenergy.2020.115775

16. Hengsbach JN, Sabel-Becker B, Ulber R, Holtmann D. Microbial electrosynthesis of methane and acetate—comparison of pure and mixed cultures. *Appl Microbiol Biotechnol*. 2022;106(12):4427-4443. doi:10.1007/s00253-022-12031-9

17. Gralnick JA, Newman DK. Extracellular respiration. *Mol Microbiol*. 2007;65(1):1-11. doi:10.1111/j.1365-2958.2007.05778.x

18. Fujikawa T, Ogura Y, Ishigami K, et al. Unexpected genomic features of high current density-producing Geobacter sulfurreducens strain YM18. *FEMS Microbiol Lett*. 2021;368(17). doi:10.1093/femsle/fnab119

19. Zhang L, Zhang Y, Liu Y, et al. High power density redox-mediated Shewanella microbial flow fuel cells. *Nat Commun*. 2024;15(1):8302. doi:10.1038/s41467-024-52498-w

20. Ross DE, Flynn JM, Baron DB, Gralnick JA, Bond DR. Towards Electrosynthesis in Shewanella: Energetics of Reversing the Mtr Pathway for Reductive Metabolism. Xu S yong, ed. *PLoS One*. 2011;6(2):e16649. doi:10.1371/journal.pone.0016649

21. Coursolle D, Baron DB, Bond DR, Gralnick JA. The Mtr respiratory pathway is essential for reducing flavins and electrodes in *Shewanella oneidensis*. *J Bacteriol*. 2010;192(2):467-474. doi:10.1128/JB.00925-09

22. Rowe AR, Salimijazi F, Trutschel L, et al. Identification of a pathway for electron uptake in *Shewanella oneidensis*. *Commun Biol*. 2021;4(1). doi:10.1038/s42003-021-02454-x

23. Kotloski NJ, Gralnick JA. Flavin electron shuttles dominate extracellular electron transfer by *Shewanella oneidensis*. *mBio*. 2013;4(1). doi:10.1128/mBio.00553-12

24. Madsen CS, TerAvest MA. NADH dehydrogenases Nuo and Nqr1 contribute to extracellular electron transfer by *Shewanella oneidensis* MR-1 in bioelectrochemical systems. *Sci Rep*. 2019;9(1):1-6. doi:10.1038/s41598-019-51452-x

25. Edwards MJ, White GF, Butt JN, Richardson DJ, Clarke TA. The Crystal Structure of a Biological Insulated Transmembrane Molecular Wire. *Cell*. Published online 2020. doi:10.1016/j.cell.2020.03.032

26. Kracke F, Vassilev I, Krömer JO. Microbial electron transport and energy conservation - The foundation for optimizing bioelectrochemical systems. *Front Microbiol*. 2015;6(JUN). doi:10.3389/fmicb.2015.00575

27. Mitchell P. Chemiosmotic coupling in oxidative and photosynthetic phosphorylation. *Biochim Biophys Acta Bioenerg*. 2011;1807(12):1507-1538. doi:10.1016/j.bbabio.2011.09.018

28. Herrmann G, Jayamani E, Mai G, Buckel W. Energy conservation via electron-transferring flavoprotein in anaerobic bacteria. *J Bacteriol*. 2008;190(3):784-791. doi:10.1128/JB.01422-07

29. Buckel W, Thauer RK. Energy conservation via electron bifurcating ferredoxin reduction and proton/Na+ translocating ferredoxin oxidation. *Biochim Biophys Acta Bioenerg*. 2013;1827(2):94-113. doi:10.1016/j.bbabio.2012.07.002

30. Müller V, Hess V. The Minimum Biological Energy Quantum. *Front Microbiol*. 2017;8(OCT):2019. doi:10.3389/fmicb.2017.02019

31. Pal Chowdhury N, Basen M. Electron Bifurcation: A Long-Hidden Energy-Coupling Mechanism. Published online 2018. doi:10.1146/annurev-micro-090816

32. Martin WF. Hydrogen, metals, bifurcating electrons, and proton gradients: The early evolution of biological energy conservation. *FEBS Lett*. 2012;586(5):485-493. doi:10.1016/j.febslet.2011.09.031

33. Buckel W, Thauer RK. Flavin-Based Electron Bifurcation, A New Mechanism of Biological Energy Coupling. *Chem Rev*. 2018;118(7):3862-3886. doi:10.1021/acs.chemrev.7b00707

34. Feng J, Jiang M, Li K, et al. Direct electron uptake from a cathode using the inward Mtr pathway in *Escherichia coli*. *Bioelectrochemistry*. 2020;134:107498. doi:10.1016/j.bioelechem.2020.107498

35. Gupta D, Sutherland MC, Rengasamy K, Mark Meacham J, Kranz RG, Bose A. Photoferrotrophs produce a PioAB electron conduit for extracellular electron

uptake. *mBio*. 2019;10(6). doi:10.1128/mBio.02668-19

36. Schuchmann K, Müller V. Energetics and application of heterotrophy in acetogenic bacteria. *Appl Environ Microbiol*. 2016;82(14):4056-4069. doi:10.1128/AEM.00882-16

37. Jourdin L, Grieger T, Monetti J, et al. High Acetic Acid Production Rate Obtained by Microbial Electrosynthesis from Carbon Dioxide. *Environ Sci Technol*. 2015;49(22):13566-13574. doi:10.1021/acs.est.5b03821

38. Franza T, Gaudu P. Quinones: more than electron shuttles. *Res Microbiol*. 2022;173(6-7):103953. doi:10.1016/J.RESMIC.2022.103953

39. Abby SS, Kazemzadeh K, Vragniau C, Pelosi L, Pierrel F. Advances in bacterial pathways for the biosynthesis of ubiquinone. *Biochim Biophys Acta Bioenerg*. 2020;1861(11). doi:10.1016/j.bbabio.2020.148259

40. Richardson DJ. *Bacterial Respiration a Flexible Process for a Changing Environment*. Vol 146.; 2000. doi:10.1099/00221287-146-3-551

41. Anraku Y. *Bacterial Electron Transport Chains*.; 1988. doi:10.1146/annurev.bi.57.070188.000533

42. Kaila VRI, Wikström M. Architecture of bacterial respiratory chains. *Nat Rev Microbiol*. 2021;19(5):319-330. doi:10.1038/s41579-020-00486-4

43. Sarewicz M, Pintscher S, Pietras R, et al. Catalytic reactions and energy conservation in the cytochrome bc1 and b6f complexes of energy-transducing membranes. *Chem Rev*. 2021;121(4):2020-2108. doi:10.1021/acs.chemrev.0c00712

44. Nelson D, Cox M. *Lehninger Principles of Biochemistry*. 8th ed.; 2021.

45. Kleijn RJ, Buescher JM, Le Chat L, Jules M, Aymerich S, Sauer U. Metabolic Fluxes during Strong Carbon Catabolite Repression by Malate in Bacillus subtilis. *Journal of Biological Chemistry*. 2010;285(3):1587-1596. doi:10.1074/JBC.M109.061747

46. Yang X, Heinemann M, Howard J, et al. Physical bioenergetics: Energy fluxes, budgets, and constraints in cells. *Proc Natl Acad Sci U S A*. 2021;118(26). doi:10.1073/pnas.2026786118

47. Schoepp-Cothenet B, Van Lis R, Atteia A, et al. On the universal core of bioenergetics. *Biochim Biophys Acta Bioenerg*. 2013;1827(2):79-93. doi:10.1016/j.bbabio.2012.09.005

48. Tefft NM, Teravest MA. Reversing an Extracellular Electron Transfer Pathway for Electrode-Driven Acetoin Reduction. *ACS Synth Biol*. 2019;8(7):1590-1600.

doi:10.1021/acssynbio.8b00498

49. Pinchuk GE, Hill EA, Geydebrekht O v., et al. Constraint-based model of *Shewanella oneidensis* MR-1 metabolism: A tool for data analysis and hypothesis generation. *PLoS Comput Biol*. 2010;6(6):1-8. doi:10.1371/journal.pcbi.1000822

50. Flynn CM, Hunt KA, Gralnick JA, Srienc F. Construction and elementary mode analysis of a metabolic model for *Shewanella oneidensis* MR-1. *BioSystems*. 2012;107(2):120-128. doi:10.1016/j.biosystems.2011.10.003

51. Kishi S, Saito K, Kato Y, Ishikita H. Redox potentials of ubiquinone, menaquinone, phylloquinone, and plastoquinone in aqueous solution. *Photosynth Res*. 2017;134(2):193-200. doi:10.1007/s11120-017-0433-4

52. Tefft NM, Ford K, TerAvest MA. NADH dehydrogenases drive inward electron transfer in *Shewanella oneidensis* MR-1. *Microb Biotechnol*. Published online 2022. doi:10.1111/1751-7915.14175

53. Breuer M, Zarzycki P, Shi L, et al. Molecular structure and free energy landscape for electron transport in the decahaem cytochrome MtrF. In: *Biochemical Society Transactions*. Vol 40. ; 2012:1198-1203. doi:10.1042/BST20120139

54. Beber ME, Gollub MG, Mozaffari D, et al. EQuilibrator 3.0: A database solution for thermodynamic constant estimation. *Nucleic Acids Res*. 2022;50(D1):D603-D609. doi:10.1093/nar/gkab1106

55. Pirbadian S, Chavez MS, El-Naggar MY. Spatiotemporal mapping of bacterial membrane potential responses to extracellular electron transfer. *Proc Natl Acad Sci U S A*. Published online August 3, 2020. doi:10.1073/pnas.2000802117

56. Ford KC, Teravest MA. The Electron Transport Chain of *Shewanella oneidensis* MR-1 can Operate Bidirectionally to Enable Microbial Electrosynthesis. *Appl Environ Microbiol*. Published online December 20, 2023. doi:10.1101/2023.08.11.553014

57. Agarwal RG, Coste SC, Groff BD, et al. Free Energies of Proton-Coupled Electron Transfer Reagents and Their Applications. *Chem Rev*. 2022;122(1):1-49. doi:10.1021/acs.chemrev.1c00521

58. Flamholz A, Noor E, Bar-Even A, Milo R. EQuilibrator - The biochemical thermodynamics calculator. *Nucleic Acids Res*. 2012;40(D1):D770-D775. doi:10.1093/nar/gkr874

59. Mohr PJ, Taylor BN. *CODATA Recommended Values of the Fundamental Physical Constants 1998*.; 1998. doi:10.1103/RevModPhys.72.351

60. Haraldsdóttir HS, Thiele I, Fleming RMT. Quantitative assignment of reaction

directionality in a multicompartmental human metabolic reconstruction. *Biophys J*. 2012;102(8):1703-1711. doi:10.1016/J.BPJ.2012.02.032

61. Bekker M, Kramer G, Hartog AF, et al. Changes in the redox state and composition of the quinone pool of *Escherichia coli* during aerobic batch-culture growth. *Microbiology (N Y)*. 2007;153(6):1974-1980. doi:10.1099/mic.0.2007/006098-0

62. van Beilen JWA, Hellingwerf KJ. All three endogenous quinone species of *Escherichia coli* are involved in controlling the activity of the aerobic/anaerobic response regulator ArcA. *Front Microbiol*. 2016;7(SEP). doi:10.3389/fmicb.2016.01339

63. G McMillan DG, Marritt SJ, Butt JN, C Jeuken LJ. Menaquinone-7 Is Specific Cofactor in Tetraheme Quinol Dehydrogenase CymA. Published online 2012. doi:10.1074/jbc.M112.348813

64. Li F, Li Y, Sun L, et al. Modular Engineering Intracellular NADH Regeneration Boosts Extracellular Electron Transfer of *Shewanella oneidensis* MR-1. *ACS Synth Biol*. 2018;7(3):885-895. doi:10.1021/acssynbio.7b00390

65. Liu Y, Landick R, Raman S. A Regulatory NADH/NAD+ Redox Biosensor for Bacteria. *ACS Synth Biol*. 2019;8(2):264-273. doi:10.1021/acssynbio.8b00485

66. Duhl KL, Tefft NM, TerAvest MA. *Shewanella oneidensis* MR-1 utilizes both sodium- and proton-pumping NADH dehydrogenases during aerobic growth. *Appl Environ Microbiol*. 2018;84(12). doi:10.1128/AEM.00415-18

67. Kane MS, Paris A, Codron P, et al. Current mechanistic insights into the CCCP-induced cell survival response. *Biochem Pharmacol*. 2018;148:100-110. doi:10.1016/J.BCP.2017.12.018

68. Ishiki K, Shiigi H. Kinetics of Intracellular Electron Generation in *Shewanella oneidensis* MR-1. *Anal Chem*. Published online 2019. doi:10.1021/acs.analchem.9b02900

69. Mancini L, Terradot G, Tian T, et al. A General Workflow for Characterization of Nernstian Dyes and Their Effects on Bacterial Physiology. *Biophys J*. 2019;118(1):4-14. doi:10.1016/j.bpj.2019.10.030

70. Rowe AR, Salimijazi F, Trutschel L, et al. Identification of a pathway for electron uptake in *Shewanella oneidensis*. *Commun Biol*. 2021;4(1). doi:10.1038/s42003-021-02454-x

71. Rowe AR, Rajeev P, Jain A, et al. Tracking electron uptake from a cathode into Shewanella cells: Implications for energy acquisition from solid-substrate electron donors. *mBio*. 2018;9(1). doi:10.1128/mBio.02203-17

72. Teravest MA, Zajdel TJ, Ajo-Franklin CM. The Mtr Pathway of *Shewanella oneidensis* MR-1 Couples Substrate Utilization to Current Production in *Escherichia coli*. *ChemElectroChem*. 2014;1(11):1874-1879. doi:10.1002/celc.201402194

73. Jensen HM, Albers AE, Malley KR, et al. Engineering of a synthetic electron conduit in living cells. *PNAS*. 2010;107(45). doi:10.1073/pnas.1009645107/-/DCSupplemental

74. Antonovsky N, Gleizer S, Jona G, Bar-Even A, Correspondence RM. Sugar Synthesis from CO 2 in *Escherichia coli*. *Cell*. 2016;166:115-125. doi:10.1016/j.cell.2016.05.064

# Chapter 3. Outward and inward electron transfer occur through distinct mechanisms for anaerobic *Shewanella oneidensis*

Shaylynn D. Miller[1], Kathryne C. Ford[2,3], and Michaela A. TerAvest[1]

[1]Department of Biochemistry and Molecular Biology, Michigan State University, East Lansing, MI, USA

[2]Department of Microbiology and Molecular Genetics, Michigan State University, East Lansing, MI, USA

[3]Department of Chemical and Biomolecular Engineering, North Carolina State University, Raleigh, NC, USA

## 3. 1. Author Contributions

All authors participated in preliminary discussions pertaining to this work. SM furthered those conceptual discussions into testable hypotheses and experimental designs. SM performed all experiments and experimental troubleshooting. SM collected all data and performed preliminary data analysis. SM and MT finalized data analysis and interpretation together, prior to SM writing the manuscript. The manuscript was edited by MT and KF.

## 3. 2. Abstract

Microbial electrosynthesis (MES) is an emerging biotechnology with the potential to help mitigate climate change by recycling carbon dioxide into organic compounds using sustainably-generated electricity as the energy source. However, for MES to meaningfully decrease net carbon emissions on an industrial scale, the rate of inward electron transfer (ET) from cathode to bacterium must increase. In this work, we investigate this challenge using *Shewanella oneidensis*, a model metal-reducing bacterium with the most extensively studied microbial extracellular electron transfer (EET) pathway. While the Mtr pathway in *S. oneidensis* is bidirectional, the magnitude of outward ET (its native

respiratory direction) consistently exceeds inward ET, the direction required for MES applications. Here, we present the first direct comparison of flavin-mediated ET for both directions using potentiometric techniques. Through chronoamperometry and turnover cyclic voltammetry, we demonstrate that the ET mechanism and flavin dependence are direction-dependent under anaerobic conditions.

Keywords: Microbial electrosynthesis, *Shewanella oneidensis*, extracellular electron uptake, inward electron transfer, outward electron transfer, electron transfer mechanism

**3. 3. Introduction**

Technologies for mitigating climate change span a wide range of fields, with recent options including biotechnologies. Microbial electrosynthesis (MES) is a biotechnology that could help decrease net $CO_2$ emissions by using microorganisms to recycle the carbon from industrial emissions into organic carbon molecules for fuels and products. Microorganisms that accept electrons from a negatively poised electrode and funnel reducing power into their cytoplasm could perform the intracellular reduction reactions needed to fix $CO_2$. However, MES systems will need an improved inward electron transfer rate before maturing into biotechnologies capable of decreasing net $CO_2$ emissions.[1,2]

To improve the electron transfer rate of an MES system, the rate of electrons transported per unit of electrode surface area (current density, $mA \cdot cm^{-2}$) must increase.[1,2] Because MES requires a robust bacteria-electrode interface, bacteria that reduce extracellular electron acceptors as a part of their native metabolism are among the promising candidates for this biotechnology; one such species is the metal-reducing bacterium, *Shewanella oneidensis*. While *S. oneidensis* lacks the high extracellular electron transfer (ET) rates of *Geobacter sulfurreducens*, its metal-reducing (Mtr) pathway is the most thoroughly understood. Electron flow through the Mtr pathway is also bidirectional,

allowing *S. oneidensis* to perform both inward and outward electron transfer (ET).[3] In this work, we define outward ET as electron flow from a bacterium to a positively poised electrode (anode). Correspondingly, inward ET is electron flow from a negatively poised electrode (cathode) to a bacterium. The well-characterized bidirectionality of the Mtr pathway makes *S. oneidensis* a suitable model organism to address inefficiencies that prevent MES from developing into an industrially relevant biotechnology. [4]

Outward and inward ETs in *S. oneidensis* share much of the Mtr pathway, yet they differ in their reported extracellular ET rates, with inward ET consistently lower in magnitude.[3–9] In our previous work, Miller et al. (2025, preprint), we described an intracellular thermodynamic bottleneck that limits inward ET from the respiratory quinone pool to the cytoplasm.[10] Specifically, we observed that ET from menaquinol to $NAD^+$ is thermodynamically unfavorable and must be coupled to dissipation of proton-motive force (PMF) to proceed; however, the PMF is limiting during inward ET in our experience. With NADH dehydrogenase flux limiting inward ET to the cytoplasm, it follows that the rate of inward ET would be lower than outward ET. However, there is a thermodynamically favorable inward ET path, where electrons from a cathode reduce periplasmic fumarate to succinate ($\Delta G'^\circ$ = -11.9 ± 7.0 $kJ \cdot mol^{-1}$).[11] Yet, when extracellular ET is thermodynamically favorable for both inward ET and outward ET, the current density magnitude of inward ET remains approximately one tenth that of outward ET under similar bioelectrochemical system (BES) setups (Table 3-1).[3–5]

Because the directional discrepancy for extracellular ET rate persists when both directions have thermodynamically favorable electron acceptors, we expect that there is a directional difference in ET kinetics. Because ET within Mtr pathway proteins is

kinetically favorable due to the Mtr cytochromes' short inter-heme distances (<8Å), we expect that the mechanistic difference is extracellular.[12,13]

For *S. oneidensis* the extracellular component of ET occurs either through direct contact with a redox active surface or indirectly through flavins, redox shuttling molecules.[3,14–20] The flavin species that *S. oneidensis* produces are flavin mononucleotide (FMN), riboflavin (RF), and flavin adenine dinucleotide (FAD), of which it secretes RF and FMN in up to μM concentrations.[4] Previous works have demonstrated that the majority of extracellular ET is flavin-dependent, consisting of approximately 70 to 85% of the extracellular ET measured.[19,20]

*Table 3-1. An estimate of the relative current density magnitude for outward ET to an anode and inward ET to fumarate. All examples used carbon-based electrodes under anaerobic conditions.*

| ET direction | Approx. peak current (mA) | Electrode material | Geometric electrode surface area ($cm^2$) | Approx. current density ($mA \cdot cm^{-2}$) | Current density magnitude relative to outward ET | Reference |
|---|---|---|---|---|---|---|
| Outward | 3.5 | Carbon felt | 18.8 | 0.186 | 1.0 | Masen and TerAvest (2019)[5] |
| Inward | -0.6 | Carbon felt | 34.5 | 0.017 | 0.09 | Ford and TerAvest (2023)[4] |
| Inward | Directly reported | Graphite | 2.5 | 0.017 | 0.09 | Ross et al. (2011)[3] |

Given that flavins are required for the majority of extracellular ET in *S. oneidensis*, we hypothesize that the mechanistic difference between inward and outward ETs stems from dissimilar reliance on flavin-mediated ET. To test our hypothesis, we compared chronoamperometric and cyclic voltametric electric current for inward and outward ETs with and without supplemental riboflavin. Before MES systems can assist with the climate crisis, their inward ET rate must increase. An essential step towards this goal is to better

understand the mechanisms of inward ET. While *S. oneidensis* has the most thoroughly understood ET pathway among metal reducing bacteria, the reason that inward ET rate remains consistently lower than outward ET rate has yet to be resolved.

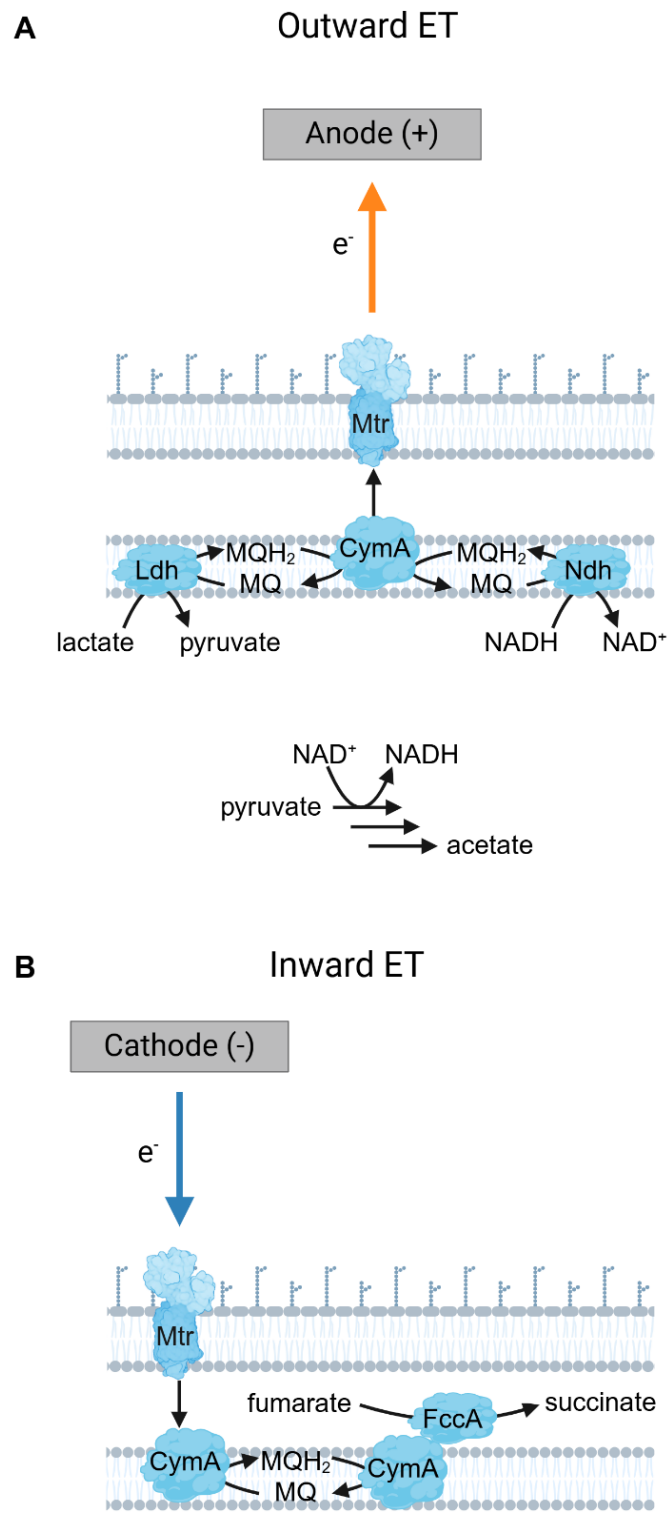


*Figure 3-1. Comparison of outward ET and inward ET through the Mtr pathway in S. oneidensis MR-1. (A) Outward ET is the ET direction used during cell respiration to funnel electrons to extracellular electron acceptors. (B) Inward ET is ET from an external electron donor to the bacterium. The bidirectionality of the Mtr pathway was first reported in Ross et al. (2011) using fumarate as the electron acceptor.*

## 3. 4. Methods

### 3. 4. 1 Bacterial culture preparation

*S. oneidensis* cells from a cryostock, stored at -80°C, were plated for single colonies on Miller's Lysogeny Broth (LB) agarose plates. Liquid cultures were each prepared by inoculating 5 ml LB with a single colony of *S. oneidensis*. After growth in liquid LB, the $OD_{600}$ was measured with a 1:10 dilution of culture to fresh LB medium. Cultures were centrifuged (8,500 x g for 3 minutes), washed in 1.0 ml of M5 minimal medium (1.29 mM $K_2HPO_4$, 1.65 mM $KH_2PO_4$, 7.87 mM NaCl, 1.70 mM $NH_4SO_4$, 475 µM $MgSO_4 \cdot 7H_2O$, 10 mM HEPES, 1X Wolfe's mineral solution (excluding both casamino acids and $AlK(SO_4)_2 \cdot 12\ H_2O$), and 1X Wolfe's vitamin solution (excluding riboflavin) to wash cells. Once resuspended in minimal medium and centrifuged (8,500 x g for 3 minutes), cultures were standardized to an $OD_{600}$ of 1.0. For each biological replicate, 100 ml of fresh minimal medium with 20 mM D,L-lactate and 0.01% (w/v) casamino acids was inoculated with 200 µl of the standardized culture ($OD_{600}$ of 1.0) in a 500 ml Erlenmeyer flask. Each flask was incubated at 30°C, 250 rpm, for 18-19 hours (to an $OD_{600}$ of ~0.55). Once the *S. oneidensis* cultures reached the specified optical density, the cells were centrifuged (8,500 x g for 5 minutes) and washed twice with 50 ml M5 minimal medium without a carbon source. We performed a final centrifugation step with 10 ml of the culture standardized to an $OD_{600}$ of 3.78 and then resuspended each cell pellet in 10 ml of M5 minimal medium without a carbon source, in an anaerobic chamber. The resuspension medium degassed for at least 48 hours prior to resuspension. We injected 9 ml of each biological replicate into an anaerobic BES.

### 3. 4. 2 Bioelectrochemical system set-up

For all BES experiments, we used a three-electrode set-up controlled by a potentiostat

(VMP, BioLogic USA). The working electrode was carbon felt (Alfa Aesar, 43200RF) cut to 50 mm x 25 mm and connected to a titanium wire with carbon adhesive (Sigma-Aldrich, 09929-30G). The reference electrode was housed in a glass tube with a magnesia frit (Sigma-Aldrich, 31408-1EA) that separated the interior of the reference electrode from the BES medium; inside the tube was a saturated (potassium chloride) Ag/AgCl reference electrode. The counter electrode was a graphite rod (Electron Microscopy Science, 07200). All electrodes were secured with butyl rubber septum stoppers.

Each BES was assembled from two blown-glass chambers, with the working electrode chamber jacketed for maintaining a temperature of 30°C via a heated water pump for *S. oneidensis* during BES experiments. The working and counter electrode chambers were separated by a cation exchange membrane (Membranes International, CMI-7000S). The counter electrode chamber was filled with phosphate buffered saline, and the working electrode chamber was filled with 150.8 ml of M5 minimal medium (100 mM HEPES, 1.29 mM $K_2HPO_4$, 1.65 mM $KH_2PO_4$, 7.87 mM NaCl, 1.70 mM $NH_4SO_4$, and 475 µM $MgSO_4 \cdot 7H_2O$, adjusted to pH = 7.2) prior to autoclave sterilization. After each BES had cooled from the autoclave, we added the following filter sterilized medium components: 1.7 ml of 100X Wolfe's vitamin solution (excluding riboflavin) and 1.7 ml of 100X Wolfe's mineral solution (excluding both casamino acids and $AlK(SO_4)_2 \cdot 12\ H_2O$). BES intended for inward ET on a cathode received 6.8 ml of 1 M sodium fumarate (40 mM final concentration), while BES for outward ET on an anode received 6.8 ml of 500 mM D,L-Lactate (20 mM final concentration).

**3. 4. 3 Riboflavin preparation**

We prepared two anaerobic riboflavin solutions, one for the anodic BESs and one for the cathodic BESs. Both riboflavin solutions received at least 12 hours of nitrogen bubbling

prior to the first use. In addition to nitrogen bubbling, the riboflavin solution for the cathodic BES was reduced to an electrode potential of -0.697 V (vs saturated Ag/AgCl reference electrode); this was to prevent electric current flow towards oxidized riboflavin from obscuring the true inward ET current. All riboflavin solutions were prepared at 170 μM so that the BES volume would remain roughly constant, and the volume of sample removed would approximately equal the volume of riboflavin added incrementally in Figure 3-3. Riboflavin stock solutions were kept wrapped in foil to protect from photodegradation during the experiment. All riboflavin solutions were filter-sterilized and kept in autoclave-sterilized glass bottles for the duration of the experiment.

### 3. 4. 4 Anaerobic riboflavin injection

Before injecting the anaerobic riboflavin solutions, each syringe was flushed 3–4 times with nitrogen gas. Just before drawing up the riboflavin solution, the remaining nitrogen gas was gradually expelled while approaching the butyl rubber stopper. While this method does not eliminate oxygen from entering the syringe or the BES entirely, it was sufficient for this experiment. This conclusion is based on: 1) the absence of injection-specific current responses in abiotic control experiments, 2) no injection-induced acetate production in biotic controls without an applied electrode potential, and 3) no visible color change in the reduced riboflavin transferred from the preparatory electrochemical cell to the BES chambers (it remained clear rather than turning bright yellow, which would indicate oxidation).

### 3. 4. 5 Potentiometric techniques

Chronoamperometry steps were performed with an electrode potential of -0.697V for cathodic BESs and +0.303 V for anodic BESs (vs a saturated Ag/AgCl reference electrode). Cyclic voltammetry steps were performed at a scan rate of 2.0 $mV \cdot s^{-1}$ and a

potential sweep from +0.303 V to -0.697V vs a saturated Ag/AgCl reference electrode.

### 3. 4. 6 HPLC analysis

After the BESs were inoculated, approximately 1 ml of culture was collected from each BES at 0, 22, and 44 hours post inoculation with a sterile syringe, and stored at -20°C until HPLC sample preparation. Each sample was thawed at 20-22°C prior to centrifugation at >16,000 RCF for 10 minutes. We prepared the HPLC samples as described in Gruenberg and TerAvest (2023), with the following change that our standards were combined solutions of four compounds (D,L-lactate, sodium fumarate, acetate, and succinate) at seven concentrations (0.5 mM, 1.0 mM, 2.5 mM, 5.0 mM,10 mM, 20 mM, and 40 mM).

### 3. 4. 7 Data processing and availability

Data were analysed with either python 3.9.7 (Dependencies: seaborn 0.11.2, scipy 1.8.1, pandas 1.3.4, numpy 1.22.4, and matplotlib 3.4.3) or Rstudio (ggplot2, reshape2, dplyr and TTR). Raw data and coding scripts are available on request.

## 3. 5. Results

### 3. 5. 1 Inward and outward electron transfers differ in their dependance on supplemental riboflavin

We used two thermodynamically favorable extracellular ET processes to assess if inward and outward ET are mechanistically distinct in *S. oneidensis*. Specifically, we compared the ET to an anode during lactate oxidation with ET from a cathode during fumarate reduction. Because RF is known to mediate extracellular ET in this organism, we compared inward and outward ET via chronoamperometry where the RF concentration was 0 μM, 2 μM, 4 μM, or 7 μM. To ensure that oxygen reduction did not contribute significantly to cathodic current, we prepared each BES with approximately 12 hours of

$N_2$ bubbling prior to applying an electrode potential. To ensure that reduction of oxidized RF (as injected) did not cause a current spike in the cathodic condition, RF was pre-reduced prior to injection in cathodic systems. Additionally, we found no notable difference in the initial $OD_{600}$ or flavin fluorescence for BES samples directly after inoculation (Figure 3-2).

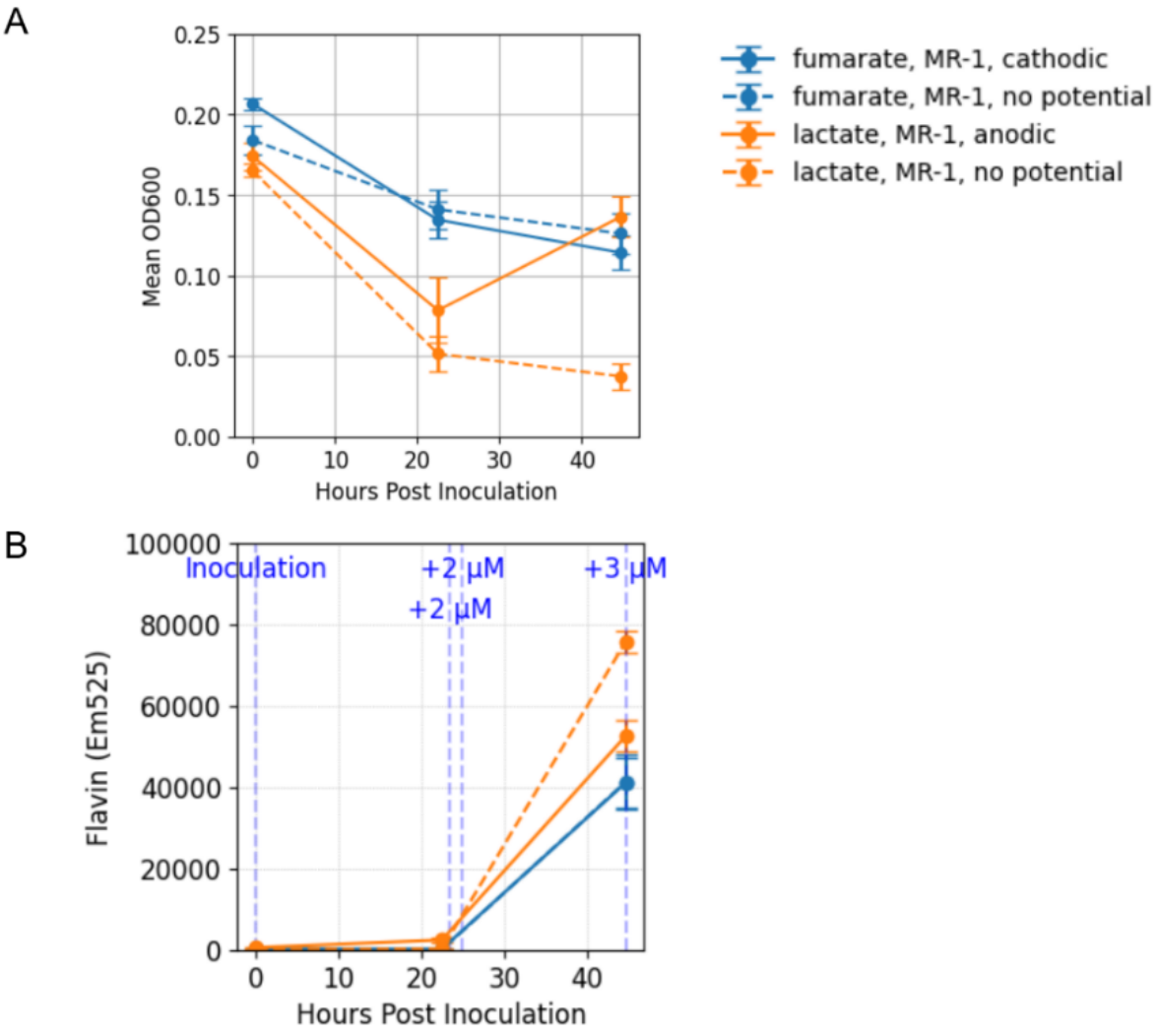


*Figure 3-2. Optical density ($OD_{600}$) and flavin fluorescence (525 nm) at three timepoints, post inoculation (0 hours), end of pre-RF (22 hours), end of post-RF (44.7 hours). The final addition of 3 µM of RF was after the sampling at 44.7 hours, to observe if there was any change in current with additional RF. Pre-RF and pos-RF refer to the 20-hour timeframe preceding or following the first RF injection at 22.5 hours, respectively.*

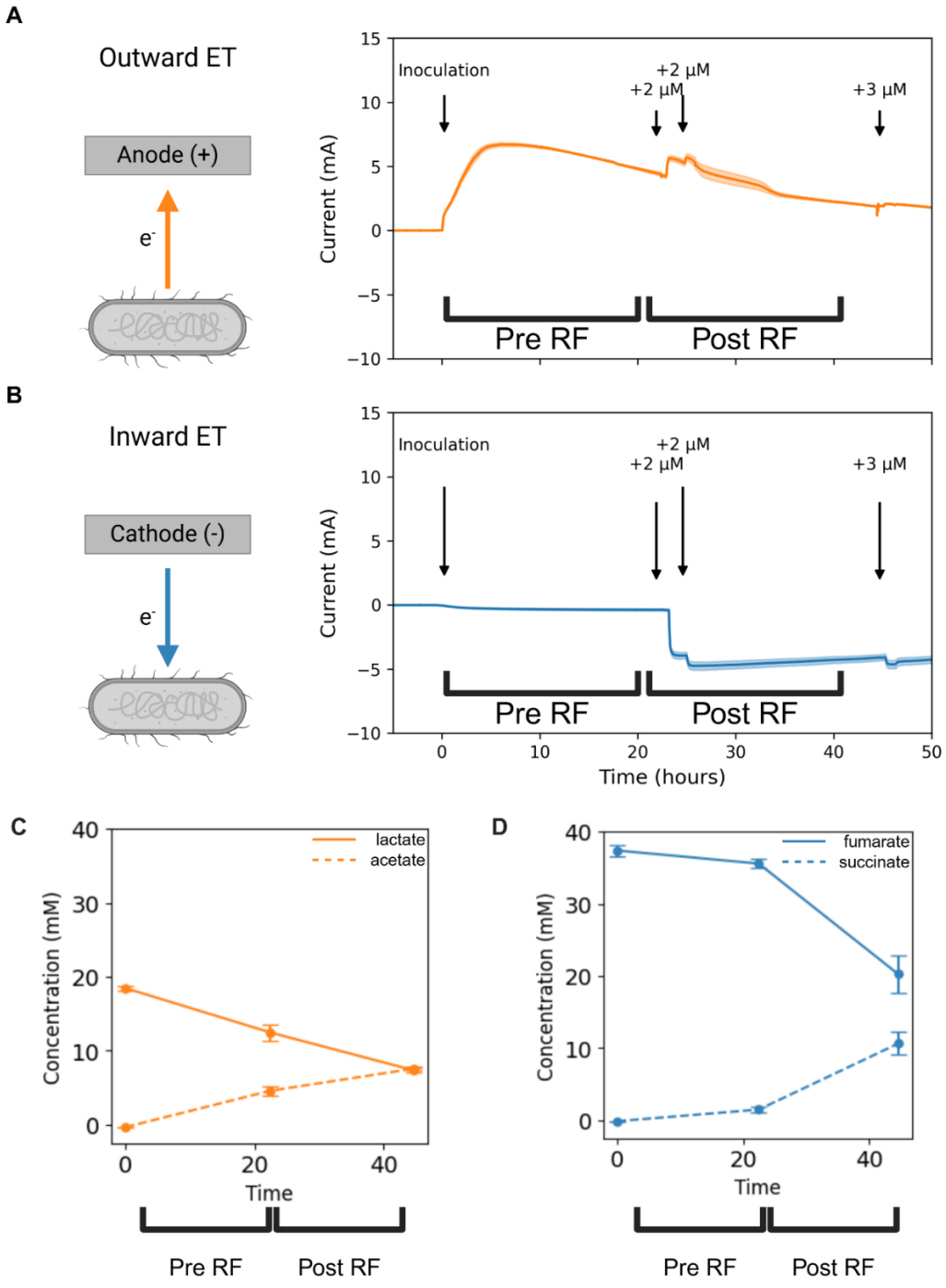


*Figure 3-3. Current versus time for (A) outward ET and (B) inward ET. Once inoculated at 0 hours, there was a 20-hour period before the first RF injection (pre-RF), and a 20-hour period with supplemental RF present (post-RF). (C) Lactate and acetate concentrations during outward ET. D) Fumarate and succinate concentrations during inward ET. The concentrations in C and D were determined through HPLC analysis.*

Prior to supplemental RF addition at 22.5 hours, significantly less charge (i.e. electrons) was passed in the inward ET condition than the outward ET condition (p=0.012, independent T-test). During inward ET, there was a significant increase in the amount of charge passed in the 20 hours after RF addition (p=0.027, paired T-test). Likewise, the peak current density ($\mu A \cdot cm^{-2}$) during the 20 hours pre-RF was significantly lower for inward ET compared to outward ET (p=0.019, independent T-test), and for inward ET pre- to post-RF (p=0.031, paired T-test).

We also measured lactate, acetate, fumarate, and succinate concentrations over time by HPLC. For outward ET (Figure 3-3), the rates of lactate decrease and acetate increase were approximately equal for the pre-RF and post-RF timeframes. However, for inward ET (Figure 3-3), the rate of fumarate reduction increased significantly after RF addition.

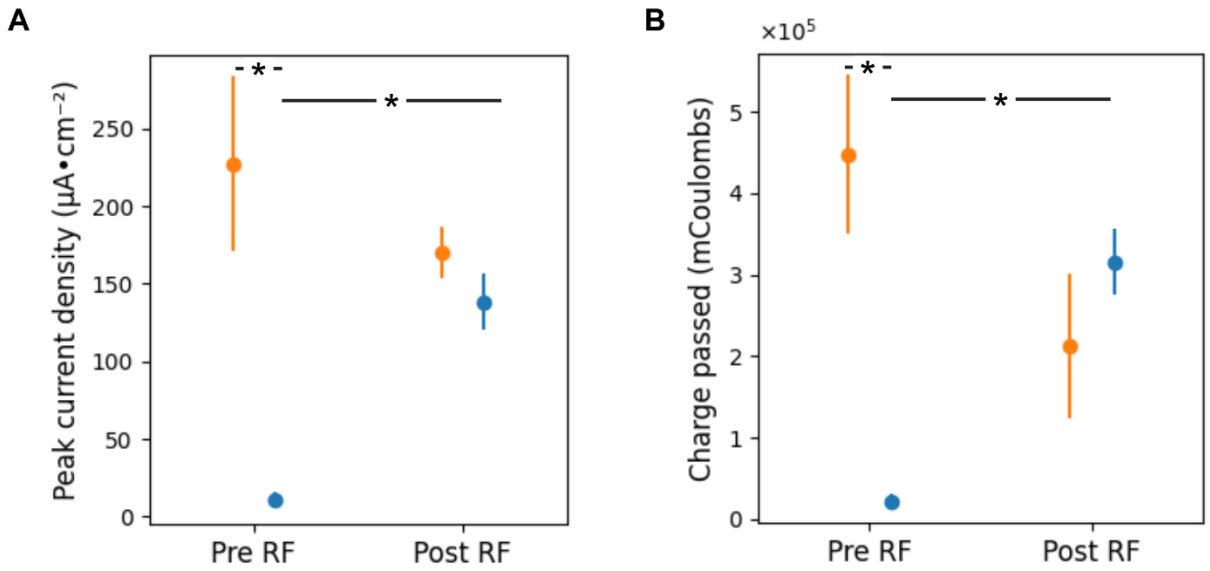


*Figure 3-4. (A) Peak current density during the 20 hours following inoculation but before RF (Pre RF), or after supplemental RF (Post RF). (B) The magnitude of charge passed during the 20-hour period indicated, either pre- or post-RF. Data points represent the mean, while the error bars are the standard error of the mean. An asterisk (*) indicates a two sample T test p-value of $p < 0.05$. Orange indicates outward ET, while blue is inward ET.*

### 3. 5. 2 Inward and outward electron transfer use distinct electron transfer mechanisms

In the chronoamperometry experiments described above, we demonstrated that inward ET is more dependent on RF than outward ET. However, to add further mechanistic insight we used cyclic voltammetry (CV). In a BES, turnover cyclic voltammetry (CV) refers to conditions where the electron-donating or -accepting substrate is present in excess.[21] For anodic conditions in this system, lactate served as the electron donor, while for cathodic conditions, fumarate was the electron acceptor. Under turnover conditions, and at a sufficiently slow scan rate (i.e., low electrode potential change per unit time), the maximum current is limited by the kinetics of the rate-limiting ET step.[21] Under these conditions, the current-potential curve exhibits a characteristic sigmoidal (S)-shape because the microbial ET system can support both oxidation and reduction at steady-state, leading to a catalytic wave rather than a peak.[21]

As above, we used anaerobic BESs for either inward or outward ET. Figure 3-5A and B show CV and chronoamperometry data for outward and inward ET, respectively. On the right-hand side is the chronoamperometry data for three biological replicates, and on the left are three CV traces that correspond to the following timepoints: Pre-inoculation ($CV_0$), post-inoculation ($CV_1$), and post-inoculation with 2 μM supplemental RF ($CV_2$). The CV traces in Figure 5, for either inward or outward ET, are shown as individual biological replicates for clarity. All biological replicate CV sets are shown in their entirety in Figure S1.

During chronoamperometry, the peak current for outward ET was 4.68 ± 1.32 mA while the peak current for inward ET was -2.47 ± 0.16 mA (Figure 3-5). Inward and outward ETs displayed different responses to inoculation and supplemental RF. Outward ET

(Figure 3-5A, right) had a sharp increase in chronoamperometric current magnitude following inoculation, but not after supplemental RF injection. Inward ET (Figure 3-5B, right) showed the opposite response, where current magnitude remained close to zero following inoculation, but increased (i.e., became more negative) following supplemental RF injection. For both inward and outward ET, the CVs prior to inoculation ($CV_0$) were featureless, aside from a peak present at 0.1 V. As this peak remained present for all CVs involving an autoclaved carbon felt electrode, we suspect that this peak was due to pseudocapacitance from heteroatom functional groups, which are a common impurity in carbon electrodes, particularly those with high surface area, such as carbon felt.[22,23]

The CVs in Figure 3-5A and Figure 3-5B (left) demonstrate both thermodynamic and kinetic differences present between outward and inward ET. The type of ET sites and their associated midpoint potentials are among the thermodynamic information we can glean from CV in BESs.[21] We can assess these thermodynamic parameters for each timepoint to gain information about the ET mechanisms used during either direction of extracellular ET. Outward ET and inward ET differ in their available ET sites, both before and after supplemental RF addition. $CV_1$ showed that prior to supplemental RF addition, one ET site was available for outward ET, but no ET sites were available for inward ET. Post-RF, $CV_2$ indicated that outward ET had two ET sites (midpoint potentials of -0.435 $V_{Ag/AgCl}$ and 0.142 $V_{Ag/AgCl}$) and inward ET had one ET site (midpoint potential of -0.455 $V_{Ag/AgCl}$).

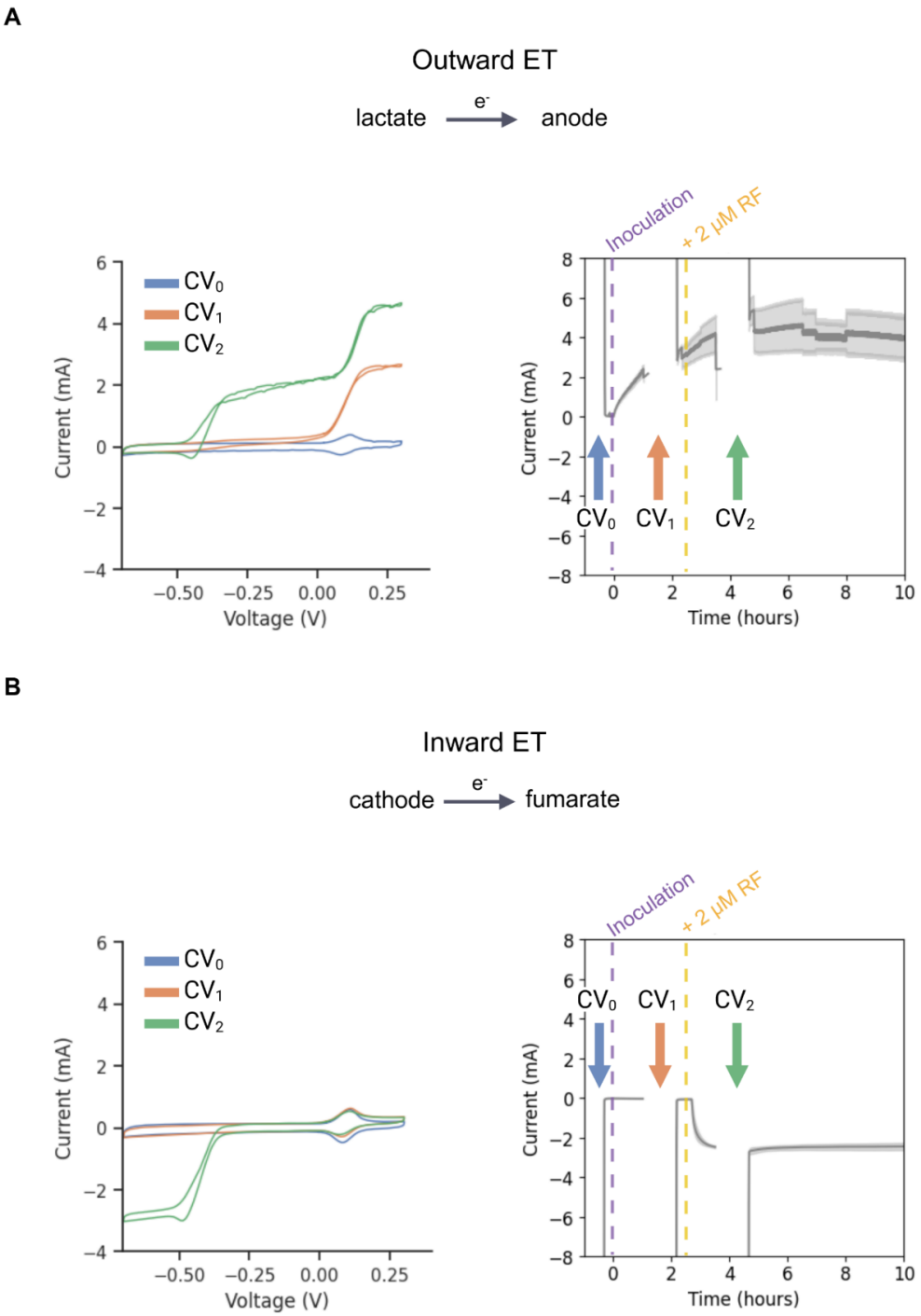


*Figure 3-5. On the right are chronoamperometric current versus time plots, and on the left are the corresponding cyclic voltammograms (CV). (A) Potentiometric data for outward ET, while (B) shows the same for inward ET. Inoculation was at 0 hours, and RF was injected just after 2 hours. For both outward ET and inward ET, there were three cyclic voltammograms at a scan rate of 2.0 mV·s$^{-1}$. $CV_0$ was the abiotic scan prior to inoculation, $CV_1$ was the scan post-inoculation, and $CV_2$ was the scan post-RF.*

## 3. 6. Discussion

Numerous studies have examined inward and outward ET in *S. oneidensis* under various conditions, yet no work has directly compared these two ET directions during extracellular electron transfer (EET). [2828]To ensure that the starting conditions in our BESs were consistent and that we did not observe significant abiotic oxygen reduction, we bubbled nitrogen through the working electrode chamber for at least 12 hours before applying an electrode potential in all BES experiments. This step, 1) standardized oxygen levels across biological replicates and conditions, and 2) prevented peroxide accumulation in the BESs for inward ET. This step was important because in our previous work, Ford and TerAvest (2023), we found that nitrogen bubbling decreased dissolved oxygen to ~1% in our glass BESs.[4] While this microoxic state did not eliminate oxygen entirely, it effectively prevented peroxide accumulation at the cathode from compromising cell viability.[4] Additionally, for BESs in the inward ET group, we pre-reduced riboflavin at a cathode before use to eliminate abiotic current contributions that could otherwise obscure inward ET measurements.

We hypothesized that the discrepancy in magnitude between inward and outward ET was due to a dissimilar reliance on flavin-mediated ET. Indeed, we found that during chronoamperometry, inward and outward ET do not have the same dependence on riboflavin (Figure 3-3 and Figure 3-4). Additionally, we found that inward and outward ET likely occur through different mechanisms under anaerobic conditions (Figure 3-5).

We show in Figure 3-3, that our initial chronoamperometry comparisons with incrementally increasing riboflavin concentration, that electric current for outward ET was not limited by supplemental riboflavin. Conversely, inward ET was dependent on supplemental riboflavin; we observed the same pattern in the concentration of lactate

oxidized to acetate and fumarate reduced to succinate. During the pre- and post-RF timeframes, approximately equal concentrations of acetate were produced via outward ET (Figure 3-3C), however, the majority of the succinate produced during inward ET was post-RF (Figure 3-3D). Additionally, RF only produced a significant difference ($p < 0.05$) in peak current density or charge for inward ET but not for outward ET (Figure 3-4).

For electric current from *S. oneidensis* to the anode, no change in chronoamperometric current was observed due to supplemental RF (Figure 3-5A). However, the difference in the number of catalytic waves during cyclic voltammetry for $CV_1$ (pre-RF) and $CV_2$ (post-RF) suggests that different ET processes occurred under these conditions. Whereas, during both chronoamperometry and cyclic voltammetry, electric current from the cathode to *S. oneidensis* only began after supplemental RF was injected (Figure 3-5B). In Figure 3-5A, $CV_1$ (pre-RF), the catalytic wave at 0.142 $V_{Ag/AgCl}$, is consistent with ET from an outer membrane cytochrome (OMC), while the midpoint potentials for $CV_2$ (post-RF), -0.435 $V_{Ag/AgCl}$ and 0.142 $V_{Ag/AgCl}$, are consistent with both RF- and OMC-mediated EET, respectively. For Figure 3-5B there was no catalytic wave pre-RF, it was only post-RF that the flavin catalytic wave appeared.[24]

Our results align with the growing body of research demonstrating that flavin-mediated ET is more complex than the original diffusion-based model, particularly under anaerobic conditions. Edwards et al. (2015) identified a highly conserved disulfide bond in MtrC that was essential for *S. oneidensis* growth under aerobic but not anaerobic conditions.[25] They concluded that this disulfide bond enables MtrC to transition between cytochrome and flavocytochrome forms while preventing reactive oxygen species.[25] Further work by Norman et al. (2023) connected this oxygen-regulated disulfide bond to regulation of

EET.[26] Under aerobic conditions, the disulfide bond forms, inducing a slight conformational change that decreases FMN-MtrC binding affinity. In contrast, under anaerobic conditions, the disulfide bond is reduced, increasing FMN-MtrC affinity and promoting flavin-based ET through the bound flavin semi-quinone form.

Building on this, Huang et al. (2023) demonstrated that flavocytochrome formation occurs in specific pairs, either FMN-MtrC or RF-OmcA, and that ET via these complexes requires continuous heme reduction from catabolic electron flow, such as lactate metabolism.[27] These findings are consistent with the flavin dependence patterns we observed. All our experiments were conducted under anaerobic conditions, however, we would expect only the outward ET group to perform EET via flavocytochrome, because lactate metabolism supplied the necessary flow of electrons for the OMC hemes to remain reduced. In contrast, the inward ET group lacked an electron source from carbon metabolism, preventing OMC heme reduction and EET via the flavocytochrome complex. Notably, Huang et al. (2023) found that the flavocytochrome complex was suppressed when the electron acceptors, fumarate or dimethyl sulfoxide were present as this led to the OMC hemes becoming oxidized.[27]

Our results suggest that inward ET is dependent on flavin diffusion for EET, while outward ET can function via either path, flavocytochrome or flavin diffusion. However, because the single ET mediated by the flavocytochrome complex proceeds much more rapidly than the 2 $e^-$ transfer that is diffusion limited, it is unsurprising that the outward ET current did not increase further with supplemental flavin.

By directly comparing inward and outward ET, we have demonstrated that *S. oneidensis* uses different EET mechanisms for inward and outward ETs under anaerobic conditions.

Additionally, we have found that our results were consistent with recent works refining the flavin-mediated EET model.

## Availability of Data and Materials

All raw data and coding scripts are available on request.

## Competing Interests

The authors declare that they have no competing interests.


## Funding

Our work was funded by the NSF CAREER award 1750785 to MT.


## Authors' Contributions

All authors participated in discussions pertaining to preliminary experiments and the conceptual framework of this project. SM performed all experiments and data processing. SM and MT interpreted the results and wrote all versions of this manuscript.


## Acknowledgements

This work was funded by the NSF CAREER award 1750785 to M. TerAvest.


## Authors' Information


### Corresponding Author

Michaela A. TerAvest – ORCID: 0000-0002-5435-3587; Email: teraves2@msu.edu

### Authors

Shaylynn D. Miller – ORCID: 0009-0007-6351-0517

Kathryne C. Ford – ORCID: 0000-0002-6357-9318

## REFERENCES


1. Jourdin L, Burdyny T. Microbial Electrosynthesis: Where Do We Go from Here? *Trends Biotechnol*. 2021;39(4):359-369. doi:10.1016/j.tibtech.2020.10.014

2. Jourdin L, Sousa J, Stralen N van, Strik DPBTB. Techno-economic assessment of microbial electrosynthesis from $CO_2$ and/or organics: An interdisciplinary roadmap towards future research and application. *Appl Energy*. 2020;279:115775. doi:10.1016/j.apenergy.2020.115775

3. Ross DE, Flynn JM, Baron DB, Gralnick JA, Bond DR. Towards Electrosynthesis in Shewanella: Energetics of Reversing the Mtr Pathway for Reductive Metabolism. Xu S yong, ed. *PLoS One*. 2011;6(2):e16649. doi:10.1371/journal.pone.0016649

4. Ford KC, Teravest MA. The Electron Transport Chain of *Shewanella oneidensis* MR-1 can Operate Bidirectionally to Enable Microbial Electrosynthesis. *Appl Environ Microbiol*. Published online December 20, 2023. doi:10.1101/2023.08.11.553014

5. Madsen CS, TerAvest MA. NADH dehydrogenases Nuo and Nqr1 contribute to extracellular electron transfer by *Shewanella oneidensis* MR-1 in bioelectrochemical systems. *Sci Rep*. 2019;9(1):1-6. doi:10.1038/s41598-019-51452-x

6. Tefft NM, Teravest MA. Reversing an Extracellular Electron Transfer Pathway for Electrode-Driven Acetoin Reduction. *ACS Synth Biol*. 2019;8(7):1590-1600. doi:10.1021/acssynbio.8b00498

7. Tefft NM, Ford K, TerAvest MA. NADH dehydrogenases drive inward electron transfer in *Shewanella oneidensis* MR-1. *Microb Biotechnol*. Published online 2022. doi:10.1111/1751-7915.14175

8. Duhl KL, Tefft NM, TerAvest MA. *Shewanella oneidensis* MR-1 utilizes both sodium- and proton-pumping NADH dehydrogenases during aerobic growth. *Appl Environ Microbiol*. 2018;84(12). doi:10.1128/AEM.00415-18

9. Rowe AR, Rajeev P, Jain A, et al. Tracking electron uptake from a cathode into Shewanella cells: Implications for energy acquisition from solid-substrate electron donors. *mBio*. 2018;9(1). doi:10.1128/mBio.02203-17

10. Miller S, Ford KC, Cross MCG, Teravest MA. Energetic constraints of metal-reducing bacteria as biocatalysts for microbial electrosynthesis. Published online April 3, 2025. doi:10.21203/RS.3.RS-4184650/V1

11. Beber ME, Gollub MG, Mozaffari D, et al. EQuilibrator 3.0: A database solution for thermodynamic constant estimation. *Nucleic Acids Res*. 2022;50(D1):D603-D609. doi:10.1093/nar/gkab1106

12. Edwards MJ, White GF, Butt JN, Richardson DJ, Clarke TA. The Crystal Structure of a Biological Insulated Transmembrane Molecular Wire. *Cell*. Published online 2020. doi:10.1016/j.cell.2020.03.032

13. Mostajabi Sarhangi S, Matyushov D V. Electron Tunneling in Biology: When Does it Matter? *ACS Omega*. 2023;8(30):27355-27365. doi:10.1021/acsomega.3c02719

14. Von Canstein H, Ogawa J, Shimizu S, Lloyd JR. Secretion of flavins by Shewanella species and their role in extracellular electron transfer. *Appl Environ Microbiol*. 2008;74(3):615-623. doi:10.1128/AEM.01387-07

15. Yang Y, Ding Y, Hu Y, et al. Enhancing Bidirectional Electron Transfer of *Shewanella oneidensis* by a Synthetic Flavin Pathway. *ACS Synth Biol*. 2015;4(7):815-823. doi:10.1021/sb500331x

16. Coursolle D, Baron DB, Bond DR, Gralnick JA. The Mtr respiratory pathway is essential for reducing flavins and electrodes in *Shewanella oneidensis*. *J Bacteriol*. 2010;192(2):467-474. doi:10.1128/JB.00925-09

17. Xu S, Jangir Y, El-Naggar MY. Disentangling the roles of free and cytochrome-bound flavins in extracellular electron transport from *Shewanella oneidensis* MR-1. *Electrochim Acta*. 2016;198:49-55. doi:10.1016/j.electacta.2016.03.074

18. Min D, Cheng L, Zhang F, et al. Enhancing Extracellular Electron Transfer of *Shewanella oneidensis* MR-1 through Coupling Improved Flavin Synthesis and Metal-Reducing Conduit for Pollutant Degradation. *Environ Sci Technol*. 2017;51(9):5082-5089. doi:10.1021/acs.est.6b04640

19. Marsili E, Baron DB, Shikhare ID, Coursolle D, Gralnick JA, Bond DR. Shewanella secretes flavins that mediate extracellular electron transfer. *Proc Natl Acad Sci U S A*. 2008;105(10):3968-3973. doi:10.1073/pnas.0710525105

20. Kotloski NJ, Gralnick JA. Flavin electron shuttles dominate extracellular electron transfer by *Shewanella oneidensis*. *mBio*. 2013;4(1). doi:10.1128/mBio.00553-12

21. Harnisch F, Freguia S. A basic tutorial on cyclic voltammetry for the investigation of electroactive microbial biofilms. *Chem Asian J*. 2012;7(3). doi:10.1002/asia.201100740

22. Jerigová M, Odziomek M, López-Salas N. “We Are Here!” Oxygen Functional Groups in Carbons for Electrochemical Applications. *ACS Omega*. 2022;7(14):11544-11554. doi:10.1021/acsomega.2c00639

23. Wang H, Fan R, Deng J. Oxygen Groups Immobilized on Micropores for Enhancing the Pseudocapacitance. Published online 2021. doi:10.1021/acssuschemeng.9b0120

24. Firer-Sherwood M, Pulcu GS, Elliott SJ. Electrochemical interrogations of the Mtr cytochromes from Shewanella: Opening a potential window. *Journal of Biological Inorganic Chemistry*. 2008;13(6):849-854. doi:10.1007/s00775-008-0398-z

25. Edwards MJ, White GF, Norman M, et al. Redox Linked Flavin Sites in Extracellular Decaheme Proteins Involved in Microbe-Mineral Electron Transfer. *Sci Rep*. 2015;5(December 2014):1-11. doi:10.1038/srep11677

26. Norman MP, Edwards MJ, White GF, et al. A Cysteine Pair Controls Flavin Reduction by Extracellular Cytochromes during Anoxic/Oxic Environmental Transitions. Brennan RG, ed. *mBio*. Published online January 16, 2023. doi:10.1128/mbio.02589-22

27. Huang W, Long X, Okamoto A. Enhancement of microbial current production by riboflavin requires the reduced heme centers in outer membrane cytochromes in *Shewanella oneidensis* MR-1. *Electrochim Acta*. 2023;464. doi:10.1016/j.electacta.2023.142860

# Chapter 4. Minimal medium primes *S. oneidensis* proteome for inward electron transfer

Shaylynn D. Miller[1, ‡], Nicholas M. Tefft[1, ‡], Andrew Scheil [1], and Michaela A. TerAvest[1, *]

[1]Department of Biochemistry and Molecular Biology, Michigan State University, East Lansing, MI, USA

[‡]These authors contributed equally

## 4. 1. Author Contributions

The differential protein abundance dataset used in this work resulted from observations by NT and MT. NT performed the experiments and sample processing to generate the proteomics dataset. SM developed the computational workflow and performed the proteomics analysis presented in this work. SM and AS created the strain of *S. oneidensis* that linked Nuo operon expression to green fluorescence protein (GFP) expression and performed the subsequent experiments reported here. SM led all data analysis reported in this work. SM and NT cowrote the section of the Methods describing sample preparation for differential protein abundance. All other areas of the manuscript were written by SM with editing from MT and NT.

## 4. 2. Abstract

Many innovative solutions for addressing the climate crisis depend on combining existing biological and technological techniques. Microbial electrosynthesis (MES) is a biotechnology that could allow the repurposing of carbon dioxide into organic carbon compounds. Advancing MES requires a deeper understanding of how microbes regulate extracellular electron transfer (ET). Here, we establish a link between increased inward ET ability and higher *nuo* operon expression in *S. oneidensis* MR-1. We observed that

pre-culture medium influenced inward ET in *S. oneidensis* and performed bioelectrochemical system (BES) experiments to test the hypothesis that growth in minimal medium enhances extracellular ET. We found that inward ET, but not outward ET, was increased in *S. oneidensis* pre-cultured in minimal medium compared to rich medium. To gain a proteome-level understanding of this result, we performed differential proteomics analysis on electrode-attached cells following BES experiments. More abundant and less abundant proteins were analyzed in Cytoscape to identify distinct functional protein modules. Additionally, we compared the expression of a differentially regulated operon using an in-genome green fluorescent protein indicator. We found that *S. oneidensis* grown in minimal medium exhibited a proteome shift favoring pathways associated with energy conservation and redox balance, suggesting a restructuring of metabolic priorities that supports inward ET. These results indicate that pre-culture conditions can influence the proteome during BES experiments conducted without a carbon source. Our findings provide new insights into the relationship between BES performance and the metabolic history of the microbes involved, with implications for optimizing microbial electrosynthesis.

**Keywords:** microbial electrochemistry, biotechnology, electrosynthesis, *Shewanella*, metabolism

### 4. 3. Introduction

Our biotechnological abilities are rapidly advancing, providing innovative solutions to address the growing climate crisis. However, even promising options face challenges related to efficiency and scalability.[1] Biotechnologies integrate traditional technologies with compatible biological systems. For example, systems that integrate electrochemical processes with bacteria capable of extracellular electron transfer (ET) are increasingly

pursued areas of study due to their versatility in bioelectrochemical applications.[2,3] Such systems leverage microbes to generate or consume electricity, enabling processes such as bioremediation, biosensing, and more. One bacterial species with a well-understood extracellular ET pathway is the metal-reducing bacterium *Shewanella oneidensis*.[4–7] Known for its metabolic flexibility, *S. oneidensis* donates electrons to extracellular electron acceptors via its metal-reduction (Mtr) pathway.[5] Beyond its ability to funnel electrons out of the cell to access extracellular terminal electron acceptors when oxygen is scarce, the Mtr pathway is bidirectional, enabling *S. oneidensis* to perform electrode-driven periplasmic and intracellular reduction reactions. When *S. oneidensis* respires using an extracellular electron acceptor, electrons are transferred from the cytoplasm to the quinone pool when an electron carrier (e.g., NADH) is oxidized by a dehydrogenase in the inner membrane (e.g., NADH dehydrogenase).[8] From the quinone pool, electrons travel to extracellular electron acceptors via several multiheme cytochromes, beginning with CymA.[8] From CymA, the periplasmic cytochrome CctA and other small tetraheme cytochromes allow electrons to cross the periplasmic space and exit through the MtrCAB electron conduit in the outer membrane.[8]

While outward ET (from bacterium to extracellular electron acceptor) is the direction used for respiratory purposes, *S. oneidensis* can also support inward ET (from extracellular electron donor to bacterium).[4] Indeed, in Tefft and TerAvest (2019), we demonstrated that *S. oneidensis* MR-1 can perform electrode-driven cytoplasmic reduction reactions when expressing the non-native NADH-dependent enzyme, butanediol dehydrogenase.[9] During this process, inward ET proceeds through the Mtr pathway and reduces the respiratory quinone pool. From the quinone pool, electrons flow from reduced quinones

to cytoplasmic $NAD^+$ via proton- or sodium-pumping NADH-dehydrogenases.[7] By replenishing the proton motive force in the periplasmic space using proteorhodopsin (PR), a light-driven proton-pump, we were able to drive the NADH-dehydrogenase to facilitate inward ET to the cytoplasm.[9] In further work with this system, we observed that pre-culture

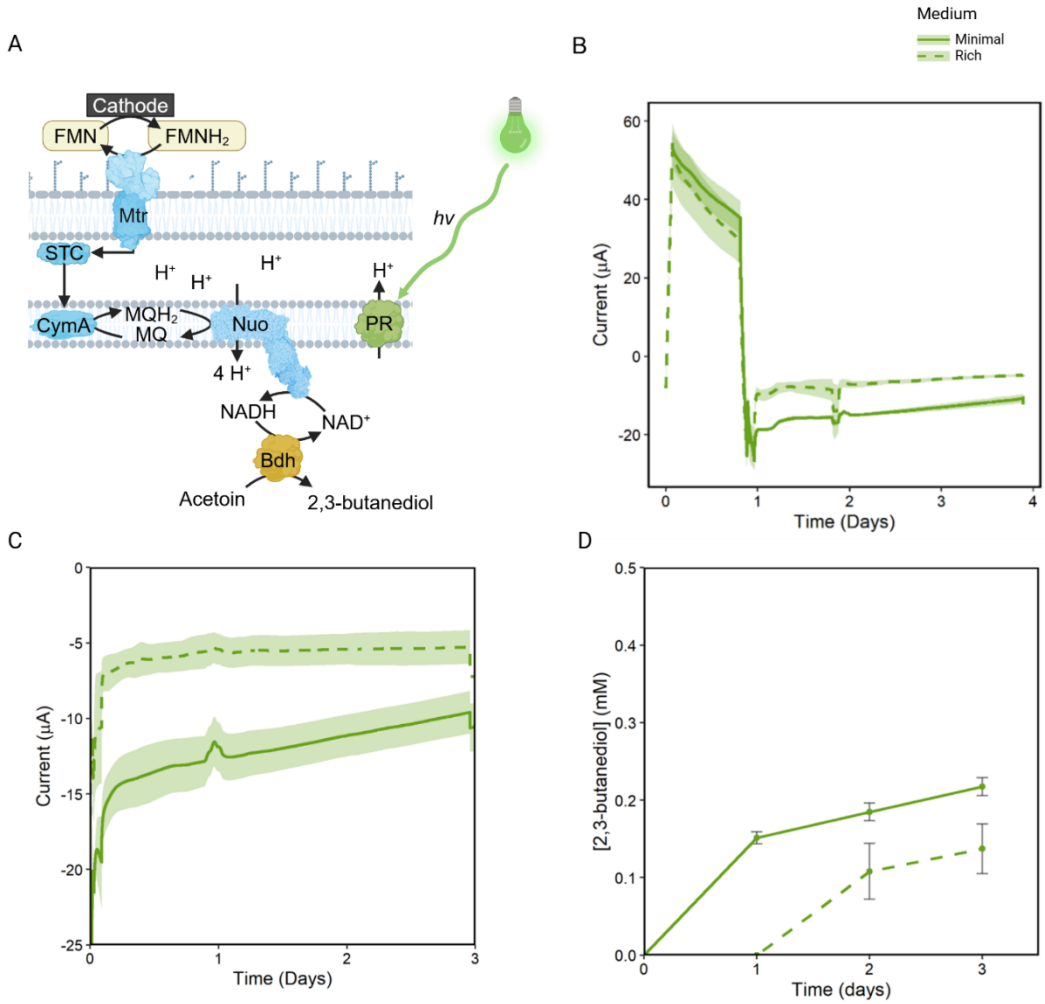


*Figure 4-1. Bioelectrochemical system data for pre-cultures in minimal medium and rich medium. Panel A, A representation of the ET pathway in S. oneidensis +Bdh-PR. The Mtr pathway (Mtr), a periplasmic small tetraheme cytochrome (STC), menaquinone (MQ), menaquinol ($MQH_2$), proteorhodopsin (PR, a light-driven proton pump), Bdh (butanediol dehydrogenase), acetoin (the substrate of Bdh), and oxidized flavin (FMN) and reduced flavin ($FMNH_2$). Panel B is the electric current passed over time, where the electrode potential was changed from an anodic potential (S. oneidensis reduces the electrode) to a cathodic potential (S. oneidensis oxidizes the electrode). Panel C is the same as Panel B, but with an adjusted y-axis scale. Panel D is the concentration of 2,3-butanediol (mM) over time. See Tefft et al. (2019) for more information on this system.*

conditions influence the rate of inward ET but not outward ET in a bioelectrochemical system (BES) (Figure 4-1).[10]

While rapid shifts in extracellular ET direction can be controlled post-translationally via a redox switch, we expected that such a temporal difference would be related to an earlier level of regulation.[10] We hypothesized that *S. oneidensis* pre-cultured in minimal versus rich medium undergoes a proteome shift that favors inward ET. To test this hypothesis, we combined bioelectrochemical measurements with proteomic analysis to determine whether the observed differences in inward ET correlate with proteomic changes associated with inward ET.

## 4. 4. Methods

### 4. 4. 1 Bioelectrochemical system setup

We prepared BESs for this work as described.[9] Briefly, all BESs consisted of two blown-glass chambers separated by a cation exchange membrane (Membranes International, CMI-7000S). We used a three-electrode system where the working electrode was carbon felt (Alfa Aesar, 43200RF) cut to 50 mm x 25 mm and connected to a titanium wire with carbon adhesive (Sigma-Aldrich, 09929-30G). The counter electrode was a graphite rod (Electron Microscopy Science, 07200). The reference electrode was housed in a glass tube with a magnesia frit (Sigma-Aldrich, 31408-1EA) that separated the interior of the reference electrode from the BES medium; inside the glass housing was a saturated (potassium chloride) Ag/AgCl reference electrode. All working electrode chambers, regardless of medium during pre-culture, contained 170 ml of M5 BES minimal medium (100 mM HEPES, 1.29 mM $K_2HPO_4$, 1.65 mM $KH_2PO_4$, 7.87 mM NaCl, 1.70 mM $NH_4SO_4$, 475 µM $MgSO_4 \cdot 7H_2O$, 50 µg·mL$^{-1}$ kanamycin (kan), 0.2 mM riboflavin, 1X Wolfe's mineral solution (without $AlK(SO_4)_2 \cdot 12\ H_2O$), and 1X Wolfe's vitamin solution (without riboflavin),

and adjusted to pH 7.2). The BES counter chamber was filled with PBS, and all electrodes were secured into a flanged port of the appropriate BES chamber via butyl rubber septum stoppers. Except for the temperature sensitive solutions that were filter-sterilized (i.e., vitamins, minerals, riboflavin, and antibiotic), we assembled and autoclaved each BES prior to use. We controlled the working electrode voltage with a potentiostat (VMP, BioLogic USA).

Prior to BES inoculation, we prepared pre-cultures in either rich medium or minimal medium. Rich medium was LB+kan, whereas minimal medium was M5+kan. In contrast to the minimal medium used in our BESs, M5 minimal medium for pre-culture had the following differences: 10 mM instead of 100 mM HEPES buffer, it included 20 mM D,L-lactate and 0.01% (w/v) casamino acids, and it lacked supplemental riboflavin. Sterile 250 ml flasks, with 50 ml of either minimal medium or rich medium were inoculated with 0.1 ml of MR-1 +Bdh-PR standardized to an optical density of 1.0 $OD_{600}$ from a 5 ml LB+kan overnight culture (approximately 16-20 hours). After inoculation, pre-culture flasks were incubated at 30°C with shaking (275 rpm) for 17 hours for minimal medium and 8 hours for rich medium ($OD_{600}$ ~0.55). The preculture flasks were then incubated an additional 1 hour with 50 µl of 20 mM trans-retinal (vitamin A aldehyde from Sigma Aldrich, R2500). Retinal was added because it is a required cofactor for proteorhodopsin, the light-driven proton pump expressed by strain MR-1 +Bdh-PR.[11]

After the 1-hour incubation with retinal, we prepared pre-cultures for BES inoculation. Regardless of pre-culture medium, each pre-culture was centrifuged for 5 minutes at 8,000 rpm (Thermo Scientific ST8R; Rotor: 75005709) and washed twice with 50 ml of sterile minimal medium lacking a carbon source. Each biological replicate was

standardized to an optical density of 3.6 $OD_{600}$ and 9 ml of the standardized culture was injected into each BES. Throughout each experiment we kept the working electrode chamber at 30°C via a water jacket and heated water pump, illuminated with green LED lights, and continuous mixing with a magnetic stir bar.

We collected abiotic background current for a minimum of 5 hours prior inoculation. All periods of anodic electrode voltage were set to +0.2 $V_{Ag/AgCl}$, while all cathodic voltage was set to -0.5 $V_{Ag/AgCl}$.

After inoculation, the first 40 hours of each experiment had a working electrode potential of +0.2 $V_{Ag/AgCl}$, before the electrode potential was changed to -0.5 $V_{Ag/AgCl}$. Three hours after the electrode potential was changed from anodic to cathodic, we injected sterile, anaerobic acetoin into the working chamber for a final concentration of 20 mM.

Additionally, there was a 6-hour period of ambient air following inoculation before we began nitrogen bubbling (99.9% $N_2$, Airgas) into the working electrode chamber through a sterile 0.2 µm filter inserted into a butyl rubber stopper at the bottom of the working chamber. Gas outflow from the working chamber was directed through another sterile filter into a glass bubbler containing RO water. After we began nitrogen bubbling, the system remained anaerobic for the duration of the experiment. Immediately after the end of each BES experiment the working electrode of each replicate was frozen (-20°C) in a sterile conical tube prior to beginning proteolytic digestion.

### 4. 4. 2 Proteomic sample processing

#### 4.4.2.1 Proteolytic Digestion

We extracted protein for differential protein analysis from the carbon felt working electrode of each biological replicate. To extract protein from *S. oneidensis* attached to carbon felt working electrodes we followed the protocol established by Grobbler et al. (2015) for *S.*

*oneidensis* on carbon cloth electrodes.[12] Aliquots from each sample equal to 50 µg of protein were precipitated using a 1:4 ratio of chloroform to methanol. Protein pellets were re-suspended in 270 µl of 4% (w/v) sodium deoxycholate (SDC) in 100 mM Tris, pH 8.5, then reduced and alkylated by adding tris-2(-carboxyethyl)-phosphine and Iodoacetamide at 10 mM and 40 mM, respectively. Samples were then incubated for 5 minutes at 45°C with shaking at 2,000 rpm in an Eppendorf ThermoMixer. Trypsin, in 50 mM ammonium bicarbonate, was added at a 1:100 ratio (w/w) and the mixture was incubated at 37°C overnight with shaking at 2,000 rpm in the ThermoMixer. The final volume of each digest was ~300 µl. After digestion, SDC was removed by adding 1% (v/v) each of ethyl acetate and trifluoracetic acid (TFA). Samples were then centrifuged at 15,7000 x g for 3 minutes to pellet the SDC mixture and the supernatant removed to a new tube. Peptides were then subjected to C18 solid phase clean up using StageTips (Rappsilber et al., 2007) to remove salts and eluates dried by vacuum centrifugation.[13]

#### 4.4.2.2 Isotopic/Isobaric Peptide Labeling

Peptide samples were re-suspended in 100 µl of 100 mM triethylammonium bicarbonate and labeled with tandem mass tag (TMT) reagents from Thermo Scientific (www.thermo.com) according to manufacturers' instructions. Aliquots of 2 µl were taken from each labeled sample and reserved for testing labeling/mixing efficiency by MS. Labeling efficiency was calculated at >97% for all labels. Remaining labeled peptides were mixed 1:1 and purified by solid phase extraction using c18 StageTips.[13] Eluted peptides were dried by vacuum centrifugation to ~2 µl and stored at -20°C. Prior to injection the purified peptides were re-suspended in 2% acetonitrile/0.1%TFA to 20 µl.

#### 4.4.2.3 LC-MS/MS Analysis

The sample was diluted 1:10 on plate in 2% acetonitrile/0.1% TFA and an injection of 5 µl was automatically made using a Thermo (www.thermo.com) EASYnLC 1200 onto a Thermo Acclaim PepMap RSLC 0.1 mm x 20 mm C18 trapping column and washed for ~5 min with buffer A. Bound peptides were then eluted over 245 min onto a Thermo Acclaim PepMap RSLC 0.075mm x 250mm resolving column with a gradient of 2%B to 28%B in 24 min, ramping to 90%B at 25 min and held at 90%B for the duration of the run (Buffer A = 99.9% water/0.1% formic acid, Buffer B = 80% acetonitrile/0.1% formic acid/19.9% water) at a constant flow rate of 300 nl/min. Column temperature was maintained at a constant temperature of 50°C using and integrated column oven (PRSO-V2, Sonation GmbH, Biberach, Germany).

Eluted peptides were sprayed into a ThermoScientific Q-Exactive HF-X mass spectrometer (www.thermo.com) using a FlexSpray spray ion source. Survey scans were taken in the Orbi trap (120,000 resolution, determined at m/z 200) and the top ten in each survey scan were subjected to automatic higher energy collision induced dissociation with fragment spectra acquired at 45,000 resolution. The resulting MS/MS spectra were converted to peak lists using MaxQuant, v1.6.3.4 (www.maxquant.org) and searched against a protein sequence database containing all entries for S. oneidensis (downloaded from www.uniprot.org on 2019-10-15), customer provided sequences and common laboratory contaminants (downloaded from www.thegpm.org, cRAP project) using the Andromeda search algorithm, a part of the MaxQuant environment.[14,15] The Mascot output was then analyzed using Scaffold, v4.11.1 (www.proteomesoftware.com), to probabilistically validate protein identifications. Assignments validated using the Scaffold 1% false discovery rate (FDR) confidence filter are considered true.

### 4. 4. 3 Differential protein expression analysis

#### 4.4.3.1 Relative protein abundance and significance

For proteins that passed the 1% FDR threshold, we proceeded with differential protein expression analysis, where we compared protein abundance for *S. oneidensis* pre-cultured in minimal medium versus rich medium. For each protein, we calculated the $\log_2$ fold change ($\log_2$FC) between the minimal medium and rich medium groups by first applying a $\log_2$ transformation to each replicate's intensity value. We computed the average $\log_2$ intensity value separately for each group (minimal medium and rich medium). The $\log_2$FC for a given protein was calculated as the difference between the group averages.

As our protein intensity distributions were not normally distributed, we used a Mann-Whitney U Test, a non-parametric test to determine which proteins differed significantly in TMT reporter ion intensity for minimal and rich medium groups. To control false positives, we used a Benjamini-Hochberg ($p < 0.03066$) false discovery rate (FDR) p-value correction, performed within Scaffold using manufacturer recommended settings. Additionally, we plotted the identified proteins in a volcano plot to visualize proteins of interest while accounting for both significance and fold change. Rather than use common, but arbitrary cut-offs for the negative logarithm transformed p-value and $\text{Log}_2$FC, we used the π-metric (pi-metric) to identify proteins of interest. The π-metric is calculated as $\pi = -\log_{10}(\text{p-value}) \times \log_2(\text{FC})$, so that both fold change and p-value can contribute simultaneously.[16] The advantage of the π-metric is that it better accounts for biologically significant proteins that would be missed in situations where either the fold change or p-value is significant, but the other value does not cross its independent threshold.[16] In this work we used the π-metric definitions established by Xiao et al. (2014), that correspond

to the commonly used cut-offs for a statistically significant fold change ($log_2FC > 2.0$ and p-value < 0.05). The high and moderate π-metric correspond to a log2FC of 2.0 with a p-value under 0.01 and 0.05, respectively.[16]

#### 4.4.3.2 Network analysis

We performed network analysis on all proteins that met the criteria of either a moderate or high π-metric. Separate protein-protein interaction (PPI) networks were generated in Cytoscape for significantly more abundant and less abundant proteins. For each group, we constructed two networks: (1) a comprehensive STRING-predicted PPI network, which includes all predicted and experimentally validated interactions based on the selected confidence score and species, and (2) a physical interaction-only network, containing only direct physical PPIs. The network analysis workflow (Figure 4-2) began with the STRING-predicted network, which represents high-level interactions encompassing both functional and physical associations. However, these clusters do not inherently reflect biologically distinct functional modules. To derive a more biologically relevant network, we applied Markov Cluster Algorithm (MCL) clustering in Cytoscape (granularity = 2.0), which grouped proteins into functionally connected clusters (e.g., metabolic pathways, protein complexes). Once MCL clustering identified functional modules, we performed STRING group-wise functional enrichment analysis, using the *S. oneidensis* genome as the reference background. This allowed us to assign enriched biological functions to individual protein clusters, facilitating pathway-level interpretation of significantly more abundant and less abundant protein groups identified in the volcano plot.

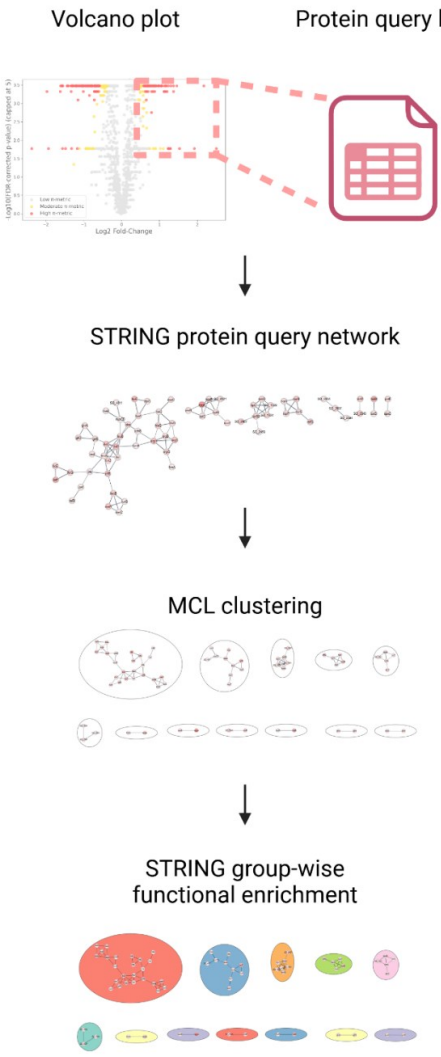


*Figure 4-2. Network analysis workflow for differential protein abundance data.*

### 4. 4. 4 Strain construction

To link green fluorescent protein (GFP) expression to *nuo* operon expression in *S. oneidensis, we* designed a gBlock (Integrated DNA Technologies) that had the superfolder GFP ribosome binding site and the superfolder GFP coding sequence flanked by the 795 bp immediately upstream of the *nuoN* stop codon and the 625 bp immediately downstream of the *nuoN* stop codon. On either side of those segments flanking the *nuoN* stop codon were SpeI restriction sites, each with an extra 33 bp of DNA sequence to

protect the SpeI restriction sites. We ligated the insert into pSMV3.0, a non-replicating vector for *S. oneidensis* that can be maintained in *Escherichia coli* WM3064, derived from strain B2155.[17] WM3064 is an *E. coli* strain that is auxotrophic for diaminopimelic acid (DAP) and, with pSMV3.0, carries kanamycin (kan) resistance. We grew WM3064 at 37°C (250 rpm) in LB (lysogeny broth, Miller, Acumedia BD) with 30 µg/mL of DAP, and 50 µg/mL of kan.

We isolated pSMV3.0 from WM3064 +pSMV3.0 with E.Z.N.A. Plasmid DNA Kit (Omega, Bio-Tek), and digested both the plasmid and the DNA insert with SpeI-HF (New England Biolabs) for approximately 2-4 hours. Following plasmid digestion, we treated the vector with Antarctic Phosphatase (New England Biolabs) to remove the 5' and 3' phosphate groups and prevent re-circularization without the DNA insert. We ligated the DNA insert into the corresponding SpeI site of the pSMV3.0 vector. Once pSMV3.0 contained the insert for adding GFP to the end of the *nuo* operon, we transformed the plasmid into WM3064. We then performed a conjugation with *S. oneidensis* and WM3064 +pSMV3.0 (NuoN:GFP insert). As pSMV3.0 carries the gene *sacB*, we isolated the mutant strain via sucrose counter selection, followed by Sanger sequencing to verify that the new *S. oneidensis* strain contained *GFP* directly downstream from *nuoN*, the end of the *nuo* operon.

**4. 4. 5 GFP fluorescence as an indicator of Nuo operon expression**

To compare *nuo* operon expression when *S. oneidensis* is cultured in either minimal or rich medium, we created the following strain: *S. oneidensis* Nuo:GFP. In *S. oneidensis* Nuo:GFP, the super folder GFP coding sequence was inserted downstream of the *nuoN* stop codon. We grew *S. oneidensis* Nuo:GFP aerobically in a 24-well plate (Greiner Bio-One, 662165) in a Synergy H1 plate reader (BioTek Instruments, Winooski, VT).

Minimal medium was M5 (10 mM HEPES, 20 mM D,L-Lactate, 0.01% (w/v) casamino acids, 1.29 mM $K_2HPO_4$, 1.65 mM $KH_2PO_4$, 7.87 mM NaCl, 1.70 mM $NH_4SO_4$, 475 µM $MgSO_4 \cdot 7H_2O$, 1X Wolfe's mineral solution (without $AlK(SO_4)_2 \cdot 12\ H_2O$), and 1X Wolfe's vitamin solution (without riboflavin), and adjusted to pH 7.2) and rich medium (LB). Cells were incubated throughout plate reader experiments at 30°C with orbital shaking. Each well had a volume of 1 ml of medium that was inoculated with 10 µl of culture standardized to an optical density ($OD_{600}$) of 1.0.

The culture OD was measured at a wavelength of 600 nm; the excitation and emission wavelengths for GFP were 485 nm and 530 nm, respectively; and the optical gain was set to 50. All GFP fluorescence values were normalized to $OD_{600}$.

## 4. 5. Results

### 4. 5. 1 Inward ET but not outward ET performance improved when cells were pre-cultured in minimal medium compared to rich medium.

We previously observed that pre-culture medium appeared to influence ET phenotype. To better understand this, we repeated BES experiments with the strain we used to demonstrate proof-of-concept for this system, *S. oneidensis* Δ*hyaB*Δ*hydA +Bdh-PR (*MR-1 +Bdh-PR*).* We assessed the current production and 2,3-butanediol concentration that each pre-culture group produced during inward ET. The BES working electrodes were initially poised at an anodic potential (+0.2 $V_{Ag/AgCl}$) to encourage oxidation of residual organic carbon, then switched to a cathodic potential. Three hours after the electrode potential was switched from anodic to cathodic potential (-0.5 $V_{Ag/AgCl}$), we injected acetoin. Prior to acetoin injection, the cathode is the electron donor, but there is no terminal electron acceptor, therefore low background current levels are observed. Once acetoin is in the BES, Bdh can reduce acetoin to 2,3-butanediol and current levels for

both groups of cells increased.

When *MR-1 +Bdh-PR* was pre-cultured in minimal medium (M5) it displayed a higher current magnitude during inward ET than when it was pre-cultured in rich medium (LB). Pre-culture medium only appeared to influence inward ET performance; outward ET between the two pre-culture groups during the initial phase of the experiment was indistinguishable. However, while inward ET in this system could be accurately assessed due to the NADH-dependent reduction of acetoin to 2,3-butanediol, the outward electron transfer period did not include an electron donating substrate, like lactate. Additionally, we found that the increase in inward ET current magnitude was reflected in an increase in 2,3-butanediol accumulation.

Because the difference between the two groups of cells persisted after being inoculated into identical bioelectrochemical cells, we hypothesized that the discrepancy in inward ET performance was due to changes in the proteome. For each BES biological replicate, protein from each electrode was extracted, digested, labeled, and analyzed via LC-MS/MS. Peptides were identified and quantified, as discussed in the Methods section allowing us to convert peptide intensities into log-transformed fold-changes ($log_2FC$). A positive $log_2FC$ represents a protein that was more abundant in the minimal medium preculture group compared to the rich medium group, whereas a negative $log_2FC$ represents a protein being less abundant in the minimal medium group compared to the rich medium group. We used a volcano plot and calculated π-metric to select proteins of interest for further analysis. A π-metric integrates both fold change and p-value to better capture biological significance, avoiding the biases of arbitrary cutoffs. Using this

approach, we identified 161 proteins that were significantly more abundant and 227 proteins that were significantly less abundant in the minimal medium compared to the rich medium pre-culture group (Figure 4-3). In addition to differential protein abundance from proteins native to *S. oneidensis*, we also observed differential protein abundance of the heterologously expressed proteins, PR and Bdh. Both PR and Bdh, expressed constitutively from the pBBR1 plasmid as described in Tefft et al. (2019), were significantly ($p<0.05$) more abundant in *S. oneidensis* pre-cultured in minimal medium compared to rich medium.

### 4. 5. 2 Pre-culture in minimal medium alters proteomic network connectivity while preserving overall structure

To assess differences in protein connectivity and network organization, we analyzed two independent STRING networks for proteins that were significantly more abundant and

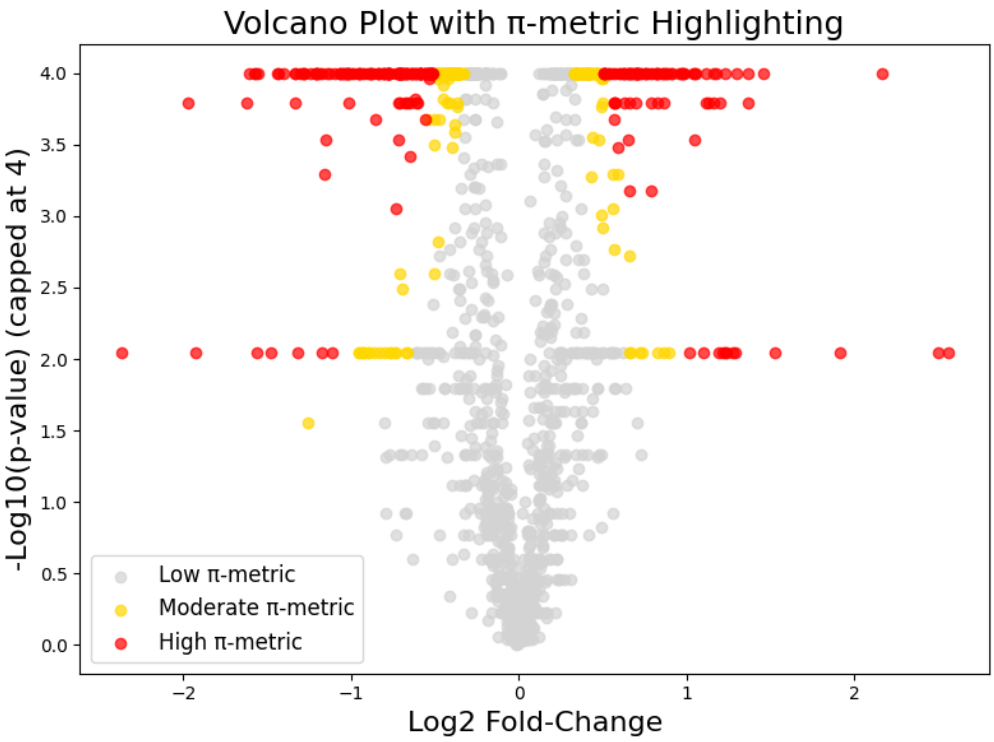


*Figure 4-3. Volcano plot for comparing significance and fold change. The line-like appearance at a Y value of 4.0 is due to the analysis software (Scaffold) capping significant p-values at 0.0001.*

less abundant in the group pre-cultured in minimal medium, compared to those pre-cultured in rich medium. Both the more abundant and less abundant MCL clustered PPI) networks were analyzed using three key network topology metrics: degree, betweenness centrality, and clustering coefficient (Figure 4-4).

In these networks, each protein is represented as a node, and each PPI is represented as an edge (a line connecting two nodes). Degree measures the number of direct connections (edges) a protein (node) has within the network, which reflects how central a protein is to cellular processes. By comparing these metrics between conditions, we can determine whether changes in protein abundance correspond to network rewiring, shifts in functional interactions, or alterations in pathway cohesion, providing a systems-level perspective on inward ET. Of these metrics, degree differed significantly between the more abundant and less abundant networks, with an FDR-corrected p-value of $1.55 \cdot 10^{-10}$ and a Wilcoxon statistic of -6.57 (Figure 4-4). The lack of significant differences in betweenness centrality and clustering coefficient indicates that while connectivity

changed, the fundamental organization of the network remained stable.

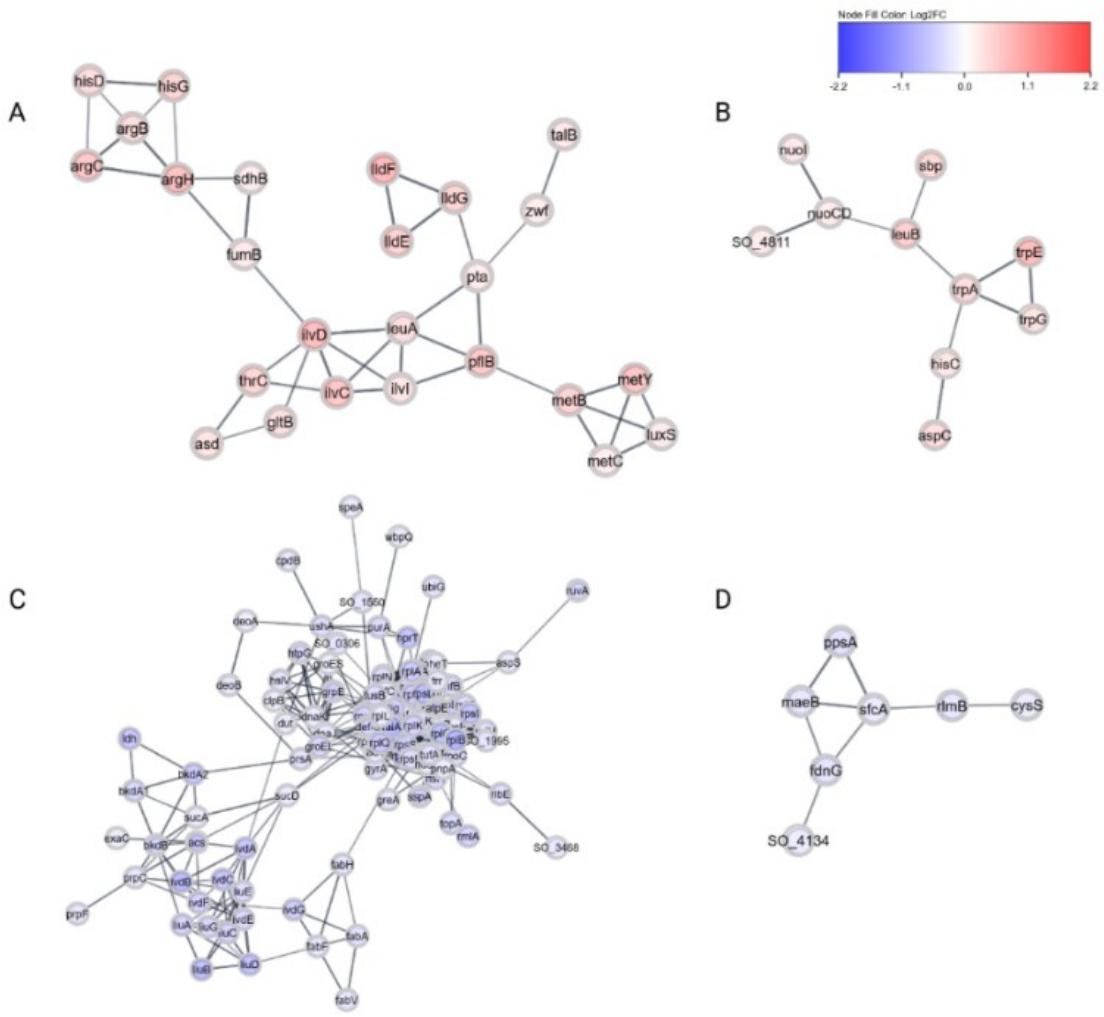


*Figure 4-4. Differential protein network analysis. Proteins that were significantly more or less abundant in minimal medium, were quieried in Cytoscape with the STRING plugin. The proteins in the protein-protein interaction (PPI) networks produced by STRING were then grouped based on functional role with MCL clustering. The largest two clusters of proteins that were more (A and B) or less (C and D) abundant in cells precultured in minimal medium are shown. Panels E, F, and G are metrics of network connectedness. Panel E shows the degree distribution, representing the number of protein-protein interactions per protein; this distribution is useful for evaluating overall interconnectedness in the network. Panel F shows the betweenness centrality distribution, indicating the probability that a given protein lies on the shortest path between two others, reflecting its role in connecting subnetworks. Panel G shows the clustering coefficient distribution, describing how frequently a protein's interaction partners also interact with each other, which reflects the extent of local clustering in the network.*

Figure 4-4 (Cont'd)

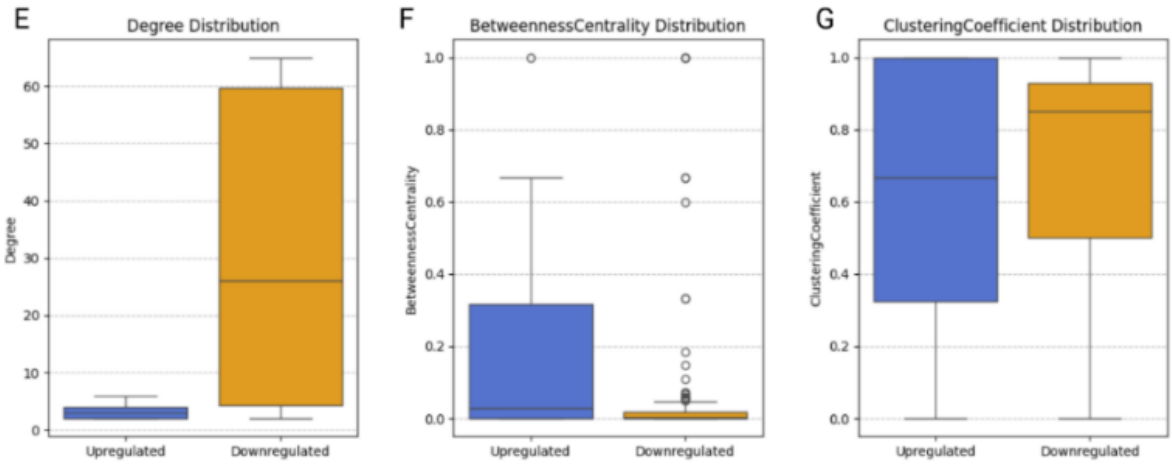


### 4. 5. 3 Pre-culture in minimal medium less abundant translation and more abundant pyruvate and lactate metabolism

We identified KEGG pathways and gene ontology (GO) terms that were enriched in differentially abundant network clusters compared to the *S. oneidensis* reference genome. The most significantly enriched terms are shown in Table 4-1 for the more abundant network and in Table 4-2 for the less abundant network. The top five terms are shown for each cluster, unless the total number is less than five. We applied STRING group-wise functional enrichment to each MCL cluster. For clarity, the enrichment tables were filtered in Cytoscape to remove redundant KEGG pathway and GO terms, only showing the most significant term for a given pathway or GO term.

The largest PPI cluster for the more abundant network (Figure 4-4) was enriched for KEGG pathways relating to metabolic flexibility, lactate metabolism, pyruvate metabolism, and amino acid biosynthesis (Table 4-1, Cluster 1).

While the second largest cluster (Table 4-1, Cluster 2) in the more abundant network was also enriched for amino acid synthesis, the enriched terms also included terms relating to quorum sensing and NADH dehydrogenase complexes. Less abundant KEGG pathway

and GO terms included those related to translation, both generally (GO:0006412; 'translation') and specifically (GO:0015934; 'large ribosomal subunit').

*Table 4-1. Enrichment table for the top most abundant clusters. Included are Kegg terms, GO Biological Process, GO Molecular Functions, and GO Cellular Components.*

| Cluster | Pathway ID | Pathway Description | FDR p-value | Genes |
|---|---|---|---|---|
| 1 | son01230 | Biosynthesis of amino acids | 3.80E-17 | *argC* \| *argB* \| *argH* \| *luxS* \| *gltB* \| *hisD* \| *hisG* \| *metC* \| *ilvI* \| *asd* \| *thrC* \| *talB* \| *metB* \| *leuA* \| *ilvD* \| *ilvC* |
| 1 | son01210 | 2-Oxocarboxylic acid metabolism | 1.04E-08 | *argC* \| *argB* \| *ilvI* \| *asd* \| *leuA* \| *ilvD* \| *ilvC* |
| 1 | son01120 | Microbial metabolism in diverse environments | 8.61E-06 | *gltB* \| *sdhB* \| *fumB* \| *zwf* \| *pflB* \| *pta* \| *asd* \| *thrC* \| *talB* |
| 1 | son00270 | Cysteine and methionine metabolism | 5.02E-05 | *metY* \| *luxS* \| *metC* \| *asd* \| *metB* |
| 1 | son00620 | Pyruvate metabolism | 8.40E-04 | *fumB* \| *pflB* \| *pta* \| *leuA* |
| 2 | son00400 | Phenylalanine, tyrosine and tryptophan biosynthesis | 1.87E-07 | *hisC* \| *aspC* \| *trpE* \| *trpG* \| *trpA* |
| 2 | son00401 | Novobiocin biosynthesis | 0.0017 | *hisC* \| *aspC* |
| 2 | son02024 | Quorum sensing | 0.0306 | *trpE* \| *trpG* |
| 2 | GO:0030964 | NADH dehydrogenase complex | 0.045 | *nuoI* \| *nuoCD* |

Both the more and less abundant networks were significantly enriched for pyruvate metabolism (son00620), albeit for different genes. Pre-culture in minimal medium led to

a decreased abundance of ribosomal proteins and an increased abundance of proteins encoded by the *nuo* operon

In addition to analyzing STRING networks for all known PPI, we separately queried the more abundant and less abundant proteins for direct physical interactions only.[18] As shown in Figure 4-5A, the largest more abundant cluster consists of proteins encoded by the *nuo* operon, while the less abundant cluster (Figure 4-5B) primarily contains ribosomal proteins from the 50S and 30S subunits. SO_4811 is not well studied but is known to be

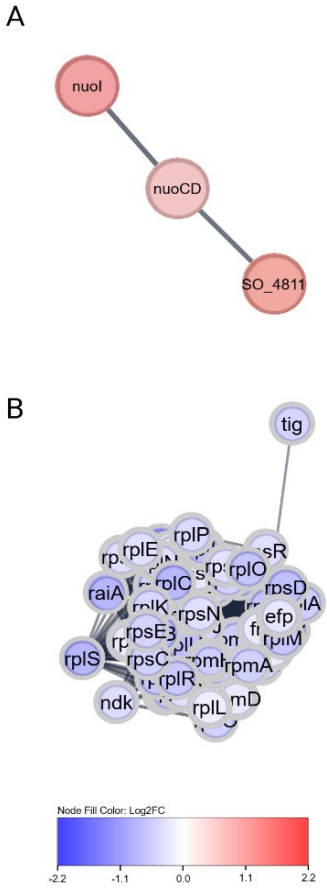


*Figure 4-5. Protein-protein network for direct physical interactions. The MCL clusters here were generated in the same way and represent a protein group with a shared molecular function. However, the MCL clusters shown above are specifically for directly physical PPIs. The clusters above are the largest MCL clusters from the group that was either more (Panel (A)) or less (Panel (B)) abundant in cells pre-cultured in minimal medium.*

from the periplasmic peptidase family M16B.[19]

*Table 4-2. Enrichment table for the least abundant clusters. Included are Kegg terms, GO Biological Process, GO Molecular Functions, and GO Cellular Components.*

| Cluster | Pathway ID | Pathway Description | FDR p-value | Genes |
|---|---|---|---|---|
| 1 | GO:0006412 | Translation | 2.85E-44 | *rpmH* \| *rplK* \| *rplA* \| *rplL* \| *rpsG* \| *tufA* \| *rpsJ* \| *rplC* \| *rplD* \| *rplB* \| *rpsS* \| *rplV* \| *rpsC* \| *rplP* \| *rpsQ* \| *rplN* \| *rplX* \| *rplE* \| *rpsN* \| *rpsH* \| *rplF* \| *rplR* \| *rpsE* \| *rpmD* \| *rplO* \| *rpsM* \| *rpsK* \| *rpsD* \| *rplQ* \| *fusB* \| *prfB* \| *nusA* \| *infB* \| *rpsO* \| *rplS* \| *rpsB* \| *tsf* \| *frr* \| *pheT* \| *infC* \| *rpmI* \| *rplT* \| *efp* \| *aspS* \| *def-3* \| *rpmF* \| *yciH* \| *rpsT* \| *rpmA* \| *rplU* \| *rplI* \| *rpsR* \| *rpsF* \| *rpsI* \| *rplM* \| *rpmG* |
| 1 | GO:0015934 | Large ribosomal subunit | 8.78E-22 | *rplK* \| *rplA* \| *rplL* \| *rplC* \| *rplB* \| *rplV* \| *rplP* \| *rplN* \| *rplX* \| *rplE* \| *rplF* \| *rplR* \| *rpmD* \| *rplO* \| *rplQ* \| *rplS* \| *rpmI* \| *rplT* \| *rpmF* \| *rpmA* \| *rplI* \| *rplM* \| *rpmG* |

Table 4-2 (cont'd)

| | | | | |
|---|---|---|---|---|
| 1 | GO:0008152 | Metabolic process | 1.77E-21 | *rpmH* \| *nusG* \| *rplK* \| *rplA* \| *rplL* \| *rpoB* \| *rpoC* \| *rpsG* \| *tufA* \| *rpsJ* \| *rplC* \| *rplD* \| *rplB* \| *rpsS* \| *rplV* \| *rpsC* \| *rplP* \| *rpsQ* \| *rplN* \| *rplX* \| *rplE* \| *rpsN* \| *rpsH* \| *rplF* \| *rplR* \| *rpsE* \| *rpmD* \| *rplO* \| *rpsM* \| *rpsK* \| *rpsD* \| *rplQ* \| *prpF* \| *prpC* \| *sspA* \| *fusB* \| *prfB* \| *dnaJ* \| *ftsH* \| *nusA* \| *infB* \| *rpsO* \| *pnpA* \| *deoA* \| *deoB* \| *rpoD* \| *rplS* \| *SO_1550* \| *rpsB* \| *tsf* \| *frr* \| *ivdA* \| *ivdB* \| *ivdC* \| *ivdE* \| *ivdF* \| *ivdG* \| *fabV* \| *fabA* \| *speA* \| *liuG* \| *liuE* \| *liuD* \| *liuC* \| *liuB* \| *liuA* \| *sucA* \| *sucD* \| *ushA* \| *adk* \| *pheT* \| *ndk* \| *infC* \| *rpmI* \| *rplT* \| *efp* \| *bkdA1* \| *bkdA2* \| *bkdB* \| *gyrA* \| *ubiG* \| *ruvA* \| *aspS* \| *def-3* \| *ldh* \| *topA* \| *acs* \| *fabF* \| *fabH* \| *rpmF* \| *wbpQ* \| *rmlA* \| *yciH* \| *raiA* \| *ribE* \| *SO_3468* \| *rpsT* \| *cpdB* \| *rpmA* \| *rplU* \| *hprT* \| *prsA* \| *rplI* \| *rpsR* \| *rpsF* \| *purA* \| *rpsI* \| *rplM* \| *hslV* \| *rpmG* \| *dut* \| *exaC* \| *atpE* |
| 1 | GO:0015935 | Small ribosomal subunit | 5.08E-16 | *rpsG* \| *rpsJ* \| *rpsS* \| *rpsC* \| *rpsQ* \| *rpsN* \| *rpsH* \| *rpsE* \| *rpsM* \| *rpsK* \| *rpsD* \| *rpsO* \| *rpsB* \| *rpsT* \| *rpsR* \| *rpsF* \| *rpsI* |
| 1 | son00280 | Valine, leucine and isoleucine degradation | 2.93E-10 | *ivdA* \| *ivdB* \| *ivdF* \| *liuG* \| *liuE* \| *liuD* \| *liuC* \| *liuB* \| *liuA* \| *bkdA1* \| *bkdA2* \| *bkdB* \| *ldh* |
| 2 | son00620 | Pyruvate metabolism | 0.0012 | *ppsA* \| *sfcA* \| *maeB* |

### 4. 5. 4 Nuo expression was higher in cells grown in minimal medium compared to rich medium at the growth phase harvested for BES experiments

Proteins encoded by the *nuo* operon were significantly enriched in the networks of proteins that were more abundant in the high-performing conditions. Our previous work has shown that Nuo, a proton-pumping NADH dehydrogenase, plays a crucial role in inward ET in *S. oneidensis*. To compare expression of the *nuo* operon in *S. oneidensis* grown to the same stage as the cultures used to inoculate the BESs in Figure 4-1, we constructed a strain of *S. oneidensis* with a gene encoding superfolder GFP downstream

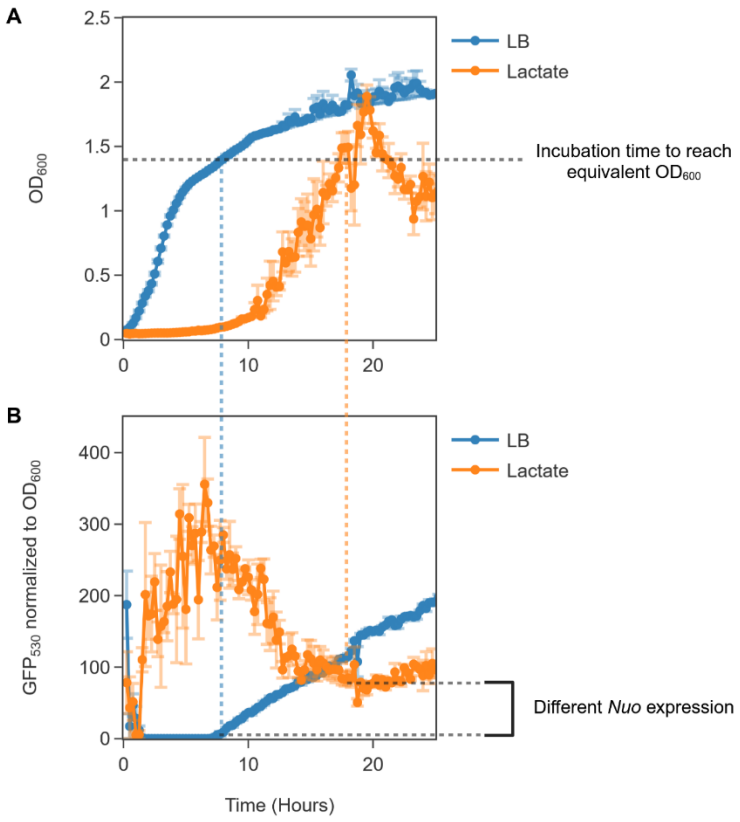


*Figure 4-6. Nuo expression tracked via GFP fluorescence during growth in rich medium (LB, blue) and minimal medium (Lactate, orange). Pannel A shows the $OD_{600}$ during growth for both rich and minimal medium conditions for S. oneidensis with a transcriptional fusion of GFP following the nuo operon. Pannel B shows the corresponding GFP fluorescence relative to $OD_{600}$. The vertical lines represent the growth point where cells were harvested for BES experiments and proteomics samples. In pannel B the horizontal lines show the difference in $OD_{600}$ normalized GFP fluorescence for cells grown in minimal and rich medium.*

of the *nuo* operon as a transcriptional fusion. We then compared the GFP fluorescence normalized to $OD_{600}$ at 8 hours for rich medium and 18 hours for minimal medium, when both cultures were at the end of the exponential growth phase. We found that cells grown in minimal medium had approximately 9.4 times higher GFP fluorescence than cells grown in rich medium for the timepoints corresponding to when pre-cultures were harvested for the BES experiments in Figure 4-6.

**4. 6. Discussion**

Here we report that proteomic shifts arising during pre-culture conditions can alter BES performance without active growth or a carbon source. In the BESs from Figure 4-1, the electron donor was a cathode, and the electron acceptor was acetoin. In this condition, the cells do not grow and the $OD_{600}$ decreases or remains stable, suggesting that there is little turnover of the proteome. We observed that *S. oneidensis* pre-cultured in minimal medium demonstrated increased inward ET compared to the same strain pre-cultured in rich medium. We harvested protein from electrode-attached cells and applied a differential protein analysis workflow to determine: 1) differences in protein abundance following identical BES experiments, and 2) differentially abundant proteins that could lead to enhanced inward ET compared to outward ET.

We found 388 differentially expressed proteins that met our statistical significance cut off. Of the 388 differentially expressed proteins, 161 were more abundant and 227 were less abundant in the group pre-cultured in minimal medium compared to rich medium. The largest functional clusters in the more abundant and less abundant PPI networks suggest that the group pre-cultured in minimal medium experienced a shift in metabolism that down regulated translation (

Table 4-2) and up regulated pathways relating to the citric acid cycle, survival in diverse

environments, pyruvate metabolism, and NADH dehydrogenases (Table 4-1).

While we identified hundreds of differentially expressed proteins, the overall structure of the proteomic network remained largely unchanged. This is evident from the distributions of betweenness centrality and clustering coefficient, which showed no statistically significant differences between more abundant and less abundant groups, indicating that key hubs and functional modules were preserved. Notably, one of the primary less abundant clusters consisted of ribosomal proteins, suggesting a shift in cellular resource allocation rather than a fundamental rewiring of metabolic pathways. These findings indicate that metabolic adaptation primarily occurred tuning existing pathways (e.g., tuning the efficiency of existing pathways) rather than structural reorganization (e.g., activating alternate pathways). That is not to imply that biological pathways operate as an on/off binary but rather to emphasize that the adaptations we observed were more consistent with flux shifting through coexisting pathways rather than a more dramatic shift that required a previously absent pathway.

Our finding that proteins from the *nuo* operon were enriched in the more abundant group (Figure 4-5), is consistent with our previous work that identified Nuo as the thermodynamically limiting step for inward ET. We hypothesized that *nuo* operon expression is higher in *S. oneidensis* grown in minimal medium compared to cells grown in rich medium at the growth phase of harvesting for our BES (late exponential growth). We tested this hypothesis by inserting GFP directly downstream of the final gene in the *nuo* operon, *nuoN*. We found that *S. oneidensis* grown to late log phase in minimal medium exhibited approximately 9.4 times higher *nuo* operon expression than cells grown to the same phase in rich medium ($OD_{600}$-normalized GFP). Although the connection

between inward ET and minimal medium was not initially clear, our experimental confirmation that *nuo* expression is elevated under these conditions reinforces the conclusions of our network analysis, suggesting a functional link between pre-culture proteomic state and inward ET capacity.

## REFERENCES


1. Prévoteau A, Carvajal-Arroyo JM, Ganigué R, Rabaey K. Microbial electrosynthesis from $CO_2$: forever a promise? *Curr Opin Biotechnol*. 2020;62:48-57. doi:10.1016/j.copbio.2019.08.014

2. Karthikeyan R, Singh R, Bose A. Microbial electron uptake in microbial electrosynthesis: a mini-review. *J Ind Microbiol Biotechnol*. 2019;46(9-10):1419-1426. doi:10.1007/s10295-019-02166-6

3. Conners EM, Rengasamy K, Bose A. Electroactive biofilms: how microbial electron transfer enables bioelectrochemical applications. *J Ind Microbiol Biotechnol*. 2022;49(4). doi:10.1093/jimb/kuac012

4. Ross DE, Flynn JM, Baron DB, Gralnick JA, Bond DR. Towards Electrosynthesis in Shewanella: Energetics of Reversing the Mtr Pathway for Reductive Metabolism. Xu S yong, ed. *PLoS One*. 2011;6(2):e16649. doi:10.1371/journal.pone.0016649

5. Coursolle D, Baron DB, Bond DR, Gralnick JA. The Mtr respiratory pathway is essential for reducing flavins and electrodes in *Shewanella oneidensis*. *J Bacteriol*. 2010;192(2):467-474. doi:10.1128/JB.00925-09

6. Gralnick JA, Bond DR. Electron Transfer Beyond the Outer Membrane: Putting Electrons to Rest. Published online 2023. doi:10.1146/annurev-micro-032221

7. Sturm G, Richter K, Doetsch A, Heide H, Louro RO, Gescher J. A dynamic periplasmic electron transfer network enables respiratory flexibility beyond a thermodynamic regulatory regime. *ISME Journal*. 2015;9(8). doi:10.1038/ismej.2014.264

8. Sun W, Lin Z, Yu Q, Cheng S, Gao H. Promoting Extracellular Electron Transfer of *Shewanella oneidensis* MR-1 by Optimizing the Periplasmic Cytochrome c Network. *Front Microbiol*. 2021;12. doi:10.3389/fmicb.2021.727709

9. Tefft NM, Teravest MA. Reversing an Extracellular Electron Transfer Pathway for Electrode-Driven Acetoin Reduction. *ACS Synth Biol*. 2019;8(7):1590-1600. doi:10.1021/acssynbio.8b00498

10. Okamoto A, Hashimoto K, Nealson KH. Flavin redox bifurcation as a mechanism for controlling the direction of electron flow during extracellular electron transfer. *Angewandte Chemie - International Edition*. 2014;53(41):10988-10991. doi:10.1002/anie.201407004

11. Fuhrman JA, Schwalbach MS, Stingl U. Proteorhodopsins: an array of physiological roles? *Nature Reviews Microbiology 2008 6:6*. 2008;6(6):488-494. doi:10.1038/NRMICRO1893

12. Grobbler C, Virdis B, Nouwens A, Harnisch F, Rabaey K, Bond PL. Use of SWATH mass spectrometry for quantitative proteomic investigation of *Shewanella oneidensis* MR-1 biofilms grown on graphite cloth electrodes. *Syst Appl Microbiol*. 2015;38(2):135-139. doi:10.1016/J.SYAPM.2014.11.007

13. Rappsilber J, Mann M, Ishihama Y. Protocol for micro-purification, enrichment, pre-fractionation and storage of peptides for proteomics using StageTips. *Nat Protoc*. 2007;2(8):1896-1906. doi:10.1038/nprot.2007.261

14. Cox J, Neuhauser N, Michalski A, Scheltema RA, Olsen J V., Mann M. Andromeda: A peptide search engine integrated into the MaxQuant environment. *J Proteome Res*. 2011;10(4):1794-1805. doi:10.1021/pr101065j

15. Cox J, Mann M. MaxQuant enables high peptide identification rates, individualized p.p.b.-range mass accuracies and proteome-wide protein quantification. *Nat Biotechnol*. 2008;26(12):1367-1372. doi:10.1038/nbt.1511

16. Xiao Y, Hsiao TH, Suresh U, et al. A novel significance score for gene selection and ranking. *Bioinformatics*. 2014;30(6):801-807. doi:10.1093/bioinformatics/btr671

17. Dehio C, Meyer M. Maintenance of broad-host-range incompatibility group P and group Q plasmids and transposition of Tn5 in Bartonella henselae following conjugal plasmid transfer from E*Escherichia coli*. *J Bacteriol*. 1997;179(2):538-540. doi:10.1128/jb.179.2.538-540.1997

18. Szklarczyk D, Gable AL, Nastou KC, et al. The STRING database in 2021: Customizable protein-protein networks, and functional characterization of user-uploaded gene/measurement sets. *Nucleic Acids Res*. 2021;49(D1):D605-D612. doi:10.1093/nar/gkaa1074

19. Heidelberg JF, Paulsen IT, Nelson KE, et al. Genome sequence of the dissimilatory metal ion–reducing bacterium *Shewanella oneidensis*. *Nat Biotechnol*. 2002;20(11):1118-1123. doi:10.1038/nbt749

# Chapter 5. Conclusions and future directions

One of the key challenges preventing MES from helping reduce net carbon emissions is the need to sufficiently improve ET from cathode to microbial cytoplasmic electron carriers. In the preceding chapters, we identified several bottlenecks that cause inward ET rates in *S. oneidensis* to be lower than outward ET rates.

## 5. 1. Inward ET through the quinone pool requires IMF

One bottleneck that limits inward ET is the thermodynamically unfavorable ET from the quinone pool to $NAD^+$. The thermodynamic model that we used to calculate the available Gibbs free energy changes assumed that ET from the reduced quinone pool to cytoplasmic $NAD^+$ was catalyzed by NADH dehydrogenases with three different energetic coupling abilities. Those NADH dehydrogenases (Nuo, Nqr, and Ndh) were coupled to PMF, SMF, or uncoupled, respectively.

We found that there were no scenarios under conditions that were biologically relevant to *S. oneidensis* where inward ET was favorable in the absence of either PMF or SMF. While this work considered the energetics of inward ET for *S. oneidensis*, there are far reaching implications for microbes performing inward ET through routes that pass through the respiratory quinone pool. As discussed previously, inward ET is the direction required for MES. As this thermodynamic bottleneck could limit MES for organisms that do not have a natural or engineered means of electrically bypassing the quinone pool, it is important to consider this limitation, and how to bypass it, in future work.[1,2] As discussed in previous chapters, we have demonstrated proof-of-concept for inward ET to the cytoplasm driven by both native and heterologous sources of PMF in *S. oneidensis*.[3,4] While sources of ion motive force must be optimized for inward ET, this is a widespread but potentially

resolvable bottleneck for inward ET in *S. oneidensis*.

**5. 2. Directional differences in flavin-mediated extracellular electron transfer**

We also compared inward and outward ET for two thermodynamically favorable electron transfers and found extracellular differences in ET mechanism. Specifically, we observed that inward and outward ET exhibit different dependence on extracellular flavin under anaerobic conditions. We found our results were consistent with recent work describing an oxygen dependent switch that toggles between a diffusive flavin and bound flavocytochrome mechanism. Under anaerobic conditions, *S. oneidensis* can use the flavocytochrome mechanism when the OMCs have a constant supply of electrons from metabolic processes, as was the case for our anaerobic condition, where lactate was the electron donor, and an anode was the electron acceptor. When the electron donor was a cathode and fumarate was the electron acceptor, we observed behavior consistent with the diffusive flavin mechanism of electron transfer.[5]

In this work we provided the first direct comparison of inward and outward ET ability for *S. oneidensis* and furthered our understanding of flavin-mediated ET in *S. oneidensis.*

**5. 3. Inward electron transfer is sensitive to proteome history**

We have also uncovered proteome-level changes that can influence inward ET ability in *S. oneidensis*. Specifically, the lingering proteome changes from growth in different pre-culture media prior to entering a BES lead to differing performance for inward ET. *S. oneidensis* precultured in minimal medium demonstrated an improved inward ET phenotype compared to *S. oneidensis* precultured in rich medium. To determine if the difference in inward ET ability was due to a proteomic difference, we performed differential proteomics analysis. We found that preculture in minimal medium compared to rich medium increased the abundance of proteins associated with cellular energy

conservation and a decrease in abundance for proteins involved in translation. We also observed that cells grown in minimal medium experienced an increased abundance of proteins from the *nuo* operon that known physical protein-protein interactions. Our results were consistent with preculture in minimal medium priming cells for inward ET due to overlap among proteins and functional modules that are important for cellular shifts towards energy conservation, and proteins that are important for inward ET.

**5. 4. Future directions**

In the preceding chapters I have identified bottlenecks that if alleviated could improve inward ET in *S. oneidensis*. While *S. oneidensis* is better known for its increasingly well-understood Mtr pathway than for achieving high current density, it remains a potential candidate for MES. There has been recent interest in improving BES efficiency by uncoupling biological and electrochemical aspects with innovative BES designs that decrease some of the issues of mass-transport limitation, ohmic drop, biofilm depth, and biofilm stratification.[6] Indeed, Zhang et al. (2024) achieved a current density of 40 $mA \cdot cm^{-2}$ with a planktonic *S. oneidensis* suspension and using artificial redox mediators in a microbial flow fuel cell.[7] It remains to be seen if this result will be replicable by other groups, but it is worth noting that the current density they reported, 40 $mA \cdot cm^{-2}$, is rather close to the current density estimated to be required for a MES given present material and electricity costs, 50-100 $mA \cdot cm^{-2}$.[6,8,9]

Additionally, as the cost of electricity is uniquely situated as a commodity that could decrease in price with support from solar panels, and electricity is ~70% of the estimated cost of such a system, it is possible that *S. oneidensis* on an anode could soon achieve a current density magnitude approaching financial feasibility. [6,8,9] In the work presented here, we have further defined the bottlenecks and mechanistic differences that distinguish

inward and outward electron transfer in *S. oneidensis*. The next steps towards a functional MES in *S. oneidensis* are to 1) alleviate the discrepancy between inward and outward ET by optimizing the supply of flavin or artificial redox carrier, 2) optimize inward ET for ion motive force generation by native or heterologous proteins, 3) replicate the high current density BES design developed by Zhang et al. (2024) and assess its utility for inward ET in *S. oneidensis* to fumarate and intracellular reduction reactions.

## REFERENCES


1. Schuchmann K, Müller V. Autotrophy at the thermodynamic limit of life: A model for energy conservation in acetogenic bacteria. *Nat Rev Microbiol*. 2014;12(12):809-821. doi:10.1038/nrmicro3365

2. Gupta D, Guzman MS, Bose A. Extracellular electron uptake by autotrophic microbes: physiological, ecological, and evolutionary implications. *J Ind Microbiol Biotechnol*. 2020;47(9-10):863-876. doi:10.1007/s10295-020-02309-0

3. Ford KC, Teravest MA. The Electron Transport Chain of *Shewanella oneidensis* MR-1 can Operate Bidirectionally to Enable Microbial Electrosynthesis. *Appl Environ Microbiol*. Published online December 20, 2023. doi:10.1101/2023.08.11.553014

4. Tefft NM, Teravest MA. Reversing an Extracellular Electron Transfer Pathway for Electrode-Driven Acetoin Reduction. *ACS Synth Biol*. 2019;8(7):1590-1600. doi:10.1021/acssynbio.8b00498

5. Miller SD, Ford KC, TerAvest MA. Outward and inward electron transfer occur through distinct mechanisms for anaerobic S. oneidensis. *Unsubmitted Intended journal: Bioelectrochemistry*. Published online 2025.

6. Jourdin L, Sousa J, Stralen N van, Strik DPBTB. Techno-economic assessment of microbial electrosynthesis from $CO_2$ and/or organics: An interdisciplinary roadmap towards future research and application. *Appl Energy*. 2020;279:115775. doi:10.1016/j.apenergy.2020.115775

7. Zhang L, Zhang Y, Liu Y, et al. High power density redox-mediated Shewanella microbial flow fuel cells. *Nat Commun*. 2024;15(1):8302. doi:10.1038/s41467-024-52498-w

8. Jourdin L, Burdyny T. Microbial Electrosynthesis: Where Do We Go from Here? *Trends Biotechnol*. 2021;39(4):359-369. doi:10.1016/j.tibtech.2020.10.014

9. Prévoteau A, Carvajal-Arroyo JM, Ganigué R, Rabaey K. Microbial electrosynthesis from $CO_2$: forever a promise? *Curr Opin Biotechnol*. 2020;62:48-57. doi:10.1016/j.copbio.2019.08.014

## APPENDIX

*Table A-1. Complete enrichment table for more abundant proteins in minimal medium group.*

| Cluster | # Background genes | # Genes | Category | Term name | Description | FDR (p-value) | Genes |
|---|---|---|---|---|---|---|---|
| 1 | 142 | 63 | STRING Clusters | CL:98 | Translation, and Protein export | 8.68E-50 | rpmH\|nusG\|rplK\|rplA\|rplL\|rpoB\|rpoC\|rpsG\|tufA\|rpsJ\|rplC\|rplD\|rplB\|rpsS\|rplV\|rpsC\|rplP\|rpsQ\|rplN\|rplX\|rplE\|rpsN\|rpsH\|rplF\|rplR\|rpsE\|rpmD\|rplO\|rpsM\|rpsK\|rpsD\|rplQ\|fusB\|prfB\|greA\|nusA\|infB\|rpsO\|rpoD\|rplS\|rpsB\|tsf\|frr\|tig\|pheT\|infC\|rpmI\|rplT\|efp\|aspS\|def-3\|rpmF\|raiA\|rpsT\|rpmA\|rplU\|rpll\|rpsR\|rpsF\|rpsI\|rplM\|rpmG\|atpE |
| 1 | 49 | 9 | STRING Clusters | CL:507 | Mixed, incl. Stress response, and Antioxidant activity | 1.10E-03 | groES\|groEL\|dnaK\|dnaJ\|ftsH\|grpE\|htpG\|clpB\|hslV |
| 1 | 591 | 36 | GO Biological Process | GO:0044281 | Small molecule metabolic process | 1.30E-03 | prpF\|prpC\|deoA\|deoB\|ivdA\|ivdE\|ivdF\|ivdG\|fabV\|fabA\|speA\|liuE |

Table A-1 (cont'd)

| | | | | | | | |
|---|---|---|---|---|---|---|---|
| | | | | | | | \|liuD\|liuB\|ushA\|adk\|pheT\|ndk\|bkdA1\|bkdA2\|bkdB\|ubiG\|aspS\|ldh\|acs\|fabF\|fabH\|wbpQ\|ribE\|SO_3468\|cpdB\|hprT\|prsA\|purA\|dut\|atpE |
| 1 | 18 | 6 | UniProt Keywords | KW-0820 | tRNA-binding | 1.30E-03 | rplA\|rpsG\|rplP\|rplE\|rpsM\|pheT |
| 1 | 290 | 22 | KEGG Pathways | son01110 | Biosynthesis of secondary metabolites | 1.70E-03 | ivdA\|ivdG\|fabV\|liuE\|sucA\|sucD\|ushA\|adk\|ndk\|bkdA1\|bkdA2\|bkdB\|ubiG\|ldh\|acs\|wbpQ\|rmlA\|ribE\|SO_3468\|hprT\|prsA\|exaC |
| 1 | 4 | 4 | GO Biological Process | GO:0006458 | De novo protein folding | 2.00E-03 | groES\|groEL\|dnaJ\|tig |
| 1 | 5 | 4 | STRING Clusters | CL:1632 | Valine catabolic process, and Acyl-CoA dehydrogenase, conserved site | 2.10E-03 | ivdB\|ivdC\|ivdE\|ivdF |
| 1 | 5 | 4 | STRING Clusters | CL:190 | Cytosolic large ribosomal subunit, and Small ribosomal subunit | 2.10E-03 | rplQ\|rplS\|rpmA\|rpsI |
| 1 | 17 | 6 | GO Molecular Function | GO:0051082 | Unfolded protein binding | 2.30E-03 | groES\|groEL\|dnaK\|dnaJ\|grpE\|htpG |

Table A-1 (cont'd)

| | | | | | | | |
|---|---|---|---|---|---|---|---|
| 1 | 340 | 24 | UniProt Keywords | KW-0547 | Nucleotide-binding | 2.50E-03 | tufA\|groEL\|fusB\|dnaK\|ftsH\|infB\|liuD\|sucD\|ushA\|htpG\|adk\|pheT\|ndk\|gyrA\|ruvA\|aspS\|ldh\|acs\|wbpQ\|cpdB\|clpB\|hprT\|prsA\|purA |
| 1 | 59 | 9 | KEGG Pathways | son00230 | Purine metabolism | 2.50E-03 | deoB\|SO_1550\|ushA\|adk\|ndk\|cpdB\|hprT\|prsA\|purA |
| 1 | 86 | 11 | STRING Clusters | CL:1203 | Carbon metabolism, and Starch and sucrose metabolism | 2.60E-03 | prpF\|prpC\|deoA\|deoB\|sucA\|sucD\|bkdA1\|bkdA2\|bkdB\|prsA\|exaC |
| 1 | 6 | 4 | STRING Clusters | CL:211 | Mixed, incl. Zinc-binding ribosomal protein, and L28p-like | 3.20E-03 | rpmF\|rpsT\|rplU\|rpmG |
| 1 | 25 | 6 | KEGG Pathways | son01212 | Fatty acid metabolism | 3.50E-03 | ivdA\|ivdG\|fabV\|fabA\|fabF\|fabH |
| 1 | 76 | 10 | STRING Clusters | CL:1204 | Carbon metabolism, and Starch and sucrose metabolism | 4.30E-03 | prpF\|prpC\|deoA\|deoB\|sucA\|sucD\|bkdA1\|bkdA2\|bkdB\|prsA |
| 1 | 5 | 4 | GO Molecular Function | GO:0070181 | Small ribosomal subunit rRNA binding | 4.50E-03 | rpsK\|rpsT\|rpsR\|rpsF |
| 1 | 87 | 11 | GO Biological Process | GO:1901565 | Organonitrogen compound catabolic process | 4.70E-03 | ftsH\|ivdC\|ivdE\|ivdF\|speA\|liuE\|liuA\|bkdA1\|bkdA2\|hslV\|dut |
| 1 | 15 | 5 | UniProt Keywor | KW-0346 | Stress response | 4.70E- | dnaK\|dnaJ\|grpE\|htpG\|clp |

Table A-1 (cont'd)

| | | | | | | | |
|---|---|---|---|---|---|---|---|
| | | | ds | | | 03 | B |
| 1 | 32 | 7 | GO Molecular Function | GO:0000049 | tRNA binding | 5.90E-03 | rplA\|rpsG\|rpsJ\|rplP\|rplE\|rpsM\|pheT |
| 1 | 18 | 5 | KEGG Pathways | son00061 | Fatty acid biosynthesis | 6.00E-03 | ivdG\|fabV\|fabA\|fabF\|fabH |
| 1 | 13 | 5 | GO Molecular Function | GO:0003746 | Translation elongation factor activity | 6.30E-03 | tufA\|fusB\|nusA\|tsf\|efp |
| 1 | 536 | 32 | GO Molecular Function | GO:0000166 | Nucleotide binding | 6.40E-03 | tufA\|groES\|groEL\|fusB\|dnaK\|dnaJ\|ftsH\|nusA\|infB\|grpE\|ivdC\|ivdF\|fabV\|liuD\|liuA\|sucD\|ushA\|htpG\|adk\|pheT\|ndk\|gyrA\|ruvA\|aspS\|ldh\|acs\|wbpQ\|cpdB\|clpB\|hprT\|prsA\|purA |
| 1 | 14 | 5 | GO Biological Process | GO:0042255 | Ribosome assembly | 6.50E-03 | rpsG\|rpsS\|rplV\|rpsK\|rplT |
| 1 | 76 | 10 | GO Biological Process | GO:0006996 | Organelle organization | 6.70E-03 | rpsG\|rpsS\|rplV\|rpsK\|fusB\|infC\|rplT\|gyrA\|ruvA\|topA |
| 1 | 7 | 4 | GO Biological Process | GO:0042026 | Protein refolding | 7.30E-03 | groEL\|dnaJ\|SO_1995\|clpB |

Table A-1 (cont'd)

| | | | | | | | |
|---|---|---|---|---|---|---|---|
| 1 | 39 | 7 | STRING Clusters | CL:1205 | Citrate cycle (TCA cycle), and Propanoate metabolism | 7.50E-03 | prpF\|prpC\|sucA\|sucD\|bkdA1\|bkdA2\|bkdB |
| 1 | 4 | 3 | KEGG Pathways | son00072 | Synthesis and degradation of ketone bodies | 9.50E-03 | ivdA\|liuG\|liuE |
| 1 | 604 | 34 | GO Molecular Function | GO:0036094 | Small molecule binding | 1.00E-02 | rpoB\|tufA\|groES\|groEL\|fusB\|dnaK\|dnaJ\|ftsH\|nusA\|infB\|grpE\|ivdC\|ivdF\|fabV\|liuD\|liuA\|sucA\|sucD\|ushA\|htpG\|adk\|pheT\|ndk\|gyrA\|ruvA\|aspS\|ldh\|acs\|wbpQ\|cpdB\|clpB\|hprT\|prsA\|purA |
| 1 | 8 | 4 | GO Biological Process | GO:0022411 | Cellular component disassembly | 1.03E-02 | fusB\|prfB\|frr\|infC |
| 1 | 10 | 4 | UniProt Keywords | KW-0275 | Fatty acid biosynthesis | 1.12E-02 | fabV\|fabA\|fabF\|fabH |
| 1 | 10 | 4 | STRING Clusters | CL:359 | RNA polymerase complex, and RNA polymerase sigma-70 | 1.26E-02 | rpoB\|rpoC\|greA\|rpoD |
| 1 | 54 | 8 | GO Biological Process | GO:0006631 | Fatty acid metabolic process | 1.35E-02 | prpF\|prpC\|ivdA\|fabV\|fabA\|liuB\|fabF\|fabH |
| 1 | 6 | 5 | InterPro Domains | IPR008991 | Translation protein SH3-like domain superfamily | 1.36E-02 | nusG\|rplB\|rplX\|rplS\|efp |
| 1 | 4 | 3 | UniProt Keywor | KW-0396 | Initiation factor | 1.41E- | infB\|infC\|yciH |

Table A-1 (cont'd)

| | | | | | | | |
|---|---|---|---|---|---|---|---|
| | | | ds | | | 02 | |
| 1 | 129 | 12 | UniProt Keywords | KW-0460 | Magnesium | 1.41E-02 | rpoC\|pnpA\|speA\|pheT\|ndk\|topA\|acs\|rmlA\|hprT\|prsA\|purA\|dut |
| 1 | 20 | 5 | STRING Clusters | CL:1207 | Citrate cycle (TCA cycle) | 1.46E-02 | sucA\|sucD\|bkdA1\|bkdA2\|bkdB |
| 1 | 3 | 3 | GO Biological Process | GO:0002181 | Cytoplasmic translation | 1.55E-02 | rplB\|rplF\|frr |
| 1 | 3 | 3 | GO Biological Process | GO:0051085 | Chaperone cofactor-dependent protein refolding | 1.55E-02 | groES\|groEL\|dnaJ |
| 1 | 32 | 6 | STRING Clusters | CL:1113 | Pyrimidine metabolism, and Purine-containing compound salvage | 1.55E-02 | SO_1550\|ushA\|adk\|ndk\|cpdB\|hprT |
| 1 | 9 | 4 | GO Molecular Function | GO:0044183 | Protein folding chaperone | 1.64E-02 | groES\|groEL\|dnaK\|tig |
| 1 | 27 | 5 | GO Cellular Component | GO:1990234 | Transferase complex | 1.72E-02 | rpoB\|rpoC\|sucA\|ribE\|prsA |
| 1 | 10 | 4 | GO Biological Process | GO:0061077 | Chaperone-mediated protein folding | 1.77E-02 | groES\|groEL\|dnaJ\|tig |
| 1 | 39 | 6 | KEGG Pathways | son00240 | Pyrimidine metabolism | 1.95E-02 | deoA\|SO_1550\|ushA\|ndk\|cpdB\|dut |
| 1 | 5 | 3 | UniProt Keywords | KW-0488 | Methylation | 1.98E-02 | rplK\|rplC\|prfB |

Table A-1 (cont'd)

| | | | | | | | |
|---|---|---|---|---|---|---|---|
| 1 | 20 | 5 | GO Biological Process | GO:0006351 | Transcription, DNA-templated | 2.05E-02 | nusG\|rpoB\|rpoC\|nusA\|rpoD |
| 1 | 12 | 4 | STRING Clusters | CL:1526 | Fatty acid biosynthesis | 2.05E-02 | fabV\|fabA\|fabF\|fabH |
| 1 | 11 | 4 | GO Biological Process | GO:0022618 | Ribonucleoprotein complex assembly | 2.22E-02 | rpsG\|rpsS\|rpsK\|rplT |
| 1 | 5 | 3 | COMPARTMENTS | GOCC:0045239 | Tricarboxylic acid cycle enzyme complex | 2.23E-02 | sucA\|sucD\|bkdA2 |
| 1 | 61 | 8 | GO Biological Process | GO:0046395 | Carboxylic acid catabolic process | 2.32E-02 | prpF\|ivdA\|ivdE\|ivdF\|speA\|liuE\|bkdA1\|bkdA2 |
| 1 | 131 | 12 | GO Biological Process | GO:0009117 | Nucleotide metabolic process | 2.42E-02 | deoB\|ushA\|adk\|ndk\|bkdB\|acs\|cpdB\|hprT\|prsA\|purA\|dut\|atpE |
| 1 | 5 | 3 | STRING Clusters | CL:363 | RNA polymerase | 2.54E-02 | rpoB\|rpoC\|rpoD |
| 1 | 48 | 7 | GO Biological Process | GO:0006164 | Purine nucleotide biosynthetic process | 2.62E-02 | adk\|ndk\|acs\|hprT\|prsA\|purA\|atpE |
| 1 | 34 | 6 | GO Biological Process | GO:0009063 | Cellular amino acid catabolic process | 2.62E-02 | ivdE\|ivdF\|speA\|liuE\|bkdA1\|bkdA2 |
| 1 | 152 | 13 | GO Biological | GO:0034654 | Nucleobase-containing compound | 2.62E-02 | nusG\|rpoB\|rpoC\|nusA\|rpoD\|adk\|ndk\|a |

Table A-1 (cont'd)

| | | | | | | | |
|---|---|---|---|---|---|---|---|
| | | | Process | | biosynthetic process | | cs\|hprT\|prsA\|purA\|dut\|atpE |
| 1 | 63 | 8 | GO Biological Process | GO:0046390 | Ribose phosphate biosynthetic process | 2.62E-02 | deoB\|adk\|ndk\|acs\|hprT\|prsA\|purA\|atpE |
| 1 | 5 | 3 | GO Biological Process | GO:0000028 | Ribosomal small subunit assembly | 3.01E-02 | rpsG\|rpsS\|rpsK |
| 1 | 4 | 3 | GO Molecular Function | GO:0003743 | Translation initiation factor activity | 3.01E-02 | infB\|infC\|yciH |
| 1 | 37 | 8 | InterPro Domains | IPR012340 | Nucleic acid-binding, OB-fold | 3.20E-02 | rplB\|rpsQ\|nusA\|pnpA\|pheT\|efp\|ruvA\|aspS |
| 1 | 4 | 4 | InterPro Domains | IPR014722 | Ribosomal protein L2, domain 2 | 3.20E-02 | nusG\|rplB\|rplX\|efp |
| 1 | 335 | 21 | GO Biological Process | GO:0019752 | Carboxylic acid metabolic process | 3.22E-02 | prpF\|prpC\|ivdA\|ivdE\|ivdF\|fabV\|fabA\|speA\|liuE\|liuD\|liuB\|pheT\|bkdA1\|bkdA2\|bkdB\|aspS\|ldh\|acs\|fabF\|fabH\|wbpQ |
| 1 | 6 | 3 | STRING Clusters | CL:1235 | e3 binding domain, and Oxidoreductase activity, acting on the aldehyde or oxo group of donors, disulfide as acceptor | 3.65E-02 | bkdA1\|bkdA2\|bkdB |

Table A-1 (cont'd)

| | | | | | | | |
|---|---|---|---|---|---|---|---|
| 1 | 6 | 3 | STRING Clusters | CL:131 | Mixed, incl. Ribosomal protein L2, domain 2, and Large ribosomal subunit rRNA binding | 3.65E-02 | rplB\|rplV\|rplX |
| 1 | 6 | 3 | STRING Clusters | CL:1330 | Mixed, incl. 5-phosphoribose 1-diphosphate metabolic process, and Pentose metabolic process | 3.65E-02 | deoA\|deoB\|prsA |
| 1 | 161 | 13 | GO Biological Process | GO:0044248 | Cellular catabolic process | 3.68E-02 | prpF\|pnpA\|deoB\|ivdA\|ivdE\|ivdF\|speA\|liuE\|ushA\|bkdA1\|bkdA2\|cpdB\|dut |
| 1 | 2 | 2 | GO Cellular Component | GO:1905202 | methylcrotonoyl-CoA carboxylase complex | 3.77E-02 | liuD\|liuB |
| 1 | 15 | 4 | GO Biological Process | GO:0009166 | Nucleotide catabolic process | 4.30E-02 | deoB\|ushA\|cpdB\|dut |
| 1 | 40 | 6 | GO Biological Process | GO:0043933 | Protein-containing complex organization | 4.40E-02 | rpsG\|rpsS\|rpsK\|prfB\|frr\|rplT |
| 1 | 169 | 13 | GO Biological Process | GO:0055086 | Nucleobase-containing small molecule metabolic process | 4.89E-02 | deoA\|deoB\|ushA\|adk\|ndk\|bkdB\|acs\|cpdB\|hprT\|prsA\|purA\|dut\|atpE |
| 1 | 126 | 43 | COMPARTMENTS | GOCC:0043232 | Intracellular non-membrane-bounded organelle | 1.04E-28 | rpmH\|rplK\|rplA\|rplL\|rpsG\|rpsJ\|rplC\|rplD\|rplB\|rpsS\|rplV\|rpsC\|rplP\|rpsQ\|rplN\|rpl |

Table A-1 (cont'd)

| | | | | | | | |
|---|---|---|---|---|---|---|---|
| | | | | | | | X\|rplE\|rpsN\|rpsH\|rplF\|rplR\|rpsE\|rpmD\|rplO\|rpsK\|rpsD\|rplQ\|infB\|rpsO\|rpsB\|rpmI\|rplT\|rpmF\|raiA\|rpsT\|rpmA\|rplU\|rplI\|rpsR\|rpsF\|rpsI\|rplM\|rpmG |
| 1 | 1435 | 100 | GO Cellular Component | GO:0005737 | Cytoplasm | 1.09E-23 | nusG\|rplK\|rplA\|rplL\|rpsG\|tufA\|rplC\|rplD\|rplB\|rpsS\|rplV\|rpsC\|rplP\|rpsQ\|rplN\|rplX\|rplE\|rpsN\|rpsH\|rplF\|rplR\|rpsE\|rpmD\|rplO\|rpsM\|rpsK\|rplQ\|prpC\|sspA\|groES\|groEL\|fusB\|prfB\|dnaK\|dnaJ\|greA\|nusA\|infB\|rpsO\|pnpA\|deoA\|deoB\|rpoD\|rplS\|grpE\|SO_1550\|rpsB\|tsf\|frr\|ivdA\|ivdB\|ivdC\|ivdG\|tig\|fabA\|liuG\|liuE\|liuA\|sucA\|sucD\|SO_1995\|htpG\|adk\|pheT\|ndk\|infC\|rpmI\|rplT\|efp\|bkdB\|gyrA\|ubiG\|aspS\|def-3\|ldh\|acs\|fabF\|fabH\|wbp |

Table A-1 (cont'd)

| | | | | | | | |
|---|---|---|---|---|---|---|---|
| | | | | | | | Q\|rmlA\|yciH\|raiA\|ribE\|SO_3468\|rpsT\|clpB\|rpmA\|rplU\|hprT\|prsA\|rplI\|rpsR\|rpsF\|purA\|rpsI\|rplM\|hslV\|rpmG\|dut\|exaC |
| 1 | 57 | 43 | UniProt Keywords | KW-0689 | Ribosomal protein | 1.12E-39 | rpmH\|rplK\|rplA\|rplL\|rpsG\|rpsJ\|rplC\|rplD\|rplB\|rpsS\|rplV\|rpsC\|rplP\|rpsQ\|rplN\|rplX\|rplE\|rpsN\|rpsH\|rplF\|rplR\|rpsE\|rpmD\|rplO\|rpsM\|rpsK\|rpsD\|rplQ\|rpsO\|rplS\|rpsB\|rpmI\|rplT\|rpmF\|rpsT\|rpmA\|rplU\|rplI\|rpsR\|rpsF\|rpsI\|rplM\|rpmG |
| 1 | 16 | 12 | COMPARTMENTS | GOCC:0022625 | Cytosolic large ribosomal subunit | 1.13E-10 | rplA\|rplL\|rplC\|rplD\|rplB\|rplV\|rplE\|rplF\|rplR\|rpmD\|rplO\|rplU |
| 1 | 12 | 9 | STRING Clusters | CL:130 | Cytosolic large ribosomal subunit | 1.13E-7 | rplC\|rplD\|rplB\|rplV\|rplN\|rplX\|rplE\|rplO\|rplM |
| 1 | 83 | 17 | STRING Clusters | CL:1520 | Mixed, incl. Fatty acid metabolism, and Valine, leucine and isoleucine degradation | 1.13E-7 | ivdA\|ivdB\|ivdC\|ivdE\|ivdF\|ivdG\|fabV\|fabA\|liuG\|liuE\|liuD\|liuC\|liuB\|liuA\|acs\|fabF\|fabH |

Table A-1 (cont'd)

| | | | | | | | |
|---|---|---|---|---|---|---|---|
| 1 | 80 | 51 | STRING Clusters | CL:108 | Structural constituent of ribosome, and Translation regulator activity | 1.1E-45 | rpmH\|nusG\|rplK\|rplA\|rplL\|rpsG\|tufA\|rpsJ\|rplC\|rplD\|rplB\|rpsS\|rplV\|rpsC\|rplP\|rpsQ\|rplN\|rplX\|rplE\|rpsN\|rpsH\|rplF\|rplR\|rpsE\|rpmD\|rplO\|rpsM\|rpsK\|rpsD\|rplQ\|fusB\|prfB\|nusA\|infB\|rpsO\|rplS\|rpsB\|tig\|infC\|rpmI\|rplT\|rpmF\|rpsT\|rpmA\|rplU\|rplI\|rpsR\|rpsF\|rpsI\|rplM\|rpmG |
| 1 | 2525 | 116 | GO Biological Process | GO:0009987 | Cellular process | 1.21E-14 | rpmH\|nusG\|rplK\|rplA\|rplL\|rpoB\|rpoC\|rpsG\|tufA\|rpsJ\|rplC\|rplD\|rplB\|rpsS\|rplV\|rpsC\|rplP\|rpsQ\|rplN\|rplX\|rplE\|rpsN\|rpsH\|rplF\|rplR\|rpsE\|rpmD\|rplO\|rpsM\|rpsK\|rpsD\|rplQ\|SO_0306\|prpF\|prpC\|sspA\|groES\|groEL\|fusB\|prfB\|dnaK\|dnaJ\|nusA\|infB\|rpsO\|pnpA\|deoA\|deoB\|rpoD\|rplS\|grpE\|rpsB\|tsf\|frr\|ivdA\|ivdB\|ivdE\|ivdF\| |

Table A-1 (cont'd)

| | | | | | | | |
|---|---|---|---|---|---|---|---|
| | | | | | | | ivdG\|tig\|fabV\|fabA\|speA\|liuG\|liuE\|liuD\|liuC\|liuB\|sucA\|sucD\|SO_1995\|ushA\|htpG\|adk\|pheT\|ndk\|infC\|rpmI\|rplT\|efp\|bkdA1\|bkdA2\|bkdB\|gyrA\|ubiG\|ruvA\|aspS\|def-3\|ldh\|topA\|acs\|fabF\|fabH\|rpmF\|wbpQ\|rmlA\|yciH\|ribE\|SO_3468\|rpsT\|cpdB\|clpB\|rpmA\|rplU\|hprT\|prsA\|rplI\|rpsR\|rpsF\|purA\|rpsI\|rplM\|rpmG\|dut\|exaC\|atpE |
| 1 | 18 | 14 | COMPARTMENTS | GOCC:0015934 | Large ribosomal subunit | 1.36E-12 | rplA\|rplL\|rplC\|rplD\|rplB\|rplV\|rplN\|rplE\|rplF\|rplR\|rpmD\|rplO\|rpmF\|rplU |
| 1 | 1661 | 107 | GO Biological Process | GO:0044237 | Cellular metabolic process | 1.39E-23 | rpmH\|nusG\|rplK\|rplA\|rplL\|rpoB\|rpoC\|rpsG\|tufA\|rpsJ\|rplC\|rplD\|rplB\|rpsS\|rplV\|rpsC\|rplP\|rpsQ\|rplN\|rplX\|rplE\|rpsN\|rpsH\|rplF\|rplR\|rpsE\|rpmD\|rplO\|rpsM\|rpsK\|rpsD\|rplQ\|pr |

Table A-1 (cont'd)

| | | | | | | | |
|---|---|---|---|---|---|---|---|
| | | | | | | | pF\|prpC\|sspA\|fusB\|prfB\|dnaJ\|nusA\|infB\|rpsO\|pnpA\|deoA\|deoB\|rpoD\|rplS\|rpsB\|tsf\|frr\|ivdA\|ivdB\|ivdE\|ivdF\|ivdG\|fabV\|fabA\|speA\|liuG\|liuE\|liuD\|liuC\|liuB\|sucA\|sucD\|ushA\|adk\|pheT\|ndk\|infC\|rpmI\|rplT\|efp\|bkdA1\|bkdA2\|bkdB\|gyrA\|ubiG\|ruvA\|aspS\|def-3\|ldh\|topA\|acs\|fabF\|fabH\|rpmF\|wbpQ\|rmlA\|yciH\|ribE\|SO_3468\|rpsT\|cpdB\|rpmA\|rplU\|hprT\|prsA\|rplI\|rpsR\|rpsF\|purA\|rpsI\|rplM\|rpmG\|dut\|exaC\|atpE |
| 1 | 675 | 80 | GO Biological Process | GO:0044249 | Cellular biosynthetic process | 1.42E-29 | rpmH\|nusG\|rplK\|rplA\|rplL\|rpoB\|rpoC\|rpsG\|tufA\|rpsJ\|rplC\|rplD\|rplB\|rpsS\|rplV\|rpsC\|rplP\|rpsQ\|rplN\|rplX\|rplE\|rpsN\|rpsH\|rplF\|rplR\|rpsE\|rpmD\|rplO\|rpsM\|rpsK\| |

Table A-1 (cont'd)

| | | | | | | | |
|---|---|---|---|---|---|---|---|
| | | | | | | | rpsD\|rplQ\|fusB\|prfB\|nusA\|infB\|rpsO\|rpoD\|rplS\|rpsB\|tsf\|frr\|fabV\|fabA\|speA\|liuE\|liuB\|adk\|pheT\|ndk\|infC\|rpmI\|rplT\|efp\|ubiG\|aspS\|def-3\|acs\|fabF\|fabH\|rpmF\|wbpQ\|rmlA\|yciH\|ribE\|SO_3468\|rpsT\|rpmA\|rplU\|hprT\|prsA\|rplI\|rpsR\|rpsF\|purA\|rpsI\|rplM\|rpmG\|dut\|atpE |
| 1 | 141 | 57 | GO Biological Process | GO:0006518 | Peptide metabolic process | 1.45E-42 | rpmH\|rplK\|rplA\|rplL\|rpsG\|tufA\|rpsJ\|rplC\|rplD\|rplB\|rpsS\|rplV\|rpsC\|rplP\|rpsQ\|rplN\|rplX\|rplE\|rpsN\|rpsH\|rplF\|rplR\|rpsE\|rpmD\|rplO\|rpsM\|rpsK\|rpsD\|rplQ\|sspA\|fusB\|prfB\|nusA\|infB\|rpsO\|rplS\|rpsB\|tsf\|frr\|pheT\|infC\|rpmI\|rplT\|efp\|aspS\|def-3\|rpmF\|yciH\|rpsT\|rpmA\|rplU\|rplI\|rpsR\|rpsF\|rpsI\|rplM |

Table A-1 (cont'd)

| | | | | | | | |
|---|---|---|---|---|---|---|---|
| | | | | | | | \|rpmG |
| 1 | 1497 | 108 | GO Cellular Component | GO:0005622 | Intracellular anatomical structure | 1.47E-29 | rpmH\|nusG\|rplK\|rplA\|rplL\|rpsG\|tufA\|rpsJ\|rplC\|rplD\|rplB\|rpsS\|rplV\|rpsC\|rplP\|rpsQ\|rplN\|rplX\|rplE\|rpsN\|rpsH\|rplF\|rplR\|rpsE\|rpmD\|rplO\|rpsM\|rpsK\|rpsD\|rplQ\|prpC\|sspA\|groES\|groEL\|fusB\|prfB\|dnaK\|dnaJ\|greA\|nusA\|infB\|rpsO\|pnpA\|deoA\|deoB\|rpoD\|rplS\|grpE\|SO_1550\|rpsB\|tsf\|frr\|ivdA\|ivdB\|ivdC\|ivdG\|tig\|fabA\|liuG\|liuE\|liuA\|sucA\|sucD\|SO_1995\|htpG\|adk\|pheT\|ndk\|infC\|rpmI\|rplT\|efp\|bkdA1\|bkdB\|gyrA\|ubiG\|ruvA\|aspS\|def-3\|ldh\|topA\|acs\|fabF\|fabH\|rpmF\|wbpQ\|rmlA\|yciH\|raiA\|ribE\|SO_3468\|rpsT\|clp |

Table A-1 (cont'd)

| | | | | | | | |
|---|---|---|---|---|---|---|---|
| | | | | | | | B\|rpmA\|rplU\|hprT\|prsA\|rplI\|rpsR\|rpsF\|purA\|rpsI\|rplM\|hslV\|rpmG\|dut\|exaC\|atpE |
| 1 | 5 | 5 | STRING Clusters | CL:178 | Mixed, incl. 5S rRNA binding, and Positive regulation of translation | 1.4E-4 | rpsS\|rplP\|rplR\|rpsE\|rpsD |
| 1 | 5 | 5 | STRING Clusters | CL:518 | De novo post-translational protein folding, and ATPase regulator activity | 1.4E-4 | groES\|groEL\|dnaK\|dnaJ\|grpE |
| 1 | 600 | 59 | GO Cellular Component | GO:0005829 | Cytosol | 1.52E-16 | nusG\|rplK\|rplA\|rplL\|rpsG\|rplC\|rplB\|rpsS\|rplV\|rpsC\|rplP\|rpsQ\|rplN\|rplX\|rplE\|rpsH\|rplF\|rplR\|rpsE\|rpmD\|rplO\|rpsM\|rpsK\|rplQ\|groEL\|dnaK\|greA\|rpsO\|pnpA\|deoA\|deoB\|rplS\|grpE\|SO_1550\|rpsB\|frr\|liuE\|sucA\|htpG\|adk\|infC\|rpmI\|rplT\|def-3\|acs\|wbpQ\|rmlA\|ribE\|SO_3468\|rpsT\|rpmA\|rplI\|rpsR\|rpsF\|rpsI\|r |

Table A-1 (cont'd)

| | | | | | | | |
|---|---|---|---|---|---|---|---|
| | | | | | | | plM\|hslV\|rpmG\|dut |
| 1 | 14 | 12 | GO Cellular Component | GO:0022627 | Cytosolic small ribosomal subunit | 1.55E-11 | rpsG\|rpsS\|rpsC\|rpsQ\|rpsH\|rpsE\|rpsK\|rpsO\|rpsB\|rpsR\|rpsF\|rpsI |
| 1 | 6 | 6 | STRING Clusters | CL:142 | Cytosolic large ribosomal subunit | 1.58E-5 | rplC\|rplD\|rplN\|rplE\|rplO\|rplM |
| 1 | 298 | 53 | COMPARTMENTS | GOCC:0043229 | Intracellular organelle | 1.61E-24 | rpmH\|nusG\|rplK\|rplA\|rplL\|rpsG\|rpsJ\|rplC\|rplD\|rplB\|rpsS\|rplV\|rpsC\|rplP\|rpsQ\|rplN\|rplX\|rplE\|rpsN\|rpsH\|rplF\|rplR\|rpsE\|rpmD\|rplO\|rpsM\|rpsK\|rpsD\|rplQ\|nusA\|infB\|rpsO\|rplS\|rpsB\|ivdC\|speA\|liuE\|liuA\|rpmI\|rplT\|bkdA1\|bkdA2\|rpmF\|raiA\|rpsT\|rpmA\|rplU\|rplI\|rpsR\|rpsF\|rpsI\|rplM\|rpmG |
| 1 | 20 | 12 | STRING Clusters | CL:1615 | Valine, leucine and isoleucine degradation, and Enoyl-CoA hydratase/isomerase | 1.62E-9 | ivdA\|ivdB\|ivdC\|ivdE\|ivdF\|liuG\|liuE\|liuD\|liuC\|liuB\|liuA\|acs |

Table A-1 (cont'd)

| | | | | | | | |
|---|---|---|---|---|---|---|---|
| 1 | 30 | 26 | STRING Clusters | CL:128 | Ribosomal subunit | 1.68E-24 | rplK\|rplA\|rplL\|rpsG\|rpsJ\|rplC\|rplD\|rplB\|rpsS\|rplV\|rpsC\|rplP\|rpsQ\|rplN\|rplX\|rplE\|rpsN\|rplF\|rplR\|rpsE\|rplO\|rpsM\|rpsD\|rpsO\|rpsB\|rplM |
| 1 | 2017 | 113 | GO Biological Process | GO:0008152 | Metabolic process | 1.77E-21 | rpmH\|nusG\|rplK\|rplA\|rplL\|rpoB\|rpoC\|rpsG\|tufA\|rpsJ\|rplC\|rplD\|rplB\|rpsS\|rplV\|rpsC\|rplP\|rpsQ\|rplN\|rplX\|rplE\|rpsN\|rpsH\|rplF\|rplR\|rpsE\|rpmD\|rplO\|rpsM\|rpsK\|rpsD\|rplQ\|prpF\|prpC\|sspA\|fusB\|prfB\|dnaJ\|ftsH\|nusA\|infB\|rpsO\|pnpA\|deoA\|deoB\|rpoD\|rplS\|SO_1550\|rpsB\|tsf\|frr\|ivdA\|ivdB\|ivdC\|ivdE\|ivdF\|ivdG\|fabV\|fabA\|speA\|liuG\|liuE\|liuD\|liuC\|liuB\|liuA\|sucA\|sucD\|ushA\|adk\|pheT\|ndk\|infC\|rpmI\|rplT\|efp\|bkdA1\|bkdA2\|bkdB\|gyrA\|ubiG\|ruvA\|aspS\|d |

Table A-1 (cont'd)

| | | | | | | | |
|---|---|---|---|---|---|---|---|
| | | | | | | | ef-3\|ldh\|topA\|acs\|fabF\|fabH\|rpmF\|wbpQ\|rmlA\|yciH\|raiA\|ribE\|SO_3468\|rpsT\|cpdB\|rpmA\|rplU\|hprT\|prsA\|rplI\|rpsR\|rpsF\|purA\|rpsI\|rplM\|hslV\|rpmG\|dut\|exaC\|atpE |
| 1 | 150 | 57 | GO Biological Process | GO:0043604 | Amide biosynthetic process | 1.82E-41 | rpmH\|rplK\|rplA\|rplL\|rpsG\|tufA\|rpsJ\|rplC\|rplD\|rplB\|rpsS\|rplV\|rpsC\|rplP\|rpsQ\|rplN\|rplX\|rplE\|rpsN\|rpsH\|rplF\|rplR\|rpsE\|rpmD\|rplO\|rpsM\|rpsK\|rpsD\|rplQ\|fusB\|prfB\|nusA\|infB\|rpsO\|rplS\|rpsB\|tsf\|frr\|pheT\|infC\|rpmI\|rplT\|efp\|aspS\|def-3\|acs\|rpmF\|yciH\|rpsT\|rpmA\|rplU\|rplI\|rpsR\|rpsF\|rpsI\|rplM\|rpmG |
| 1 | 41 | 34 | GO Cellular Component | GO:0022626 | Cytosolic ribosome | 1.89E-32 | rplK\|rplA\|rplL\|rpsG\|rplC\|rplB\|rpsS\|rplV\|rpsC\|rplP\|rpsQ\|rplN\|rplX\|rplE\|rpsH\|rplF\|rplR\|rpsE\|rpmD\|rplO\|rps |

Table A-1 (cont'd)

| | | | | | | | |
|---|---|---|---|---|---|---|---|
| | | | | | | | K\|rplQ\|rpsO\|rplS\|rpsB\|rpmI\|rplT\|rpmA\|rplI\|rpsR\|rpsF\|rpsI\|rplM\|rpmG |
| 1 | 3153 | 115 | GO Cellular Component | GO:0110165 | Cellular anatomical entity | 1.95E-5 | rpmH\|nusG\|rplK\|rplA\|rplL\|rpsG\|tufA\|rpsJ\|rplC\|rplD\|rplB\|rpsS\|rplV\|rpsC\|rplP\|rpsQ\|rplN\|rplX\|rplE\|rpsN\|rpsH\|rplF\|rplR\|rpsE\|rpmD\|rplO\|rpsM\|rpsK\|rpsD\|rplQ\|SO_0306\|prpF\|prpC\|sspA\|groES\|groEL\|fusB\|prfB\|dnaK\|dnaJ\|greA\|ftsH\|nusA\|infB\|rpsO\|pnpA\|deoA\|deoB\|rpoD\|rplS\|grpE\|SO_1550\|rpsB\|tsf\|frr\|ivdA\|ivdB\|ivdC\|ivdG\|tig\|fabA\|speA\|liuG\|liuE\|liuA\|sucA\|sucD\|SO_1995\|ushA\|htpG\|adk\|pheT\|ndk\|infC\|rpmI\|rplT\|efp\|bkdA1\|bkdA2\|bkdB\|gyrA\|ubiG\|ruvA\|aspS\|def-3\|ldh\|topA\|acs\|fabF\|fabH\|r |

Table A-1 (cont'd)

| | | | | | | | |
|---|---|---|---|---|---|---|---|
| | | | | | | | pmF\|wbpQ\|rmlA\|yciH\|raiA\|ribE\|SO_3468\|rpsT\|cpdB\|clpB\|rpmA\|rplU\|hprT\|prsA\|rplI\|rpsR\|rpsF\|purA\|rpsI\|rplM\|hslV\|rpmG\|dut\|exaC\|atpE |
| 1 | 1489 | 101 | GO Biological Process | GO:0044238 | Primary metabolic process | 1.98E-22 | rpmH\|nusG\|rplK\|rplA\|rplL\|rpoB\|rpoC\|rpsG\|tufA\|rpsJ\|rplC\|rplD\|rplB\|rpsS\|rplV\|rpsC\|rplP\|rpsQ\|rplN\|rplX\|rplE\|rpsN\|rpsH\|rplF\|rplR\|rpsE\|rpmD\|rplO\|rpsM\|rpsK\|rpsD\|rplQ\|prpF\|prpC\|fusB\|prfB\|dnaJ\|ftsH\|nusA\|infB\|rpsO\|pnpA\|deoA\|deoB\|rpoD\|rplS\|rpsB\|tsf\|frr\|ivdA\|ivdE\|ivdF\|fabV\|fabA\|speA\|liuE\|liuD\|liuB\|sucA\|sucD\|ushA\|adk\|pheT\|ndk\|infC\|rpmI\|rplT\|efp\|bkdA1\|bkdA2\|bkdB\|gyrA\|ruvA\|aspS\|def-3\|ldh\|topA\|acs\|fabF\|fabH\|r |

Table A-1 (cont'd)

| | | | | | | | |
|---|---|---|---|---|---|---|---|
| | | | | | | | pmF\|wbpQ\|rmlA\|yciH\|raiA\|rpsT\|cpdB\|rpmA\|rplU\|hprT\|prsA\|rplI\|rpsR\|rpsF\|purA\|rpsI\|rplM\|hslV\|rpmG\|dut\|atpE |
| 1 | 101 | 13 | GO Cellular Component | GO:1902494 | Catalytic complex | 1.9E-4 | rpoB\|rpoC\|liuD\|liuC\|liuB\|sucA\|sucD\|pheT\|bkdB\|ruvA\|ribE\|prsA\|hslV |
| 1 | 586 | 62 | GO Biological Process | GO:0044260 | Cellular macromolecule metabolic process | 2.09E-18 | rpmH\|rplK\|rplA\|rplL\|rpsG\|tufA\|rpsJ\|rplC\|rplD\|rplB\|rpsS\|rplV\|rpsC\|rplP\|rpsQ\|rplN\|rplX\|rplE\|rpsN\|rpsH\|rplF\|rplR\|rpsE\|rpmD\|rplO\|rpsM\|rpsK\|rpsD\|rplQ\|fusB\|prfB\|dnaJ\|nusA\|infB\|rpsO\|pnpA\|rplS\|rpsB\|tsf\|frr\|pheT\|infC\|rpmI\|rplT\|efp\|gyrA\|ruvA\|aspS\|def-3\|topA\|rpmF\|rmlA\|yciH\|rpsT\|rpmA\|rplU\|rplI\|rpsR\|rpsF\|rpsI\|rplM\|rpmG |

Table A-1 (cont'd)

| | | | | | | | |
|---|---|---|---|---|---|---|---|
| 1 | 105 | 46 | GO Cellular Component | GO:0043232 | Intracellular non-membrane-bounded organelle | 2.0E-35 | rpmH\|rplK\|rplA\|rplL\|rpsG\|rpsJ\|rplC\|rplD\|rplB\|rpsS\|rplV\|rpsC\|rplP\|rpsQ\|rplN\|rplX\|rplE\|rpsN\|rpsH\|rplF\|rplR\|rpsE\|rpmD\|rplO\|rpsM\|rpsK\|rpsD\|rplQ\|rpsO\|rplS\|rpsB\|rpmI\|rplT\|gyrA\|topA\|rpmF\|raiA\|rpsT\|rpmA\|rplU\|rplI\|rpsR\|rpsF\|rpsI\|rplM\|rpmG |
| 1 | 56 | 43 | GO Molecular Function | GO:0003735 | Structural constituent of ribosome | 2.17E-39 | rpmH\|rplK\|rplA\|rplL\|rpsG\|rpsJ\|rplC\|rplD\|rplB\|rpsS\|rplV\|rpsC\|rplP\|rpsQ\|rplN\|rplX\|rplE\|rpsN\|rpsH\|rplF\|rplR\|rpsE\|rpmD\|rplO\|rpsM\|rpsK\|rpsD\|rplQ\|rpsO\|rplS\|rpsB\|rpmI\|rplT\|rpmF\|rpsT\|rpmA\|rplU\|rplI\|rpsR\|rpsF\|rpsI\|rplM\|rpmG |
| 1 | 646 | 42 | KEGG Pathways | son01100 | Metabolic pathways | 2.24E-5 | prpF\|prpC\|deoA\|deoB\|SO_1550\|ivdA\|ivdB\|ivdF\|ivdG\|fabV\|fabA\|speA\|liuG\|liuE\|liuD\|liuC\|liuB\|liuA\|suc |

Table A-1 (cont'd)

| | | | | | | | |
|---|---|---|---|---|---|---|---|
| | | | | | | | A\|sucD\|ushA\|adk\|ndk\|bkdA1\|bkdA2\|bkdB\|ubiG\|ldh\|acs\|fabF\|fabH\|wbpQ\|rmlA\|ribE\|SO_3468\|cpdB\|hprT\|prsA\|purA\|dut\|exaC\|atpE |
| 1 | 1174 | 79 | GO Molecular Function | GO:0097159 | Organic cyclic compound binding | 2.29E-13 | nusG\|rplK\|rplA\|rplL\|rpoB\|rpoC\|rpsG\|tufA\|rpsJ\|rplC\|rplD\|rplB\|rpsS\|rplV\|rpsC\|rplP\|rpsQ\|rplN\|rplX\|rplE\|rpsN\|rpsH\|rplF\|rplR\|rpsE\|rplO\|rpsM\|rpsK\|rpsD\|groES\|groEL\|fusB\|prfB\|dnaK\|dnaJ\|greA\|ftsH\|nusA\|infB\|rpsO\|pnpA\|rpoD\|grpE\|tsf\|ivdC\|ivdF\|fabV\|liuD\|liuA\|sucA\|sucD\|ushA\|htpG\|adk\|pheT\|ndk\|infC\|rplT\|efp\|gyrA\|ruvA\|aspS\|ldh\|topA\|acs\|wbpQ\|yciH\|rpsT\|cpdB\|clpB\|rplU\|hprT\|prsA\|rplI\|rpsR\|rpsF\|purA\|rpsI\|rplM |

Table A-1 (cont'd)

| | | | | | | | |
|---|---|---|---|---|---|---|---|
| 1 | 1174 | 79 | GO Molecular Function | GO:1901363 | Heterocyclic compound binding | 2.29E-13 | nusG\|rplK\|rplA\|rplL\|rpoB\|rpoC\|rpsG\|tufA\|rpsJ\|rplC\|rplD\|rplB\|rpsS\|rplV\|rpsC\|rplP\|rpsQ\|rplN\|rplX\|rplE\|rpsN\|rpsH\|rplF\|rplR\|rpsE\|rplO\|rpsM\|rpsK\|rpsD\|groES\|groEL\|fusB\|prfB\|dnaK\|dnaJ\|greA\|ftsH\|nusA\|infB\|rpsO\|pnpA\|rpoD\|grpE\|tsf\|ivdC\|ivdF\|fabV\|liuD\|liuA\|sucA\|sucD\|ushA\|htpG\|adk\|pheT\|ndk\|infC\|rplT\|efp\|gyrA\|ruvA\|aspS\|ldh\|topA\|acs\|wbpQ\|yciH\|rpsT\|cpdB\|clpB\|rplU\|hprT\|prsA\|rplI\|rpsR\|rpsF\|purA\|rpsI\|rplM |
| 1 | 5 | 5 | GO Biological Process | GO:0009083 | Branched-chain amino acid catabolic process | 2.2E-4 | ivdE\|ivdF\|liuE\|bkdA1\|bkdA2 |
| 1 | 415 | 58 | GO Biological Process | GO:0019538 | Protein metabolic process | 2.34E-22 | rpmH\|rplK\|rplA\|rplL\|rpsG\|tufA\|rpsJ\|rplC\|rplD\|rplB\|rpsS\|rplV\|rpsC\|rplP\|rpsQ\|rplN\|rplX\|rplE\|r |

Table A-1 (cont'd)

| | | | | | | | |
|---|---|---|---|---|---|---|---|
| | | | | | | | psN\|rpsH\|rplF\|rplR\|rpsE\|rpmD\|rplO\|rpsM\|rpsK\|rpsD\|rplQ\|fusB\|prfB\|ftsH\|nusA\|infB\|rpsO\|rplS\|rpsB\|tsf\|frr\|pheT\|infC\|rpmI\|rplT\|efp\|aspS\|def-3\|rpmF\|yciH\|rpsT\|rpmA\|rplU\|rplI\|rpsR\|rpsF\|rpsI\|rplM\|hslV\|rpmG |
| 1 | 742 | 50 | COMPARTMENTS | GOCC:0005829 | Cytosol | 2.3E-7 | nusG\|rplA\|rplL\|rpsG\|rplC\|rplD\|rplB\|rplV\|rpsC\|rpsQ\|rplE\|rpsN\|rpsH\|rplF\|rplR\|rpsE\|rpmD\|rplO\|rpsD\|sspA\|groES\|groEL\|prfB\|greA\|nusA\|rpsO\|deoA\|deoB\|SO_1550\|frr\|fabA\|speA\|htpG\|ndk\|efp\|ubiG\|aspS\|def-3\|topA\|acs\|fabF\|fabH\|wbpQ\|rmlA\|raiA\|SO_3468\|rpsT\|clpB\|rplU\|dut |
| 1 | 133 | 37 | GO Molecular Function | GO:0003723 | RNA binding | 2.51E-21 | rplK\|rplA\|rplL\|rpsG\|rpsJ\|rplC\|rplD\|rplB\|rpsS\|rplV\|rpsC\|rplP\|rpsQ\|rplN\|rplX\|rplE\| |

Table A-1 (cont'd)

| | | | | | | | |
|---|---|---|---|---|---|---|---|
| | | | | | | | rpsN\|rpsH\|rplF\|rplR\|rpsE\|rplO\|rpsM\|rpsK\|rpsD\|nusA\|rpsO\|pnpA\|pheT\|rplT\|rpsT\|rplU\|rplI\|rpsR\|rpsF\|rpsI\|rplM |
| 1 | 58 | 44 | STRING Clusters | CL:120 | Structural constituent of ribosome | 2.63E-41 | rpmH\|rplK\|rplA\|rplL\|rpsG\|tufA\|rpsJ\|rplC\|rplD\|rplB\|rpsS\|rplV\|rpsC\|rplP\|rpsQ\|rplN\|rplX\|rplE\|rpsN\|rpsH\|rplF\|rplR\|rpsE\|rpmD\|rplO\|rpsM\|rpsK\|rpsD\|rplQ\|rpsO\|rplS\|rpsB\|rpmI\|rplT\|rpmF\|rpsT\|rpmA\|rplU\|rplI\|rpsR\|rpsF\|rpsI\|rplM\|rpmG |
| 1 | 39 | 30 | UniProt Keywords | KW-0699 | rRNA-binding | 2.67E-27 | rplK\|rplA\|rpsG\|rplC\|rplD\|rplB\|rpsS\|rplV\|rpsC\|rplP\|rpsQ\|rplN\|rplX\|rplE\|rpsN\|rpsH\|rplF\|rplR\|rpsE\|rplO\|rpsM\|rpsK\|rpsD\|rpsO\|rplT\|rpsT\|rplU\|rplI\|rpsR\|rpsF |
| 1 | 43 | 36 | STRING Clusters | CL:124 | Ribosomal subunit | 2.72E-34 | rplK\|rplA\|rplL\|rpsG\|rpsJ\|rplC\|rplD\|rplB\|rpsS\|rplV\|rpsC\|rplP\|rpsQ\|r |

Table A-1 (cont'd)

| | | | | | | | |
|---|---|---|---|---|---|---|---|
| | | | | | | | plN\|rplX\|rplE\|rpsN\|rplF\|rplR\|rpsE\|rpmD\|rplO\|rpsM\|rpsD\|rplQ\|rpsO\|rplS\|rpsB\|rpmI\|rplT\|rpmA\|rplI\|rpsR\|rpsF\|rpsI\|rplM |
| 1 | 1181 | 78 | COMPARTMENTS | GOCC:0005737 | Cytoplasm | 2.73E-13 | nusG\|rplA\|rplL\|rpsG\|tufA\|rplC\|rplD\|rplB\|rplV\|rpsC\|rpsQ\|rplE\|rpsN\|rpsH\|rplF\|rplR\|rpsE\|rpmD\|rplO\|rpsM\|rpsD\|prpF\|prpC\|sspA\|groES\|groEL\|fusB\|prfB\|dnaK\|greA\|nusA\|rpsO\|pnpA\|deoA\|deoB\|rplS\|grpE\|SO_1550\|tsf\|frr\|ivdA\|ivdC\|ivdG\|tig\|fabA\|speA\|liuG\|liuE\|liuC\|liuA\|sucA\|sucD\|htpG\|pheT\|ndk\|infC\|efp\|bkdA2\|bkdB\|ubiG\|aspS\|def-3\|ldh\|topA\|acs\|fabF\|fabH\|wbpQ\|rmlA\|yciH\|raiA\|SO_3468\|rpsT\|clpB\|rplU\|hprT\|purA\|dut |

Table A-1 (cont'd)

| | | | | | | | |
|---|---|---|---|---|---|---|---|
| 1 | 7 | 6 | STRING Clusters | CL:1641 | Synthesis and degradation of ketone bodies, and methylcrotonoyl-CoA carboxylase complex | 2.76E-5 | liuG\|liuE\|liuD\|liuC\|liuB\|liuA |
| 1 | 894 | 82 | GO Biological Process | GO:0034641 | Cellular nitrogen compound metabolic process | 2.82E-23 | rpmH\|nusG\|rplK\|rplA\|rplL\|rpoB\|rpoC\|rpsG\|tufA\|rpsJ\|rplC\|rplD\|rplB\|rpsS\|rplV\|rpsC\|rplP\|rpsQ\|rplN\|rplX\|rplE\|rpsN\|rpsH\|rplF\|rplR\|rpsE\|rpmD\|rplO\|rpsM\|rpsK\|rpsD\|rplQ\|sspA\|fusB\|prfB\|dnaJ\|nusA\|infB\|rpsO\|pnpA\|deoA\|deoB\|rpoD\|rplS\|rpsB\|tsf\|frr\|speA\|ushA\|adk\|pheT\|ndk\|infC\|rpmI\|rplT\|efp\|bkdB\|gyrA\|ruvA\|aspS\|def-3\|topA\|acs\|rpmF\|yciH\|ribE\|SO_3468\|rpsT\|cpdB\|rpmA\|rplU\|hprT\|prsA\|rplI\|rpsR\|rpsF\|purA\|rpsI\|rplM\|rpmG\|dut\|atpE |

Table A-1 (cont'd)

| | | | | | | | |
|---|---|---|---|---|---|---|---|
| 1 | 118 | 56 | GO Biological Process | GO:0006412 | Translation | 2.85E-44 | rpmH\|rplK\|rplA\|rplL\|rpsG\|tufA\|rpsJ\|rplC\|rplD\|rplB\|rpsS\|rplV\|rpsC\|rplP\|rpsQ\|rplN\|rplX\|rplE\|rpsN\|rpsH\|rplF\|rplR\|rpsE\|rpmD\|rplO\|rpsM\|rpsK\|rpsD\|rplQ\|fusB\|prfB\|nusA\|infB\|rpsO\|rplS\|rpsB\|tsf\|frr\|pheT\|infC\|rpmI\|rplT\|efp\|aspS\|def-3\|rpmF\|yciH\|rpsT\|rpmA\|rplU\|rplI\|rpsR\|rpsF\|rpsI\|rplM\|rpmG |
| 1 | 633 | 54 | GO Molecular Function | GO:0003676 | Nucleic acid binding | 2.8E-11 | nusG\|rplK\|rplA\|rplL\|rpoB\|rpoC\|rpsG\|tufA\|rpsJ\|rplC\|rplD\|rplB\|rpsS\|rplV\|rpsC\|rplP\|rpsQ\|rplN\|rplX\|rplE\|rpsN\|rpsH\|rplF\|rplR\|rpsE\|rplO\|rpsM\|rpsK\|rpsD\|fusB\|prfB\|greA\|nusA\|infB\|rpsO\|pnpA\|rpoD\|tsf\|pheT\|infC\|rplT\|efp\|gyrA\|ruvA\|aspS\|topA\|yciH\|rpsT\|rplU\|rplI\|rpsR\|rpsF\|rpsI\|r |

Table A-1 (cont'd)

| | | | | | | | |
|---|---|---|---|---|---|---|---|
| | | | | | | | plM |
| 1 | 22 | 13 | KEGG Pathways | son00280 | Valine, leucine and isoleucine degradation | 2.93E-10 | ivdA\|ivdB\|ivdF\|liuG\|liuE\|liuD\|liuC\|liuB\|liuA\|bkdA1\|bkdA2\|bkdB\|ldh |
| 1 | 680 | 81 | GO Biological Process | GO:1901576 | Organic substance biosynthetic process | 3.0E-30 | rpmH\|nusG\|rplK\|rplA\|rplL\|rpoB\|rpoC\|rpsG\|tufA\|rpsJ\|rplC\|rplD\|rplB\|rpsS\|rplV\|rpsC\|rplP\|rpsQ\|rplN\|rplX\|rplE\|rpsN\|rpsH\|rplF\|rplR\|rpsE\|rpmD\|rplO\|rpsM\|rpsK\|rpsD\|rplQ\|fusB\|prfB\|nusA\|infB\|rpsO\|deoB\|rpoD\|rplS\|rpsB\|tsf\|frr\|fabV\|fabA\|speA\|liuE\|liuB\|adk\|pheT\|ndk\|infC\|rpmI\|rplT\|efp\|ubiG\|aspS\|def-3\|acs\|fabF\|fabH\|rpmF\|wbpQ\|rmlA\|yciH\|ribE\|SO_3468\|rpsT\|rpmA\|rplU\|hprT\|prsA\|rplI\|rpsR\|rpsF\|purA\|rpsI\|rplM\|rpmG\|dut\|atp |

Table A-1 (cont'd)

| | | | | | | | |
|---|---|---|---|---|---|---|---|
| | | | | | | | E |
| 1 | 87 | 55 | STRING Clusters | CL:105 | Structural constituent of ribosome, and Translation regulator activity | 3.13E-49 | rpmH\|nusG\|rplK\|rplA\|rplL\|rpsG\|tufA\|rpsJ\|rplC\|rplD\|rplB\|rpsS\|rplV\|rpsC\|rplP\|rpsQ\|rplN\|rplX\|rplE\|rpsN\|rpsH\|rplF\|rplR\|rpsE\|rpmD\|rplO\|rpsM\|rpsK\|rpsD\|rplQ\|fusB\|prfB\|nusA\|infB\|rpsO\|rplS\|rpsB\|tsf\|frr\|tig\|infC\|rpmI\|rplT\|def-3\|rpmF\|raiA\|rpsT\|rpmA\|rplU\|rplI\|rpsR\|rpsF\|rpsI\|rplM\|rpmG |
| 1 | 2697 | 109 | COMPARTMENTS | GOCC:0110165 | Cellular anatomical entity | 3.14E-7 | rpmH\|nusG\|rplK\|rplA\|rplL\|rpsG\|tufA\|rpsJ\|rplC\|rplD\|rplB\|rpsS\|rplV\|rpsC\|rplP\|rpsQ\|rplN\|rplX\|rplE\|rpsN\|rpsH\|rplF\|rplR\|rpsE\|rpmD\|rplO\|rpsM\|rpsK\|rpsD\|rplQ\|SO_0306\|prpF\|prpC\|sspA\| |

Table A-1 (cont'd)

| | | | | | | | |
|---|---|---|---|---|---|---|---|
| | | | | | | | groES\|groEL\|fusB\|prfB\|dnaK\|dnaJ\|greA\|ftsH\|nusA\|infB\|rpsO\|pnpA\|deoA\|deoB\|rplS\|grpE\|SO_1550\|rpsB\|tsf\|frr\|ivdA\|ivdC\|ivdE\|ivdG\|tig\|fabA\|speA\|liuG\|liuE\|liuC\|liuA\|sucA\|sucD\|SO_1995\|ushA\|htpG\|adk\|pheT\|ndk\|infC\|rpmI\|rplT\|efp\|bkdA1\|bkdA2\|bkdB\|ubiG\|aspS\|def-3\|ldh\|topA\|acs\|fabF\|fabH\|rpmF\|wbpQ\|rmlA\|yciH\|raiA\|SO_3468\|rpsT\|cpdB\|clpB\|rpmA\|rplU\|hprT\|rplI\|rpsR\|rpsF\|purA\|rpsI\|rplM\|rpmG\|dut\|atpE |
| 1 | 37 | 31 | STRING Clusters | CL:126 | Ribosomal subunit | 3.22E-29 | rplK\|rplA\|rplL\|rpsG\|rpsJ\|rplC\|rplD\|rplB\|rpsS\|rplV\|rpsC\|rplP\|rpsQ\|rplN\|rplX\|rplE\|rpsN\|rplF\|rplR\|rpsE\|rpmD\|rplO\|rpsM\|rpsD\|rplQ\|rpsO\|rplS\|rpsB\|rpmA\|rpsI\|rplM |

Table A-1 (cont'd)

| | | | | | | | |
|---|---|---|---|---|---|---|---|
| 1 | 990 | 68 | GO Biological Process | GO:0043170 | Macromolecule metabolic process | 3.33E-11 | rpmH\|nusG\|rplK\|rplA\|rplL\|rpoB\|rpoC\|rpsG\|tufA\|rpsJ\|rplC\|rplD\|rplB\|rpsS\|rplV\|rpsC\|rplP\|rpsQ\|rplN\|rplX\|rplE\|rpsN\|rpsH\|rplF\|rplR\|rpsE\|rpmD\|rplO\|rpsM\|rpsK\|rpsD\|rplQ\|fusB\|prfB\|dnaJ\|ftsH\|nusA\|infB\|rpsO\|pnpA\|rpoD\|rplS\|rpsB\|tsf\|frr\|pheT\|infC\|rpmI\|rplT\|efp\|gyrA\|ruvA\|aspS\|def-3\|topA\|rpmF\|rmlA\|yciH\|rpsT\|rpmA\|rplU\|rplI\|rpsR\|rpsF\|rpsI\|rplM\|hslV\|rpmG |
| 1 | 13 | 6 | STRING Clusters | CL:1616 | Mixed, incl. Benzoate degradation, and Valine catabolic process | 3.3E-4 | ivdA\|ivdB\|ivdC\|ivdE\|ivdF\|acs |

Table A-1 (cont'd)

| | | | | | | | |
|---|---|---|---|---|---|---|---|
| 1 | 1761 | 109 | GO Biological Process | GO:0071704 | Organic substance metabolic process | 3.52E-23 | rpmH\|nusG\|rplK\|rplA\|rplL\|rpoB\|rpoC\|rpsG\|tufA\|rpsJ\|rplC\|rplD\|rplB\|rpsS\|rplV\|rpsC\|rplP\|rpsQ\|rplN\|rplX\|rplE\|rpsN\|rpsH\|rplF\|rplR\|rpsE\|rpmD\|rplO\|rpsM\|rpsK\|rpsD\|rplQ\|prpF\|prpC\|sspA\|fusB\|prfB\|dnaJ\|ftsH\|nusA\|infB\|rpsO\|pnpA\|deoA\|deoB\|rpoD\|rplS\|rpsB\|tsf\|frr\|ivdA\|ivdB\|ivdC\|ivdE\|ivdF\|ivdG\|fabV\|fabA\|speA\|liuG\|liuE\|liuD\|liuC\|liuB\|liuA\|ushA\|adk\|pheT\|ndk\|infC\|rpmI\|rplT\|efp\|bkdA1\|bkdA2\|bkdB\|gyrA\|ubiG\|ruvA\|aspS\|def-3\|ldh\|topA\|acs\|fabF\|fabH\|rpmF\|wbpQ\|rmlA\|yciH\|ribE\|SO_3468\|rpsT\|cpdB\|rpmA\|rplU\|hprT\|prsA\|rplI\|rpsR\|rpsF\|purA\|rpsI\|rplM\|hslV\|rpmG\|dut |

Table A-1 (cont'd)

| | | | | | | | |
|---|---|---|---|---|---|---|---|
| | | | | | | | \|exaC\|atpE |
| 1 | 9 | 8 | STRING Clusters | CL:161 | Small ribosomal subunit | 3.5E-7 | rpsG\|rpsJ\|rpsC\|rpsQ\|rpsN\|rpsM\|rpsO\|rpsB |
| 1 | 1414 | 96 | GO Biological Process | GO:0006807 | Nitrogen compound metabolic process | 3.6E-20 | rpmH\|nusG\|rplK\|rplA\|rplL\|rpoB\|rpoC\|rpsG\|tufA\|rpsJ\|rplC\|rplD\|rplB\|rpsS\|rplV\|rpsC\|rplP\|rpsQ\|rplN\|rplX\|rplE\|rpsN\|rpsH\|rplF\|rplR\|rpsE\|rpmD\|rplO\|rpsM\|rpsK\|rpsD\|rplQ\|sspA\|fusB\|prfB\|dnaJ\|ftsH\|nusA\|infB\|rpsO\|pnpA\|deoA\|deoB\|rpoD\|rplS\|rpsB\|tsf\|frr\|ivdB\|ivdC\|ivdE\|ivdF\|speA\|liuE\|liuD\|liuA\|ushA\|adk\|pheT\|ndk\|infC\|rpmI\|rplT\|efp\|bkdA1\|bkdA2\|bkdB\|gyrA\|ruvA\|aspS\|d |

Table A-1 (cont'd)

| | | | | | | | |
|---|---|---|---|---|---|---|---|
| | | | | | | | ef-3\|ldh\|topA\|acs\|rpmF\|wbpQ\|yciH\|ribE\|SO_3468\|rpsT\|cpdB\|rpmA\|rplU\|hprT\|prsA\|rplI\|rpsR\|rpsF\|purA\|rpsI\|rplM\|hslV\|rpmG\|dut\|exaC\|atpE |
| 1 | 588 | 54 | COMPARTMENTS | GOCC:0032991 | Protein-containing complex | 3.79E-13 | nusG\|rplA\|rplL\|rpoB\|rpoC\|rpsG\|rplC\|rplD\|rplB\|rpsS\|rplV\|rpsC\|rpsQ\|rplN\|rplE\|rpsN\|rpsH\|rplF\|rplR\|rpsE\|rpmD\|rplO\|rpsD\|groES\|groEL\|nusA\|rpsO\|rpoD\|SO_1550\|rpsB\|ivdB\|ivdF\|liuE\|liuD\|liuB\|sucA\|sucD\|pheT\|bkdA2\|bkdB\|gyrA\|ubiG\|ruvA\|rpmF\|yciH\|raiA\|ribE\|rpsT\|clpB\|rplU\|prsA\|hslV\|exaC\|atpE |
| 1 | 75 | 49 | STRING Clusters | CL:109 | Structural constituent of ribosome, and Translation regulator activity | 3.86E-44 | rpmH\|nusG\|rplK\|rplA\|rplL\|rpsG\|tufA\|rpsJ\|rplC\|rplD\|rplB\|rpsS\|rplV\|rpsC\|rplP\|rpsQ\|rplN\|rplX\|rplE\|rpsN\|rpsH\|rplF\|rplR\|r |

Table A-1 (cont'd)

| | | | | | | | |
|---|---|---|---|---|---|---|---|
| | | | | | | | psE\|rpmD\|rplO\|rpsM\|rpsK\|rpsD\|rplQ\|fusB\|prfB\|rpsO\|rplS\|rpsB\|tig\|infC\|rpmI\|rplT\|rpmF\|rpsT\|rpmA\|rplU\|rplI\|rpsR\|rpsF\|rpsI\|rplM\|rpmG |
| 1 | 69 | 48 | STRING Clusters | CL:111 | Structural constituent of ribosome, and Elongation factor Tu GTP binding domain | 3.98E-44 | rpmH\|nusG\|rplK\|rplA\|rplL\|rpsG\|tufA\|rpsJ\|rplC\|rplD\|rplB\|rpsS\|rplV\|rpsC\|rplP\|rpsQ\|rplN\|rplX\|rplE\|rpsN\|rpsH\|rplF\|rplR\|rpsE\|rpmD\|rplO\|rpsM\|rpsK\|rpsD\|rplQ\|fusB\|rpsO\|rplS\|rpsB\|tig\|infC\|rpmI\|rplT\|rpmF\|rpsT\|rpmA\|rplU\|rplI\|rpsR\|rpsF\|rpsI\|rplM\|rpmG |
| 1 | 36 | 13 | GO Biological Process | GO:0006417 | Regulation of translation | 4.03E-8 | rplA\|tufA\|rpsD\|fusB\|prfB\|nusA\|infB\|tsf\|infC\|efp\|yciH\|raiA\|rplM |
| 1 | 454 | 68 | GO Biological Process | GO:1901566 | Organonitrogen compound biosynthetic process | 4.17E-29 | rpmH\|rplK\|rplA\|rplL\|rpsG\|tufA\|rpsJ\|rplC\|rplD\|rplB\|rpsS\|rplV\|rpsC\|rplP\|rpsQ\|rplN\|rplX\|rplE\|rpsN\|rpsH\|rplF\|rplR\|rpsE\|r |

Table A-1 (cont'd)

| | | | | | | | |
|---|---|---|---|---|---|---|---|
| | | | | | | | pmD\|rplO\|rpsM\|rpsK\|rpsD\|rplQ\|fusB\|prfB\|nusA\|infB\|rpsO\|rplS\|rpsB\|tsf\|frr\|speA\|adk\|pheT\|ndk\|infC\|rpmI\|rplT\|efp\|aspS\|def-3\|acs\|rpmF\|wbpQ\|yciH\|ribE\|SO_3468\|rpsT\|rpmA\|rplU\|hprT\|prsA\|rplI\|rpsR\|rpsF\|purA\|rpsI\|rplM\|rpmG\|dut\|atpE |
| 1 | 368 | 71 | GO Biological Process | GO:0044271 | Cellular nitrogen compound biosynthetic process | 4.29E-37 | rpmH\|nusG\|rplK\|rplA\|rplL\|rpoB\|rpoC\|rpsG\|tufA\|rpsJ\|rplC\|rplD\|rplB\|rpsS\|rplV\|rpsC\|rplP\|rpsQ\|rplN\|rplX\|rplE\|rpsN\|rpsH\|rplF\|rplR\|rpsE\|rpmD\|rplO\|rpsM\|rpsK\|rpsD\|rplQ\|fusB\|prfB\|nusA\|infB\|rpsO\|rpoD\|rplS\|rpsB\|tsf\|frr\|speA\|adk\|pheT\|ndk\|infC\|rpmI\|rplT\|efp\|aspS\|def-3\|acs\|rpmF\|yciH\|ribE\|SO_3468\|rpsT\|rpmA\|rplU\|hpr |

Table A-1 (cont'd)

| | | | | | | | |
|---|---|---|---|---|---|---|---|
| | | | | | | | T\|prsA\|rplI\|rpsR\|rpsF\|purA\|rpsI\|rplM\|rpmG\|dut\|atpE |
| 1 | 31 | 8 | UniProt Keywords | KW-0143 | Chaperone | 4.3E-4 | groES\|groEL\|dnaK\|dnaJ\|grpE\|tig\|htpG\|clpB |
| 1 | 49 | 40 | GO Cellular Component | GO:0044391 | Ribosomal subunit | 4.58E-38 | rplK\|rplA\|rplL\|rpsG\|rpsJ\|rplC\|rplB\|rpsS\|rplV\|rpsC\|rplP\|rpsQ\|rplN\|rplX\|rplE\|rpsN\|rpsH\|rplF\|rplR\|rpsE\|rpmD\|rplO\|rpsM\|rpsK\|rpsD\|rplQ\|rpsO\|rplS\|rpsB\|rpmI\|rplT\|rpmF\|rpsT\|rpmA\|rplI\|rpsR\|rpsF\|rpsI\|rplM\|rpmG |
| 1 | 62 | 44 | GO Cellular Component | GO:0005840 | Ribosome | 4.58E-40 | rpmH\|rplK\|rplA\|rplL\|rpsG\|rpsJ\|rplC\|rplD\|rplB\|rpsS\|rplV\|rpsC\|rplP\|rpsQ\|rplN\|rplX\|rplE\|rpsN\|rpsH\|rplF\|rplR\|rpsE\|rpmD\|rplO\|rpsM\|rpsK\|rpsD\|rplQ\|rpsO\|rplS\|rpsB\|rpmI\|rplT\|rpmF\|raiA\|rpsT\|rpmA\|rplU\|rplI\|rpsR\|rpsF\|rpsI\|rplM |

Table A-1 (cont'd)

| | | | | | | | |
|---|---|---|---|---|---|---|---|
| | | | | | | | \|rpmG |
| 1 | 337 | 30 | UniProt Keywords | KW-0963 | Cytoplasm | 4.65E-6 | tufA\|groES\|groEL\|fusB\|prfB\|dnaJ\|nusA\|infB\|pnpA\|deoB\|rpoD\|grpE\|tsf\|frr\|tig\|fabA\|htpG\|adk\|pheT\|ndk\|infC\|efp\|gyrA\|aspS\|fabH\|clpB\|hprT\|prsA\|purA\|hslV |
| 1 | 14 | 13 | STRING Clusters | CL:160 | Small ribosomal subunit | 4.7E-12 | rpsG\|rpsJ\|rpsS\|rpsC\|rplP\|rpsQ\|rpsN\|rplR\|rpsE\|rpsM\|rpsD\|rpsO\|rpsB |
| 1 | 21 | 17 | GO Cellular Component | GO:0015935 | Small ribosomal subunit | 5.08E-16 | rpsG\|rpsJ\|rpsS\|rpsC\|rpsQ\|rpsN\|rpsH\|rpsE\|rpsM\|rpsK\|rpsD\|rpsO\|rpsB\|rpsT\|rpsR\|rpsF\|rpsI |
| 1 | 47 | 30 | GO Molecular Function | GO:0019843 | rRNA binding | 5.0E-25 | rplK\|rplA\|rpsG\|rplC\|rplD\|rplB\|rpsS\|rplV\|rpsC\|rplP\|rpsQ\|rplN\|rplX\|rplE\|rpsN\|rpsH\|rplF\|rplR\|rpsE\|rplO\|rpsM\|rpsK\|rpsD\|rpsO\|rplT\|rpsT\|rplU\|rplI\|rpsR\|rpsF |

Table A-1 (cont'd)

| | | | | | | | |
|---|---|---|---|---|---|---|---|
| 1 | 1677 | 89 | GO Molecular Function | GO:0005488 | Binding | 5.61E-10 | nusG\|rplK\|rplA\|rplL\|rpoB\|rpoC\|rpsG\|tufA\|rpsJ\|rplC\|rplD\|rplB\|rpsS\|rplV\|rpsC\|rplP\|rpsQ\|rplN\|rplX\|rplE\|rpsN\|rpsH\|rplF\|rplR\|rpsE\|rplO\|rpsM\|rpsK\|rpsD\|groES\|groEL\|fusB\|prfB\|dnaK\|dnaJ\|greA\|ftsH\|nusA\|infB\|rpsO\|pnpA\|deoB\|rpoD\|grpE\|tsf\|frr\|ivdC\|ivdF\|tig\|fabV\|speA\|liuD\|liuA\|sucA\|sucD\|ushA\|htpG\|adk\|pheT\|ndk\|infC\|rplT\|efp\|gyrA\|ruvA\|aspS\|def-3\|ldh\|topA\|acs\|wbpQ\|rmlA\|yciH\|raiA\|rpsT\|cpdB\|clpB\|rplU\|hprT\|prsA\|rplI\|rpsR\|rpsF\|purA\|rpsI\|rplM\|hslV\|dut\|atpE |
| 1 | 118 | 59 | STRING Clusters | CL:100 | Translation, and ATP synthesis | 5.61E-49 | rpmH\|nusG\|rplK\|rplA\|rplL\|rpsG\|tufA\|rpsJ\|rplC\|rplD\|rplB\|rpsS\|rplV\|rpsC\|rplP\|rpsQ\|rplN\|rplX\|rplE\|rpsN\|rps |

Table A-1 (cont'd)

| | | | | | | | |
|---|---|---|---|---|---|---|---|
| | | | | | | | H\|rplF\|rplR\|rpsE\|rpmD\|rplO\|rpsM\|rpsK\|rpsD\|rplQ\|fusB\|prfB\|nusA\|infB\|rpsO\|rplS\|rpsB\|tsf\|frr\|tig\|pheT\|infC\|rpmI\|rplT\|efp\|aspS\|def-3\|rpmF\|raiA\|rpsT\|rpmA\|rplU\|rplI\|rpsR\|rpsF\|rpsI\|rplM\|rpmG\|atpE |
| 1 | 51 | 41 | STRING Clusters | CL:123 | Ribosome | 5.64E-39 | rpmH\|rplK\|rplA\|rplL\|rpsG\|rpsJ\|rplC\|rplD\|rplB\|rpsS\|rplV\|rpsC\|rplP\|rpsQ\|rplN\|rplX\|rplE\|rpsN\|rplF\|rplR\|rpsE\|rpmD\|rplO\|rpsM\|rpsD\|rplQ\|rpsO\|rplS\|rpsB\|rpmI\|rplT\|rpmF\|rpsT\|rpmA\|rplU\|rplI\|rpsR\|rpsF\|rpsI\|rplM\|rpmG |
| 1 | 10 | 8 | STRING Clusters | CL:515 | Stress response, and Proteasome complex | 5.66E-7 | groES\|groEL\|dnaK\|dnaJ\|grpE\|htpG\|clpB\|hslV |
| 1 | 190 | 58 | GO Biological Process | GO:0043603 | Cellular amide metabolic process | 5.75E-38 | rpmH\|rplK\|rplA\|rplL\|rpsG\|tufA\|rpsJ\|rplC\|rplD\|rplB\|rpsS\|rplV\|rpsC\|rplP\|rpsQ\|rplN\|rplX\|rplE\|rpsN\|rpsH\|rpl |

Table A-1 (cont'd)

| | | | | | | | |
|---|---|---|---|---|---|---|---|
| | | | | | | | F\|rplR\|rpsE\|rpmD\|rplO\|rpsM\|rpsK\|rpsD\|rplQ\|sspA\|fusB\|prfB\|nusA\|infB\|rpsO\|rplS\|rpsB\|tsf\|frr\|pheT\|infC\|rpmI\|rplT\|efp\|aspS\|def-3\|acs\|rpmF\|yciH\|rpsT\|rpmA\|rplU\|rplI\|rpsR\|rpsF\|rpsI\|rplM\|rpmG |
| 1 | 13 | 10 | COMPARTMENTS | GOCC:0022627 | Cytosolic small ribosomal subunit | 5.89E-9 | rpsG\|rpsC\|rpsQ\|rpsN\|rpsH\|rpsE\|rpsD\|rpsO\|raiA\|rpsT |
| 1 | 258 | 61 | GO Biological Process | GO:0009059 | Macromolecule biosynthetic process | 6.03E-35 | rpmH\|nusG\|rplK\|rplA\|rplL\|rpoB\|rpoC\|rpsG\|tufA\|rpsJ\|rplC\|rplD\|rplB\|rpsS\|rplV\|rpsC\|rplP\|rpsQ\|rplN\|rplX\|rplE\|rpsN\|rpsH\|rplF\|rplR\|rpsE\|rpmD\|rplO\|rpsM\|rpsK\|rpsD\|rplQ\|fusB\|prfB\|nusA\|infB\|rpsO\|rpoD\|rplS\|rpsB\|tsf\|frr\|pheT\|infC\|rpmI\|rplT\|efp\|aspS\|def-3\|rpmF\|rmlA\|yciH\|rpsT\|rpmA\|rplU\|rplI\|rpsR\|rpsF\|rps |

Table A-1 (cont'd)

| | | | | | | | |
|---|---|---|---|---|---|---|---|
| | | | | | | | I\|rplM\|rpmG |
| 1 | 48 | 13 | UniProt Keywords | KW-0648 | Protein biosynthesis | 6.04E-7 | tufA\|fusB\|prfB\|greA\|infB\|tsf\|frr\|pheT\|infC\|efp\|aspS\|def-3\|yciH |
| 1 | 64 | 47 | STRING Clusters | CL:115 | Structural constituent of ribosome | 6.17E-44 | rpmH\|nusG\|rplK\|rplA\|rplL\|rpsG\|tufA\|rpsJ\|rplC\|rplD\|rplB\|rpsS\|rplV\|rpsC\|rplP\|rpsQ\|rplN\|rplX\|rplE\|rpsN\|rpsH\|rplF\|rplR\|rpsE\|rpmD\|rplO\|rpsM\|rpsK\|rpsD\|rplQ\|fusB\|rpsO\|rplS\|rpsB\|tig\|rpmI\|rplT\|rpmF\|rpsT\|rpmA\|rplU\|rplI\|rpsR\|rpsF\|rpsI\|rplM\|rpmG |
| 1 | 42 | 9 | GO Biological Process | GO:0006457 | Protein folding | 6.2E-4 | groES\|groEL\|dnaK\|dnaJ\|grpE\|tig\|SO_1995\|htpG\|clpB |
| 1 | 142 | 47 | GO Cellular Component | GO:0043229 | Intracellular organelle | 6.41E-32 | rpmH\|rplK\|rplA\|rplL\|rpsG\|rpsJ\|rplC\|rplD\|rplB\|rpsS\|rplV\|rpsC\|rplP\|rpsQ\|rplN\|rplX\|rplE\|rpsN\|rpsH\|rplF\|rpl |

Table A-1 (cont'd)

| | | | | | | | |
|---|---|---|---|---|---|---|---|
| | | | | | | | R\|rpsE\|rpmD\|rplO\|rpsM\|rpsK\|rpsD\|rplQ\|rpsO\|rplS\|rpsB\|rpmI\|rplT\|bkdA1\|gyrA\|topA\|rpmF\|raiA\|rpsT\|rpmA\|rplU\|rplI\|rpsR\|rpsF\|rpsI\|rplM\|rpmG |
| 1 | 86 | 33 | UniProt Keywords | KW-0694 | RNA-binding | 6.76E-23 | rplK\|rplA\|rpsG\|rplC\|rplD\|rplB\|rpsS\|rplV\|rpsC\|rplP\|rpsQ\|rplN\|rplX\|rplE\|rpsN\|rpsH\|rplF\|rplR\|rpsE\|rplO\|rpsM\|rpsK\|rpsD\|nusA\|rpsO\|pnpA\|pheT\|rplT\|rpsT\|rplU\|rplI\|rpsR\|rpsF |
| 1 | 272 | 61 | GO Biological Process | GO:0010467 | Gene expression | 6.8E-34 | rpmH\|nusG\|rplK\|rplA\|rplL\|rpoB\|rpoC\|rpsG\|tufA\|rpsJ\|rplC\|rplD\|rplB\|rpsS\|rplV\|rpsC\|rplP\|rpsQ\|rplN\|rplX\|rplE\|rpsN\|rpsH\|rplF\|rplR\|rpsE\|rpmD\|rplO\|rpsM\|rpsK\|rpsD\|rplQ\|fusB\|prfB\|nusA\|infB\|rpsO\|pnpA\|rpoD\|rplS\|rpsB\|tsf\|frr\|pheT\|infC\|rpmI\|rplT\|efp\|aspS\|def- |

Table A-1 (cont'd)

| | | | | | | | |
|---|---|---|---|---|---|---|---|
| | | | | | | | 3\|rpmF\|yciH\|rpsT\|rpmA\|rplU\|rplI\|rpsR\|rpsF\|rpsI\|rplM\|rpmG |
| 1 | 181 | 18 | GO Biological Process | GO:1901575 | Organic substance catabolic process | 6.9E-4 | prpF\|ftsH\|pnpA\|deoB\|ivdA\|ivdC\|ivdE\|ivdF\|speA\|liuE\|liuA\|ushA\|bkdA1\|bkdA2\|bkdB\|cpdB\|hslV\|dut |
| 1 | 15 | 12 | COMPARTMENTS | GOCC:0015935 | Small ribosomal subunit | 7.12E-11 | rpsG\|rpsS\|rpsC\|rpsQ\|rpsN\|rpsH\|rpsE\|rpsD\|rpsO\|rpsB\|raiA\|rpsT |
| 1 | 97 | 56 | STRING Clusters | CL:104 | Structural constituent of ribosome, and Translation regulator activity | 7.29E-49 | rpmH\|nusG\|rplK\|rplA\|rplL\|rpsG\|tufA\|rpsJ\|rplC\|rplD\|rplB\|rpsS\|rplV\|rpsC\|rplP\|rpsQ\|rplN\|rplX\|rplE\|rpsN\|rpsH\|rplF\|rplR\|rpsE\|rpmD\|rplO\|rpsM\|rpsK\|rpsD\|rplQ\|fusB\|prfB\|nusA\|infB\|rpsO\|rplS\|rpsB\|tsf\|frr\|tig\|infC\|rpmI\|rplT\|def-3\|rpmF\|raiA\|rpsT\|rpmA\|rplU\|rplI\|rpsR\|rpsF\|rpsI\|rplM\|rpmG\|atpE |

Table A-1 (cont'd)

| | | | | | | | |
|---|---|---|---|---|---|---|---|
| 1 | 315 | 56 | GO Cellular Component | GO:0032991 | Protein-containing complex | 7.42E-27 | rplK\|rplA\|rplL\|rpoB\|rpoC\|rpsG\|rpsJ\|rplC\|rplB\|rpsS\|rplV\|rpsC\|rplP\|rpsQ\|rplN\|rplX\|rplE\|rpsN\|rpsH\|rplF\|rplR\|rpsE\|rpmD\|rplO\|rpsM\|rpsK\|rpsD\|rplQ\|groEL\|rpsO\|rplS\|rpsB\|ivdF\|liuD\|liuC\|liuB\|sucA\|sucD\|pheT\|rpmI\|rplT\|bkdB\|ruvA\|rpmF\|ribE\|rpsT\|rpmA\|prsA\|rplI\|rpsR\|rpsF\|rpsI\|rplM\|hslV\|rpmG\|atpE |
| 1 | 1531 | 110 | COMPARTMENTS | GOCC:0005622 | Intracellular | 7.6E-30 | rpmH\|nusG\|rplK\|rplA\|rplL\|rpoB\|rpoC\|rpsG\|tufA\|rpsJ\|rplC\|rplD\|rplB\|rpsS\|rplV\|rpsC\|rplP\|rpsQ\|rplN\|rplX\|rplE\|rpsN\|rpsH\|rplF\|rplR\|rpsE\|rpmD\|rplO\|rpsM\|rpsK\|rpsD\|rplQ\|prpF\|prpC\|sspA\|groES\|groEL\|fusB\|prfB\|dnaK\|dnaJ\|greA\|nusA\|infB\|rpsO\|pnpA\|deoA\|deoB\|rpoD\|rplS\|grp |

Table A-1 (cont'd)

| | | | | | | | |
|---|---|---|---|---|---|---|---|
| | | | | | | | E\|SO_1550\|rpsB\|tsf\|frr\|ivdA\|ivdC\|ivdG\|tig\|fabA\|speA\|liuG\|liuE\|liuC\|liuA\|sucA\|sucD\|SO_1995\|htpG\|adk\|pheT\|ndk\|infC\|rpmI\|rplT\|efp\|bkdA1\|bkdA2\|bkdB\|gyrA\|ubiG\|ruvA\|aspS\|def-3\|ldh\|topA\|acs\|fabF\|fabH\|rpmF\|wbpQ\|rmlA\|yciH\|raiA\|SO_3468\|rpsT\|clpB\|rpmA\|rplU\|hprT\|rplI\|rpsR\|rpsF\|purA\|rpsI\|rplM\|hslV\|rpmG\|dut\|atpE |
| 1 | 29 | 22 | COMPARTMENTS | GOCC:0022626 | Cytosolic ribosome | 7.88E-20 | rplA\|rplL\|rpsG\|rplC\|rplD\|rplB\|rplV\|rpsC\|rpsQ\|rplE\|rpsN\|rpsH\|rplF\|rplR\|rpsE\|rpmD\|rplO\|rpsD\|rpsO\|raiA\|rpsT\|rplU |
| 1 | 896 | 84 | GO Biological Process | GO:1901564 | Organonitrogen compound metabolic process | 8.1E-25 | rpmH\|rplK\|rplA\|rplL\|rpsG\|tufA\|rpsJ\|rplC\|rplD\|rplB\|rpsS\|rplV\|rpsC\|rplP\|rpsQ\|rplN\|rplX\|rplE\|rpsN\|rpsH\|rplF\|rplR\|rpsE\|rpmD\|rplO\|rp |

Table A-1 (cont'd)

| | | | | | | | |
|---|---|---|---|---|---|---|---|
| | | | | | | | sM\|rpsK\|rpsD\|rplQ\|sspA\|fusB\|prfB\|ftsH\|nusA\|infB\|rpsO\|deoA\|rplS\|rpsB\|tsf\|frr\|ivdB\|ivdC\|ivdE\|ivdF\|speA\|liuE\|liuD\|liuA\|adk\|pheT\|ndk\|infC\|rpmI\|rplT\|efp\|bkdA1\|bkdA2\|bkdB\|aspS\|def-3\|ldh\|acs\|rpmF\|wbpQ\|yciH\|ribE\|SO_3468\|rpsT\|rpmA\|rplU\|hprT\|prsA\|rplI\|rpsR\|rpsF\|purA\|rpsI\|rplM\|hslV\|rpmG\|dut\|exaC\|atpE |
| 1 | 53 | 41 | COMPARTMENTS | GOCC:0005840 | Ribosome | 8.28E-38 | rpmH\|rplK\|rplA\|rplL\|rpsG\|rpsJ\|rplC\|rplD\|rplB\|rpsS\|rplV\|rpsC\|rplP\|rpsQ\|rplN\|rplX\|rplE\|rpsN\|rpsH\|rplF\|rplR\|rpsE\|rpmD\|rplO\|rpsK\|rpsD\|rpsO\|rpsB\|rpmI\|rplT\|rpmF\|raiA\|rpsT\|rpmA\|rplU\|rplI\|rpsR\|rpsF\|rpsI\|rplM\|rpmG |

Table A-1 (cont'd)

| | | | | | | | |
|---|---|---|---|---|---|---|---|
| 1 | 212 | 57 | GO Biological Process | GO:0034645 | Cellular macromolecule biosynthetic process | 8.42E-35 | rpmH\|rplK\|rplA\|rplL\|rpsG\|tufA\|rpsJ\|rplC\|rplD\|rplB\|rpsS\|rplV\|rpsC\|rplP\|rpsQ\|rplN\|rplX\|rplE\|rpsN\|rpsH\|rplF\|rplR\|rpsE\|rpmD\|rplO\|rpsM\|rpsK\|rpsD\|rplQ\|fusB\|prfB\|nusA\|infB\|rpsO\|rplS\|rpsB\|tsf\|frr\|pheT\|infC\|rpmI\|rplT\|efp\|aspS\|def-3\|rpmF\|rmlA\|yciH\|rpsT\|rpmA\|rplU\|rplI\|rpsR\|rpsF\|rpsI\|rplM\|rpmG |
| 1 | 27 | 22 | GO Cellular Component | GO:0022625 | Cytosolic large ribosomal subunit | 8.6E-21 | rplK\|rplA\|rplL\|rplC\|rplB\|rplV\|rplP\|rplN\|rplX\|rplE\|rplF\|rplR\|rpmD\|rplO\|rplQ\|rplS\|rpmI\|rplT\|rpmA\|rplI\|rplM\|rpmG |
| 1 | 28 | 23 | GO Cellular Component | GO:0015934 | Large ribosomal subunit | 8.78E-22 | rplK\|rplA\|rplL\|rplC\|rplB\|rplV\|rplP\|rplN\|rplX\|rplE\|rplF\|rplR\|rpmD\|rplO\|rplQ\|rplS\|rpmI\|rplT\|rpmF\|rpmA\|rplI\|rplM\|rpmG |
| 1 | 33 | 26 | COMPARTMENTS | GOCC:0044391 | Ribosomal subunit | 9.09E-24 | rplA\|rplL\|rpsG\|rplC\|rplD\|rplB\|rpsS\|rplV |

Table A-1 (cont'd)

| | | | | | | | |
|---|---|---|---|---|---|---|---|
| | | | | | | | \|rpsC\|rpsQ\|rplN\|rplE\|rpsN\|rpsH\|rplF\|rplR\|rpsE\|rpmD\|rplO\|rpsD\|rpsO\|rpsB\|rpmF\|raiA\|rpsT\|rplU |
| 1 | 21 | 9 | GO Molecular Function | GO:0008135 | Translation factor activity, RNA binding | 9.09E-6 | tufA\|fusB\|prfB\|nusA\|infB\|tsf\|infC\|efp\|yciH |
| 1 | 7 | 5 | GO Molecular Function | GO:0003729 | mRNA binding | 9.0E-4 | rplL\|rpsG\|rpsC\|rpsK\|rplM |
| 1 | 24 | 9 | KEGG Pathways | son00640 | Propanoate metabolism | 9.24E-6 | prpF\|prpC\|ivdA\|ivdB\|sucD\|bkdA1\|bkdA2\|bkdB\|acs |
| 1 | 54 | 43 | KEGG Pathways | son03010 | Ribosome | 9.71E-41 | rpmH\|rplK\|rplA\|rplL\|rpsG\|rpsJ\|rplC\|rplD\|rplB\|rpsS\|rplV\|rpsC\|rplP\|rpsQ\|rplN\|rplX\|rplE\|rpsN\|rpsH\|rplF\|rplR\|rpsE\|rpmD\|rplO\|rpsM\|rpsK\|rpsD\|rplQ\|rpsO\|rplS\|rpsB\|rpmI\|rplT\|rpmF\|rpsT\|rpmA\|rplU\|rplI\|rpsR\|rpsF\|rpsI\|rplM\|rpmG |
| 1 | 9 | 5 | UniProt Keywords | KW-0251 | Elongation factor | 9.7E-4 | tufA\|fusB\|greA\|tsf\|efp |

Table A-1 (cont'd)

| | | | | | | | |
|---|---|---|---|---|---|---|---|
| 1 | 39 | 27 | COMPARTMENTS | GOCC:1990904 | Ribonucleoprotein complex | 9.87E-24 | rplA\|rplL\|rpsG\|rplC\|rplD\|rplB\|rpsS\|rplV\|rpsC\|rpsQ\|rplN\|rplE\|rpsN\|rpsH\|rplF\|rplR\|rpsE\|rpmD\|rplO\|rpsD\|rpsO\|rpsB\|rpmF\|yciH\|raiA\|rpsT\|rplU |
| 1 | 197 | 64 | STRING Clusters | CL:95 | Translation, and Catalytic activity, acting on RNA | 9.96E-45 | rpmH\|nusG\|rplK\|rplA\|rplL\|rpoB\|rpoC\|rpsG\|tufA\|rpsJ\|rplC\|rplD\|rplB\|rpsS\|rplV\|rpsC\|rplP\|rpsQ\|rplN\|rplX\|rplE\|rpsN\|rpsH\|rplF\|rplR\|rpsE\|rpmD\|rplO\|rpsM\|rpsK\|rpsD\|rplQ\|fusB\|prfB\|greA\|nusA\|infB\|rpsO\|pnpA\|rpoD\|rplS\|rpsB\|tsf\|frr\|tig\|pheT\|infC\|rpmI\|rplT\|efp\|aspS\|def-3\|rpmF\|raiA\|rpsT\|rpmA\|rplU\|rplI\|rpsR\|rpsF\|rpsI\|rplM\|rpmG\|atpE |
| 2 | 33 | 3 | KEGG Pathways | son00620 | Pyruvate metabolism | 1.20E-03 | ppsA\|sfcA\|maeB |
| 2 | 95 | 4 | KEGG Pathways | son01200 | Carbon metabolism | 1.20E-03 | fdnG\|ppsA\|sfcA\|maeB |

Table A-1 (cont'd)

| | | | | | | | |
|---|---|---|---|---|---|---|---|
| 2 | 2 | 2 | SMART Domains | SM00919 | Malic enzyme, NAD binding domain | 2.10E-03 | sfcA\|maeB |
| 2 | 2 | 2 | SMART Domains | SM01274 | Malic enzyme, N-terminal domain | 2.10E-03 | sfcA\|maeB |
| 2 | 22 | 3 | GO Biological Process | GO:0006090 | Pyruvate metabolic process | 1.04E-02 | ppsA\|sfcA\|maeB |
| 2 | 2 | 2 | GO Molecular Function | GO:0004471 | Malate dehydrogenase (decarboxylating) (NAD+) activity | 1.21E-02 | sfcA\|maeB |
| 2 | 3 | 2 | GO Biological Process | GO:0006108 | Malate metabolic process | 1.86E-02 | sfcA\|maeB |
| 2 | 350 | 5 | UniProt Keywords | KW-0479 | Metal-binding | 2.12E-02 | fdnG\|cysS\|ppsA\|sfcA\|maeB |
| 2 | 2 | 2 | InterPro Domains | IPR001891 | Malic oxidoreductase | 2.56E-02 | sfcA\|maeB |
| 2 | 2 | 2 | InterPro Domains | IPR012301 | Malic enzyme, N-terminal domain | 2.56E-02 | sfcA\|maeB |
| 2 | 2 | 2 | InterPro Domains | IPR012302 | Malic enzyme, NAD-binding | 2.56E-02 | sfcA\|maeB |
| 2 | 2 | 2 | InterPro Domains | IPR015884 | Malic enzyme, conserved site | 2.56E-02 | sfcA\|maeB |
| 2 | 2 | 2 | InterPro Domains | IPR037062 | Malic enzyme, N-terminal domain superfamily | 2.56E-02 | sfcA\|maeB |
| 2 | 6 | 2 | InterPro Domains | IPR046346 | Aminoacid dehydrogenase-like, N-terminal domain superfamily | 2.56E-02 | sfcA\|maeB |

*Table A-2. Complete enrichment table for less abundant proteins in minimal medium group.*

| Cluster | # Background genes | # Genes | Category | Term name | Description | FDR (p-value) | Genes |
|---|---|---|---|---|---|---|---|
| 1 | 109 | 16 | KEGG Pathways | son01230 | Biosynthesis of amino acids | 3.80E-17 | argC\|argB\|argH\|luxS\|gltB\|hisD\|hisG\|metC\|ilvI\|asd\|thrC\|talB\|metB\|leuA\|ilvD\|ilvC |
| 1 | 290 | 18 | KEGG Pathways | son01110 | Biosynthesis of secondary metabolites | 5.96E-14 | argC\|argB\|argH\|gltB\|sdhB\|hisD\|hisG\|metC\|fumB\|ilvI\|zwf\|asd\|thrC\|talB\|metB\|leuA\|ilvD\|ilvC |
| 1 | 646 | 22 | KEGG Pathways | son01100 | Metabolic pathways | 1.80E-13 | argC\|argB\|argH\|metY\|luxS\|gltB\|sdhB\|hisD\|hisG\|metC\|fumB\|ilvI\|zwf\|pflB\|pta\|asd\|thrC\|talB\|metB\|leuA\|ilvD\|ilvC |
| 1 | 72 | 11 | STRING Clusters | CL:876 | Amino-acid biosynthesis, and Valine, leucine and isoleucine biosynthesis | 4.04E-10 | argC\|argB\|argH\|hisD\|hisG\|ilvI\|asd\|thrC\|leuA\|ilvD\|ilvC |
| 1 | 187 | 14 | GO Biological Process | GO:0006520 | Cellular amino acid metabolic process | 4.50E-10 | argC\|argB\|argH\|metY\|gltB\|hisD\|hisG\|metC\|asd\|thrC\|metB\|leuA\|ilvD\|ilvC |
| 1 | 335 | 17 | GO Biological Process | GO:0019752 | Carboxylic acid metabolic process | 4.50E-10 | argC\|argB\|argH\|metY\|gltB\|lldG\|lldF\|hisD\|hisG\|metC\|ilvI\|asd\|thrC\|met |

Table A-2 (cont'd)

| | | | | | | | |
|---|---|---|---|---|---|---|---|
| | | | | | | | B\|leuA\|ilvD\|ilvC |
| 1 | 591 | 20 | GO Biological Process | GO:0044281 | Small molecule metabolic process | 4.50E-10 | argC\|argB\|argH\|metY\|gltB\|lldG\|lldF\|hisD\|hisG\|metC\|ilvI\|zwf\|pflB\|pta\|asd\|thrC\|metB\|leuA\|ilvD\|ilvC |
| 1 | 119 | 12 | STRING Clusters | CL:875 | Amino-acid biosynthesis, and Ribonucleoside monophosphate biosynthetic process | 1.20E-09 | argC\|argB\|argH\|gltB\|hisD\|hisG\|ilvI\|asd\|thrC\|leuA\|ilvD\|ilvC |
| 1 | 40 | 9 | STRING Clusters | CL:878 | 2-Oxocarboxylic acid metabolism, and Lysine biosynthetic process | 1.30E-09 | argC\|argB\|argH\|ilvI\|asd\|thrC\|leuA\|ilvD\|ilvC |
| 1 | 101 | 11 | GO Biological Process | GO:0008652 | Cellular amino acid biosynthetic process | 3.13E-09 | argC\|argB\|argH\|gltB\|hisD\|hisG\|asd\|thrC\|leuA\|ilvD\|ilvC |
| 1 | 138 | 12 | GO Biological Process | GO:1901605 | Alpha-amino acid metabolic process | 3.13E-09 | argC\|argB\|argH\|metY\|gltB\|metC\|asd\|thrC\|metB\|leuA\|ilvD\|ilvC |
| 1 | 73 | 10 | UniProt Keywords | KW-0028 | Amino-acid biosynthesis | 4.13E-09 | argC\|argB\|argH\|hisD\|hisG\|ilvI\|asd\|leuA\|ilvD\|ilvC |

Table A-2 (cont'd)

| | | | | | | | |
|---|---|---|---|---|---|---|---|
| 1 | 25 | 7 | KEGG Pathways | son01210 | 2-Oxocarboxylic acid metabolism | 1.04E-08 | argC\|argB\|ilvI\|asd\|leuA\|ilvD\|ilvC |
| 1 | 85 | 9 | GO Biological Process | GO:1901607 | Alpha-amino acid biosynthetic process | 2.69E-07 | argC\|argB\|argH\|gltB\|asd\|thrC\|leuA\|ilvD\|ilvC |
| 1 | 96 | 9 | STRING Clusters | CL:1201 | Carbon metabolism, and Starch and sucrose metabolism | 9.33E-07 | lldG\|lldF\|lldE\|sdhB\|fumB\|zwf\|pflB\|pta\|talB |
| 1 | 164 | 9 | KEGG Pathways | son01120 | Microbial metabolism in diverse environments | 8.61E-06 | gltB\|sdhB\|fumB\|zwf\|pflB\|pta\|asd\|thrC\|talB |
| 1 | 1661 | 23 | GO Biological Process | GO:0044237 | Cellular metabolic process | 1.69E-05 | argC\|argB\|argH\|metY\|gltB\|lldG\|lldF\|lldE\|sdhB\|hisD\|hisG\|metC\|fumB\|ilvI\|zwf\|pta\|asd\|thrC\|talB\|metB\|leuA\|ilvD\|ilvC |
| 1 | 19 | 5 | STRING Clusters | CL:880 | Lysine biosynthesis, and Arginine biosynthesis | 3.44E-05 | argC\|argB\|argH\|asd\|thrC |
| 1 | 34 | 5 | KEGG Pathways | son00270 | Cysteine and methionine metabolism | 5.02E-05 | metY\|luxS\|metC\|asd\|metB |

Table A-2 (cont'd)

| | | | | | | | |
|---|---|---|---|---|---|---|---|
| 1 | 15 | 4 | KEGG Pathways | son00290 | Valine, leucine and isoleucine biosynthesis | 6.09E-05 | ilvI\|leuA\|ilvD\|ilvC |
| 1 | 9 | 4 | UniProt Keywords | KW-0100 | Branched-chain amino acid biosynthesis | 6.45E-05 | ilvI\|leuA\|ilvD\|ilvC |
| 1 | 121 | 8 | UniProt Keywords | KW-0456 | Lyase | 6.45E-05 | argH\|metY\|luxS\|metC\|fumB\|pflB\|thrC\|ilvD |
| 1 | 2017 | 24 | GO Biological Process | GO:0008152 | Metabolic process | 7.78E-05 | argC\|argB\|argH\|metY\|gltB\|lldG\|lldF\|lldE\|sdhB\|hisD\|hisG\|metC\|fumB\|ilvI\|zwf\|pflB\|pta\|asd\|thrC\|talB\|metB\|leuA\|ilvD\|ilvC |
| 1 | 1435 | 21 | GO Cellular Component | GO:0005737 | Cytoplasm | 1.30E-04 | argC\|argB\|argH\|luxS\|gltB\|lldG\|hisD\|hisG\|metC\|fumB\|ilvI\|zwf\|pflB\|pta\|asd\|thrC\|talB\|metB\|leuA\|ilvD\|ilvC |
| 1 | 11 | 4 | GO Biological Process | GO:0009082 | Branched-chain amino acid biosynthetic process | 1.50E-04 | asd\|leuA\|ilvD\|ilvC |
| 1 | 11 | 4 | STRING Clusters | CL:931 | Branched-chain amino acid biosynthesis | 1.70E-04 | ilvI\|leuA\|ilvD\|ilvC |
| 1 | 12 | 4 | STRING Clusters | CL:2653 | Homoserine metabolic | 2.00E-04 | metY\|luxS\|metC\|metB |

Table A-2 (cont'd)

| | | | | | | | |
|---|---|---|---|---|---|---|---|
| | | | | | process, and Methionine metabolic process | | |
| 1 | 454 | 12 | GO Biological Process | GO:1901566 | Organonitrogen compound biosynthetic process | 4.90E-04 | argC\|argB\|argH\|gltB\|hisD\|hisG\|pta\|asd\|thrC\|leuA\|ilvD\|ilvC |
| 1 | 1181 | 19 | COMPARTMENTS | GOCC:0005737 | Cytoplasm | 5.70E-04 | argC\|argB\|metY\|luxS\|gltB\|lldG\|hisD\|hisG\|fumB\|ilvI\|zwf\|pflB\|pta\|asd\|thrC\|talB\|leuA\|ilvD\|ilvC |
| 1 | 742 | 15 | COMPARTMENTS | GOCC:0005829 | Cytosol | 7.40E-04 | metY\|luxS\|gltB\|lldG\|hisD\|fumB\|zwf\|pflB\|pta\|asd\|thrC\|talB\|leuA\|ilvD\|ilvC |
| 1 | 33 | 4 | KEGG Pathways | son00620 | Pyruvate metabolism | 8.40E-04 | fumB\|pflB\|pta\|leuA |
| 1 | 5 | 3 | GO Biological Process | GO:0019346 | Transsulfuration | 9.60E-04 | metY\|metC\|metB |
| 1 | 5 | 3 | STRING Clusters | CL:1378 | LUD domain, and Cysteine-rich domain | 0.001 | lldG\|lldF\|lldE |
| 1 | 86 | 6 | STRING Clusters | CL:1203 | Carbon metabolism, and Starch and sucrose metabolism | 0.0012 | sdhB\|fumB\|zwf\|pflB\|pta\|talB |

Table A-2 (cont'd)

| | | | | | | | |
|---|---|---|---|---|---|---|---|
| 1 | 6 | 3 | GO Biological Process | GO:0009097 | Isoleucine biosynthetic process | 0.0013 | asd\|ilvD\|ilvC |
| 1 | 13 | 3 | KEGG Pathways | son00220 | Arginine biosynthesis | 0.0013 | argC\|argB\|argH |
| 1 | 6 | 3 | STRING Clusters | CL:904 | Arginine biosynthesis | 0.0013 | argC\|argB\|argH |
| 1 | 25 | 4 | GO Biological Process | GO:0009084 | Glutamine family amino acid biosynthetic process | 0.0016 | argC\|argB\|argH\|gltB |
| 1 | 27 | 4 | GO Biological Process | GO:0000096 | Sulfur amino acid metabolic process | 0.002 | metY\|metC\|asd\|metB |
| 1 | 1531 | 20 | COMPARTMENTS | GOCC:0005622 | Intracellular | 0.0022 | argC\|argB\|metY\|luxS\|gltB\|lldG\|sdhB\|hisD\|hisG\|fumB\|ilvI\|zwf\|pflB\|pta\|asd\|thrC\|talB\|leuA\|ilvD\|ilvC |
| 1 | 1761 | 21 | GO Biological Process | GO:0071704 | Organic substance metabolic process | 0.0023 | argC\|argB\|argH\|metY\|gltB\|lldG\|lldF\|hisD\|hisG\|metC\|ilvI\|zwf\|pflB\|pta\|asd\|thrC\|talB\|metB\|leuA\|ilvD\|ilvC |
| 1 | 896 | 15 | GO Biological Process | GO:1901564 | Organonitrogen compound metabolic process | 0.0029 | argC\|argB\|argH\|metY\|gltB\|hisD\|hisG\|metC\|pta\|asd\|thrC\|metB\|leuA\|ilvD\|ilvC |
| 1 | 95 | 5 | KEGG Pathways | son01200 | Carbon metabolism | 0.0031 | sdhB\|fumB\|zwf\|pta\|talB |

Table A-2 (cont'd)

| | | | | | | | |
|---|---|---|---|---|---|---|---|
| 1 | 20 | 3 | KEGG Pathways | son00770 | Pantothenate and CoA biosynthesis | 0.0032 | ilvI\|ilvD\|ilvC |
| 1 | 10 | 3 | UniProt Keywords | KW-0055 | Arginine biosynthesis | 0.0033 | argC\|argB\|argH |
| 1 | 1489 | 19 | GO Biological Process | GO:0044238 | Primary metabolic process | 0.0042 | argC\|argB\|argH\|metY\|gltB\|sdhB\|hisD\|hisG\|metC\|zwf\|pflB\|pta\|asd\|thrC\|talB\|metB\|leuA\|ilvD\|ilvC |
| 1 | 600 | 12 | GO Cellular Component | GO:0005829 | Cytosol | 0.0046 | argH\|luxS\|gltB\|lldG\|hisD\|fumB\|zwf\|asd\|talB\|leuA\|ilvD\|ilvC |
| 1 | 38 | 4 | UniProt Keywords | KW-0521 | NADP | 0.005 | argC\|zwf\|asd\|ilvC |
| 1 | 38 | 4 | UniProt Keywords | KW-0663 | Pyridoxal phosphate | 0.005 | metY\|metC\|thrC\|metB |
| 1 | 2525 | 24 | GO Biological Process | GO:0009987 | Cellular process | 0.0062 | argC\|argB\|argH\|metY\|luxS\|gltB\|lldG\|lldF\|lldE\|sdhB\|hisD\|hisG\|metC\|fumB\|ilvI\|zwf\|pta\|asd\|thrC\|talB\|metB\|leuA\|ilvD\|ilvC |
| 1 | 27 | 3 | KEGG Pathways | son00650 | Butanoate metabolism | 0.0066 | sdhB\|ilvI\|pflB |
| 1 | 76 | 5 | STRING Clusters | CL:1204 | Carbon metabolism, and Starch and sucrose metabolism | 0.007 | sdhB\|fumB\|zwf\|pta\|talB |

Table A-2 (cont'd)

| | | | | | | | |
|---|---|---|---|---|---|---|---|
| 1 | 2032 | 23 | GO Molecular Function | GO:0003824 | Catalytic activity | 0.008 | argC\|argB\|argH\|metY\|luxS\|gltB\|lldG\|sdhB\|hisD\|hisG\|metC\|fumB\|ilvI\|zwf\|pflB\|pta\|asd\|thrC\|talB\|metB\|leuA\|ilvD\|ilvC |
| 1 | 48 | 5 | GO Molecular Function | GO:0019842 | Vitamin binding | 0.008 | metY\|metC\|ilvI\|thrC\|metB |
| 1 | 975 | 16 | GO Molecular Function | GO:0043167 | Ion binding | 0.008 | argB\|metY\|luxS\|gltB\|lldF\|lldE\|sdhB\|hisD\|hisG\|metC\|fumB\|ilvI\|thrC\|metB\|ilvD\|ilvC |
| 1 | 104 | 6 | GO Molecular Function | GO:0051536 | Iron-sulfur cluster binding | 0.008 | gltB\|lldF\|lldE\|sdhB\|fumB\|ilvD |
| 1 | 119 | 6 | GO Molecular Function | GO:0016829 | Lyase activity | 0.0092 | argH\|luxS\|metC\|fumB\|thrC\|ilvD |
| 1 | 34 | 4 | GO Molecular Function | GO:0030170 | Pyridoxal phosphate binding | 0.0092 | metY\|metC\|thrC\|metB |
| 1 | 16 | 3 | GO Biological Process | GO:0006526 | Arginine biosynthetic process | 0.0097 | argC\|argB\|argH |
| 1 | 4 | 3 | InterPro Domains | IPR000277 | Cys/Met metabolism, pyridoxal phosphate-dependent enzyme | 0.0117 | metY\|metC\|metB |
| 1 | 675 | 12 | GO Biological Process | GO:0044249 | Cellular biosynthetic process | 0.0139 | argC\|argB\|argH\|gltB\|hisD\|hisG\|pta\|asd\|thrC\|leuA\|ilvD\|ilvC |

Table A-2 (cont'd)

| | | | | | | | |
|---|---|---|---|---|---|---|---|
| 1 | 3 | 2 | GO Biological Process | GO:0042450 | Arginine biosynthetic process via ornithine | 0.0164 | argB\|argH |
| 1 | 241 | 7 | UniProt Keywords | KW-0560 | Oxidoreductase | 0.0176 | argC\|gltB\|sdhB\|hisD\|zwf\|asd\|ilvC |
| 1 | 106 | 5 | GO Biological Process | GO:0006790 | Sulfur compound metabolic process | 0.0184 | metY\|metC\|pta\|asd\|metB |
| 1 | 12 | 2 | KEGG Pathways | son00450 | Selenocompound metabolism | 0.0259 | metC\|metB |
| 1 | 572 | 11 | GO Molecular Function | GO:0046872 | Metal ion binding | 0.0263 | luxS\|gltB\|lldF\|lldE\|sdhB\|hisD\|hisG\|fumB\|ilvI\|ilvD\|ilvC |
| 1 | 350 | 8 | UniProt Keywords | KW-0479 | Metal-binding | 0.0271 | luxS\|sdhB\|hisD\|hisG\|fumB\|ilvI\|ilvD\|ilvC |
| 1 | 5 | 2 | GO Biological Process | GO:0009099 | Valine biosynthetic process | 0.0287 | ilvD\|ilvC |
| 1 | 2 | 2 | SMART Domains | SM00859 | Semialdehyde dehydrogenase, NAD binding domain | 0.029 | argC\|asd |
| 1 | 14 | 2 | KEGG Pathways | son00340 | Histidine metabolism | 0.0315 | hisD\|hisG |
| 1 | 1677 | 19 | GO Molecular Function | GO:0005488 | Binding | 0.0337 | argC\|argB\|metY\|luxS\|gltB\|lldF\|lldE\|sdhB\|hisD\|hisG\|metC\|fumB\|ilvI\|zwf\|asd\|thrC\|metB\|ilv |

Table A-2 (cont'd)

| | | | | | | | |
|---|---|---|---|---|---|---|---|
| | | | | | | | D\|ilvC |
| 1 | 604 | 11 | GO Molecular Function | GO:0036094 | Small molecule binding | 0.0337 | argC\|argB\|metY\|hisD\|hisG\|metC\|ilvI\|zwf\|asd\|thrC\|metB |
| 1 | 4 | 2 | GO Molecular Function | GO:0051538 | 3 iron, 4 sulfur cluster binding | 0.0337 | gltB\|sdhB |
| 1 | 7 | 2 | GO Biological Process | GO:0006089 | Lactate metabolic process | 0.0464 | lldG\|lldF |
| 1 | 7 | 2 | GO Biological Process | GO:0006098 | Pentose-phosphate shunt | 0.0464 | zwf\|talB |
| 1 | 5 | 2 | STRING Clusters | CL:933 | Valine biosynthetic process, and Acetolactate synthase, large subunit, biosynthetic | 0.0464 | ilvD\|ilvC |
| 1 | 29 | 3 | STRING Clusters | CL:1284 | Pentose phosphate pathway, and Glycolysis / Gluconeogenesis | 0.0496 | zwf\|pta\|talB |
| 2 | 21 | 5 | KEGG Pathways | son00400 | Phenylalanine, tyrosine and | 1.87E-07 | hisC\|aspC\|trpE\|trpG\|trpA |

Table A-2 (cont'd)

| | | | | | | | |
|---|---|---|---|---|---|---|---|
| | | | | | tryptophan biosynthesis | | |
| 2 | 109 | 6 | KEGG Pathways | son01230 | Biosynthesis of amino acids | 4.57E-06 | hisC\|aspC\|trpE\|trpG\|trpA\|leuB |
| 2 | 72 | 5 | STRING Clusters | CL:876 | Amino-acid biosynthesis, and Valine, leucine and isoleucine biosynthesis | 4.60E-04 | hisC\|trpE\|trpG\|trpA\|leuB |
| 2 | 29 | 4 | STRING Clusters | CL:962 | Phenylalanine, tyrosine and tryptophan biosynthesis, and Histidine biosynthesis | 4.60E-04 | hisC\|trpE\|trpG\|trpA |
| 2 | 646 | 8 | KEGG Pathways | son01100 | Metabolic pathways | 5.00E-04 | nuoI\|nuoCD\|hisC\|aspC\|trpE\|trpG\|trpA\|leuB |
| 2 | 290 | 6 | KEGG Pathways | son01110 | Biosynthesis of secondary metabolites | 6.20E-04 | hisC\|aspC\|trpE\|trpG\|trpA\|leuB |
| 2 | 4 | 2 | KEGG Pathways | son00401 | Novobiocin biosynthesis | 0.0017 | hisC\|aspC |

Table A-2 (cont'd)

| | | | | | | | |
|---|---|---|---|---|---|---|---|
| 2 | 16 | 3 | STRING Clusters | CL:964 | Aromatic amino acid biosynthesis, and Anthranilate synthase/para-aminobenzoate synthase like domain | 0.0024 | trpE\|trpG\|trpA |
| 2 | 8 | 2 | KEGG Pathways | son00360 | Phenylalanine metabolism | 0.0043 | hisC\|aspC |
| 2 | 73 | 4 | UniProt Keywords | KW-0028 | Amino-acid biosynthesis | 0.0054 | hisC\|trpE\|trpA\|leuB |
| 2 | 26 | 3 | STRING Clusters | CL:3097 | Oxidoreduction-driven active transmembrane transporter activity, and Peptidase M16, C-terminal | 0.0059 | nuoI\|nuoCD\|SO_4811 |
| 2 | 11 | 2 | KEGG Pathways | son00350 | Tyrosine metabolism | 0.0064 | hisC\|aspC |
| 2 | 5 | 2 | UniProt Keywords | KW-0822 | Tryptophan biosynthesis | 0.0135 | trpE\|trpA |

Table A-2 (cont'd)

| | | | | | | | |
|---|---|---|---|---|---|---|---|
| 2 | 6 | 2 | STRING Clusters | CL:981 | Tryptophan biosynthesis, and Anthranilate synthase component I-like | 0.0168 | trpG\|trpA |
| 2 | 8 | 2 | STRING Clusters | CL:3102 | NADH dehydrogenase (quinone) activity | 0.0227 | nuoI\|nuoCD |
| 2 | 10 | 2 | UniProt Keywords | KW-0874 | Quinone | 0.0281 | nuoI\|nuoCD |
| 2 | 28 | 2 | KEGG Pathways | son02024 | Quorum sensing | 0.0306 | trpE\|trpG |
| 2 | 67 | 3 | UniProt Keywords | KW-0520 | NAD | 0.0319 | nuoI\|nuoCD\|leuB |
| 2 | 18 | 2 | UniProt Keywords | KW-0032 | Aminotransferase | 0.04 | hisC\|aspC |
| 2 | 9 | 2 | GO Cellular Component | GO:0030964 | NADH dehydrogenase complex | 0.045 | nuoI\|nuoCD |
| 3 | 21 | 7 | STRING Clusters | CL:5638 | Mixed, incl. Transmembrane beta strand, and TonB, C-terminal | 3.03E-13 | SO_1824\|ttpC\|exbD\|tonB2\|SO_1829\|SO_2469\|SO_2907 |
| 3 | 10 | 6 | STRING Clusters | CL:5640 | Mixed, incl. TonB, C-terminal, and | 2.77E-12 | SO_1824\|ttpC\|exbD\|tonB2\|SO_1829\|SO_2907 |

Table A-2 (cont'd)

| | | | | | | | |
|---|---|---|---|---|---|---|---|
| | | | | | MotA/TolQ/ExbB proton channel | | |
| 3 | 5 | 4 | STRING Clusters | CL:5644 | MotA/TolQ/ExbB proton channel, and Gram-negative bacterial TonB protein | 4.51E-08 | SO_1824\|ttpC\|exbD\|tonB2 |
| 3 | 31 | 3 | UniProt Keywords | KW-0653 | Protein transport | 0.0043 | ttpC\|exbD\|tonB2 |
| 3 | 20 | 3 | GO Biological Process | GO:0034755 | Iron ion transmembrane transport | 0.008 | tonB2\|SO_2469\|SO_2907 |
| 3 | 218 | 5 | GO Biological Process | GO:0071702 | Organic substance transport | 0.008 | ttpC\|exbD\|tonB2\|SO_2469\|SO_2907 |
| 4 | 19 | 5 | STRING Clusters | CL:3524 | Sodium transport, and Rnf-Nqr subunit, membrane protein | 4.30E-09 | nqrA\|nqrB\|nqrC\|nqrF\|rnfG |
| 4 | 41 | 5 | UniProt Keywords | KW-1278 | Translocase | 3.52E-08 | nqrA\|nqrB\|nqrC\|nqrF\|rnfG |
| 4 | 12 | 4 | STRING Clusters | CL:3525 | Sodium transport | 1.87E-07 | nqrA\|nqrB\|nqrC\|nqrF |
| 4 | 15 | 4 | UniProt Keywords | KW-0739 | Sodium transport | 2.02E-07 | nqrA\|nqrB\|nqrC\|nqrF |
| 4 | 26 | 4 | UniProt Keywords | KW-0830 | Ubiquinone | 7.11E-07 | nqrA\|nqrB\|nqrC\|nqrF |
| 4 | 57 | 4 | UniProt | KW- | Flavoprot | 8.98E- | nqrB\|nqrC\|nqrF\|r |

Table A-2 (cont'd)

| | | | | | | | |
|---|---|---|---|---|---|---|---|
| | | | Keywords | 0285 | ein | 06 | nfG |
| 4 | 5 | 3 | STRING Clusters | CL:3538 | Sodium transport | 9.36E-06 | nqrA\|nqrB\|nqrC |
| 4 | 202 | 5 | UniProt Keywords | KW-0813 | Transport | 1.11E-05 | nqrA\|nqrB\|nqrC\|nqrF\|rnfG |
| 4 | 28 | 4 | GO Molecular Function | GO:0016655 | Oxidoreductase activity, acting on NAD(P)H, quinone or similar compound as acceptor | 1.25E-05 | nqrA\|nqrB\|nqrC\|nqrF |
| 4 | 67 | 4 | UniProt Keywords | KW-0520 | NAD | 1.25E-05 | nqrA\|nqrB\|nqrC\|nqrF |
| 4 | 24 | 4 | GO Biological Process | GO:0006814 | Sodium ion transport | 1.32E-05 | nqrA\|nqrB\|nqrC\|nqrF |
| 4 | 27 | 3 | UniProt Keywords | KW-0288 | FMN | 9.49E-05 | nqrB\|nqrC\|rnfG |
| 4 | 182 | 4 | UniProt Keywords | KW-0997 | Cell inner membrane | 4.90E-04 | nqrB\|nqrC\|nqrF\|rnfG |
| 4 | 241 | 4 | UniProt Keywords | KW-0560 | Oxidoreductase | 0.0013 | nqrA\|nqrB\|nqrC\|nqrF |
| 4 | 32 | 3 | GO Molecular Function | GO:0010181 | FMN binding | 0.0015 | nqrB\|nqrC\|rnfG |
| 4 | 379 | 5 | GO Molecular Function | GO:0016491 | Oxidoreductase activity | 0.0015 | nqrA\|nqrB\|nqrC\|nqrF\|rnfG |
| 4 | 85 | 3 | UniProt Keywords | KW-0597 | Phosphoprotein | 0.0017 | nqrB\|nqrC\|rnfG |

Table A-2 (cont'd)

| | | | | | | | |
|---|---|---|---|---|---|---|---|
| 4 | 5 | 2 | SMART Domains | SM00900 | This conserved region includes the FMN-binding site of the NqrC protein as well as the NosR and NirI regulatory proteins. | 0.0034 | nqrC\|rnfG |
| 4 | 5 | 2 | InterPro Domains | IPR007329 | FMN-binding | 0.0426 | nqrC\|rnfG |
| 4 | 103 | 3 | GO Biological Process | GO:0022900 | Electron transport chain | 0.0488 | nqrB\|nqrF\|rnfG |
| 5 | 60 | 4 | STRING Clusters | CL:4138 | Mixed, incl. HlyD family secretion protein, and Multidrug efflux transporter AcrB TolC docking domain, DN/DC subdomains | 2.60E-04 | tolC\|bpfA\|aggB\|SO_4321 |
| 5 | 11 | 3 | STRING Clusters | CL:4233 | Mixed, incl. ABC transporter transmembrane region, and | 2.60E-04 | bpfA\|aggB\|SO_4321 |

Table A-2 (cont'd)

| | | | | | | | |
|---|---|---|---|---|---|---|---|
| | | | | | Secretion protein HlyD, conserved site | | |

*Table A-3. Complete enrichment table for less abundant proteins in minimal medium group.*

| Cluster | # Background genes | # Genes | Category | Term name | Description | FDR (p-value) | Genes |
|---|---|---|---|---|---|---|---|
| 1 | 142 | 63 | STRING Clusters | CL:98 | Translation, and Protein export | 8.68E-50 | rpmH\|nusG\|rplK\|rplA\|rplL\|rpoB\|rpoC\|rpsG\|tufA\|rpsJ\|rplC\|rplD\|rplB\|rpsS\|rplV\|rpsC\|rplP\|rpsQ\|rplN\|rplX\|rplE\|rpsN\|rpsH\|rplF\|rplR\|rpsE\|rpmD\|rplO\|rpsM\|rpsK\|rpsD\|rplQ\|fusB\|prfB\|greA\|nusA\|infB\|rpsO\|rpoD\|rplS\|rpsB\|tsf\|frr\|tig\|pheT\|infC\|rpmI\|rplT\|efp\|aspS\|def-3\|rpmF\|raiA\|rpsT\|rpmA\|rplU\|rplI\|rpsR\|rpsF\|rpsI\|rplM\|rpmG\|atpE |
| 1 | 49 | 9 | STRING Clusters | CL:507 | Mixed, incl. Stress response, and Antioxidant activity | 1.10E-03 | groES\|groEL\|dnaK\|dnaJ\|ftsH\|grpE\|htpG\|clpB\|hslV |
| 1 | 591 | 36 | GO Biological Process | GO:0044281 | Small molecule metabolic process | 1.30E-03 | prpF\|prpC\|deoA\|deoB\|ivdA\|ivdE\|ivdF\|ivdG\|fabV\|fabA\|speA\|liuE |

Table A-3 (cont'd)

| | | | | | | | |
|---|---|---|---|---|---|---|---|
| | | | | | | | \|liuD\|liuB\|ushA\|adk\|pheT\|ndk\|bkdA1\|bkdA2\|bkdB\|ubiG\|aspS\|ldh\|acs\|fabF\|fabH\|wbpQ\|ribE\|SO_3468\|cpdB\|hprT\|prsA\|purA\|dut\|atpE |
| 1 | 18 | 6 | UniProt Keywords | KW-0820 | tRNA-binding | 1.30E-03 | rplA\|rpsG\|rplP\|rplE\|rpsM\|pheT |
| 1 | 290 | 22 | KEGG Pathways | son01110 | Biosynthesis of secondary metabolites | 1.70E-03 | ivdA\|ivdG\|fabV\|liuE\|sucA\|sucD\|ushA\|adk\|ndk\|bkdA1\|bkdA2\|bkdB\|ubiG\|ldh\|acs\|wbpQ\|rmlA\|ribE\|SO_3468\|hprT\|prsA\|exaC |
| 1 | 4 | 4 | GO Biological Process | GO:0006458 | De novo protein folding | 2.00E-03 | groES\|groEL\|dnaJ\|tig |
| 1 | 5 | 4 | STRING Clusters | CL:1632 | Valine catabolic process, and Acyl-CoA dehydrogenase, conserved site | 2.10E-03 | ivdB\|ivdC\|ivdE\|ivdF |
| 1 | 5 | 4 | STRING Clusters | CL:190 | Cytosolic large ribosomal subunit, and Small ribosomal subunit | 2.10E-03 | rplQ\|rplS\|rpmA\|rpsI |

Table A-3 (cont'd)

| | | | | | | | |
|---|---|---|---|---|---|---|---|
| 1 | 17 | 6 | GO Molecular Function | GO:0051082 | Unfolded protein binding | 2.30E-03 | groES\|groEL\|dnaK\|dnaJ\|grpE\|htpG |
| 1 | 340 | 24 | UniProt Keywords | KW-0547 | Nucleotide-binding | 2.50E-03 | tufA\|groEL\|fusB\|dnaK\|ftsH\|infB\|liuD\|sucD\|ushA\|htpG\|adk\|pheT\|ndk\|gyrA\|ruvA\|aspS\|ldh\|acs\|wbpQ\|cpdB\|clpB\|hprT\|prsA\|purA |
| 1 | 59 | 9 | KEGG Pathways | son00230 | Purine metabolism | 2.50E-03 | deoB\|SO_1550\|ushA\|adk\|ndk\|cpdB\|hprT\|prsA\|purA |
| 1 | 86 | 11 | STRING Clusters | CL:1203 | Carbon metabolism, and Starch and sucrose metabolism | 2.60E-03 | prpF\|prpC\|deoA\|deoB\|sucA\|sucD\|bkdA1\|bkdA2\|bkdB\|prsA\|exaC |
| 1 | 6 | 4 | STRING Clusters | CL:211 | Mixed, incl. Zinc-binding ribosomal protein, and L28p-like | 3.20E-03 | rpmF\|rpsT\|rplU\|rpmG |
| 1 | 25 | 6 | KEGG Pathways | son01212 | Fatty acid metabolism | 3.50E-03 | ivdA\|ivdG\|fabV\|fabA\|fabF\|fabH |
| 1 | 76 | 10 | STRING Clusters | CL:1204 | Carbon metabolism, and Starch and sucrose metabolism | 4.30E-03 | prpF\|prpC\|deoA\|deoB\|sucA\|sucD\|bkdA1\|bkdA2\|bkdB\|prsA |
| 1 | 5 | 4 | GO Molecular Function | GO:0070181 | Small ribosomal subunit rRNA binding | 4.50E-03 | rpsK\|rpsT\|rpsR\|rpsF |

Table A-3 (cont'd)

| | | | | | | | |
|---|---|---|---|---|---|---|---|
| 1 | 87 | 11 | GO Biological Process | GO:1901565 | Organonitrogen compound catabolic process | 4.70E-03 | ftsH\|ivdC\|ivdE\|ivdF\|speA\|liuE\|liuA\|bkdA1\|bkdA2\|hslV\|dut |
| 1 | 15 | 5 | UniProt Keywords | KW-0346 | Stress response | 4.70E-03 | dnaK\|dnaJ\|grpE\|htpG\|clpB |
| 1 | 32 | 7 | GO Molecular Function | GO:0000049 | tRNA binding | 5.90E-03 | rplA\|rpsG\|rpsJ\|rplP\|rplE\|rpsM\|pheT |
| 1 | 18 | 5 | KEGG Pathways | son00061 | Fatty acid biosynthesis | 6.00E-03 | ivdG\|fabV\|fabA\|fabF\|fabH |
| 1 | 13 | 5 | GO Molecular Function | GO:0003746 | Translation elongation factor activity | 6.30E-03 | tufA\|fusB\|nusA\|tsf\|efp |
| 1 | 536 | 32 | GO Molecular Function | GO:0000166 | Nucleotide binding | 6.40E-03 | tufA\|groES\|groEL\|fusB\|dnaK\|dnaJ\|ftsH\|nusA\|infB\|grpE\|ivdC\|ivdF\|fabV\|liuD\|liuA\|sucD\|ushA\|htpG\|adk\|pheT\|ndk\|gyrA\|ruvA\|aspS\|ldh\|acs\|wbpQ\|cpdB\|clpB\|hprT\|prsA\|purA |
| 1 | 14 | 5 | GO Biological Process | GO:0042255 | Ribosome assembly | 6.50E-03 | rpsG\|rpsS\|rplV\|rpsK\|rplT |
| 1 | 76 | 10 | GO Biological | GO:0006996 | Organelle organization | 6.70E-03 | rpsG\|rpsS\|rplV\|rpsK\|fusB\|infC\|rplT\|gyrA\|ruvA\|topA |

Table A-3 (cont'd)

| | | | | | | | |
|---|---|---|---|---|---|---|---|
| | | | Process | | | | |
| 1 | 7 | 4 | GO Biological Process | GO:0042026 | Protein refolding | 7.30E-03 | groEL\|dnaJ\|SO_1995\|clpB |
| 1 | 39 | 7 | STRING Clusters | CL:1205 | Citrate cycle (TCA cycle), and Propanoate metabolism | 7.50E-03 | prpF\|prpC\|sucA\|sucD\|bkdA1\|bkdA2\|bkdB |
| 1 | 4 | 3 | KEGG Pathways | son00072 | Synthesis and degradation of ketone bodies | 9.50E-03 | ivdA\|liuG\|liuE |
| 1 | 604 | 34 | GO Molecular Function | GO:0036094 | Small molecule binding | 1.00E-02 | rpoB\|tufA\|groES\|groEL\|fusB\|dnaK\|dnaJ\|ftsH\|nusA\|infB\|grpE\|ivdC\|ivdF\|fabV\|liuD\|liuA\|sucA\|sucD\|ushA\|htpG\|adk\|pheT\|ndk\|gyrA\|ruvA\|aspS\|ldh\|acs\|wbpQ\|cpdB\|clpB\|hprT\|prsA\|purA |
| 1 | 8 | 4 | GO Biological Process | GO:0022411 | Cellular component disassembly | 1.03E-02 | fusB\|prfB\|frr\|infC |
| 1 | 10 | 4 | UniProt Keywords | KW-0275 | Fatty acid biosynthesis | 1.12E-02 | fabV\|fabA\|fabF\|fabH |
| 1 | 10 | 4 | STRING Clusters | CL:359 | RNA polymerase complex, and RNA | 1.26E-02 | rpoB\|rpoC\|greA\|rpoD |

Table A-3 (cont'd)

| | | | | | | | |
|---|---|---|---|---|---|---|---|
| | | | | | polymerase sigma-70 | | |
| 1 | 54 | 8 | GO Biological Process | GO:0006631 | Fatty acid metabolic process | 1.35E-02 | prpF\|prpC\|ivdA\|fabV\|fabA\|liuB\|fabF\|fabH |
| 1 | 6 | 5 | InterPro Domains | IPR008991 | Translation protein SH3-like domain superfamily | 1.36E-02 | nusG\|rplB\|rplX\|rplS\|efp |
| 1 | 4 | 3 | UniProt Keywords | KW-0396 | Initiation factor | 1.41E-02 | infB\|infC\|yciH |
| 1 | 129 | 12 | UniProt Keywords | KW-0460 | Magnesium | 1.41E-02 | rpoC\|pnpA\|speA\|pheT\|ndk\|topA\|acs\|rmlA\|hprT\|prsA\|purA\|dut |
| 1 | 20 | 5 | STRING Clusters | CL:1207 | Citrate cycle (TCA cycle) | 1.46E-02 | sucA\|sucD\|bkdA1\|bkdA2\|bkdB |
| 1 | 3 | 3 | GO Biological Process | GO:0002181 | Cytoplasmic translation | 1.55E-02 | rplB\|rplF\|frr |
| 1 | 3 | 3 | GO Biological Process | GO:0051085 | Chaperone cofactor-dependent protein refolding | 1.55E-02 | groES\|groEL\|dnaJ |
| 1 | 32 | 6 | STRING Clusters | CL:1113 | Pyrimidine metabolism, and Purine-containing compound salvage | 1.55E-02 | SO_1550\|ushA\|adk\|ndk\|cpdB\|hprT |
| 1 | 9 | 4 | GO Molecular | GO:0044183 | Protein folding chaperone | 1.64E-02 | groES\|groEL\|dnaK\|tig |

Table A-3 (cont'd)

| | | | | | | | |
|---|---|---|---|---|---|---|---|
| | | | Function | | | | |
| 1 | 27 | 5 | GO Cellular Component | GO:1990234 | Transferase complex | 1.72E-02 | rpoB\|rpoC\|sucA\|ribE\|prsA |
| 1 | 10 | 4 | GO Biological Process | GO:0061077 | Chaperone-mediated protein folding | 1.77E-02 | groES\|groEL\|dnaJ\|tig |
| 1 | 39 | 6 | KEGG Pathways | son00240 | Pyrimidine metabolism | 1.95E-02 | deoA\|SO_1550\|ushA\|ndk\|cpdB\|dut |
| 1 | 5 | 3 | UniProt Keywords | KW-0488 | Methylation | 1.98E-02 | rplK\|rplC\|prfB |
| 1 | 20 | 5 | GO Biological Process | GO:0006351 | Transcription, DNA-templated | 2.05E-02 | nusG\|rpoB\|rpoC\|nusA\|rpoD |
| 1 | 12 | 4 | STRING Clusters | CL:1526 | Fatty acid biosynthesis | 2.05E-02 | fabV\|fabA\|fabF\|fabH |
| 1 | 11 | 4 | GO Biological Process | GO:0022618 | Ribonucleoprotein complex assembly | 2.22E-02 | rpsG\|rpsS\|rpsK\|rplT |
| 1 | 5 | 3 | COMPARTMENTS | GOCC:0045239 | Tricarboxylic acid cycle enzyme complex | 2.23E-02 | sucA\|sucD\|bkdA2 |
| 1 | 61 | 8 | GO Biological Process | GO:0046395 | Carboxylic acid catabolic process | 2.32E-02 | prpF\|ivdA\|ivdE\|ivdF\|speA\|liuE\|bkdA1\|bkdA2 |
| 1 | 131 | 12 | GO Biological | GO:0009117 | Nucleotide metabolic process | 2.42E-02 | deoB\|ushA\|adk\|ndk\|bkdB\|acs\|cpdB\|hpr |

Table A-3 (cont'd)

| | | | | | | | |
|---|---|---|---|---|---|---|---|
| | | | Process | | | | T\|prsA\|purA\|dut\|atpE |
| 1 | 5 | 3 | STRING Clusters | CL:363 | RNA polymerase | 2.54E-02 | rpoB\|rpoC\|rpoD |
| 1 | 48 | 7 | GO Biological Process | GO:0006164 | Purine nucleotide biosynthetic process | 2.62E-02 | adk\|ndk\|acs\|hprT\|prsA\|purA\|atpE |
| 1 | 34 | 6 | GO Biological Process | GO:0009063 | Cellular amino acid catabolic process | 2.62E-02 | ivdE\|ivdF\|speA\|liuE\|bkdA1\|bkdA2 |
| 1 | 152 | 13 | GO Biological Process | GO:0034654 | Nucleobase-containing compound biosynthetic process | 2.62E-02 | nusG\|rpoB\|rpoC\|nusA\|rpoD\|adk\|ndk\|acs\|hprT\|prsA\|purA\|dut\|atpE |
| 1 | 63 | 8 | GO Biological Process | GO:0046390 | Ribose phosphate biosynthetic process | 2.62E-02 | deoB\|adk\|ndk\|acs\|hprT\|prsA\|purA\|atpE |
| 1 | 5 | 3 | GO Biological Process | GO:0000028 | Ribosomal small subunit assembly | 3.01E-02 | rpsG\|rpsS\|rpsK |
| 1 | 4 | 3 | GO Molecular Function | GO:0003743 | Translation initiation factor activity | 3.01E-02 | infB\|infC\|yciH |
| 1 | 37 | 8 | InterPro Domains | IPR012340 | Nucleic acid-binding, OB-fold | 3.20E-02 | rplB\|rpsQ\|nusA\|pnpA\|pheT\|efp\|ruvA\|aspS |
| 1 | 4 | 4 | InterPro Domains | IPR014722 | Ribosomal protein L2, domain 2 | 3.20E-02 | nusG\|rplB\|rplX\|efp |

Table A-3 (cont'd)

| | | | | | | | |
|---|---|---|---|---|---|---|---|
| 1 | 335 | 21 | GO Biological Process | GO:0019752 | Carboxylic acid metabolic process | 3.22E-02 | prpF\|prpC\|ivdA\|ivdE\|ivdF\|fabV\|fabA\|speA\|liuE\|liuD\|liuB\|pheT\|bkdA1\|bkdA2\|bkdB\|aspS\|ldh\|acs\|fabF\|fabH\|wbpQ |
| 1 | 6 | 3 | STRING Clusters | CL:1235 | e3 binding domain, and Oxidoreductase activity, acting on the aldehyde or oxo group of donors, disulfide as acceptor | 3.65E-02 | bkdA1\|bkdA2\|bkdB |
| 1 | 6 | 3 | STRING Clusters | CL:131 | Mixed, incl. Ribosomal protein L2, domain 2, and Large ribosomal subunit rRNA binding | 3.65E-02 | rplB\|rplV\|rplX |
| 1 | 6 | 3 | STRING Clusters | CL:1330 | Mixed, incl. 5-phosphoribose 1-diphosphate metabolic process, and Pentose metabolic process | 3.65E-02 | deoA\|deoB\|prsA |
| 1 | 161 | 13 | GO Biological Process | GO:0044248 | Cellular catabolic process | 3.68E-02 | prpF\|pnpA\|deoB\|ivdA\|ivdE\|ivdF\|speA\|liuE\|ushA\|bkdA1\|bkdA2\|cpdB\|dut |

Table A-3 (cont'd)

| | | | | | | | |
|---|---|---|---|---|---|---|---|
| 1 | 2 | 2 | GO Cellular Component | GO:1905202 | methylcrotonoyl-CoA carboxylase complex | 3.77E-02 | liuD\|liuB |
| 1 | 15 | 4 | GO Biological Process | GO:0009166 | Nucleotide catabolic process | 4.30E-02 | deoB\|ushA\|cpdB\|dut |
| 1 | 40 | 6 | GO Biological Process | GO:0043933 | Protein-containing complex organization | 4.40E-02 | rpsG\|rpsS\|rpsK\|prfB\|frr\|rplT |
| 1 | 169 | 13 | GO Biological Process | GO:0055086 | Nucleobase-containing small molecule metabolic process | 4.89E-02 | deoA\|deoB\|ushA\|adk\|ndk\|bkdB\|acs\|cpdB\|hprT\|prsA\|purA\|dut\|atpE |
| 1 | 126 | 43 | COMPARTMENTS | GOCC:0043232 | Intracellular non-membrane-bounded organelle | 1.04E-28 | rpmH\|rplK\|rplA\|rplL\|rpsG\|rpsJ\|rplC\|rplD\|rplB\|rpsS\|rplV\|rpsC\|rplP\|rpsQ\|rplN\|rplX\|rplE\|rpsN\|rpsH\|rplF\|rplR\|rpsE\|rpmD\|rplO\|rpsK\|rpsD\|rplQ\|infB\|rpsO\|rpsB\|rpmI\|rplT\|rpmF\|raiA\|rpsT\|rpmA\|rplU\|rplI\|rpsR\|rpsF\|rpsI\|rplM\|rpmG |

Table A-3 (cont'd)

| | | | | | | | |
|---|---|---|---|---|---|---|---|
| 1 | 1435 | 100 | GO Cellular Component | GO:0005737 | Cytoplasm | 1.09E-23 | nusG\|rplK\|rplA\|rplL\|rpsG\|tufA\|rplC\|rplD\|rplB\|rpsS\|rplV\|rpsC\|rplP\|rpsQ\|rplN\|rplX\|rplE\|rpsN\|rpsH\|rplF\|rplR\|rpsE\|rpmD\|rplO\|rpsM\|rpsK\|rplQ\|prpC\|sspA\|groES\|groEL\|fusB\|prfB\|dnaK\|dnaJ\|greA\|nusA\|infB\|rpsO\|pnpA\|deoA\|deoB\|rpoD\|rplS\|grpE\|SO_1550\|rpsB\|tsf\|frr\|ivdA\|ivdB\|ivdC\|ivdG\|tig\|fabA\|liuG\|liuE\|liuA\|sucA\|sucD\|SO_1995\|htpG\|adk\|pheT\|ndk\|infC\|rpmI\|rplT\|efp\|bkdB\|gyrA\|ubiG\|aspS\|def-3\|ldh\|acs\|fabF\|fabH\|wbpQ\|rmlA\|yciH\|raiA\|ribE\|SO_3468\|rpsT\|clpB\|rpmA\|rplU\|hprT\|prsA\|rplI\|rpsR\|rpsF\|purA\|rpsI\|rplM\|hslV\|rpmG\|dut\|exaC |

Table A-3 (cont'd)

| | | | | | | | |
|---|---|---|---|---|---|---|---|
| 1 | 57 | 43 | UniProt Keywords | KW-0689 | Ribosomal protein | 1.12E-39 | rpmH\|rplK\|rplA\|rplL\|rpsG\|rpsJ\|rplC\|rplD\|rplB\|rpsS\|rplV\|rpsC\|rplP\|rpsQ\|rplN\|rplX\|rplE\|rpsN\|rpsH\|rplF\|rplR\|rpsE\|rpmD\|rplO\|rpsM\|rpsK\|rpsD\|rplQ\|rpsO\|rplS\|rpsB\|rpmI\|rplT\|rpmF\|rpsT\|rpmA\|rplU\|rplI\|rpsR\|rpsF\|rpsI\|rplM\|rpmG |
| 1 | 16 | 12 | COMPARTMENTS | GOCC:0022625 | Cytosolic large ribosomal subunit | 1.13E-10 | rplA\|rplL\|rplC\|rplD\|rplB\|rplV\|rplE\|rplF\|rplR\|rpmD\|rplO\|rplU |
| 1 | 12 | 9 | STRING Clusters | CL:130 | Cytosolic large ribosomal subunit | 1.13E-7 | rplC\|rplD\|rplB\|rplV\|rplN\|rplX\|rplE\|rplO\|rplM |
| 1 | 83 | 17 | STRING Clusters | CL:1520 | Mixed, incl. Fatty acid metabolism, and Valine, leucine and isoleucine degradation | 1.13E-7 | ivdA\|ivdB\|ivdC\|ivdE\|ivdF\|ivdG\|fabV\|fabA\|liuG\|liuE\|liuD\|liuC\|liuB\|liuA\|acs\|fabF\|fabH |
| 1 | 80 | 51 | STRING Clusters | CL:108 | Structural constituent of ribosome, and Translation regulator activity | 1.1E-45 | rpmH\|nusG\|rplK\|rplA\|rplL\|rpsG\|tufA\|rpsJ\|rplC\|rplD\|rplB\|rpsS\|rplV\|rpsC\|rplP\|rpsQ\|rplN\|rplX\|rplE\|rpsN\|rpsH\|rplF\|rplR\|rpsE\|rpmD\|rplO\|rpsM\|rpsK\| |

Table A-3 (cont'd)

| | | | | | | | |
|---|---|---|---|---|---|---|---|
| | | | | | | | rpsD\|rplQ\|fusB\|prfB\|nusA\|infB\|rpsO\|rplS\|rpsB\|tig\|infC\|rpmI\|rplT\|rpmF\|rpsT\|rpmA\|rplU\|rplI\|rpsR\|rpsF\|rpsI\|rplM\|rpmG |
| 1 | 2525 | 116 | GO Biological Process | GO:0009987 | Cellular process | 1.21E-14 | rpmH\|nusG\|rplK\|rplA\|rplL\|rpoB\|rpoC\|rpsG\|tufA\|rpsJ\|rplC\|rplD\|rplB\|rpsS\|rplV\|rpsC\|rplP\|rpsQ\|rplN\|rplX\|rplE\|rpsN\|rpsH\|rplF\|rplR\|rpsE\|rpmD\|rplO\|rpsM\|rpsK\|rpsD\|rplQ\|SO_0306\|prpF\|prpC\|sspA\|groES\|groEL\|fusB\|prfB\|dnaK\|dnaJ\|nusA\|infB\|rpsO\|pnpA\|deoA\|deoB\|rpoD\|rplS\|grpE\|rpsB\|tsf\|frr\|ivdA\|ivdB\|ivdE\|ivdF\|ivdG\|tig\|fabV\|fabA\|speA\|liuG\|liuE\|liuD\|liuC\|liuB\|sucA\|sucD\|SO_1995\|ushA\|htpG\|adk\|pheT\|ndk\|infC\|rpmI\|rplT\|efp\|bkdA1\|bkdA2\|bkdB\|gyrA\|u |

Table A-3 (cont'd)

| | | | | | | | |
|---|---|---|---|---|---|---|---|
| | | | | | | | biG\|ruvA\|asp S\|def-3\|ldh\|topA\|ac s\|fabF\|fabH\|r pmF\|wbpQ\|r mlA\|yciH\|rib E\|SO_3468\|r psT\|cpdB\|clp B\|rpmA\|rplU\| hprT\|prsA\|rpl I\|rpsR\|rpsF\|p urA\|rpsI\|rplM \|rpmG\|dut\|ex aC\|atpE |
| 1 | 18 | 14 | COMP ARTME NTS | GOCC:0 015934 | Large ribosomal subunit | 1.36 E-12 | rplA\|rplL\|rplC \|rplD\|rplB\|rpl V\|rplN\|rplE\|r plF\|rplR\|rpm D\|rplO\|rpmF\| rplU |
| 1 | 1661 | 107 | GO Biologic al Proces s | GO:004 4237 | Cellular metabolic process | 1.39 E-23 | rpmH\|nusG\|r plK\|rplA\|rplL\| rpoB\|rpoC\|rp sG\|tufA\|rpsJ\| rplC\|rplD\|rpl B\|rpsS\|rplV\|r psC\|rplP\|rps Q\|rplN\|rplX\|r plE\|rpsN\|rps H\|rplF\|rplR\|r psE\|rpmD\|rpl O\|rpsM\|rpsK\| rpsD\|rplQ\|pr pF\|prpC\|ssp A\|fusB\|prfB\|d naJ\|nusA\|inf B\|rpsO\|pnpA \|deoA\|deoB\|r poD\|rplS\|rps B\|tsf\|frr\|ivdA\| ivdB\|ivdE\|ivd F\|ivdG\|fabV\|f abA\|speA\|liu G\|liuE\|liuD\|li |

Table A-3 (cont'd)

| | | | | | | | |
|---|---|---|---|---|---|---|---|
| | | | | | | | uC\|liuB\|sucA\|sucD\|ushA\|adk\|pheT\|ndk\|infC\|rpmI\|rplT\|efp\|bkdA1\|bkdA2\|bkdB\|gyrA\|ubiG\|ruvA\|aspS\|def-3\|ldh\|topA\|acs\|fabF\|fabH\|rpmF\|wbpQ\|rmlA\|yciH\|ribE\|SO_3468\|rpsT\|cpdB\|rpmA\|rplU\|hprT\|prsA\|rplI\|rpsR\|rpsF\|purA\|rpsI\|rplM\|rpmG\|dut\|exaC\|atpE |
| 1 | 675 | 80 | GO Biological Process | GO:0044249 | Cellular biosynthetic process | 1.42E-29 | rpmH\|nusG\|rplK\|rplA\|rplL\|rpoB\|rpoC\|rpsG\|tufA\|rpsJ\|rplC\|rplD\|rplB\|rpsS\|rplV\|rpsC\|rplP\|rpsQ\|rplN\|rplX\|rplE\|rpsN\|rpsH\|rplF\|rplR\|rpsE\|rpmD\|rplO\|rpsM\|rpsK\|rpsD\|rplQ\|fusB\|prfB\|nusA\|infB\|rpsO\|rpoD\|rplS\|rpsB\|tsf\|frr\|fabV\|fabA\|speA\|liuE\|liuB\|adk\|pheT\|ndk\|infC\|rpmI\|rplT\|efp\|ubiG\|aspS\|def- |

Table A-3 (cont'd)

| | | | | | | | |
|---|---|---|---|---|---|---|---|
| | | | | | | | 3\|acs\|fabF\|fabH\|rpmF\|wbpQ\|rmlA\|yciH\|ribE\|SO_3468\|rpsT\|rpmA\|rplU\|hprT\|prsA\|rplI\|rpsR\|rpsF\|purA\|rpsI\|rplM\|rpmG\|dut\|atpE |
| 1 | 141 | 57 | GO Biological Process | GO:0006518 | Peptide metabolic process | 1.45E-42 | rpmH\|rplK\|rplA\|rplL\|rpsG\|tufA\|rpsJ\|rplC\|rplD\|rplB\|rpsS\|rplV\|rpsC\|rplP\|rpsQ\|rplN\|rplX\|rplE\|rpsN\|rpsH\|rplF\|rplR\|rpsE\|rpmD\|rplO\|rpsM\|rpsK\|rpsD\|rplQ\|sspA\|fusB\|prfB\|nusA\|infB\|rpsO\|rplS\|rpsB\|tsf\|frr\|pheT\|infC\|rpmI\|rplT\|efp\|aspS\|def-3\|rpmF\|yciH\|rpsT\|rpmA\|rplU\|rplI\|rpsR\|rpsF\|rpsI\|rplM\|rpmG |

Table A-3 (cont'd)

| | | | | | | | |
|---|---|---|---|---|---|---|---|
| 1 | 1497 | 108 | GO Cellular Component | GO:0005622 | Intracellular anatomical structure | 1.47E-29 | rpmH\|nusG\|rplK\|rplA\|rplL\|rpsG\|tufA\|rpsJ\|rplC\|rplD\|rplB\|rpsS\|rplV\|rpsC\|rplP\|rpsQ\|rplN\|rplX\|rplE\|rpsN\|rpsH\|rplF\|rplR\|rpsE\|rpmD\|rplO\|rpsM\|rpsK\|rpsD\|rplQ\|prpC\|sspA\|groES\|groEL\|fusB\|prfB\|dnaK\|dnaJ\|greA\|nusA\|infB\|rpsO\|pnpA\|deoA\|deoB\|rpoD\|rplS\|grpE\|SO_1550\|rpsB\|tsf\|frr\|ivdA\|ivdB\|ivdC\|ivdG\|tig\|fabA\|liuG\|liuE\|liuA\|sucA\|sucD\|SO_1995\|htpG\|adk\|pheT\|ndk\|infC\|rpmI\|rplT\|efp\|bkdA1\|bkdB\|gyrA\|ubiG\|ruvA\|aspS\|def-3\|ldh\|topA\|acs\|fabF\|fabH\|rpmF\|wbpQ\|rmlA\|yciH\|raiA\|ribE\|SO_3468\|rpsT\|clpB\|rpmA\|rplU\|hprT\|prsA\|rplI\|rpsR\|rpsF\|purA\|rpsI\|rplM |

Table A-3 (cont'd)

| | | | | | | | |
|---|---|---|---|---|---|---|---|
| | | | | | | | \|hslV\|rpmG\|dut\|exaC\|atpE |
| 1 | 5 | 5 | STRING Clusters | CL:178 | Mixed, incl. 5S rRNA binding, and Positive regulation of translation | 1.4E-4 | rpsS\|rplP\|rplR\|rpsE\|rpsD |
| 1 | 5 | 5 | STRING Clusters | CL:518 | De novo post-translational protein folding, and ATPase regulator activity | 1.4E-4 | groES\|groEL\|dnaK\|dnaJ\|grpE |
| 1 | 600 | 59 | GO Cellular Component | GO:0005829 | Cytosol | 1.52E-16 | nusG\|rplK\|rplA\|rplL\|rpsG\|rplC\|rplB\|rpsS\|rplV\|rpsC\|rplP\|rpsQ\|rplN\|rplX\|rplE\|rpsH\|rplF\|rplR\|rpsE\|rpmD\|rplO\|rpsM\|rpsK\|rplQ\|groEL\|dnaK\|greA\|rpsO\|pnpA\|deoA\|deoB\|rplS\|grpE\|SO_1550\|rpsB\|frr\|liuE\|sucA\|htpG\|adk\|infC\|rpmI\|rplT\|def- |

Table A-3 (cont'd)

| | | | | | | | |
|---|---|---|---|---|---|---|---|
| | | | | | | | 3\|acs\|wbpQ\|rmlA\|ribE\|SO_3468\|rpsT\|rpmA\|rplI\|rpsR\|rpsF\|rpsI\|rplM\|hslV\|rpmG\|dut |
| 1 | 14 | 12 | GO Cellular Component | GO:0022627 | Cytosolic small ribosomal subunit | 1.55E-11 | rpsG\|rpsS\|rpsC\|rpsQ\|rpsH\|rpsE\|rpsK\|rpsO\|rpsB\|rpsR\|rpsF\|rpsI |
| 1 | 6 | 6 | STRING Clusters | CL:142 | Cytosolic large ribosomal subunit | 1.58E-5 | rplC\|rplD\|rplN\|rplE\|rplO\|rplM |
| 1 | 298 | 53 | COMPARTMENTS | GOCC:0043229 | Intracellular organelle | 1.61E-24 | rpmH\|nusG\|rplK\|rplA\|rplL\|rpsG\|rpsJ\|rplC\|rplD\|rplB\|rpsS\|rplV\|rpsC\|rplP\|rpsQ\|rplN\|rplX\|rplE\|rpsN\|rpsH\|rplF\|rplR\|rpsE\|rpmD\|rplO\|rpsM\|rpsK\|rpsD\|rplQ\|nusA\|infB\|rpsO\|rplS\|rpsB\|ivdC\|speA\|liuE\|liuA\|rpmI\|rplT\|bkdA1\|bkdA2\|rpmF\|raiA\|rpsT\|rpmA\|rplU\|rplI\|rpsR\|rpsF\|rpsI\|rplM\|rpmG |
| 1 | 20 | 12 | STRING Clusters | CL:1615 | Valine, leucine and isoleucine degradation, and Enoyl-CoA | 1.62E-9 | ivdA\|ivdB\|ivdC\|ivdE\|ivdF\|liuG\|liuE\|liuD\|liuC\|liuB\|liuA\|acs |

Table A-3 (cont'd)

| | | | | | | | |
|---|---|---|---|---|---|---|---|
| | | | | | hydratase/isomerase | | |
| 1 | 30 | 26 | STRING Clusters | CL:128 | Ribosomal subunit | 1.68E-24 | rplK\|rplA\|rplL\|rpsG\|rpsJ\|rplC\|rplD\|rplB\|rpsS\|rplV\|rpsC\|rplP\|rpsQ\|rplN\|rplX\|rplE\|rpsN\|rplF\|rplR\|rpsE\|rplO\|rpsM\|rpsD\|rpsO\|rpsB\|rplM |
| 1 | 2017 | 113 | GO Biological Process | GO:0008152 | Metabolic process | 1.77E-21 | rpmH\|nusG\|rplK\|rplA\|rplL\|rpoB\|rpoC\|rpsG\|tufA\|rpsJ\|rplC\|rplD\|rplB\|rpsS\|rplV\|rpsC\|rplP\|rpsQ\|rplN\|rplX\|rplE\|rpsN\|rpsH\|rplF\|rplR\|rpsE\|rpmD\|rplO\|rpsM\|rpsK\|rpsD\|rplQ\|prpF\|prpC\|sspA\|fusB\|prfB\|dnaJ\|ftsH\|nusA\|infB\|rpsO\|pnpA\|deoA\|deoB\|rpoD\|rplS\|SO_1550\|rpsB\|tsf\|frr\|ivdA\|ivdB\|ivdC\|ivdE\|ivdF\|ivdG\|fabV\|fabA\|speA\|liuG\|liuE\|liuD\|liuC\|liuB\|liuA\|sucA\|sucD\|ushA\|adk\|pheT\|ndk\|infC\|rpmI\|r |

Table A-3 (cont'd)

| | | | | | | | |
|---|---|---|---|---|---|---|---|
| | | | | | | | plT\|efp\|bkdA1\|bkdA2\|bkdB\|gyrA\|ubiG\|ruvA\|aspS\|def-3\|ldh\|topA\|acs\|fabF\|fabH\|rpmF\|wbpQ\|rmlA\|yciH\|raiA\|ribE\|SO_3468\|rpsT\|cpdB\|rpmA\|rplU\|hprT\|prsA\|rplI\|rpsR\|rpsF\|purA\|rpsI\|rplM\|hslV\|rpmG\|dut\|exaC\|atpE |
| 1 | 150 | 57 | GO Biological Process | GO:0043604 | Amide biosynthetic process | 1.82E-41 | rpmH\|rplK\|rplA\|rplL\|rpsG\|tufA\|rpsJ\|rplC\|rplD\|rplB\|rpsS\|rplV\|rpsC\|rplP\|rpsQ\|rplN\|rplX\|rplE\|rpsN\|rpsH\|rplF\|rplR\|rpsE\|rpmD\|rplO\|rpsM\|rpsK\|rpsD\|rplQ\|fusB\|prfB\|nusA\|infB\|rpsO\|rplS\|rpsB\|tsf\|frr\|pheT\|infC\|rpmI\|rplT\|efp\|aspS\|def-3\|acs\|rpmF\|yciH\|rpsT\|rpmA\|rplU\|rplI\|rpsR\|rpsF\|rpsI\|rplM\|rpmG |
| 1 | 41 | 34 | GO Cellular Component | GO:0022626 | Cytosolic ribosome | 1.89E-32 | rplK\|rplA\|rplL\|rpsG\|rplC\|rplB\|rpsS\|rplV\|rpsC\|rplP\|rps |

Table A-3 (cont'd)

| | | | | | | | |
|---|---|---|---|---|---|---|---|
| | | | | | | | Q\|rplN\|rplX\|rplE\|rpsH\|rplF\|rplR\|rpsE\|rpmD\|rplO\|rpsK\|rplQ\|rpsO\|rplS\|rpsB\|rpmI\|rplT\|rpmA\|rplI\|rpsR\|rpsF\|rpsI\|rplM\|rpmG |
| 1 | 3153 | 115 | GO Cellular Component | GO:0110165 | Cellular anatomical entity | 1.95E-5 | rpmH\|nusG\|rplK\|rplA\|rplL\|rpsG\|tufA\|rpsJ\|rplC\|rplD\|rplB\|rpsS\|rplV\|rpsC\|rplP\|rpsQ\|rplN\|rplX\|rplE\|rpsN\|rpsH\|rplF\|rplR\|rpsE\|rpmD\|rplO\|rpsM\|rpsK\|rpsD\|rplQ\|SO_0306\|prpF\|prpC\|sspA\|groES\|groEL\|fusB\|prfB\|dnaK\|dnaJ\|greA\|ftsH\|nusA\|infB\|rpsO\|pnpA\|deoA\|deoB\|rpoD\|rplS\|grpE\|SO_1550\|rpsB\|tsf\|frr\|ivdA\|ivdB\|ivdC\|ivdG\|tig\|fabA\|speA\|liuG\|liuE\|liuA\|sucA\|sucD\|SO_1995\|ushA\|htpG\|adk\|pheT\|ndk\|infC\|rpmI\|rplT\|efp\|bkdA1\|bkdA2\|bkdB\|gyr |

Table A-3 (cont'd)

| | | | | | | | |
|---|---|---|---|---|---|---|---|
| | | | | | | | A\|ubiG\|ruvA\|aspS\|def-3\|ldh\|topA\|acs\|fabF\|fabH\|rpmF\|wbpQ\|rmlA\|yciH\|raiA\|ribE\|SO_3468\|rpsT\|cpdB\|clpB\|rpmA\|rplU\|hprT\|prsA\|rplI\|rpsR\|rpsF\|purA\|rpsI\|rplM\|hslV\|rpmG\|dut\|exaC\|atpE |
| 1 | 1489 | 101 | GO Biological Process | GO:0044238 | Primary metabolic process | 1.98E-22 | rpmH\|nusG\|rplK\|rplA\|rplL\|rpoB\|rpoC\|rpsG\|tufA\|rpsJ\|rplC\|rplD\|rplB\|rpsS\|rplV\|rpsC\|rplP\|rpsQ\|rplN\|rplX\|rplE\|rpsN\|rpsH\|rplF\|rplR\|rpsE\|rpmD\|rplO\|rpsM\|rpsK\|rpsD\|rplQ\|prpF\|prpC\|fusB\|prfB\|dnaJ\|ftsH\|nusA\|infB\|rpsO\|pnpA\|deoA\|deoB\|rpoD\|rplS\|rpsB\|tsf\|frr\|ivdA\|ivdE\|ivdF\|fabV\|fabA\|speA\|liuE\|liuD\|liuB\|sucA\|sucD\|ushA\|adk\|pheT\|ndk\|infC\|rpmI\|rplT\|efp\|bkdA1\|bkdA2\|bkdB\|gyrA\|ru |

Table A-3 (cont'd)

| | | | | | | | |
|---|---|---|---|---|---|---|---|
| | | | | | | | vA\|aspS\|def-3\|ldh\|topA\|acs\|fabF\|fabH\|rpmF\|wbpQ\|rmlA\|yciH\|raiA\|rpsT\|cpdB\|rpmA\|rplU\|hprT\|prsA\|rplI\|rpsR\|rpsF\|purA\|rpsI\|rplM\|hslV\|rpmG\|dut\|atpE |
| 1 | 101 | 13 | GO Cellular Component | GO:1902494 | Catalytic complex | 1.9E-4 | rpoB\|rpoC\|liuD\|liuC\|liuB\|sucA\|sucD\|pheT\|bkdB\|ruvA\|ribE\|prsA\|hslV |
| 1 | 586 | 62 | GO Biological Process | GO:0044260 | Cellular macromolecule metabolic process | 2.09E-18 | rpmH\|rplK\|rplA\|rplL\|rpsG\|tufA\|rpsJ\|rplC\|rplD\|rplB\|rpsS\|rplV\|rpsC\|rplP\|rpsQ\|rplN\|rplX\|rplE\|rpsN\|rpsH\|rplF\|rplR\|rpsE\|rpmD\|rplO\|rpsM\|rpsK\|rpsD\|rplQ\|fusB\|prfB\|dnaJ\|nusA\|infB\|rpsO\|pnpA\|rplS\|rpsB\|tsf\|frr\|pheT\|infC\|rpmI\|rplT\|efp\|gyrA\|ruvA\|aspS\|def-3\|topA\|rpmF\|rmlA\|yciH\|rpsT\|rpmA\|rplU\|rplI\|rpsR\|rpsF\|rpsI\|rplM\|rpmG |

Table A-3 (cont'd)

| | | | | | | | |
|---|---|---|---|---|---|---|---|
| 1 | 105 | 46 | GO Cellular Component | GO:0043232 | Intracellular non-membrane-bounded organelle | 2.0E-35 | rpmH\|rplK\|rplA\|rplL\|rpsG\|rpsJ\|rplC\|rplD\|rplB\|rpsS\|rplV\|rpsC\|rplP\|rpsQ\|rplN\|rplX\|rplE\|rpsN\|rpsH\|rplF\|rplR\|rpsE\|rpmD\|rplO\|rpsM\|rpsK\|rpsD\|rplQ\|rpsO\|rplS\|rpsB\|rpmI\|rplT\|gyrA\|topA\|rpmF\|raiA\|rpsT\|rpmA\|rplU\|rplI\|rpsR\|rpsF\|rpsI\|rplM\|rpmG |
| 1 | 56 | 43 | GO Molecular Function | GO:0003735 | Structural constituent of ribosome | 2.17E-39 | rpmH\|rplK\|rplA\|rplL\|rpsG\|rpsJ\|rplC\|rplD\|rplB\|rpsS\|rplV\|rpsC\|rplP\|rpsQ\|rplN\|rplX\|rplE\|rpsN\|rpsH\|rplF\|rplR\|rpsE\|rpmD\|rplO\|rpsM\|rpsK\|rpsD\|rplQ\|rpsO\|rplS\|rpsB\|rpmI\|rplT\|rpmF\|rpsT\|rpmA\|rplU\|rplI\|rpsR\|rpsF\|rpsI\|rplM\|rpmG |
| 1 | 646 | 42 | KEGG Pathways | son01100 | Metabolic pathways | 2.24E-5 | prpF\|prpC\|deoA\|deoB\|SO_1550\|ivdA\|ivdB\|ivdF\|ivdG\|fabV\|fabA\|speA\|liuG\|liuE\|liuD\|liuC\|liuB\|liuA\|suc |

Table A-3 (cont'd)

| | | | | | | | |
|---|---|---|---|---|---|---|---|
| | | | | | | | A\|sucD\|ushA\|adk\|ndk\|bkdA1\|bkdA2\|bkdB\|ubiG\|ldh\|acs\|fabF\|fabH\|wbpQ\|rmlA\|ribE\|SO_3468\|cpdB\|hprT\|prsA\|purA\|dut\|exaC\|atpE |
| 1 | 1174 | 79 | GO Molecular Function | GO:0097159 | Organic cyclic compound binding | 2.29E-13 | nusG\|rplK\|rplA\|rplL\|rpoB\|rpoC\|rpsG\|tufA\|rpsJ\|rplC\|rplD\|rplB\|rpsS\|rplV\|rpsC\|rplP\|rpsQ\|rplN\|rplX\|rplE\|rpsN\|rpsH\|rplF\|rplR\|rpsE\|rplO\|rpsM\|rpsK\|rpsD\|groES\|groEL\|fusB\|prfB\|dnaK\|dnaJ\|greA\|ftsH\|nusA\|infB\|rpsO\|pnpA\|rpoD\|grpE\|tsf\|ivdC\|ivdF\|fabV\|liuD\|liuA\|sucA\|sucD\|ushA\|htpG\|adk\|pheT\|ndk\|infC\|rplT\|efp\|gyrA\|ruvA\|aspS\|ldh\|topA\|acs\|wbpQ\|yciH\|rpsT\|cpdB\|clpB\|rplU\|hprT\|prsA\|rplI\|rpsR\|rpsF\|purA\|rpsI\|rplM |

Table A-3 (cont'd)

| | | | | | | | |
|---|---|---|---|---|---|---|---|
| 1 | 1174 | 79 | GO Molecular Function | GO:1901363 | Heterocyclic compound binding | 2.29E-13 | nusG\|rplK\|rplA\|rplL\|rpoB\|rpoC\|rpsG\|tufA\|rpsJ\|rplC\|rplD\|rplB\|rpsS\|rplV\|rpsC\|rplP\|rpsQ\|rplN\|rplX\|rplE\|rpsN\|rpsH\|rplF\|rplR\|rpsE\|rplO\|rpsM\|rpsK\|rpsD\|groES\|groEL\|fusB\|prfB\|dnaK\|dnaJ\|greA\|ftsH\|nusA\|infB\|rpsO\|pnpA\|rpoD\|grpE\|tsf\|ivdC\|ivdF\|fabV\|liuD\|liuA\|sucA\|sucD\|ushA\|htpG\|adk\|pheT\|ndk\|infC\|rplT\|efp\|gyrA\|ruvA\|aspS\|ldh\|topA\|acs\|wbpQ\|yciH\|rpsT\|cpdB\|clpB\|rplU\|hprT\|prsA\|rplI\|rpsR\|rpsF\|purA\|rpsI\|rplM |
| 1 | 5 | 5 | GO Biological Process | GO:0009083 | Branched-chain amino acid catabolic process | 2.2E-4 | ivdE\|ivdF\|liuE\|bkdA1\|bkdA2 |
| 1 | 415 | 58 | GO Biological Process | GO:0019538 | Protein metabolic process | 2.34E-22 | rpmH\|rplK\|rplA\|rplL\|rpsG\|tufA\|rpsJ\|rplC\|rplD\|rplB\|rpsS\|rplV\|rpsC\|rplP\|rpsQ\|rplN\|rplX\|rplE\|r |

Table A-3 (cont'd)

| | | | | | | | |
|---|---|---|---|---|---|---|---|
| | | | | | | | psN\|rpsH\|rplF\|rplR\|rpsE\|rpmD\|rplO\|rpsM\|rpsK\|rpsD\|rplQ\|fusB\|prfB\|ftsH\|nusA\|infB\|rpsO\|rplS\|rpsB\|tsf\|frr\|pheT\|infC\|rpmI\|rplT\|efp\|aspS\|def-3\|rpmF\|yciH\|rpsT\|rpmA\|rplU\|rplI\|rpsR\|rpsF\|rpsI\|rplM\|hslV\|rpmG |
| 1 | 742 | 50 | COMPARTMENTS | GOCC:0005829 | Cytosol | 2.3E-7 | nusG\|rplA\|rplL\|rpsG\|rplC\|rplD\|rplB\|rplV\|rpsC\|rpsQ\|rplE\|rpsN\|rpsH\|rplF\|rplR\|rpsE\|rpmD\|rplO\|rpsD\|sspA\|groES\|groEL\|prfB\|greA\|nusA\|rpsO\|deoA\|deoB\|SO_1550\|frr\|fabA\|speA\|htpG\|ndk\|efp\|ubiG\|aspS\|def-3\|topA\|acs\|fabF\|fabH\|wbpQ\|rmlA\|raiA\|SO_3468\|rpsT\|clpB\|rplU\|dut |
| 1 | 133 | 37 | GO Molecular Function | GO:0003723 | RNA binding | 2.51E-21 | rplK\|rplA\|rplL\|rpsG\|rpsJ\|rplC\|rplD\|rplB\|rpsS\|rplV\|rpsC\|rplP\|rpsQ\|rplN\|rplX\|rplE\| |

Table A-3 (cont'd)

| | | | | | | | |
|---|---|---|---|---|---|---|---|
| | | | | | | | rpsN\|rpsH\|rplF\|rplR\|rpsE\|rplO\|rpsM\|rpsK\|rpsD\|nusA\|rpsO\|pnpA\|pheT\|rplT\|rpsT\|rplU\|rplI\|rpsR\|rpsF\|rpsI\|rplM |
| 1 | 58 | 44 | STRING Clusters | CL:120 | Structural constituent of ribosome | 2.63E-41 | rpmH\|rplK\|rplA\|rplL\|rpsG\|tufA\|rpsJ\|rplC\|rplD\|rplB\|rpsS\|rplV\|rpsC\|rplP\|rpsQ\|rplN\|rplX\|rplE\|rpsN\|rpsH\|rplF\|rplR\|rpsE\|rpmD\|rplO\|rpsM\|rpsK\|rpsD\|rplQ\|rpsO\|rplS\|rpsB\|rpmI\|rplT\|rpmF\|rpsT\|rpmA\|rplU\|rplI\|rpsR\|rpsF\|rpsI\|rplM\|rpmG |
| 1 | 39 | 30 | UniProt Keywords | KW-0699 | rRNA-binding | 2.67E-27 | rplK\|rplA\|rpsG\|rplC\|rplD\|rplB\|rpsS\|rplV\|rpsC\|rplP\|rpsQ\|rplN\|rplX\|rplE\|rpsN\|rpsH\|rplF\|rplR\|rpsE\|rplO\|rpsM\|rpsK\|rpsD\|rpsO\|rplT\|rpsT\|rplU\|rplI\|rpsR\|rpsF |
| 1 | 43 | 36 | STRING Clusters | CL:124 | Ribosomal subunit | 2.72E-34 | rplK\|rplA\|rplL\|rpsG\|rpsJ\|rplC\|rplD\|rplB\|rpsS\|rplV\|rpsC\|rplP\|rpsQ\|r |

Table A-3 (cont'd)

| | | | | | | | |
|---|---|---|---|---|---|---|---|
| | | | | | | | plN\|rplX\|rplE\|rpsN\|rplF\|rplR\|rpsE\|rpmD\|rplO\|rpsM\|rpsD\|rplQ\|rpsO\|rplS\|rpsB\|rpmI\|rplT\|rpmA\|rplI\|rpsR\|rpsF\|rpsI\|rplM |
| 1 | 1181 | 78 | COMPARTMENTS | GOCC:0005737 | Cytoplasm | 2.73E-13 | nusG\|rplA\|rplL\|rpsG\|tufA\|rplC\|rplD\|rplB\|rplV\|rpsC\|rpsQ\|rplE\|rpsN\|rpsH\|rplF\|rplR\|rpsE\|rpmD\|rplO\|rpsM\|rpsD\|prpF\|prpC\|sspA\|groES\|groEL\|fusB\|prfB\|dnaK\|greA\|nusA\|rpsO\|pnpA\|deoA\|deoB\|rplS\|grpE\|SO_1550\|tsf\|frr\|ivdA\|ivdC\|ivdG\|tig\|fabA\|speA\|liuG\|liuE\|liuC\|liuA\|sucA\|sucD\|htpG\|pheT\|ndk\|infC\|efp\|bkdA2\|bkdB\|ubiG\|aspS\|def-3\|ldh\|topA\|acs\|fabF\|fabH\|wbpQ\|rmlA\|yciH\|raiA\|SO_3468\|rpsT\|clpB\|rplU\|hprT\|purA\|dut |

Table A-3 (cont'd)

| | | | | | | | |
|---|---|---|---|---|---|---|---|
| 1 | 7 | 6 | STRING Clusters | CL:1641 | Synthesis and degradation of ketone bodies, and methylcrotonoyl-CoA carboxylase complex | 2.76 E-5 | liuG\|liuE\|liuD\|liuC\|liuB\|liuA |
| 1 | 894 | 82 | GO Biological Process | GO:0034641 | Cellular nitrogen compound metabolic process | 2.82 E-23 | rpmH\|nusG\|rplK\|rplA\|rplL\|rpoB\|rpoC\|rpsG\|tufA\|rpsJ\|rplC\|rplD\|rplB\|rpsS\|rplV\|rpsC\|rplP\|rpsQ\|rplN\|rplX\|rplE\|rpsN\|rpsH\|rplF\|rplR\|rpsE\|rpmD\|rplO\|rpsM\|rpsK\|rpsD\|rplQ\|sspA\|fusB\|prfB\|dnaJ\|nusA\|infB\|rpsO\|pnpA\|deoA\|deoB\|rpoD\|rplS\|rpsB\|tsf\|frr\|speA\|ushA\|adk\|pheT\|ndk\|infC\|rpmI\|rplT\|efp\|bkdB\|gyrA\|ruvA\|aspS\|def-3\|topA\|acs\|rpmF\|yciH\|ribE\|SO_3468\|rpsT\|cpdB\|rpmA\|rplU\|hprT\|prsA\|rplI\|rpsR\|rpsF\|purA\|rpsI\|rplM\|rpmG\|dut\|atpE |

Table A-3 (cont'd)

| | | | | | | | |
|---|---|---|---|---|---|---|---|
| 1 | 118 | 56 | GO Biological Process | GO:0006412 | Translation | 2.85E-44 | rpmH\|rplK\|rplA\|rplL\|rpsG\|tufA\|rpsJ\|rplC\|rplD\|rplB\|rpsS\|rplV\|rpsC\|rplP\|rpsQ\|rplN\|rplX\|rplE\|rpsN\|rpsH\|rplF\|rplR\|rpsE\|rpmD\|rplO\|rpsM\|rpsK\|rpsD\|rplQ\|fusB\|prfB\|nusA\|infB\|rpsO\|rplS\|rpsB\|tsf\|frr\|pheT\|infC\|rpmI\|rplT\|efp\|aspS\|def-3\|rpmF\|yciH\|rpsT\|rpmA\|rplU\|rplI\|rpsR\|rpsF\|rpsI\|rplM\|rpmG |
| 1 | 633 | 54 | GO Molecular Function | GO:0003676 | Nucleic acid binding | 2.8E-11 | nusG\|rplK\|rplA\|rplL\|rpoB\|rpoC\|rpsG\|tufA\|rpsJ\|rplC\|rplD\|rplB\|rpsS\|rplV\|rpsC\|rplP\|rpsQ\|rplN\|rplX\|rplE\|rpsN\|rpsH\|rplF\|rplR\|rpsE\|rplO\|rpsM\|rpsK\|rpsD\|fusB\|prfB\|greA\|nusA\|infB\|rpsO\|pnpA\|rpoD\|tsf\|pheT\|infC\|rplT\|efp\|gyrA\|ruvA\|aspS\|topA\|yciH\|rpsT\|rplU\|rplI\|rps |

Table A-3 (cont'd)

| | | | | | | | |
|---|---|---|---|---|---|---|---|
| | | | | | | | R\|rpsF\|rpsI\|rplM |
| 1 | 22 | 13 | KEGG Pathways | son00280 | Valine, leucine and isoleucine degradation | 2.93E-10 | ivdA\|ivdB\|ivdF\|liuG\|liuE\|liuD\|liuC\|liuB\|liuA\|bkdA1\|bkdA2\|bkdB\|ldh |
| 1 | 680 | 81 | GO Biological Process | GO:1901576 | Organic substance biosynthetic process | 3.0E-30 | rpmH\|nusG\|rplK\|rplA\|rplL\|rpoB\|rpoC\|rpsG\|tufA\|rpsJ\|rplC\|rplD\|rplB\|rpsS\|rplV\|rpsC\|rplP\|rpsQ\|rplN\|rplX\|rplE\|rpsN\|rpsH\|rplF\|rplR\|rpsE\|rpmD\|rplO\|rpsM\|rpsK\|rpsD\|rplQ\|fusB\|prfB\|nusA\|infB\|rpsO\|deoB\|rpoD\|rplS\|rpsB\|tsf\|frr\|fabV\|fabA\|speA\|liuE\|liuB\|adk\|pheT\|ndk\|infC\|rpmI\|rplT\|efp\|ubiG\|aspS\|def-3\|acs\|fabF\|fabH\|rpmF\|wbpQ\|rmlA\|yciH\|ribE\|SO_3468\|rpsT\|rpmA\|rplU\|hprT\|prsA\|rplI\|rpsR\|rpsF\|purA\|rpsI\|rplM\|r |

Table A-3 (cont'd)

| | | | | | | | |
|---|---|---|---|---|---|---|---|
| | | | | | | | pmG\|dut\|atpE |
| 1 | 87 | 55 | STRING Clusters | CL:105 | Structural constituent of ribosome, and Translation regulator activity | 3.13E-49 | rpmH\|nusG\|rplK\|rplA\|rplL\|rpsG\|tufA\|rpsJ\|rplC\|rplD\|rplB\|rpsS\|rplV\|rpsC\|rplP\|rpsQ\|rplN\|rplX\|rplE\|rpsN\|rpsH\|rplF\|rplR\|rpsE\|rpmD\|rplO\|rpsM\|rpsK\|rpsD\|rplQ\|fusB\|prfB\|nusA\|infB\|rpsO\|rplS\|rpsB\|tsf\|frr\|tig\|infC\|rpmI\|rplT\|def-3\|rpmF\|raiA\|rpsT\|rpmA\|rplU\|rplI\|rpsR\|rpsF\|rpsI\|rplM\|rpmG |
| 1 | 2697 | 109 | COMPARTMENTS | GOCC:0110165 | Cellular anatomical entity | 3.14E-7 | rpmH\|nusG\|rplK\|rplA\|rplL\|rpsG\|tufA\|rpsJ\|rplC\|rplD\|rplB\|rpsS\|rplV\|rpsC\|rplP\|rpsQ\|rplN\|rplX\|rplE\|rpsN\|rpsH\|rplF\|rplR\|rpsE\|rpmD\|rplO\|rpsM\|rpsK\|rpsD\|rplQ\|SO_0306\|prpF\|prpC\|sspA\| |

Table A-3 (cont'd)

| | | | | | | | |
|---|---|---|---|---|---|---|---|
| | | | | | | | groES\|groEL\|fusB\|prfB\|dnaK\|dnaJ\|greA\|ftsH\|nusA\|infB\|rpsO\|pnpA\|deoA\|deoB\|rplS\|grpE\|SO_1550\|rpsB\|tsf\|frr\|ivdA\|ivdC\|ivdE\|ivdG\|tig\|fabA\|speA\|liuG\|liuE\|liuC\|liuA\|sucA\|sucD\|SO_1995\|ushA\|htpG\|adk\|pheT\|ndk\|infC\|rpmI\|rplT\|efp\|bkdA1\|bkdA2\|bkdB\|ubiG\|aspS\|def-3\|ldh\|topA\|acs\|fabF\|fabH\|rpmF\|wbpQ\|rmlA\|yciH\|raiA\|SO_3468\|rpsT\|cpdB\|clpB\|rpmA\|rplU\|hprT\|rplI\|rpsR\|rpsF\|purA\|rpsI\|rplM\|rpmG\|dut\|atpE |
| 1 | 37 | 31 | STRING Clusters | CL:126 | Ribosomal subunit | 3.22E-29 | rplK\|rplA\|rplL\|rpsG\|rpsJ\|rplC\|rplD\|rplB\|rpsS\|rplV\|rpsC\|rplP\|rpsQ\|rplN\|rplX\|rplE\|rpsN\|rplF\|rplR\|rpsE\|rpmD\|rplO\|rpsM\|rpsD\|rplQ\|rpsO\|rplS\|rpsB\|rpmA\|rpsI\|rplM |

Table A-3 (cont'd)

| | | | | | | | |
|---|---|---|---|---|---|---|---|
| 1 | 990 | 68 | GO Biological Process | GO:0043170 | Macromolecule metabolic process | 3.33E-11 | rpmH\|nusG\|rplK\|rplA\|rplL\|rpoB\|rpoC\|rpsG\|tufA\|rpsJ\|rplC\|rplD\|rplB\|rpsS\|rplV\|rpsC\|rplP\|rpsQ\|rplN\|rplX\|rplE\|rpsN\|rpsH\|rplF\|rplR\|rpsE\|rpmD\|rplO\|rpsM\|rpsK\|rpsD\|rplQ\|fusB\|prfB\|dnaJ\|ftsH\|nusA\|infB\|rpsO\|pnpA\|rpoD\|rplS\|rpsB\|tsf\|frr\|pheT\|infC\|rpmI\|rplT\|efp\|gyrA\|ruvA\|aspS\|def-3\|topA\|rpmF\|rmlA\|yciH\|rpsT\|rpmA\|rplU\|rplI\|rpsR\|rpsF\|rpsI\|rplM\|hslV\|rpmG |
| 1 | 13 | 6 | STRING Clusters | CL:1616 | Mixed, incl. Benzoate degradation, and Valine catabolic process | 3.3E-4 | ivdA\|ivdB\|ivdC\|ivdE\|ivdF\|acs |

Table A-3 (cont'd)

| | | | | | | | |
|---|---|---|---|---|---|---|---|
| 1 | 1761 | 109 | GO Biological Process | GO:0071704 | Organic substance metabolic process | 3.52E-23 | rpmH\|nusG\|rplK\|rplA\|rplL\|rpoB\|rpoC\|rpsG\|tufA\|rpsJ\|rplC\|rplD\|rplB\|rpsS\|rplV\|rpsC\|rplP\|rpsQ\|rplN\|rplX\|rplE\|rpsN\|rpsH\|rplF\|rplR\|rpsE\|rpmD\|rplO\|rpsM\|rpsK\|rpsD\|rplQ\|prpF\|prpC\|sspA\|fusB\|prfB\|dnaJ\|ftsH\|nusA\|infB\|rpsO\|pnpA\|deoA\|deoB\|rpoD\|rplS\|rpsB\|tsf\|frr\|ivdA\|ivdB\|ivdC\|ivdE\|ivdF\|ivdG\|fabV\|fabA\|speA\|liuG\|liuE\|liuD\|liuC\|liuB\|liuA\|ushA\|adk\|pheT\|ndk\|infC\|rpmI\|rplT\|efp\|bkdA1\|bkdA2\|bkdB\|gyrA\|ubiG\|ruvA\|aspS\|def-3\|ldh\|topA\|acs\|fabF\|fabH\|rpmF\|wbpQ\|rmlA\|yciH\|ribE\|SO_3468\|rpsT\|cpdB\|rpmA\|rplU\|hprT\|prsA\|rplI\|rpsR\|rpsF\|purA\|rpsI\|rplM\|h |

Table A-3 (cont'd)

| | | | | | | | |
|---|---|---|---|---|---|---|---|
| | | | | | | | slV\|rpmG\|dut\|exaC\|atpE |
| 1 | 9 | 8 | STRING Clusters | CL:161 | Small ribosomal subunit | 3.5E-7 | rpsG\|rpsJ\|rpsC\|rpsQ\|rpsN\|rpsM\|rpsO\|rpsB |
| 1 | 1414 | 96 | GO Biological Process | GO:0006807 | Nitrogen compound metabolic process | 3.6E-20 | rpmH\|nusG\|rplK\|rplA\|rplL\|rpoB\|rpoC\|rpsG\|tufA\|rpsJ\|rplC\|rplD\|rplB\|rpsS\|rplV\|rpsC\|rplP\|rpsQ\|rplN\|rplX\|rplE\|rpsN\|rpsH\|rplF\|rplR\|rpsE\|rpmD\|rplO\|rpsM\|rpsK\|rpsD\|rplQ\|sspA\|fusB\|prfB\|dnaJ\|ftsH\|nusA\|infB\|rpsO\|pnpA\|deoA\|deoB\|rpoD\|rplS\|rpsB\|tsf\|frr\|ivdB\|ivdC\|ivdE\|ivdF\|speA\|liuE\|liuD\|liuA\|ushA\|adk\|pheT\|ndk\|infC\|rpmI\|rplT\|efp\|bkdA1\|bkdA2\|bkdB\|gyrA\|ruvA\|aspS\|d |

Table A-3 (cont'd)

| | | | | | | | |
|---|---|---|---|---|---|---|---|
| | | | | | | | ef-3\|ldh\|topA\|acs\|rpmF\|wbpQ\|yciH\|ribE\|SO_3468\|rpsT\|cpdB\|rpmA\|rplU\|hprT\|prsA\|rplI\|rpsR\|rpsF\|purA\|rpsI\|rplM\|hslV\|rpmG\|dut\|exaC\|atpE |
| 1 | 588 | 54 | COMPARTMENTS | GOCC:0032991 | Protein-containing complex | 3.79E-13 | nusG\|rplA\|rplL\|rpoB\|rpoC\|rpsG\|rplC\|rplD\|rplB\|rpsS\|rplV\|rpsC\|rpsQ\|rplN\|rplE\|rpsN\|rpsH\|rplF\|rplR\|rpsE\|rpmD\|rplO\|rpsD\|groES\|groEL\|nusA\|rpsO\|rpoD\|SO_1550\|rpsB\|ivdB\|ivdF\|liuE\|liuD\|liuB\|sucA\|sucD\|pheT\|bkdA2\|bkdB\|gyrA\|ubiG\|ruvA\|rpmF\|yciH\|raiA\|ribE\|rpsT\|clpB\|rplU\|prsA\|hslV\|exaC\|atpE |
| 1 | 75 | 49 | STRING Clusters | CL:109 | Structural constituent of ribosome, and Translation regulator activity | 3.86E-44 | rpmH\|nusG\|rplK\|rplA\|rplL\|rpsG\|tufA\|rpsJ\|rplC\|rplD\|rplB\|rpsS\|rplV\|rpsC\|rplP\|rpsQ\|rplN\|rplX\|rplE\|rpsN\|rpsH\|rplF\|rplR\|r |

Table A-3 (cont'd)

| | | | | | | | |
|---|---|---|---|---|---|---|---|
| | | | | | | | psE\|rpmD\|rplO\|rpsM\|rpsK\|rpsD\|rplQ\|fusB\|prfB\|rpsO\|rplS\|rpsB\|tig\|infC\|rpmI\|rplT\|rpmF\|rpsT\|rpmA\|rplU\|rplI\|rpsR\|rpsF\|rpsI\|rplM\|rpmG |
| 1 | 69 | 48 | STRING Clusters | CL:111 | Structural constituent of ribosome, and Elongation factor Tu GTP binding domain | 3.98E-44 | rpmH\|nusG\|rplK\|rplA\|rplL\|rpsG\|tufA\|rpsJ\|rplC\|rplD\|rplB\|rpsS\|rplV\|rpsC\|rplP\|rpsQ\|rplN\|rplX\|rplE\|rpsN\|rpsH\|rplF\|rplR\|rpsE\|rpmD\|rplO\|rpsM\|rpsK\|rpsD\|rplQ\|fusB\|rpsO\|rplS\|rpsB\|tig\|infC\|rpmI\|rplT\|rpmF\|rpsT\|rpmA\|rplU\|rplI\|rpsR\|rpsF\|rpsI\|rplM\|rpmG |
| 1 | 36 | 13 | GO Biological Process | GO:0006417 | Regulation of translation | 4.03E-8 | rplA\|tufA\|rpsD\|fusB\|prfB\|nusA\|infB\|tsf\|infC\|efp\|yciH\|raiA\|rplM |
| 1 | 454 | 68 | GO Biological Process | GO:1901566 | Organonitrogen compound biosynthetic process | 4.17E-29 | rpmH\|rplK\|rplA\|rplL\|rpsG\|tufA\|rpsJ\|rplC\|rplD\|rplB\|rpsS\|rplV\|rpsC\|rplP\|rpsQ\|rplN\|rplX\|rplE\|rpsN\|rpsH\|rplF\|rplR\|rpsE\|r |

Table A-3 (cont'd)

| | | | | | | | |
|---|---|---|---|---|---|---|---|
| | | | | | | | pmD\|rplO\|rpsM\|rpsK\|rpsD\|rplQ\|fusB\|prfB\|nusA\|infB\|rpsO\|rplS\|rpsB\|tsf\|frr\|speA\|adk\|pheT\|ndk\|infC\|rpmI\|rplT\|efp\|aspS\|def-3\|acs\|rpmF\|wbpQ\|yciH\|ribE\|SO_3468\|rpsT\|rpmA\|rplU\|hprT\|prsA\|rplI\|rpsR\|rpsF\|purA\|rpsI\|rplM\|rpmG\|dut\|atpE |
| 1 | 368 | 71 | GO Biological Process | GO:0044271 | Cellular nitrogen compound biosynthetic process | 4.29E-37 | rpmH\|nusG\|rplK\|rplA\|rplL\|rpoB\|rpoC\|rpsG\|tufA\|rpsJ\|rplC\|rplD\|rplB\|rpsS\|rplV\|rpsC\|rplP\|rpsQ\|rplN\|rplX\|rplE\|rpsN\|rpsH\|rplF\|rplR\|rpsE\|rpmD\|rplO\|rpsM\|rpsK\|rpsD\|rplQ\|fusB\|prfB\|nusA\|infB\|rpsO\|rpoD\|rplS\|rpsB\|tsf\|frr\|speA\|adk\|pheT\|ndk\|infC\|rpmI\|rplT\|efp\|aspS\|def-3\|acs\|rpmF\|yciH\|ribE\|SO_3468\|rpsT\|rpmA\|rplU\|hpr |

Table A-3 (cont'd)

| | | | | | | | |
|---|---|---|---|---|---|---|---|
| | | | | | | | T\|prsA\|rplI\|rpsR\|rpsF\|purA\|rpsI\|rplM\|rpmG\|dut\|atpE |
| 1 | 31 | 8 | UniProt Keywords | KW-0143 | Chaperone | 4.3E-4 | groES\|groEL\|dnaK\|dnaJ\|grpE\|tig\|htpG\|clpB |
| 1 | 49 | 40 | GO Cellular Component | GO:0044391 | Ribosomal subunit | 4.58E-38 | rplK\|rplA\|rplL\|rpsG\|rpsJ\|rplC\|rplB\|rpsS\|rplV\|rpsC\|rplP\|rpsQ\|rplN\|rplX\|rplE\|rpsN\|rpsH\|rplF\|rplR\|rpsE\|rpmD\|rplO\|rpsM\|rpsK\|rpsD\|rplQ\|rpsO\|rplS\|rpsB\|rpmI\|rplT\|rpmF\|rpsT\|rpmA\|rplI\|rpsR\|rpsF\|rpsI\|rplM\|rpmG |
| 1 | 62 | 44 | GO Cellular Component | GO:0005840 | Ribosome | 4.58E-40 | rpmH\|rplK\|rplA\|rplL\|rpsG\|rpsJ\|rplC\|rplD\|rplB\|rpsS\|rplV\|rpsC\|rplP\|rpsQ\|rplN\|rplX\|rplE\|rpsN\|rpsH\|rplF\|rplR\|rpsE\|rpmD\|rplO\|rpsM\|rpsK\|rpsD\|rplQ\|rpsO\|rplS\|rpsB\|rpmI\|rplT\|rpmF\|raiA\|rpsT\|rpmA\|rplU\|rplI\|rpsR\|r |

Table A-3 (cont'd)

| | | | | | | | |
|---|---|---|---|---|---|---|---|
| | | | | | | | psF\|rpsI\|rplM\|rpmG |
| 1 | 337 | 30 | UniProt Keywords | KW-0963 | Cytoplasm | 4.65E-6 | tufA\|groES\|groEL\|fusB\|prfB\|dnaJ\|nusA\|infB\|pnpA\|deoB\|rpoD\|grpE\|tsf\|frr\|tig\|fabA\|htpG\|adk\|pheT\|ndk\|infC\|efp\|gyrA\|aspS\|fabH\|clpB\|hprT\|prsA\|purA\|hslV |
| 1 | 14 | 13 | STRING Clusters | CL:160 | Small ribosomal subunit | 4.7E-12 | rpsG\|rpsJ\|rpsS\|rpsC\|rplP\|rpsQ\|rpsN\|rplR\|rpsE\|rpsM\|rpsD\|rpsO\|rpsB |
| 1 | 21 | 17 | GO Cellular Component | GO:0015935 | Small ribosomal subunit | 5.08E-16 | rpsG\|rpsJ\|rpsS\|rpsC\|rpsQ\|rpsN\|rpsH\|rpsE\|rpsM\|rpsK\|rpsD\|rpsO\|rpsB\|rpsT\|rpsR\|rpsF\|rpsI |
| 1 | 47 | 30 | GO Molecular Function | GO:0019843 | rRNA binding | 5.0E-25 | rplK\|rplA\|rpsG\|rplC\|rplD\|rplB\|rpsS\|rplV\|rpsC\|rplP\|rpsQ\|rplN\|rplX\|rplE\|rpsN\|rpsH\|rplF\|rplR\|rpsE\|rplO\|rpsM\|rpsK\|rpsD\|rpsO\|rplT\|rpsT\|rplU\|rplI\|rpsR\|rpsF |

Table A-3 (cont'd)

| | | | | | | | |
|---|---|---|---|---|---|---|---|
| 1 | 1677 | 89 | GO Molecular Function | GO:0005488 | Binding | 5.61E-10 | nusG\|rplK\|rplA\|rplL\|rpoB\|rpoC\|rpsG\|tufA\|rpsJ\|rplC\|rplD\|rplB\|rpsS\|rplV\|rpsC\|rplP\|rpsQ\|rplN\|rplX\|rplE\|rpsN\|rpsH\|rplF\|rplR\|rpsE\|rplO\|rpsM\|rpsK\|rpsD\|groES\|groEL\|fusB\|prfB\|dnaK\|dnaJ\|greA\|ftsH\|nusA\|infB\|rpsO\|pnpA\|deoB\|rpoD\|grpE\|tsf\|frr\|ivdC\|ivdF\|tig\|fabV\|speA\|liuD\|liuA\|sucA\|sucD\|ushA\|htpG\|adk\|pheT\|ndk\|infC\|rplT\|efp\|gyrA\|ruvA\|aspS\|def-3\|ldh\|topA\|acs\|wbpQ\|rmlA\|yciH\|raiA\|rpsT\|cpdB\|clpB\|rplU\|hprT\|prsA\|rplI\|rpsR\|rpsF\|purA\|rpsI\|rplM\|hslV\|dut\|atpE |
| 1 | 118 | 59 | STRING Clusters | CL:100 | Translation, and ATP synthesis | 5.61E-49 | rpmH\|nusG\|rplK\|rplA\|rplL\|rpsG\|tufA\|rpsJ\|rplC\|rplD\|rplB\|rpsS\|rplV\|rpsC\|rplP\|rpsQ\|rplN\|rplX\|rplE\|rpsN\|rps |

Table A-3 (cont'd)

| | | | | | | | |
|---|---|---|---|---|---|---|---|
| | | | | | | | H\|rplF\|rplR\|rpsE\|rpmD\|rplO\|rpsM\|rpsK\|rpsD\|rplQ\|fusB\|prfB\|nusA\|infB\|rpsO\|rplS\|rpsB\|tsf\|frr\|tig\|pheT\|infC\|rpmI\|rplT\|efp\|aspS\|def-3\|rpmF\|raiA\|rpsT\|rpmA\|rplU\|rplI\|rpsR\|rpsF\|rpsI\|rplM\|rpmG\|atpE |
| 1 | 51 | 41 | STRING Clusters | CL:123 | Ribosome | 5.64E-39 | rpmH\|rplK\|rplA\|rplL\|rpsG\|rpsJ\|rplC\|rplD\|rplB\|rpsS\|rplV\|rpsC\|rplP\|rpsQ\|rplN\|rplX\|rplE\|rpsN\|rplF\|rplR\|rpsE\|rpmD\|rplO\|rpsM\|rpsD\|rplQ\|rpsO\|rplS\|rpsB\|rpmI\|rplT\|rpmF\|rpsT\|rpmA\|rplU\|rplI\|rpsR\|rpsF\|rpsI\|rplM\|rpmG |
| 1 | 10 | 8 | STRING Clusters | CL:515 | Stress response, and Proteasome complex | 5.66E-7 | groES\|groEL\|dnaK\|dnaJ\|grpE\|htpG\|clpB\|hslV |
| 1 | 190 | 58 | GO Biological Process | GO:0043603 | Cellular amide metabolic process | 5.75E-38 | rpmH\|rplK\|rplA\|rplL\|rpsG\|tufA\|rpsJ\|rplC\|rplD\|rplB\|rpsS\|rplV\|rpsC\|rplP\|rpsQ\|rplN\|rplX\|rplE\|r |

Table A-3 (cont'd)

| | | | | | | | |
|---|---|---|---|---|---|---|---|
| | | | | | | | psN\|rpsH\|rplF\|rplR\|rpsE\|rpmD\|rplO\|rpsM\|rpsK\|rpsD\|rplQ\|sspA\|fusB\|prfB\|nusA\|infB\|rpsO\|rplS\|rpsB\|tsf\|frr\|pheT\|infC\|rpmI\|rplT\|efp\|aspS\|def-3\|acs\|rpmF\|yciH\|rpsT\|rpmA\|rplU\|rplI\|rpsR\|rpsF\|rpsI\|rplM\|rpmG |
| 1 | 13 | 10 | COMPARTMENTS | GOCC:0022627 | Cytosolic small ribosomal subunit | 5.89E-9 | rpsG\|rpsC\|rpsQ\|rpsN\|rpsH\|rpsE\|rpsD\|rpsO\|raiA\|rpsT |
| 1 | 258 | 61 | GO Biological Process | GO:0009059 | Macromolecule biosynthetic process | 6.03E-35 | rpmH\|nusG\|rplK\|rplA\|rplL\|rpoB\|rpoC\|rpsG\|tufA\|rpsJ\|rplC\|rplD\|rplB\|rpsS\|rplV\|rpsC\|rplP\|rpsQ\|rplN\|rplX\|rplE\|rpsN\|rpsH\|rplF\|rplR\|rpsE\|rpmD\|rplO\|rpsM\|rpsK\|rpsD\|rplQ\|fusB\|prfB\|nusA\|infB\|rpsO\|rpoD\|rplS\|rpsB\|tsf\|frr\|pheT\|infC\|rpmI\|rplT\|efp\|aspS\|def-3\|rpmF\|rmlA\|yciH\|rpsT\|rpmA\|rplU\|rplI\|r |

Table A-3 (cont'd)

| | | | | | | | |
|---|---|---|---|---|---|---|---|
| | | | | | | | psR\|rpsF\|rpsI\|rplM\|rpmG |
| 1 | 48 | 13 | UniProt Keywords | KW-0648 | Protein biosynthesis | 6.04E-7 | tufA\|fusB\|prfB\|greA\|infB\|tsf\|frr\|pheT\|infC\|efp\|aspS\|def-3\|yciH |
| 1 | 64 | 47 | STRING Clusters | CL:115 | Structural constituent of ribosome | 6.17E-44 | rpmH\|nusG\|rplK\|rplA\|rplL\|rpsG\|tufA\|rpsJ\|rplC\|rplD\|rplB\|rpsS\|rplV\|rpsC\|rplP\|rpsQ\|rplN\|rplX\|rplE\|rpsN\|rpsH\|rplF\|rplR\|rpsE\|rpmD\|rplO\|rpsM\|rpsK\|rpsD\|rplQ\|fusB\|rpsO\|rplS\|rpsB\|tig\|rpmI\|rplT\|rpmF\|rpsT\|rpmA\|rplU\|rplI\|rpsR\|rpsF\|rpsI\|rplM\|rpmG |
| 1 | 42 | 9 | GO Biological Process | GO:0006457 | Protein folding | 6.2E-4 | groES\|groEL\|dnaK\|dnaJ\|grpE\|tig\|SO_1995\|htpG\|clpB |
| 1 | 142 | 47 | GO Cellular Component | GO:0043229 | Intracellular organelle | 6.41E-32 | rpmH\|rplK\|rplA\|rplL\|rpsG\|rpsJ\|rplC\|rplD\|rplB\|rpsS\|rplV\|rpsC\|rplP\|rpsQ\|rplN\|rplX\|rplE\|rpsN\|rpsH\|rplF\|rpl |

Table A-3 (cont'd)

| | | | | | | | |
|---|---|---|---|---|---|---|---|
| | | | | | | | R\|rpsE\|rpmD\|rplO\|rpsM\|rpsK\|rpsD\|rplQ\|rpsO\|rplS\|rpsB\|rpmI\|rplT\|bkdA1\|gyrA\|topA\|rpmF\|raiA\|rpsT\|rpmA\|rplU\|rplI\|rpsR\|rpsF\|rpsI\|rplM\|rpmG |
| 1 | 86 | 33 | UniProt Keywords | KW-0694 | RNA-binding | 6.76E-23 | rplK\|rplA\|rpsG\|rplC\|rplD\|rplB\|rpsS\|rplV\|rpsC\|rplP\|rpsQ\|rplN\|rplX\|rplE\|rpsN\|rpsH\|rplF\|rplR\|rpsE\|rplO\|rpsM\|rpsK\|rpsD\|nusA\|rpsO\|pnpA\|pheT\|rplT\|rpsT\|rplU\|rplI\|rpsR\|rpsF |
| 1 | 272 | 61 | GO Biological Process | GO:0010467 | Gene expression | 6.8E-34 | rpmH\|nusG\|rplK\|rplA\|rplL\|rpoB\|rpoC\|rpsG\|tufA\|rpsJ\|rplC\|rplD\|rplB\|rpsS\|rplV\|rpsC\|rplP\|rpsQ\|rplN\|rplX\|rplE\|rpsN\|rpsH\|rplF\|rplR\|rpsE\|rpmD\|rplO\|rpsM\|rpsK\|rpsD\|rplQ\|fusB\|prfB\|nusA\|infB\|rpsO\|pnpA\|rpoD\|rplS\|rpsB\|tsf\|frr\|pheT\|infC\|rpmI\|rplT\|efp\|aspS\|def- |

Table A-3 (cont'd)

| | | | | | | | |
|---|---|---|---|---|---|---|---|
| | | | | | | | 3\|rpmF\|yciH\|rpsT\|rpmA\|rplU\|rplI\|rpsR\|rpsF\|rpsI\|rplM\|rpmG |
| 1 | 181 | 18 | GO Biological Process | GO:1901575 | Organic substance catabolic process | 6.9E-4 | prpF\|ftsH\|pnpA\|deoB\|ivdA\|ivdC\|ivdE\|ivdF\|speA\|liuE\|liuA\|ushA\|bkdA1\|bkdA2\|bkdB\|cpdB\|hslV\|dut |
| 1 | 15 | 12 | COMPARTMENTS | GOCC:0015935 | Small ribosomal subunit | 7.12E-11 | rpsG\|rpsS\|rpsC\|rpsQ\|rpsN\|rpsH\|rpsE\|rpsD\|rpsO\|rpsB\|raiA\|rpsT |
| 1 | 97 | 56 | STRING Clusters | CL:104 | Structural constituent of ribosome, and Translation regulator activity | 7.29E-49 | rpmH\|nusG\|rplK\|rplA\|rplL\|rpsG\|tufA\|rpsJ\|rplC\|rplD\|rplB\|rpsS\|rplV\|rpsC\|rplP\|rpsQ\|rplN\|rplX\|rplE\|rpsN\|rpsH\|rplF\|rplR\|rpsE\|rpmD\|rplO\|rpsM\|rpsK\|rpsD\|rplQ\|fusB\|prfB\|nusA\|infB\|rpsO\|rplS\|rpsB\|tsf\|frr\|tig\|infC\|rpmI\|rplT\|def-3\|rpmF\|raiA\|rpsT\|rpmA\|rplU\|rplI\|rpsR\|rpsF\|rpsI\|rplM\|rpmG\|atpE |

Table A-3 (cont'd)

| | | | | | | | |
|---|---|---|---|---|---|---|---|
| 1 | 315 | 56 | GO Cellular Component | GO:0032991 | Protein-containing complex | 7.42E-27 | rplK\|rplA\|rplL\|rpoB\|rpoC\|rpsG\|rpsJ\|rplC\|rplB\|rpsS\|rplV\|rpsC\|rplP\|rpsQ\|rplN\|rplX\|rplE\|rpsN\|rpsH\|rplF\|rplR\|rpsE\|rpmD\|rplO\|rpsM\|rpsK\|rpsD\|rplQ\|groEL\|rpsO\|rplS\|rpsB\|ivdF\|liuD\|liuC\|liuB\|sucA\|sucD\|pheT\|rpmI\|rplT\|bkdB\|ruvA\|rpmF\|ribE\|rpsT\|rpmA\|prsA\|rplI\|rpsR\|rpsF\|rpsI\|rplM\|hslV\|rpmG\|atpE |
| 1 | 1531 | 110 | COMPARTMENTS | GOCC:0005622 | Intracellular | 7.6E-30 | rpmH\|nusG\|rplK\|rplA\|rplL\|rpoB\|rpoC\|rpsG\|tufA\|rpsJ\|rplC\|rplD\|rplB\|rpsS\|rplV\|rpsC\|rplP\|rpsQ\|rplN\|rplX\|rplE\|rpsN\|rpsH\|rplF\|rplR\|rpsE\|rpmD\|rplO\|rpsM\|rpsK\|rpsD\|rplQ\|prpF\|prpC\|sspA\|groES\|groEL\|fusB\|prfB\|dnaK\|dnaJ\|greA\|nusA\|infB\|rpsO\|pnpA\|deoA\|deoB\|rpoD\|rplS\|grp |

Table A-3 (cont'd)

| | | | | | | | |
|---|---|---|---|---|---|---|---|
| | | | | | | | E\|SO_1550\|rpsB\|tsf\|frr\|ivdA\|ivdC\|ivdG\|tig\|fabA\|speA\|liuG\|liuE\|liuC\|liuA\|sucA\|sucD\|SO_1995\|htpG\|adk\|pheT\|ndk\|infC\|rpmI\|rplT\|efp\|bkdA1\|bkdA2\|bkdB\|gyrA\|ubiG\|ruvA\|aspS\|def-3\|ldh\|topA\|acs\|fabF\|fabH\|rpmF\|wbpQ\|rmlA\|yciH\|raiA\|SO_3468\|rpsT\|clpB\|rpmA\|rplU\|hprT\|rplI\|rpsR\|rpsF\|purA\|rpsI\|rplM\|hslV\|rpmG\|dut\|atpE |
| 1 | 29 | 22 | COMPARTMENTS | GOCC:0022626 | Cytosolic ribosome | 7.88E-20 | rplA\|rplL\|rpsG\|rplC\|rplD\|rplB\|rplV\|rpsC\|rpsQ\|rplE\|rpsN\|rpsH\|rplF\|rplR\|rpsE\|rpmD\|rplO\|rpsD\|rpsO\|raiA\|rpsT\|rplU |
| 1 | 896 | 84 | GO Biological Process | GO:1901564 | Organonitrogen compound metabolic process | 8.1E-25 | rpmH\|rplK\|rplA\|rplL\|rpsG\|tufA\|rpsJ\|rplC\|rplD\|rplB\|rpsS\|rplV\|rpsC\|rplP\|rpsQ\|rplN\|rplX\|rplE\|rpsN\|rpsH\|rplF\|rplR\|rpsE\|rpmD\|rplO\|rp |

Table A-3 (cont'd)

| | | | | | | | |
|---|---|---|---|---|---|---|---|
| | | | | | | | sM\|rpsK\|rpsD\|rplQ\|sspA\|fusB\|prfB\|ftsH\|nusA\|infB\|rpsO\|deoA\|rplS\|rpsB\|tsf\|frr\|ivdB\|ivdC\|ivdE\|ivdF\|speA\|liuE\|liuD\|liuA\|adk\|pheT\|ndk\|infC\|rpmI\|rplT\|efp\|bkdA1\|bkdA2\|bkdB\|aspS\|def-3\|ldh\|acs\|rpmF\|wbpQ\|yciH\|ribE\|SO_3468\|rpsT\|rpmA\|rplU\|hprT\|prsA\|rplI\|rpsR\|rpsF\|purA\|rpsI\|rplM\|hslV\|rpmG\|dut\|exaC\|atpE |
| 1 | 53 | 41 | COMPARTMENTS | GOCC:0005840 | Ribosome | 8.28E-38 | rpmH\|rplK\|rplA\|rplL\|rpsG\|rpsJ\|rplC\|rplD\|rplB\|rpsS\|rplV\|rpsC\|rplP\|rpsQ\|rplN\|rplX\|rplE\|rpsN\|rpsH\|rplF\|rplR\|rpsE\|rpmD\|rplO\|rpsK\|rpsD\|rpsO\|rpsB\|rpmI\|rplT\|rpmF\|raiA\|rpsT\|rpmA\|rplU\|rplI\|rpsR\|rpsF\|rpsI\|rplM\|rpmG |

Table A-3 (cont'd)

| | | | | | | | |
|---|---|---|---|---|---|---|---|
| 1 | 212 | 57 | GO Biological Process | GO:0034645 | Cellular macromolecule biosynthetic process | 8.42E-35 | rpmH\|rplK\|rplA\|rplL\|rpsG\|tufA\|rpsJ\|rplC\|rplD\|rplB\|rpsS\|rplV\|rpsC\|rplP\|rpsQ\|rplN\|rplX\|rplE\|rpsN\|rpsH\|rplF\|rplR\|rpsE\|rpmD\|rplO\|rpsM\|rpsK\|rpsD\|rplQ\|fusB\|prfB\|nusA\|infB\|rpsO\|rplS\|rpsB\|tsf\|frr\|pheT\|infC\|rpmI\|rplT\|efp\|aspS\|def-3\|rpmF\|rmlA\|yciH\|rpsT\|rpmA\|rplU\|rplI\|rpsR\|rpsF\|rpsI\|rplM\|rpmG |
| 1 | 27 | 22 | GO Cellular Component | GO:0022625 | Cytosolic large ribosomal subunit | 8.6E-21 | rplK\|rplA\|rplL\|rplC\|rplB\|rplV\|rplP\|rplN\|rplX\|rplE\|rplF\|rplR\|rpmD\|rplO\|rplQ\|rplS\|rpmI\|rplT\|rpmA\|rplI\|rplM\|rpmG |
| 1 | 28 | 23 | GO Cellular Component | GO:0015934 | Large ribosomal subunit | 8.78E-22 | rplK\|rplA\|rplL\|rplC\|rplB\|rplV\|rplP\|rplN\|rplX\|rplE\|rplF\|rplR\|rpmD\|rplO\|rplQ\|rplS\|rpmI\|rplT\|rpmF\|rpmA\|rplI\|rplM\|rpmG |
| 1 | 33 | 26 | COMPARTMENTS | GOCC:0044391 | Ribosomal subunit | 9.09E-24 | rplA\|rplL\|rpsG\|rplC\|rplD\|rplB\|rpsS\|rplV |

Table A-3 (cont'd)

| | | | | | | | |
|---|---|---|---|---|---|---|---|
| | | | | | | | \|rpsC\|rpsQ\|rplN\|rplE\|rpsN\|rpsH\|rplF\|rplR\|rpsE\|rpmD\|rplO\|rpsD\|rpsO\|rpsB\|rpmF\|raiA\|rpsT\|rplU |
| 1 | 21 | 9 | GO Molecular Function | GO:0008135 | Translation factor activity, RNA binding | 9.09E-6 | tufA\|fusB\|prfB\|nusA\|infB\|tsf\|infC\|efp\|yciH |
| 1 | 7 | 5 | GO Molecular Function | GO:0003729 | mRNA binding | 9.0E-4 | rplL\|rpsG\|rpsC\|rpsK\|rplM |
| 1 | 24 | 9 | KEGG Pathways | son00640 | Propanoate metabolism | 9.24E-6 | prpF\|prpC\|ivdA\|ivdB\|sucD\|bkdA1\|bkdA2\|bkdB\|acs |
| 1 | 54 | 43 | KEGG Pathways | son03010 | Ribosome | 9.71E-41 | rpmH\|rplK\|rplA\|rplL\|rpsG\|rpsJ\|rplC\|rplD\|rplB\|rpsS\|rplV\|rpsC\|rplP\|rpsQ\|rplN\|rplX\|rplE\|rpsN\|rpsH\|rplF\|rplR\|rpsE\|rpmD\|rplO\|rpsM\|rpsK\|rpsD\|rplQ\|rpsO\|rplS\|rpsB\|rpmI\|rplT\|rpmF\|rpsT\|rpmA\|rplU\|rplI\|rpsR\|rpsF\|rpsI\|rplM\|rpmG |
| 1 | 9 | 5 | UniProt Keywords | KW-0251 | Elongation factor | 9.7E-4 | tufA\|fusB\|greA\|tsf\|efp |

Table A-3 (cont'd)

| | | | | | | | |
|---|---|---|---|---|---|---|---|
| 1 | 39 | 27 | COMPARTMENTS | GOCC:1990904 | Ribonucleoprotein complex | 9.87E-24 | rplA\|rplL\|rpsG\|rplC\|rplD\|rplB\|rpsS\|rplV\|rpsC\|rpsQ\|rplN\|rplE\|rpsN\|rpsH\|rplF\|rplR\|rpsE\|rpmD\|rplO\|rpsD\|rpsO\|rpsB\|rpmF\|yciH\|raiA\|rpsT\|rplU |
| 1 | 197 | 64 | STRING Clusters | CL:95 | Translation, and Catalytic activity, acting on RNA | 9.96E-45 | rpmH\|nusG\|rplK\|rplA\|rplL\|rpoB\|rpoC\|rpsG\|tufA\|rpsJ\|rplC\|rplD\|rplB\|rpsS\|rplV\|rpsC\|rplP\|rpsQ\|rplN\|rplX\|rplE\|rpsN\|rpsH\|rplF\|rplR\|rpsE\|rpmD\|rplO\|rpsM\|rpsK\|rpsD\|rplQ\|fusB\|prfB\|greA\|nusA\|infB\|rpsO\|pnpA\|rpoD\|rplS\|rpsB\|tsf\|frr\|tig\|pheT\|infC\|rpmI\|rplT\|efp\|aspS\|def-3\|rpmF\|raiA\|rpsT\|rpmA\|rplU\|rplI\|rpsR\|rpsF\|rpsI\|rplM\|rpmG\|atpE |
| 2 | 33 | 3 | KEGG Pathways | son00620 | Pyruvate metabolism | 1.20E-03 | ppsA\|sfcA\|maeB |
| 2 | 95 | 4 | KEGG Pathways | son01200 | Carbon metabolism | 1.20E-03 | fdnG\|ppsA\|sfcA\|maeB |

Table A-3 (cont'd)

| | | | | | | | |
|---|---|---|---|---|---|---|---|
| 2 | 2 | 2 | SMART Domains | SM00919 | Malic enzyme, NAD binding domain | 2.10E-03 | sfcA\|maeB |
| 2 | 2 | 2 | SMART Domains | SM01274 | Malic enzyme, N-terminal domain | 2.10E-03 | sfcA\|maeB |
| 2 | 22 | 3 | GO Biological Process | GO:0006090 | Pyruvate metabolic process | 1.04E-02 | ppsA\|sfcA\|maeB |
| 2 | 2 | 2 | GO Molecular Function | GO:0004471 | Malate dehydrogenase (decarboxylating) (NAD+) activity | 1.21E-02 | sfcA\|maeB |
| 2 | 3 | 2 | GO Biological Process | GO:0006108 | Malate metabolic process | 1.86E-02 | sfcA\|maeB |
| 2 | 350 | 5 | UniProt Keywords | KW-0479 | Metal-binding | 2.12E-02 | fdnG\|cysS\|ppsA\|sfcA\|maeB |
| 2 | 2 | 2 | InterPro Domains | IPR00189 | Malic oxidoreductase | 2.56E-02 | sfcA\|maeB |
| 2 | 2 | 2 | InterPro Domains | IPR01230 | Malic enzyme, N-terminal domain | 2.56E-02 | sfcA\|maeB |
| 2 | 2 | 2 | InterPro Domains | IPR01230 | Malic enzyme, NAD-binding | 2.56E-02 | sfcA\|maeB |
| 2 | 2 | 2 | InterPro Domains | IPR01584 | Malic enzyme, conserved site | 2.56E-02 | sfcA\|maeB |
| 2 | 2 | 2 | InterPro Domains | IPR03706 | Malic enzyme, N-terminal | 2.56E-02 | sfcA\|maeB |

Table A-3 (cont'd)

| | | | | | | | |
|---|---|---|---|---|---|---|---|
| | | | | | domain superfamily | | |
| 2 | 6 | 2 | InterPro Domains | IPR046346 | Aminoacid dehydrogenase-like, N-terminal domain superfamily | 2.56E-02 | sfcA\|maeB |